(5)

BALLISTIC IMPACT RESISTANCE OF MULTI-LAYER TEXTILE FABRICS

J.W.S. Hearle
C.M. Leech
A. Adeyefa
C.R. Cork

University of Manchester Institute of Science and Technology
Department of Textile Technology

Contract No. DAJA37-79-C-0532

Final
Technical Report
October, 1981.

UNCLASSIFIED

SECURITY CLASSIFICATION OF THIS PAGE (When Data Entered)

R&D 2762-MS

REPORT DOCUMENTATION PAGE

READ INSTRUCTIONS BEFORE COMPLETING FORM

REPORT NUMBER	2. GOVT ACCESSION NO. AD-A127641
3. RECIPIENT'S CATALOG NUMBER	
TITLE (and Subtitle)	5. TYPE OF REPORT & PERIOD COVERED
Ballistic Impact Resistance of Multi-Layer Textile Fabrics	Final Technical Report October 1979-October 1981
	6. PERFORMING ORG. REPORT NUMBER
AUTHOR(s)	8. CONTRACT OR GRANT NUMBER(s)
J.W.S. Hearle, C.M. Leech, A. Adeyefa, C.R. Cork	DAJA37-79-C-0532
PERFORMING ORGANIZATION NAME AND ADDRESS University of Manchester Institute of Science and Technology P.O. Box 88, Manchester M60 1QD	10. PROGRAM ELEMENT, PROJECT, TASK AREA & WORK UNIT NUMBERS 6.11.02A 1T16 1102BH57-04
CONTROLLING OFFICE NAME AND ADDRESS USARDSG-UK Box 65 FPO New York 09510	12. REPORT DATE October 1981
	13. NUMBER OF PAGES 104
MONITORING AGENCY NAME & ADDRESS (if different from Controlling Office)	15. SECURITY CLASS. (of this report) Unclassified
	15a. DECLASSIFICATION/DOWNGRADING SCHEDULE

DISTRIBUTION STATEMENT (of this Report)

Approved for public release; Distribution unlimited.

DISTRIBUTION STATEMENT (of the abstract entered in Block 20, if different from Report)

SUPPLEMENTARY NOTES

KEY WORDS (Continue on reverse side if necessary and identify by block number)

Textile materials, ballistic impact, impact testing, multi-layer impact, finishes, triaxial fabric, impact modelling, characteristics model, finite element model.

ABSTRACT (Continue on reverse side if necessary and identify by block number)

Experimental and theoretical work on the transverse ballistic impact of Kevlar and nylon fabrics is presented in two parts. Part I is an experimental investigation into a) the relation between the multi-layer and single layer impact; b) the effect of fabric finishes; and c) the effect of weave. A simple model of impact together with the experimental data showed that inter-layer effects are of second order. High friction finishes and bonding

FORM 1 JAN 73 1473 EDITION OF 1 NOV 65 IS OBSOLETE

UNCLASSIFIED

SECURITY CLASSIFICATION OF THIS PAGE (When Data Entered)

agents were found to be detrimental to the performance of Kevlar. Triaxial fabrics were found to be inferior to biaxial fabrics. Part II describes the development and applications of computer models of impact using both characteristics and finite element methods.

BALLISTIC IMPACT RESISTANCE OF MULTI-LAYER TEXTILE FABRICS

J.W.S. Hearle
C.M. Leech
A. Adeyefa
C.R. Cork

University of Manchester Institute of Science and Technology

Department of Textile Technology

Contract No. DAJA37-79-C-0532

Final

Technical Report

October, 1981.

The research reported in this document has been made possible through the support and sponsorship of the U.S. government through its European Research Office, this report is intended only for the internal management use of the grantee and the U.S. government.

GENERAL INTRODUCTION

This report, presented in two parts, describes the investigation carried out in UMIST in the period 1979-1981 into the performance of textile structures under ballistic impact. The investigation follows two complementary routes, namely an exhaustive program of experimentation centred around ballistic impact tests and secondly a detailed survey and development of theoretical and computer models for simulation of the textile and projectile dynamics. The design and evaluation of textile structures for protection against high speed normal impact must hinge upon the many material, surface and structure parameters intrinsic in the structure design. - The projectile, impacting in the range 150 m/s - 550 m/s, and with a nominal mass of 1 gm, encounters the textile structure both at the fibre level and at the weave level. In the first instance, one must consider firstly for the arrest of the projectile, resistance to cutting by the projectile edges, and opening of the weave structures. These are not important considerations in the present configuration, but would obviously be considered for very small projectiles where the projectile diameter is of the order of the weave pitch. A more important consideration is in the indentation of fabric surface, leading to high fibre strains, and when these strains exceed the fibre fracture strain, the structure will fail. The structure is also considered inadequate if the total indentation is sufficiently large as to present a hazard to the sensitive zone behind the fabric, even through the fibre fracture strain is never exceeded. Important to these two criteria are firstly fibre material properties quantified by fracture strain, modulus of elasticity and fibre weight (denier). Then the method of assembly into the textile

material is important, quantified by the warp and weft pitch leading to the area density (textile weight) and crimp parameters, by the fibre friction which impede the relative motions of the fibres in accommodating the impact energy and finally by the assembly of textile layers into a structure considering layer mixes and layer fixing by stitching or by resin bonding. The important projectile impact parameters are projectile mass, and impact velocity or energy.

In the first part of this report, the results of an experimental research programme are presented. The main aspects of this work were investigations of the effects of the addition of finishes designed to alter the degree of yarn to yarn cohesion within a fabric and also the compare the multi-ply response to impact to that of the single layer.

In the second part of this report, various theoretical considerations are examined with the motives of generating procedures for predicting and stimulating textile structure performances. The first considerations examine the mode of propagation to stress signals through the structure, leading to the ideas in fibre matching at the nodes (intersection of warp and wefts) and then describes the variational model applied to triaxial fabrics. This model has previously been developed and applied to regular orthoganal weaves (Journal of Textile Institute Vol 70, No. 111, page 469 et seq, 1972) and is applicable in the very approximate sense to single and then multilayer structures with no slip either between fibres or layers. Then, the method of characteristics is examined, this leading to a computer simulation which is very applicable to single layer structures in which the fibre materials and fibre orientation are significant. The high speed impact results are quite accurate since this model is stress wave based. The next set of models are finite element models, focussing on various details in the structure. The first model, the

membrane model incorporates the crimp effects into the element and is appropriate to single layer structures. The second looks at the detail of the fibres in the node area. The third and fourth programs consider the multilayer structure the former considering the layers bonded by a resin or glue effective only in shear, and the latter the more important of the two, allowing layers to slide relative to each other.

PART I

EXPERIMENTAL

List of Figures

21 Renormalised Plot of Projectile Energy Loss Against the Combined Area Density of the Multilayered Kevlar. Comparison between Kevlar 29 and Kevlar 49.

1.1 Introduction

The aims of the present study were to construct a ballistic range capable of impacting 1 gm steel projectiles onto fabric samples and to also provide apparatus for the measurement of impact velocity and the energy absorbed by penetration. Apparatus was also developed in order to (1) provide multi-flash photographs of fabrics under impact (2) measure the arrival of the stress wave at the fabric boundary. In addition work was undertaken to:

1) establish the effects on the ballistic performance of the addition to fabrics of chemical finishes designed to alter the degree of yarn to yarn cohesion within a fabric;
2) compare the multi-ply response to impact to that of the single layer over a range of impact velocities.

These two factors were known to be of importance because:

1) Laible[1] has found that the addition of high friction finishes significantly improved the ballistic performance of polypropylene fabrics; alternatively Morrison[2] has shown that when Kevlar is used in either a polyester resin or a silicone rubber composite, the ballistic resistance is reduced when compared to the untreated fabric;
2) most theoretical work has only been developed to the level of single layer impact.

In addition to the ballistic performances of the above, two triaxial weave fabrics and a lightweight nylon fabric were compared to a heavyweight biaxial fabric more representative of those normally used for ballistic protection.

1.2 Development of the Ballistic Range

During the previous research programme supported by the Ministry of Defence, SCRDE, facilities were developed to allow transverse ballistic impact onto fabrics. Lead airgun pellets were fired from a cartridge gun at velocities within the range 100 m s^{-1} to 550 m s^{-1}.

The velocities of the projectile, before impact (V_{in}) and after penetration of the fabric (V_{out}), were measured in the following manner. Four pencil leads were aligned along the path of the projectile; two in front of the fabric, and two behind. The pencil leads formed part of a simple resistive circuit with an input to a storage oscilliscope. As each pencil lead in turn was broken by the projectile, the voltage input to the oscilloscope was consequently reduced. From the stored display the time between contact breaks and thus the V_{in} and V_{out} velocities, were obtained.

Photographs of the deformation process after impact but before penetration were obtained by illuminating the event with a single flash of light of 1.2 μ s duration. These experiments were performed in a darkened room with the camera lens open. The time of the flash, in relation to a contact break a short distance before impact, was varied using a simple delay circuit. By varying this delay for each trial, plots of pellet position against time were obtained. This method, however, gave a large scatter of results as both a constant impact velocity for each trial, and identical modes of penetration for each sample, from the same fabric, had to be assumed.

This apparatus was modified for the present research in order to minimise the energy absorption due to projectile deformation. Steel, rather than lead projectiles were required. Cylindrical steel projectiles of diameter 5.5 mm, length 5.5 mm and mass 1.004 ($\pm$ 0.0008)g.

were obtained. The projectiles are located in plastic sabots and fired from a 0.303 inch (.769 mm) rifle barrel. So far, muzzle velocities of between 262 ms^{-1} and 550 ms^{-1} have been achieved. Multiple flash photographs show that before impact the projectiles yaw slightly but do not spin. As there was a danger that the steel projectiles might richochet, the whole apparatus was enclosed in a steel box. Polycarbonate windows were included in the structure to allow the fabric sample to be photographed. The present apparatus is shown in Figure 1.

In order to trigger a series of light flashes to obtain multiple image photographs of the projectile-fabric interaction; a 'Bowen' ten channel delay was acquired.

This unit produces electronic delays, in either parallel or series, down to intervals of 1 μs (± 0.01%). A projectile moving at a velocity of say 550 m s^{-1} moves .55 mm in 1 μs, thus six stages of fabric deformation can, in theory be observed before the pyramidal deformation has reached 3.3 mm. Therefore the delay is more than adequate for the present research.

Previously a single flash of a stroboscope was used as the light source for photography. Although this flash was of a relatively short duration and of reasonable brightness, image quality was impaired due to either; (a) blur caused by projectile movement during the time of the flash, b) a small depth of focus due to the large lens apertures required for the low light level or (c) high graininess due to the fast film which was required. These effects were exaggerated when negatives were greatly enlarged for analysis. In order to improve image quality, three 'Pulse' double flash argon arc light sources have been obtained. The manufacturer quotes a flash duration of 0.3 μs.

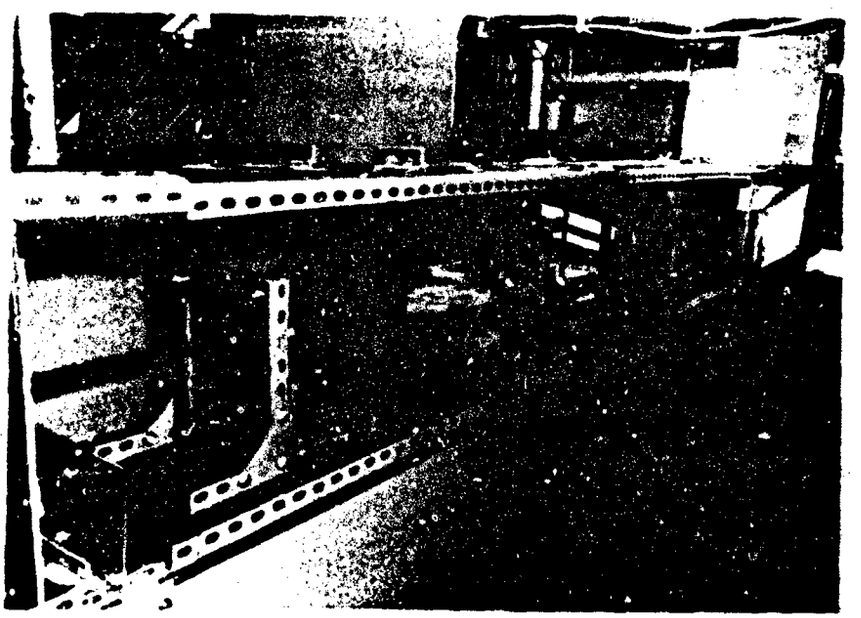

Figure 1

The Cartridge Gun Apparatus

Two still cameras, for exclusive use on the present research programme, were purchased to enable simultaneous 'side on' and 'end on' photographs of the deformation to be obtained.

Previously there was a relatively large error in the measured values of V_{in} and V_{out}. It is particularly important to reduce the errors of these measurements, as the energy loss of the projectile is obtained from the difference of the squares of V_{in} and V_{out}. Previously, time intervals could only be measured to an accuracy of $\pm$ 2%. In order to improve on this two digital timers were purchased. These can each measure time intervals down to 0.1 μs. The separation of the velocity measuring stations are now of the order of 80 cm. Therefore, timing errors now contribute to only 0.07% of the error in velocity measurement for a velocity of 550 m s^{-1}.

The above facilities were used to obtain micrographs of fabric systems under impact.

Figure 2 shows three such single flash photographs of the deformation of a double-layered nylon fabric. The impact velocity is approximately 350 ms^{-1} in each case. A general view of the whole fabric is shown in figure 2A. Lines were drawn on this fabric at 0.5 cm separation, parallel to both the warp and weft directions. From this photograph the pyramidal form of the transverse deformation is clearly seen. A line drawn on the print parallel to one of the grid lines helps to show the in-plane displacement of the fabric towards the point of impact. Figures 2B and 2C show the region of the fabric near the impact zone at approximately 20 μs and 60 μs after impact. In figure 2B the projectile, which is moving in a direction from bottom to top of the photograph, has not yet penetrated the fabric while in 2C the whole of the cylindrical projectile is visible.

FIG. 2

A Fabric Undergoing Ballistic Impact.

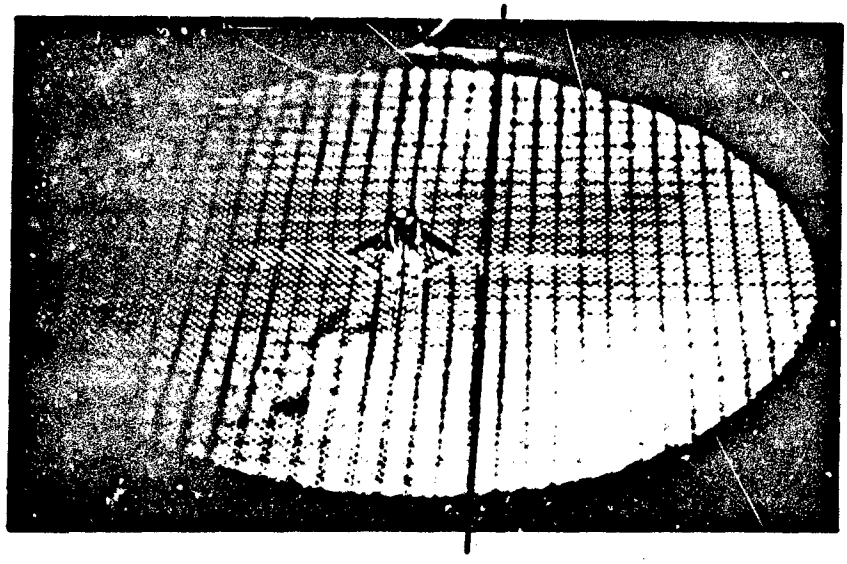

A

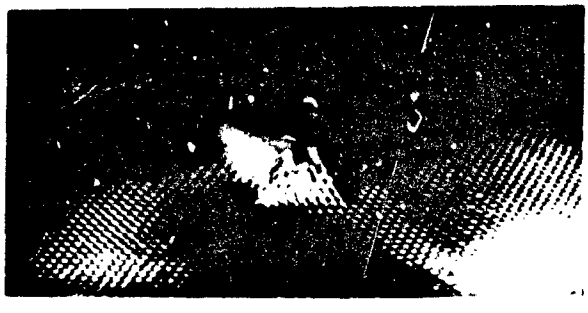

B

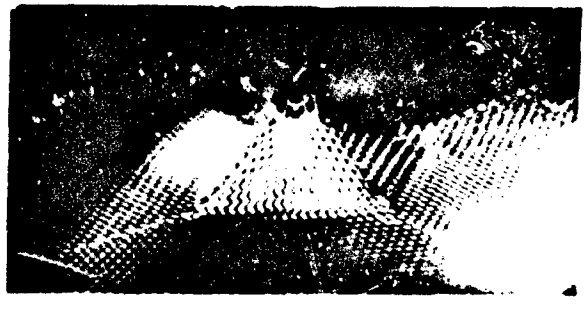

C

FIG. 3

Double Layer Fabric Undergoing Ballistic Impact.

FIG. 4

Projectile in Flight.

A

B

C

Fig. 5
Side View of Fabric Under Impact

(figures 5B and 5C) as much original detail is lost during reproduction. In figure 5A the time between flashes is 10 μs while in figure 5B this interval is 20 μs. Figure 5A shows the fabric at times before penetration. In figure 5B, however, one image shows the fabric before and two images show the fabric after penetration. The multiple flash technique has been used by previous researchers in the same field. However much previous work using multiple flash methods has been at low impact velocities in order to be able to observe large deformations before penetration. In figure 5A, the pyramid height is only 0.8 cm at the time of failure. (Approximately 50 μs after impact).

Strain Measurement

It would be of enormous theoretical interest to be able to measure the spacial and temporal distribution of strain during impact. The measurement of the level and distribution of stress and strain throughout a fabric during impact, does however, present serious experimental problems, as the measuring instruments could easily themselves influence the strain distribution. A partial solution is to restrict measurements to the fabric boundary. For this purpose a commercial pressure transducer has been mounted in such a manner as to enable tensile forces to be measured. One yarn from the fabric was clamped to the transducer. The sample holder was then adjusted in order to ensure that the yarns intersected the impact zone.

The force transducer alone has a resonant frequency of 200 kHz. The output is therefore filtered by a 180 kHz low pass filter. Stress wave reflections at the boundary would be expected to give rise to frequencies (f) in the region of

$$f = \frac{v}{dx2}$$

where v = sonic velocity

d = distance from impact zone to fabric edge.

This is only an approximation, as no consideration was made of crimp.

For Kevlar

$$f \quad \frac{4 \times 10^3}{0.075 \times 2} = 26.6 \text{ kHz}$$

Thus the apparatus was adequate for the present research.

The output from the transducer was fed into a transient recorded via a change amplifier. The resulting data was displayed and then stored on floppy disc.

To allow the force measurements to be synchronised with micrographs of the fabric during impact, the output from a photodiode was displayed on one channel of the transient recorder. A typical trace is shown in figure 6. One yarn from the last layer of a multilayered sample was attached to the force transducer. The uppermost trace is the output from the force transducer. Below, the photodiode output is shown. The large decay time of the photodiode output does not reflect the light flash duration, but is merely attributable to the electrical system. The peak output occurs as the projectile is arrested.

Figure 7 shows the synchronised output from another trial. Here, although the cone deformation has already occurred and the photograph shows the fabric at a time of at least 20 μs after impact, no signal is recorded by the transducer until 22 μs later. It can be seen from the micrograph that the fabric is not completely flat in the region near the transducer. It seems that this has resulted in a delay of the stress wave.

FIG. 6

Fabric Undergoing Ballistic Impact together with Synchronised Force Measurement.

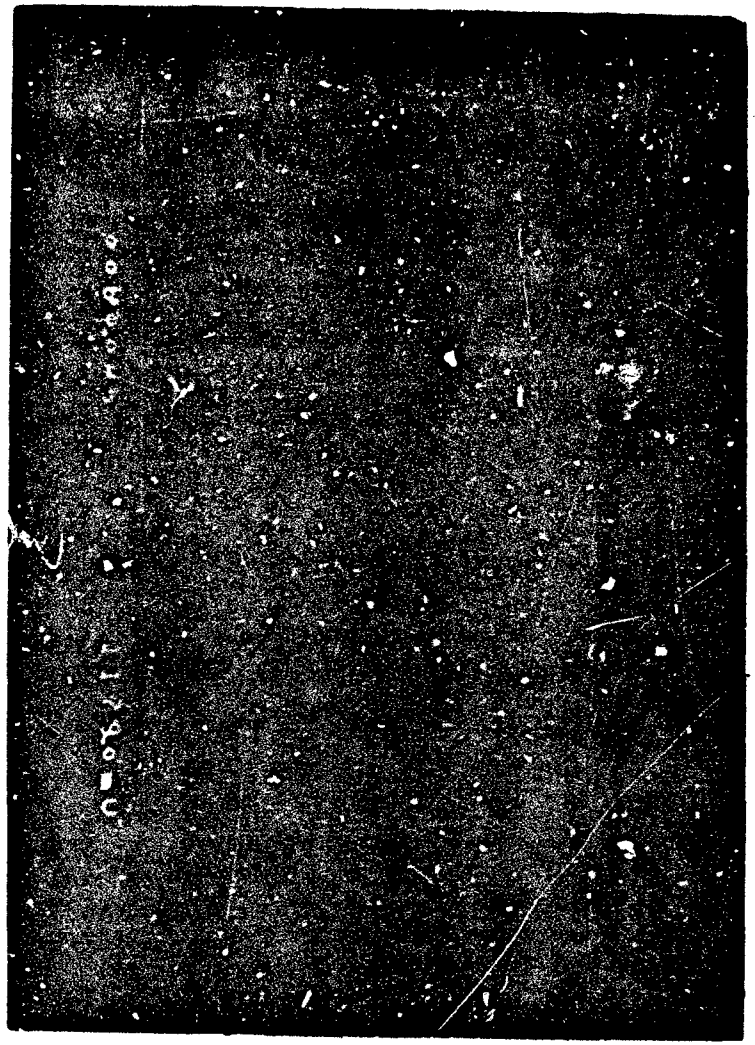

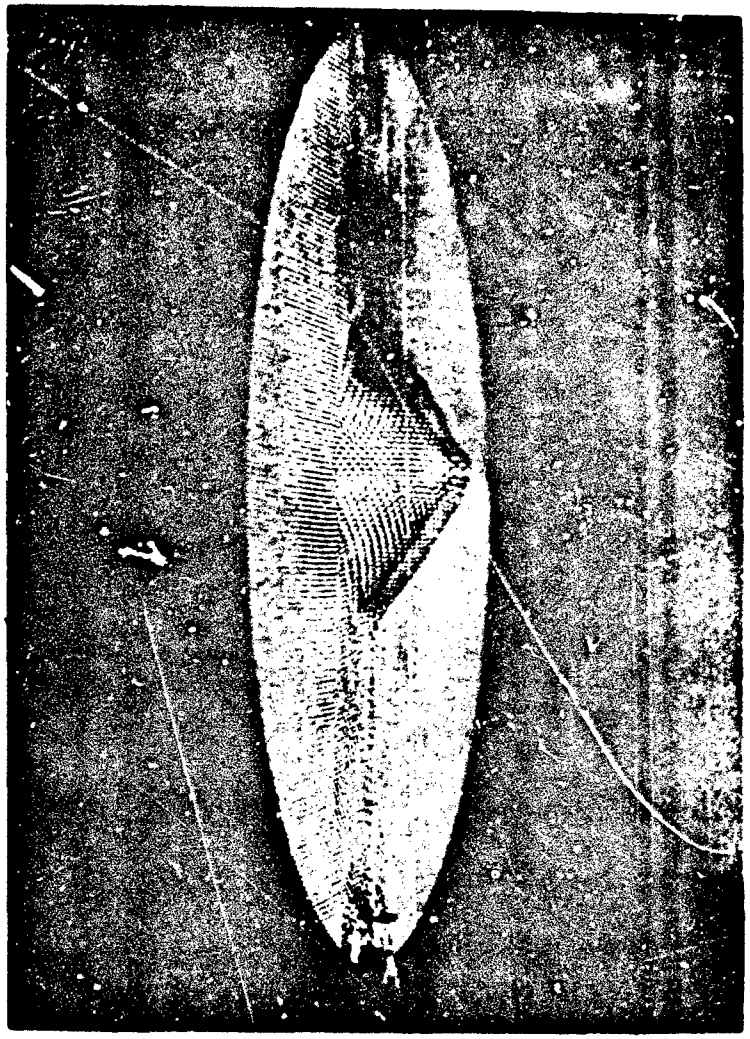

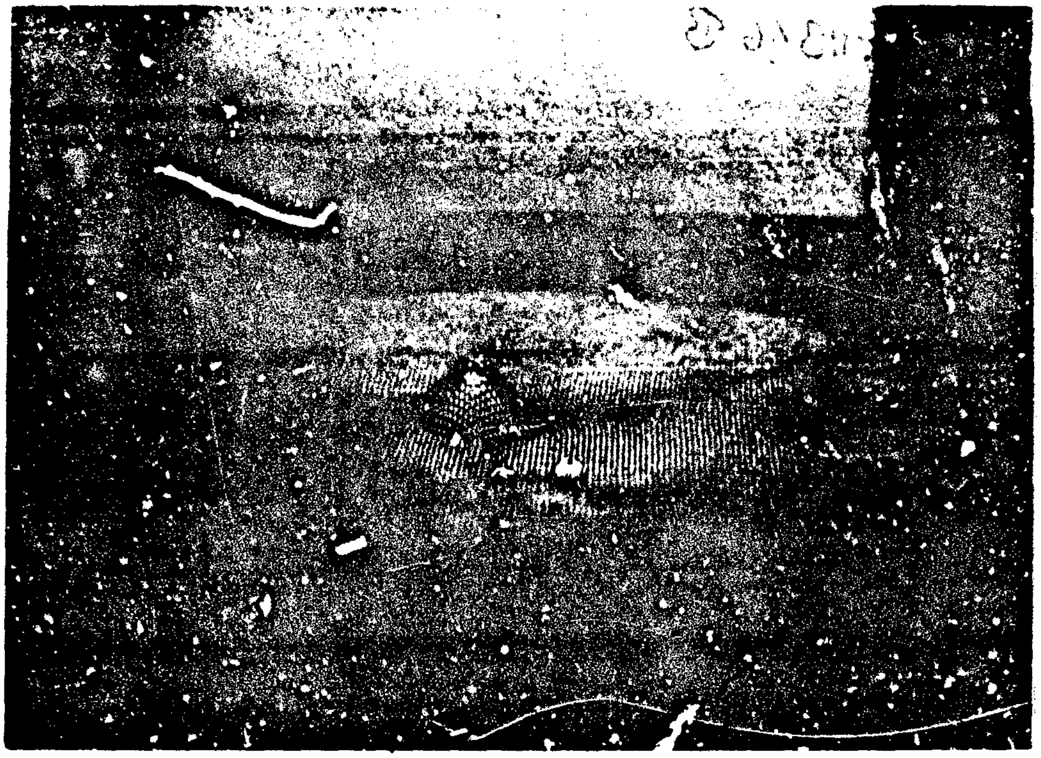

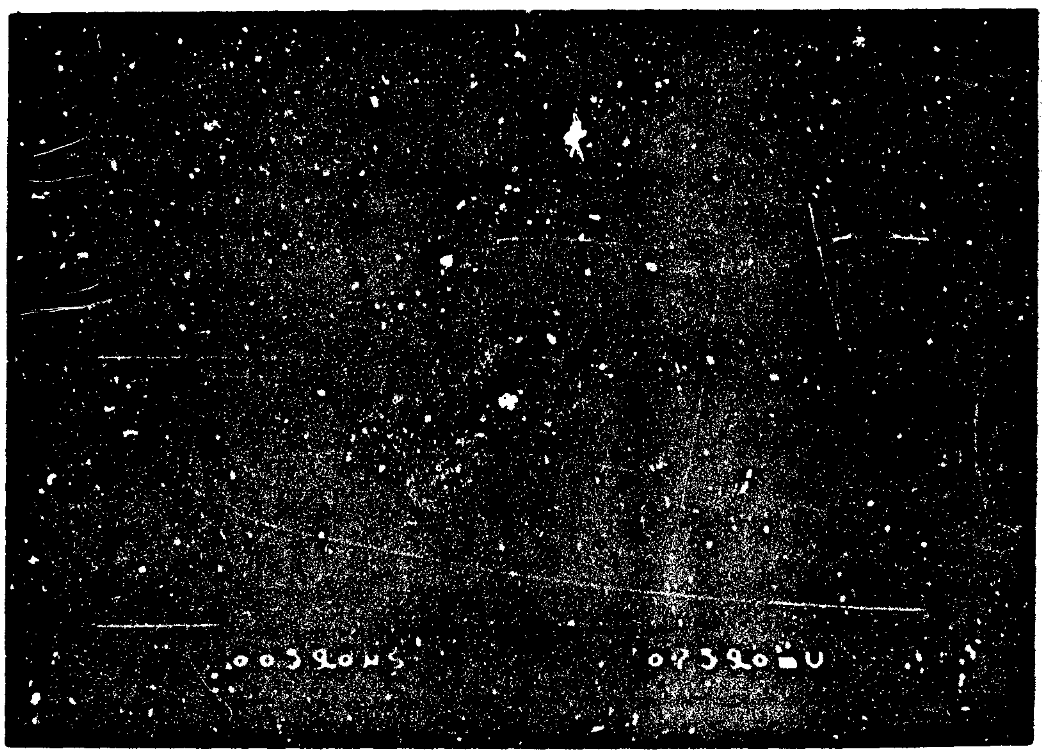

Only preliminary work has so far been undertaken using the multiple flash and the boundary transducer but results will be obtained on the deceleration of the projectile and the resulting force at the boundary in the following research programme.

1.3 The Ballistic Performance of a Lightweight Fabric

During the course of the current project the author was asked to compare a lightweight and a heavyweight nylon fabric on the ballistic range as a part of preliminary work for a proposed project. Details of the two fabrics are shown in Table 1. Figucia[4] reports that the ballistic performance of a multilayered fabric of given weight increases as the area density of the individual layers is reduced.

Fabric Area Density gm^{-2}	Yarns per cm.		Tex of yarns		Mean breaking load (Kgf)		Mean % extension	
	Warp	Weft	Warp	Weft	Warp	Weft	Warp	Weft
42.8	38.7	39.7	5.40	5.19	0.137	0.132	17.0	16.1
378.0	9.75	9.75	197.1	193.6	13.3	13.6	23.8	23.6

Table 1

The fabrics were tested on the ballistic range. The results are presented as a plot of the energy loss against the combined area density of the multilayered samples, (fig. 8). It is clear that weight for weight, less energy is absorbed by the lightweight fabric. It is of interest to compare the V_{50} energies. The data from tests on 28 layers (= 1198 gm^{-2}) of the lightweight fabric are shown as a plot of absorbed energy against impact velocity (fig. 8b). The V_{50} energy was found to be 27.3 J. From the V_{50} energy curve of the heavyweight fabric, the

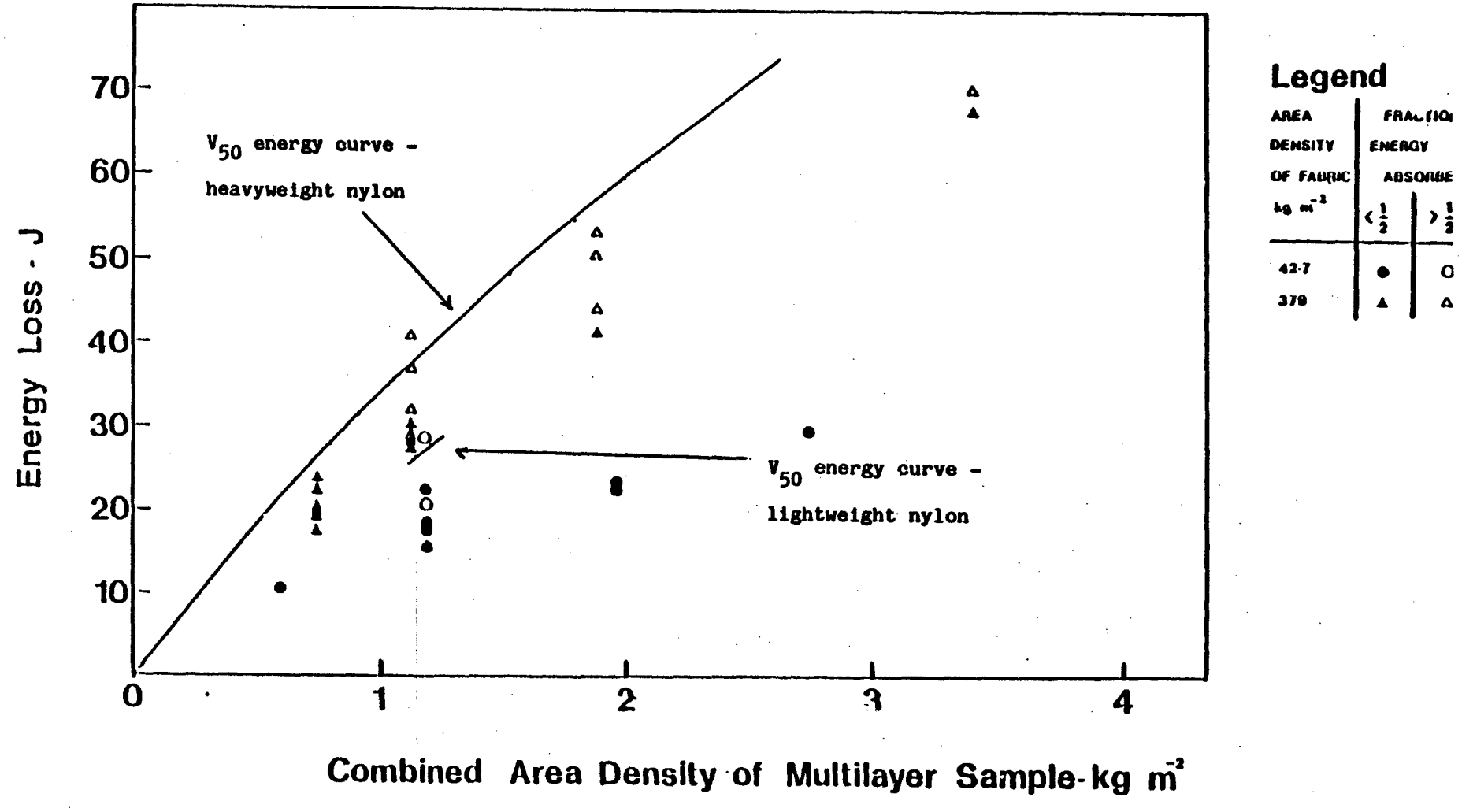
Energy Loss - J
70
60
50
40
30
20
10
0
1
2
3
4
V_{50} energy curve - heavyweight nylon
V_{50} energy curve - lightweight nylon
Combined Area Density of Multilayer Sample - kg m^{-2}
Legend
AREA DENSITY OF FABRIC kg m^{-2}
FRACTION ENERGY ABSORBED
$< \frac{1}{2}$
$> \frac{1}{2}$
42·7
379

FIG. 8 Energy

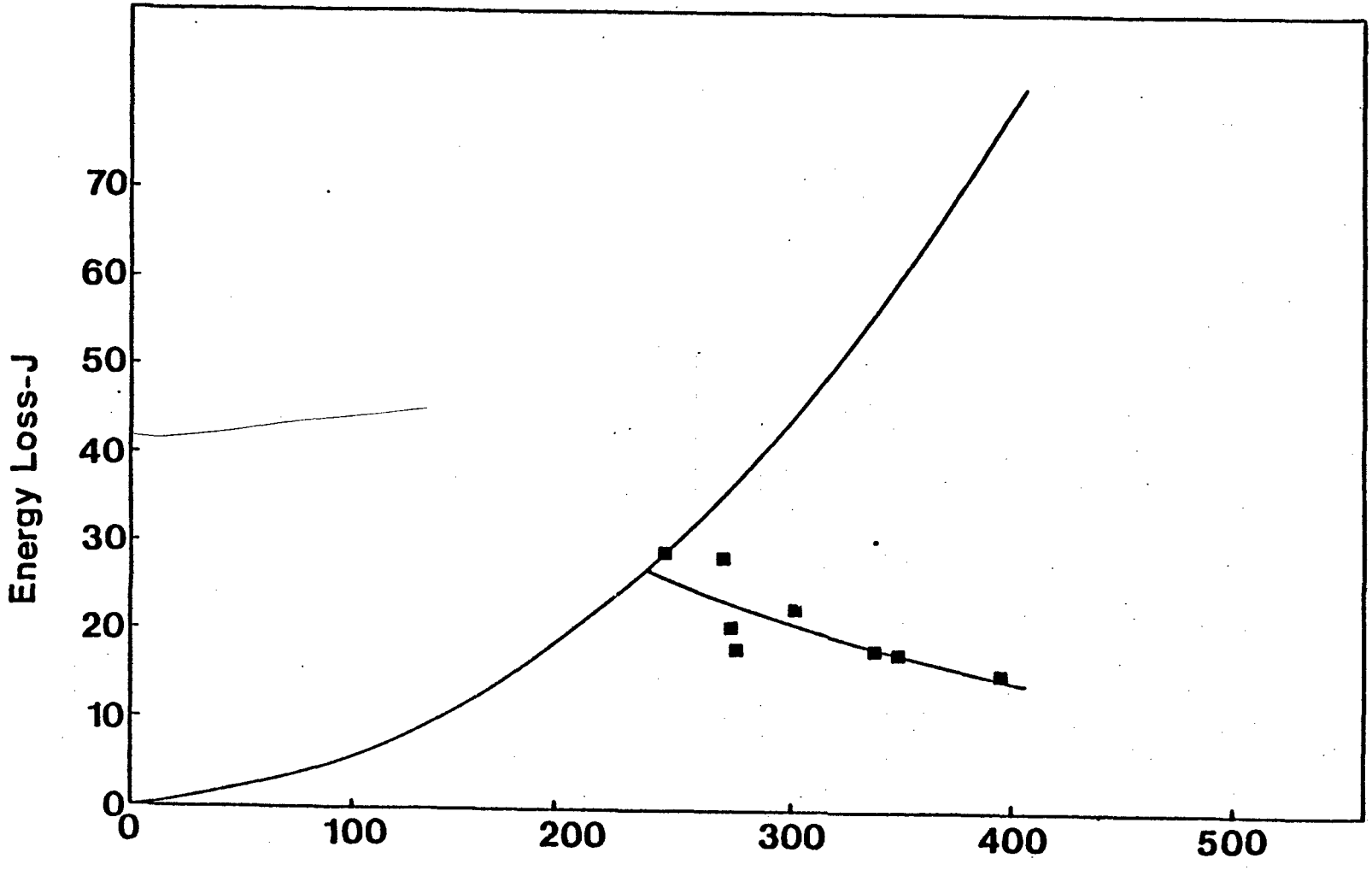

Fig. 8b Plot of Energy Absorbed against Impact Velocity

V_{50} energy at 1198 gm^{-2} was calculated to be 40.3 J. This difference could be a reflection of the differences in the quasi-static work of rupture of the constituent yarns. Assuming that the tensile strain energy is the only mode of energy absorption and that only yarns which make contact with the projectile are strained then the expected projectile energy loss per unit area density was calculated to be -

heavy duty nylon = 5.29 J per Kg/m^2

lightweight nylon = 3.39 J per Kg/m^2

(Typical quasi-static stress strain curves are shown in figure 9). These results are only one sixth of the V_{50} energies found by experiment, however, the ratios of the experimental and calculated energies are similar:

Ratio of specific work of rupture of principal yarns - $\frac{5.29}{27.3}$ = 1.56

Ratio of V_{50} energies - $\frac{40.3}{27.3}$ = 1.48

However, the ballistic performance of the two nylon fabrics might have been expected to be more similar as the work of rupture is not the only mode of energy absorption. For example, the transverse kinetic energy of the fabric accounts for some of the energy absorbed from the projectile.

One possible cause of the inferior ballistic performance of the lightweight fabric is a difference in the mode of penetration. Many photgraphs of the projectile in flight after penetration revealed a small object travelling ahead of the projectile. This was identified as a fused plug of nylon. It is known[5,6] that fibre melting is a factor in the failure mechanism but no plugging has been observed before. The nylon plug travels ahead of the impact projectile but was slowed due to air friction. It must be concluded that the plug was ejected before the final disengagement of the projectile from the fabric. The exact mechanism is however unknown.

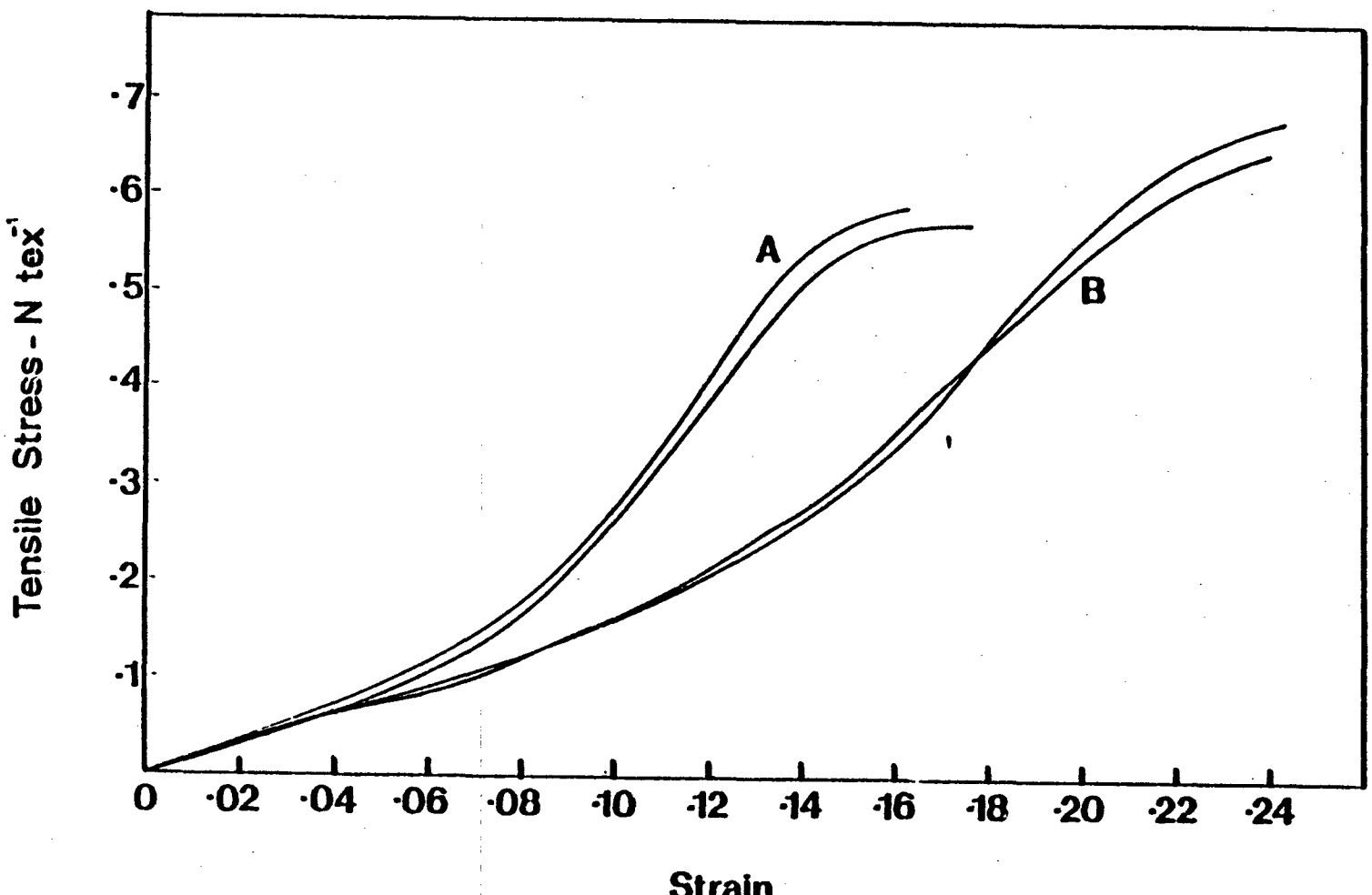

FIG. 9 Typical quais-static stress strain curves for yarns extracted from (A) a heavyweight and (B) a lightweight fabric.

1.4 The Ballistic Performance of Two Triaxial Fabrics

In normal (biaxial) fabrics two sets of parallel threads intersect at 90°. In triaxial fabrics, three sets of parallel threads intersect at 60° intervals. There are reasons for believing that the ballistic performances of otherwise identical fabrics would be different for biaxial and triaxial fabrics, although as yet the superiority of either cannot be confidently demonstrated due to lack of knowledge of the importance of various effects of weave. For example a triaxial weave might confer added ballistic performance due to the spreading of load more evenly around the impact zone or alternatively might confer a reduced ballistic performance due to the inherent openness of the triaxial weave.

Two triaxial fabrics (A and B) were therefore compared on the ballistic range. First consider fabric A which became available early on in the research program. As the ballistic rig was only partially operational at the time, and the fabric quantity was limited the triaxial fabric was compared to a biaxial fabric using a simple ad hoc procedure. The fabric parameters are shown in Table 2. The ballistic performance of each fabric was assessed by finding the number of layers required to stop the projectile at a known velocity.

The results are shown in Table 3. It is clear that the total area density of the biaxial fabric (2400 gm^{-2}), which is required to stop the projectile, is much less than that required in the case of the triaxial fabric (3094 ms^{-1}).

	Area density (gm^{-2})	Yarns per cm		Tex of yarns		Breaking load of yarn (Newtons)		Breaking Extension (%)	
		WARP	WEFT	WARP	WEFT	WARP	WEFT	WARP	WEFT
iaxial ylon	240	11.4	12.3	103	101	67.1	68.5	24.9	25.5

	Area density (gm^{-2})	Yarns per cm			Tex of yarns			Breaking load of yarn (Newtons)			Breaking Extension (%)		
		A	B	C	A	B	C	A	B	C	A	B	C
riaxial ylon	221	3.8	3.9	3.7	200	205	201	109	128	130	20.8	22.2	23.2

Table 2

Although the fabrics had similar area densities, it cannot be concluded that the difference in construction was the sole reason for the difference in ballistic resistance, as the triaxial was of a very open structure. A triaxial fabric of a much closer weave was therefore tested ballistically.

Fabric	No. of layers	Area Density of sample (gm^{-2})	Impact velocity (ms^{-1})	Was sample penetrated
Biaxial nylon	8	1920	392	Yes
	9	2160	405	Yes
	10	2400	407	No
	11	2640	399	No
Triaxial nylon	11	2431	376	Yes
	13	2783	378	Yes
	14	3094	387	No
	15	3315	385	No

Table 3

The area density of three layered sample was 1281 gm^{-2}. The V_{50} energy was found to be 38.3 J. The equivalent V_{50} limit of the heavy duty nylon described earlier can be found from the plot of V_{50} energy against area density (figure 8). By this method the V_{50} limit for the biaxial nylon of combined area density 1281 gm^{-2} is 42.5 J.

The V_{50} energy of the triaxial fabric was thus marginally lower than the biaxial fabric, but this is not statistically significant. It is concluded that the performance of the biaxial and triaxial fabrics were similar.

In part II of this report it is demonstrated that a computer model of the impact onto triaxial structures predicts that the triaxial weave is ballistically inferior to the biaxial weave. Conversely it might be expected that the triaxial fabric might be more efficient by considering differences in the transverse wave front.

Adeyefa predicts that for triaxial weaves, the transverse wave front would be hexagonal. A photograph of the reverse side of the triaxial fabric during impact is shown in figure 10. The wave front is confirmed to be hexagonal. Figure 10b shows a biaxial nylon and a biaxial Kevlar by way of comparison. In these cases the transverse wave front is rhomboidal.

By geometrical considerations it is found that the area bounded by the transverse wave front is greater for the triaxial wave over the biaxial weave by 1 : 1.3. It is expected that the kinetic energy of the transversely moving region of the fabric would be greater for triaxial than biaxial weaves. This effect would make the triaxial weave a better absorbant of projectile energy.

FIG. 10

Triaxial Fabric Undergoing Ballistic Impact.

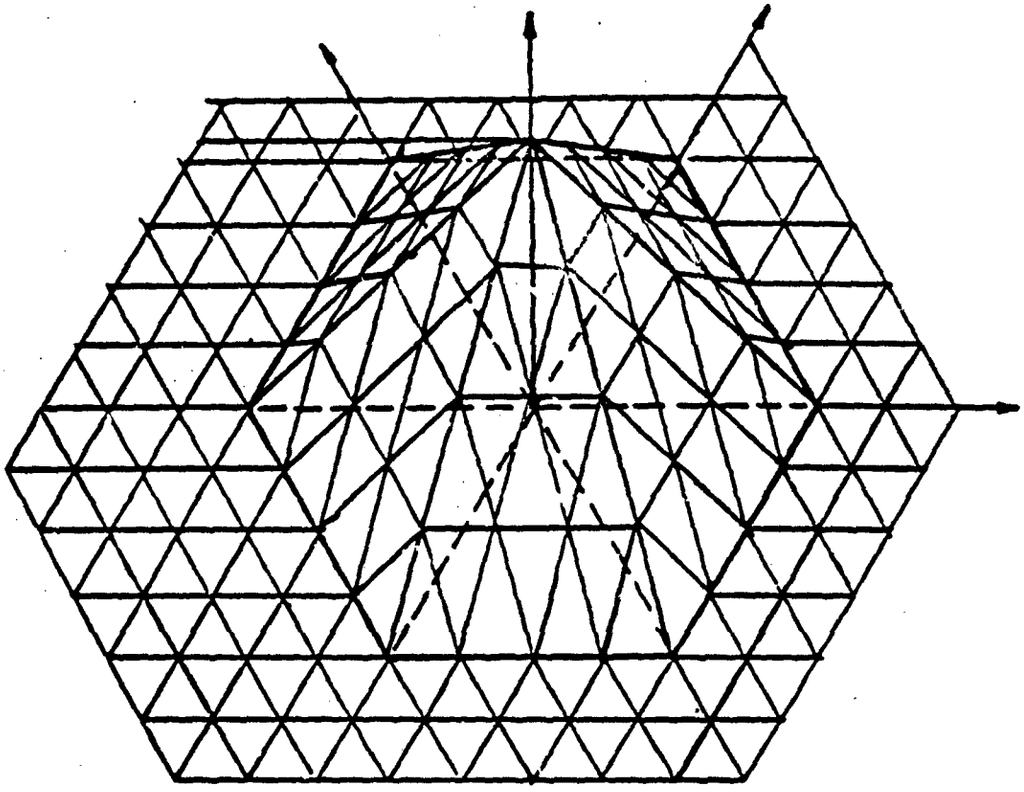

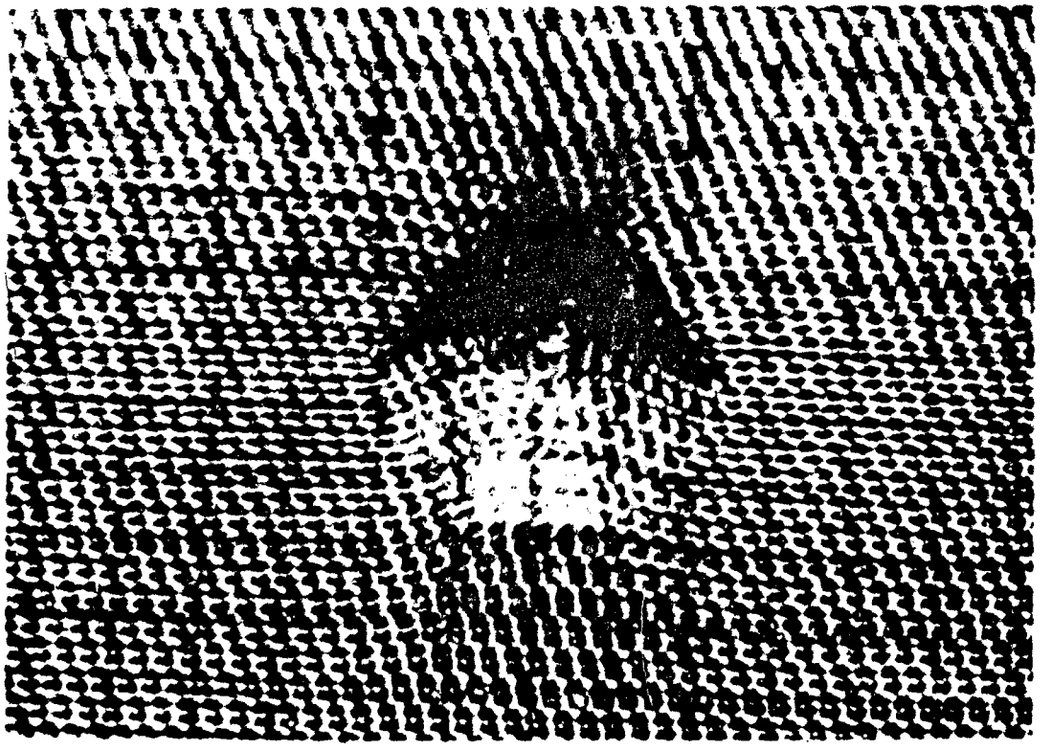

FIG. 10b

A Biaxial nylon (top) and a Biaxial Kevlar (bottom) under ballistic impact.

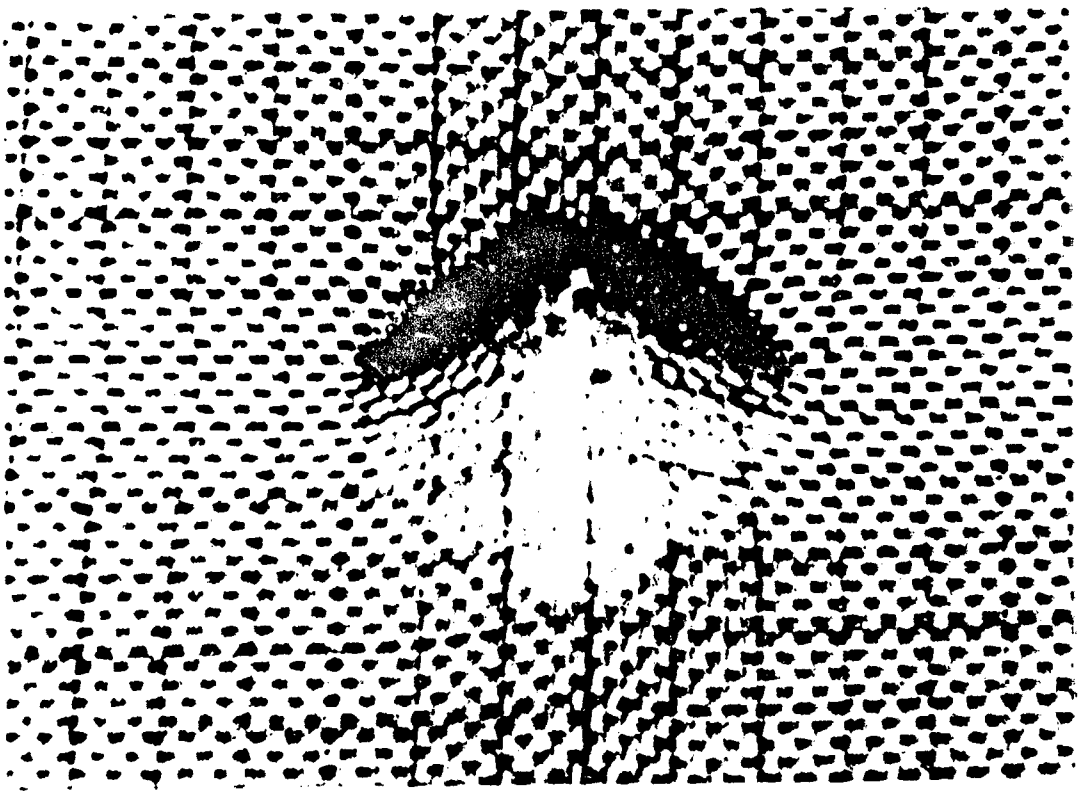

A

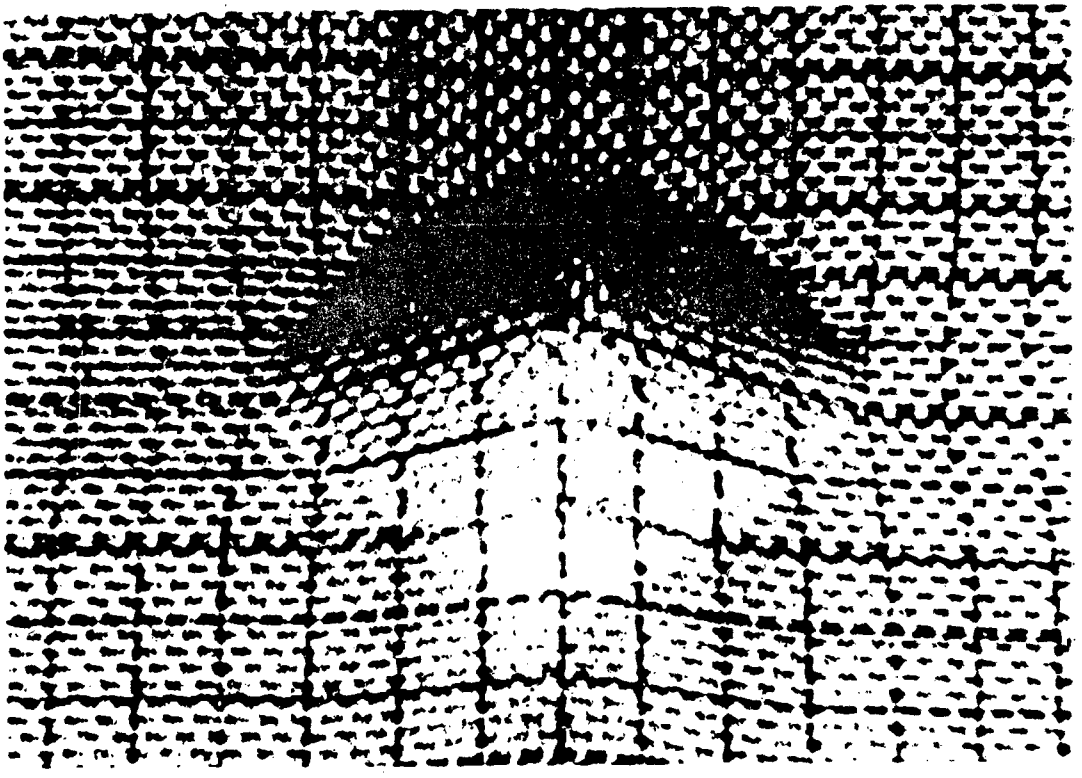

B

1.5 Main Research Programme

Experimental Procedure

For the purposes of the present research two methods of quantifying the ballistic performance of textile materials have been adopted.

First, the variation of energy loss against impact velocity is established, and from this the V_{50} limit is obtained. The variation of impact velocity provides an independent input parameter for models. The experimental and theoretical results can then be compared. This method also provides a means of comparing the ballistic properties of different fabrics. The V_{50} limit can be found for samples composed of different number of layers. The variation of the V_{50} limit with the combined area density of the multilayered sample enables the ballistic performance to be quantified. This method has the advantage that the V_{50} limit is a widely accepted way of assessing ballistic resistance. A great disadvantage is the large number of tests required to establish the V_{50} limit even for a single layered sample. Difficulties also arise due to the large scatter of results at velocities near the V_{50} limit.

The second technique is to impact a series of multilayered samples at one impact velocity (approx. 500 m s^{-1}). In this procedure fabric performance is established by the variation of energy absorbed with the combined area density of the multilayer sample. Figucia (ref. 4) reports that, for Kevlar, this relation is linear. Figucia also reports that the projectile energy loss was found to be independent of impact velocity in the range tested. Figucia only considers results where less than 50-60% of the available energy is absorbed. The author's technique was to include all results for velocities where penetration occurred, for it has been found that although the absolute

value of the experimental scatter was high, the fractional variation in absorbed energy was acceptable. The second method has proved very successful in quantifying fabric differences.

Fabric Finishes

Many computer models have been developed to predict behaviour of woven textiles when subjected to impact by a free flying projectile. A common approach is to treat the woven fabric as a pin jointed net. However, previous research by the author has produced evidence that longitudinal movements of the principal yarns can occur relative to the crossing yarns. The evidence originates from observations of residual displacements, and residual damage of the principal yarns (ref.6). It is expected that changing the ability of yarns to pass freely over each other might change the energy absorbing characteristics of the fabric. Three possible effects are postulated. First, an increase in crossover stability will cause an increase in the reflected part of the longitudinal wave at each crossover. This leads to increased strain at the impact zone, and early failure. Second, an increase in crossover stability increases the energy transfer to parallel yarns. Third, a decrease in crossover stability would increase the ability of yarns to move laterally at the impact zone and allow the projectile to pass without yarn failure.

Morrison[2] has shown that the addition of a rubber matrix to a Kevlar fabric seriously reduces the ballistic performance. Morrison concludes that for the materials tested, the second effect i.e. the increase of nodal reflections must be predominant.

Alternatively, it is known that wet samples of Kevlar are seriously weaker than dry samples (ref 7). One possible explanation is that water has seriously reduced the yarn to yarn friction. Alterations to the stress-strain behaviour of wetted Kevlar were not found to be large enough to explain this.

Laible[1] has shown experimentally that the ballistic performance of polypropylene fabrics is improved by the addition of high friction finishes.

Lateral yarn movements have been observed by the author (ref 6). In some cases single layer fabrics were penetrated without any yarns being broken.

The above observations indicate that there is an optimum yarn to yarn cohesion.

In order to investigate whether yarn to yarn friction affected the ballistic properties of fabrics and in order to observe whether any such effects are dependent on impact velocity, multilayer fabrics of nylon and Kevlar were tested on the ballistic range. The fabrics had previously been treated with chemical treatments designed to either decrease or increase the degree of yarn to yarn friction at crossovers within the fabric. Ideally it would have been desirable to find a treatment which would have reduced the friction in Kevlar fabrics, but none was found. Even a finish (Siligen E) which is designed to reduce friction was found to increase the level of friction for Kevlar. The results are shown in figures 11 to 16 as plots of the energy loss of the projectile against the impact velocity. The scatter of data is a consequence of real differences in absorbed energy for each trial. As no measurements of rebound velocity were measured, the energy loss is strictly the loss of kinetic energy of forward momentum. Thus, for tests where the fabric was not penetrated, the data points lie on the curve of formula

$$E = \tfrac{1}{2}mV^2$$

where m is the mass of the projectile. For cases where the fabric was penetrated the curve was fitted statistically to fit the exponential curve

$$E = ae^{bv}.$$

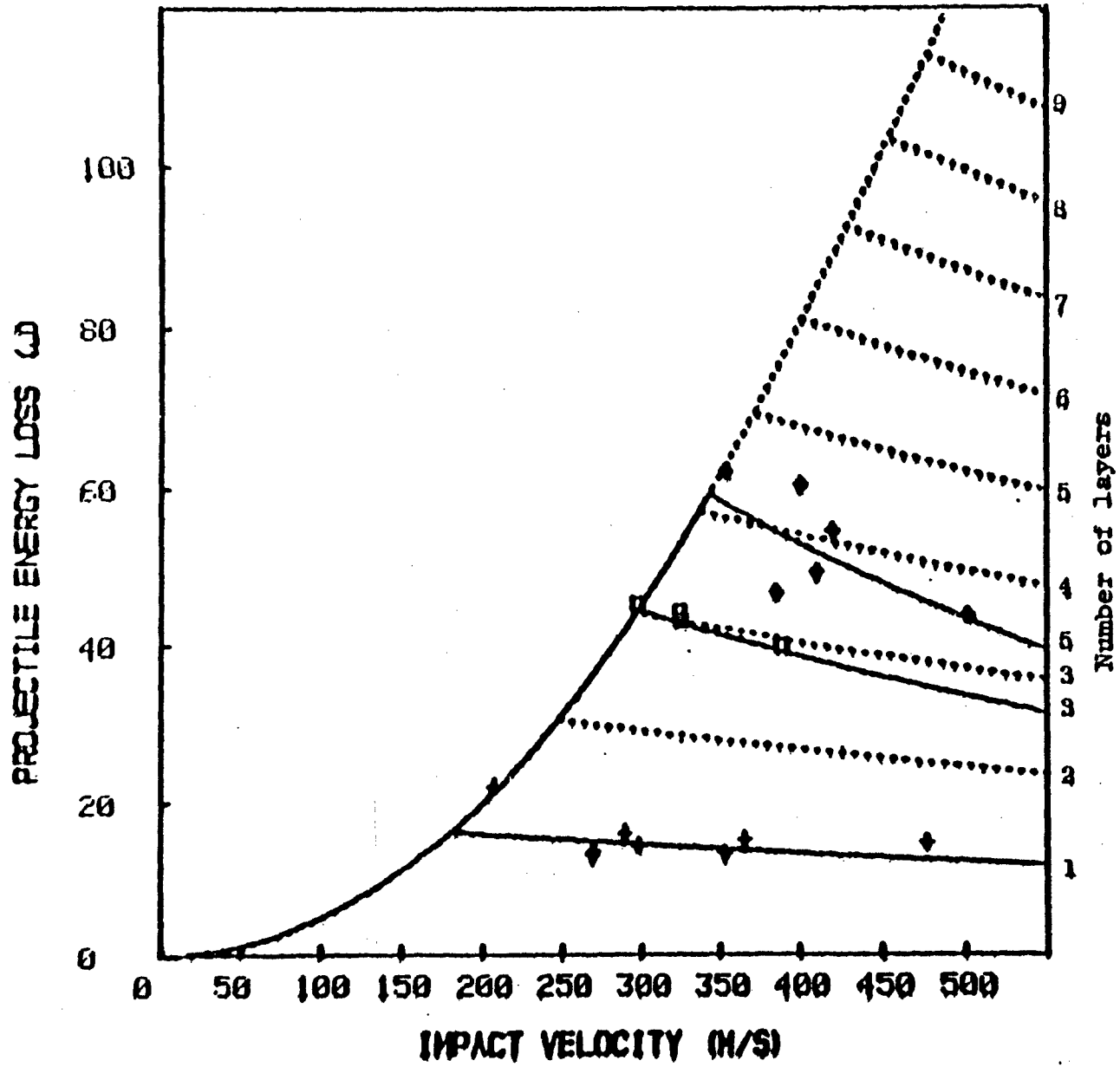

Projectile energy loss against impact velocity for a nylon fabric treated with a high friction finish.

FIG. 11

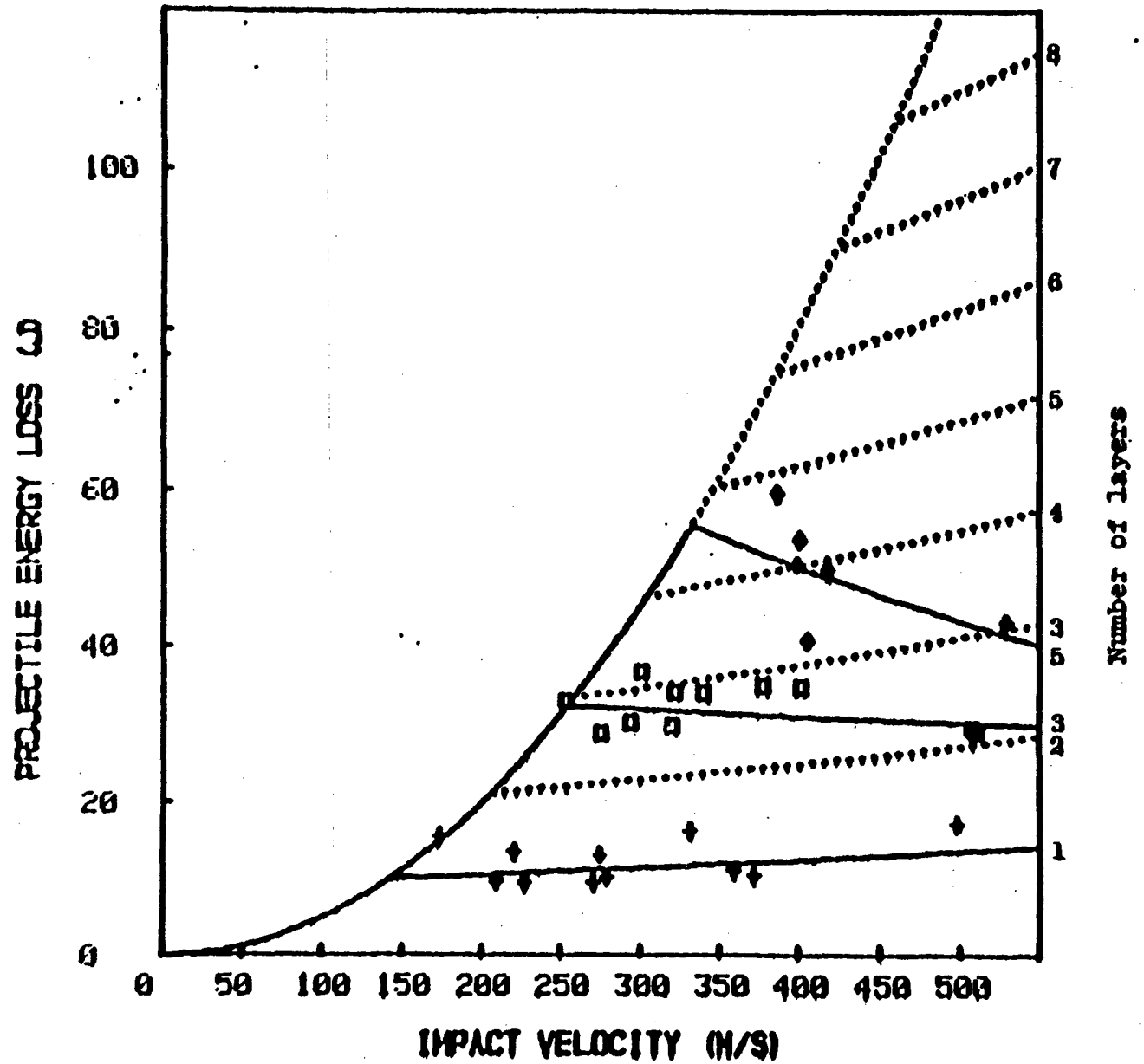

Legend

Full curves - f
to experimental

Broken curves -
layer response
polated from si
layer data.

Projectile energy loss against impact velocity for a nylon fabric treated with a low friction finish.

FIG. 12

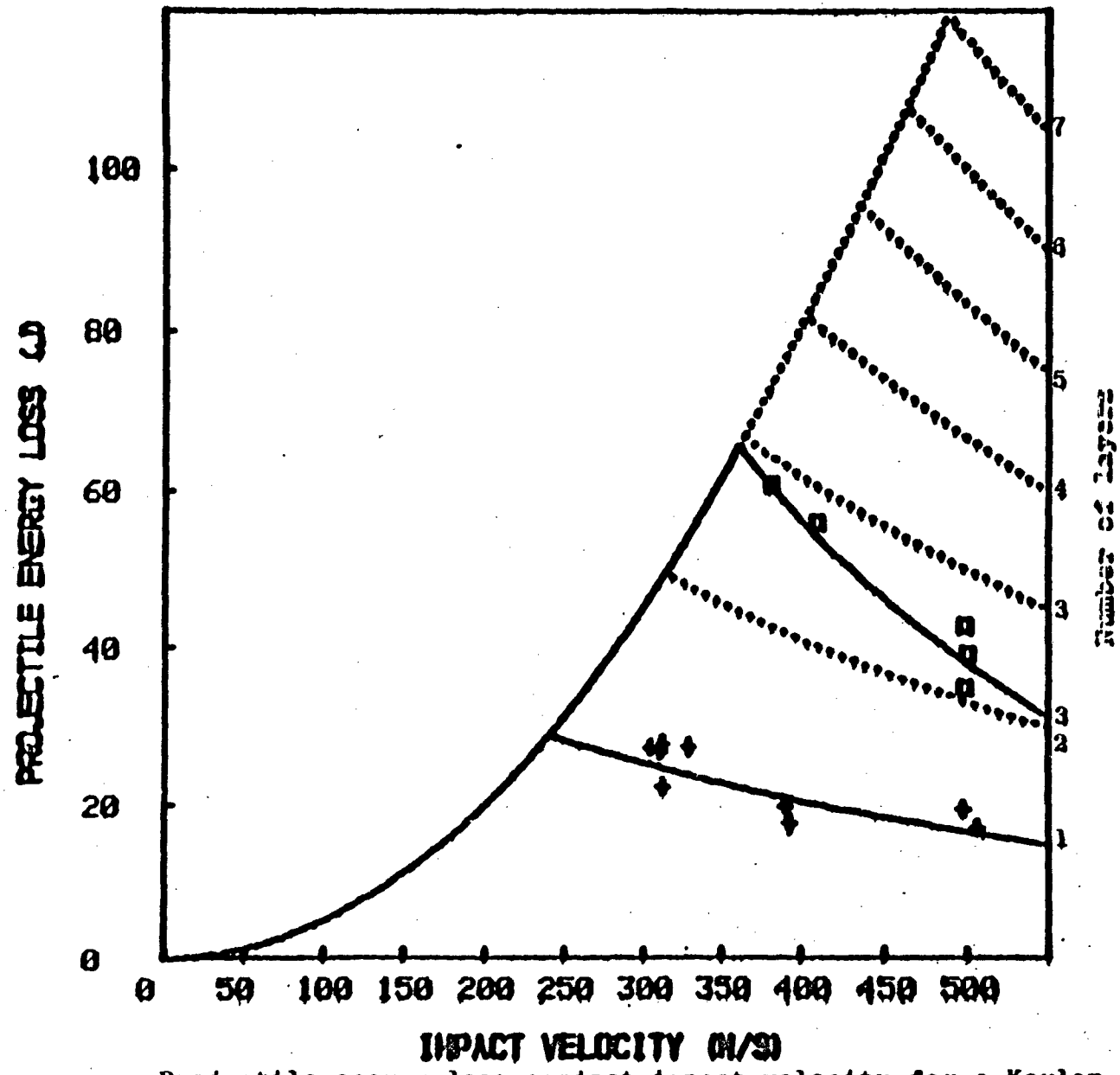

Legend

Full curves - fits to experimental data.

Broken curves - multil response extrapolated single layer data.

Projectile energy loss against impact velocity for a Kevlar fabric (As received).

FIG. 13

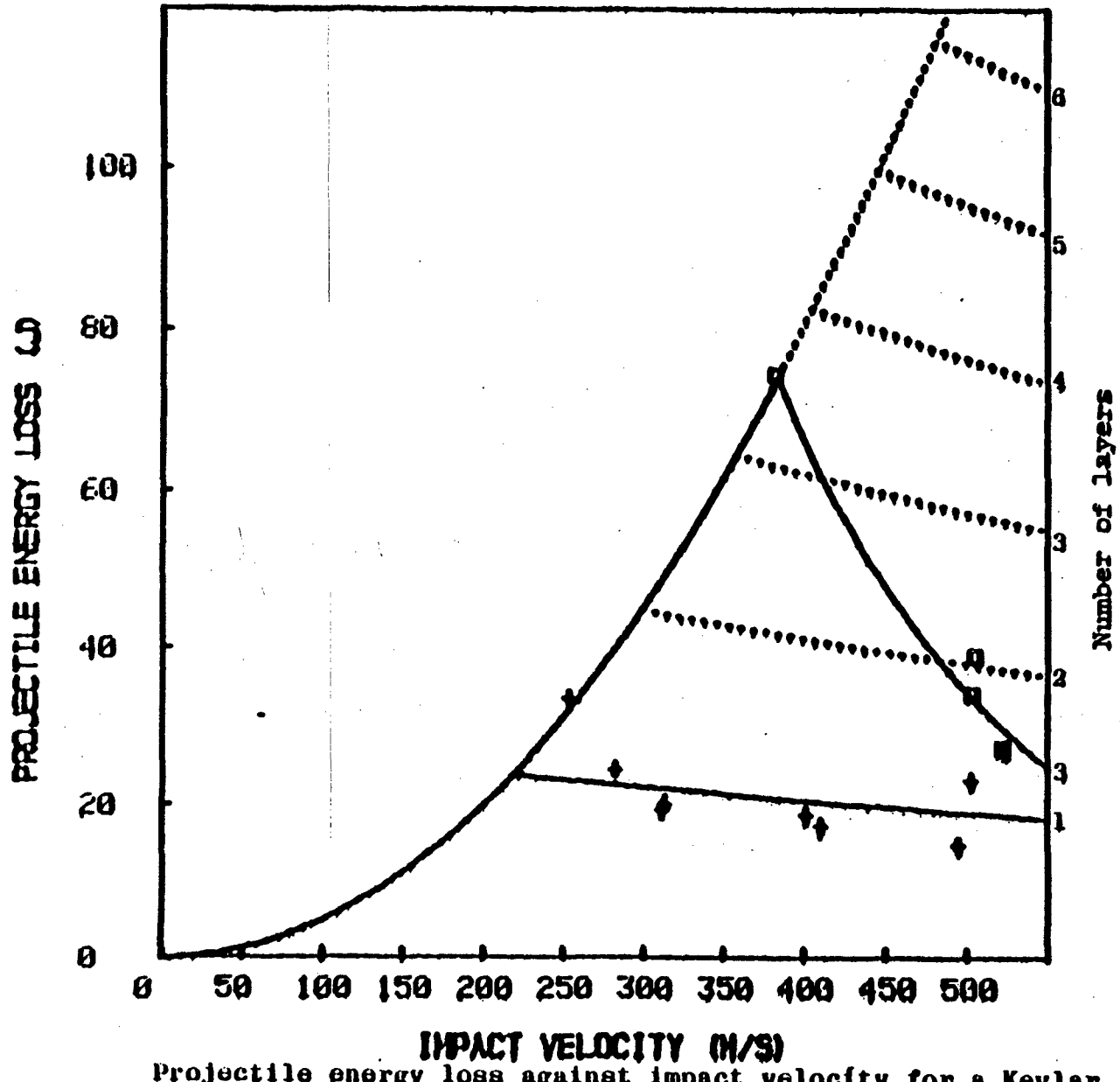

Legend

Full curves - fits t
experimental data.

Broken curves - mult
response extrapolate
single layer data.

Projectile energy loss against impact velocity for a Kevlar fabric after subjection to washing and heating to 110°C

FIG. 14

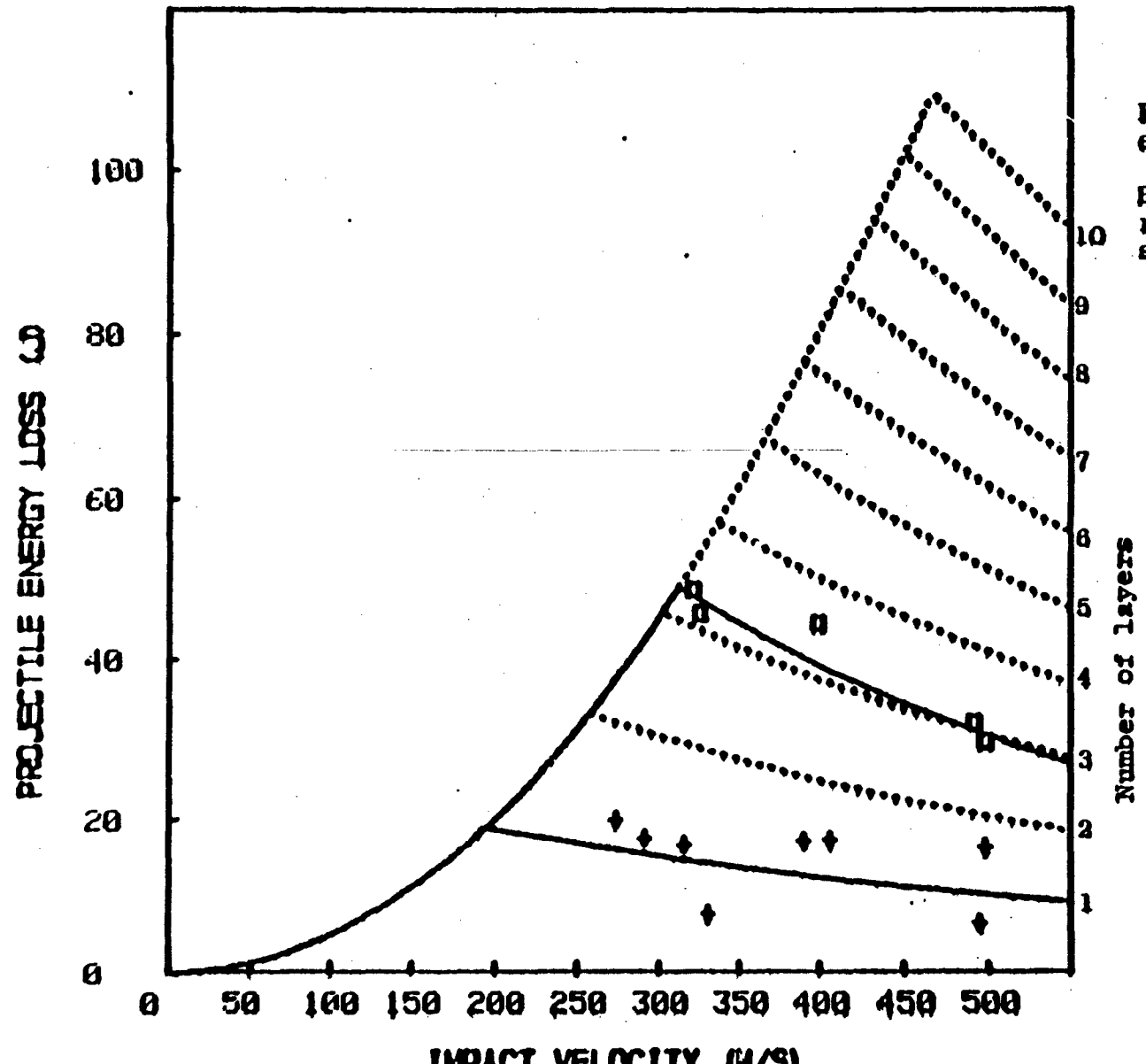

Legend

Full curves - fits to experimental data.

Broken curves - multila response extrapolated f single layer data.

Projectile energy loss against impact velocity for a Kevlar fabric treated with Silicon E.

FIG. 15

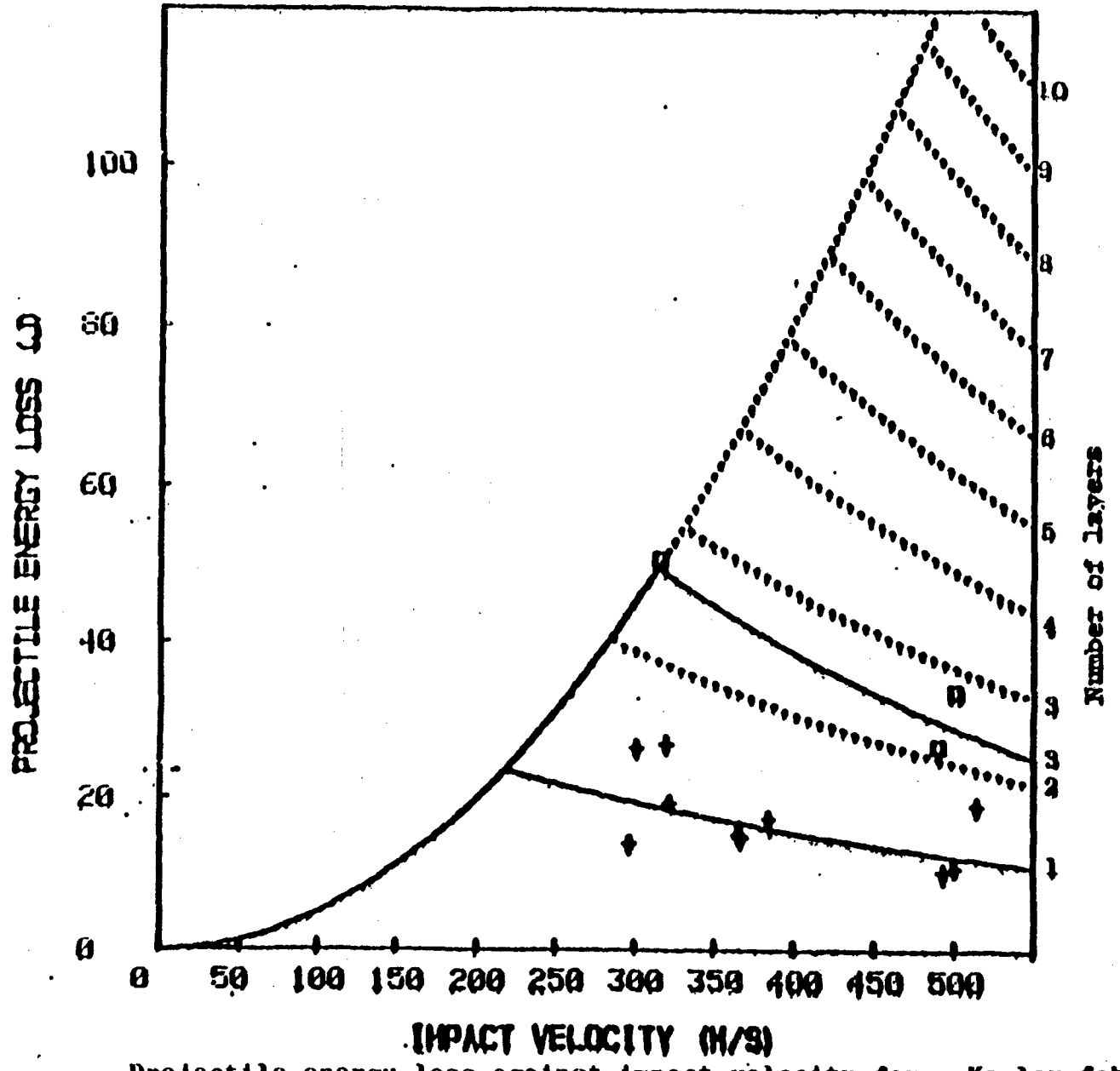

Legend

Full curves - fits experimental data

Broken curves - multilayer response extrapolated from a layer data.

Projectile energy loss against impact velocity for a Kevlar fabric treated with a high friction finish.

FIG. 16

The choice of this form of curve is somewhat arbitrary, however the aim was to be able to apply a systematic routine to evaluate differences between the two fabric finishes. When the constants a and b have been evaluated, the V_{50} limit is predicted by solving

$$ae^{bv} - \tfrac{1}{2}mv^2 = 0.$$

The V_{50} energy can then be calculated. The relative performance of these fabrics can be found from the plot of the V_{50} energy against the combined area density of the multilayered fabric. The ballistic performance for these tests were qualified by then calculating the V_{50} energy loss at an area density of 1000 gm^{-2}. This value was chosen arbitrarily, but is well in the range of the area densities tested in the current research. The results are shown in table 4. The following conclusions can be drawn:

1) the high friction finish conferred an improved ballistic performance on the nylon fabric compared to the addition of a low friction finish;

2) both the high friction treatments produced a large reduction in ballistic performance of the Kevlar fabric;

3) the water treatment improved the ballistic performance over the 'as received' fabric possibly because residual finishes were removed;

4) none of the treatments conferred any strong velocity dependent effects.

In view of this last conclusion, it was decided to adopt Figucia's method for any further quantification of ballistic performance. In the next phase of research a more open weave fabric was tested as it was felt that the inherent freedom of yarns would provide plenty of scope for modification of yarn to yarn cohesion. Samples of these fabrics

were immersed in aqueous solution of the fabric finish and then cured at 120° for 15 minutes. As a control, a set of samples was immersed in water and dried at the same temperature. One of two finishes were applied:-

i) LURAPRET + B30. This confers a high yarn to yarn friction. Chemically it is an aqueous solution of silic acid.

(ii) PARAPRET HVN + LURAPRET B30. 50/50 mixture. Parapret is an aqueous dispersion of an anionic polyacrylate.

The effects of these treatments were quantified using the yarn pull test described in the previous report. A typical force-extension curve obtained from this test is shown in figure 17. For each test, the first two maxima (A,B) were recorded. The results for the Kevlar fabrics treated with finishes are shown in table 5. As expected the maximum forces were greatest for the Lurapret-Parapret (bonded) samples and least for the control samples (water treatment). For the bonded samples there was a 66.8% reduction in force between the first and second peaks, whereas for the other samples this figure was in the region of 15%. It is concluded that the yarn to yarn bonds are broken at the first peak and that the level of the second peak is determined by frictional forces. There appears to be very little yarn to yarn bonding for the fabrics which were treated with the higher friction finish.

Results of the ballistic tests on treated fabrics

Weight for weight the water treated samples we found to be significantly superior in ballistic performance than either the 'high friction' or bonded samples. The latter two fabrics were found to be of equal ballistic performance, even though there was a large difference between the levels of force in the yarn pull test. The BPI's (Ballistic performance Indicator), the slope of the energy - area density relation is

+Registered trade made of BASF, England.

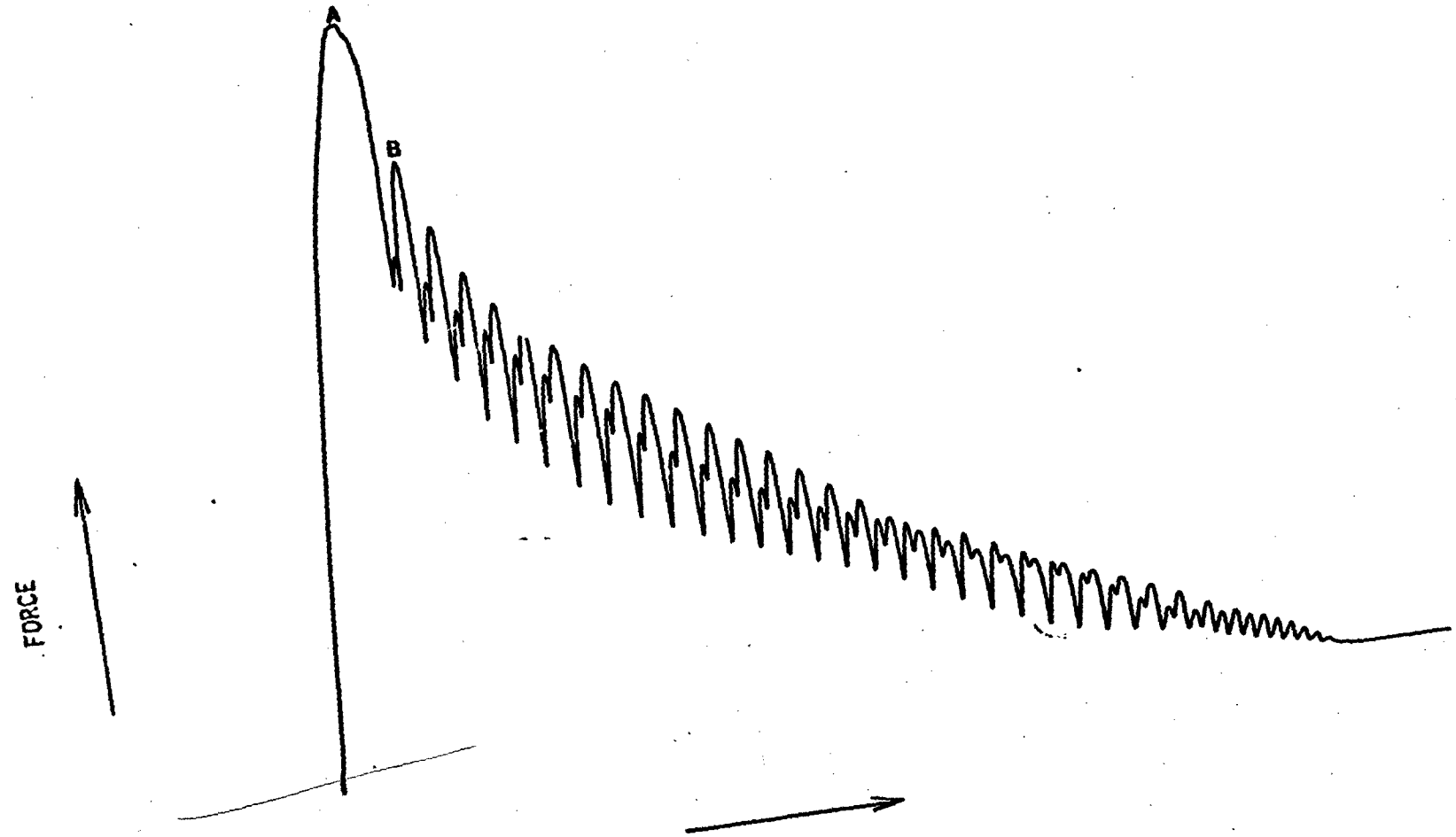

Typical force-extension curve obtained for yarn pull test.

FIG. 17

listed in table 5. The results are presented graphically in figure 18. These results hold even if the add on weight of the finishes is not included when calculating the B.P.I, although the differences are lower. The reason for this, of course, is that the fabric treatment adds weight but not strength. These renormalised results are shown graphically in figure 19.

Conclusions on the effect of increased yarn to yarn friction

Although it is possible that similarity in ballistic performance between the bonded and the high friction finish is coincidental, and the some intermediary level of cohesion would produce different results; it seems probable that there exists a relatively low level of yarn to yarn cohesion which significantly reduces the resistance of Kevlar fabric. Above this level the ballistic resistance becomes insensitive to any further increase in friction or bonding, alternatively the add-on weight of the finishes could have modified the response to impact.

Fig.5.29a and 5.29b show strain histories, at the point of impact of an identical fabric, as predicted by the methods described in part II. Fig. 5.29a shows the case where slipping is allowed at yarn crossovers and fig.5.29b models the case where the yarns are rigidly connected. Although the time to projectile arrest is less for the latter case, the strains are generally higher. Thus a strain failure criterion is applied to both cases, it is predicted that the fabric with rigidly connected yarns would fail at a lower impact velocity than the fabric where yarn slip is allowed. This is consistent with the experimental results.

Ballistic Resistance of Kevlar 29 and Kevlar 49

Kevlar 29 exhibits twice the tensile breaking strain but almost half the tensile modulus of Kevlar 49. Roylance(ref. 8) has developed

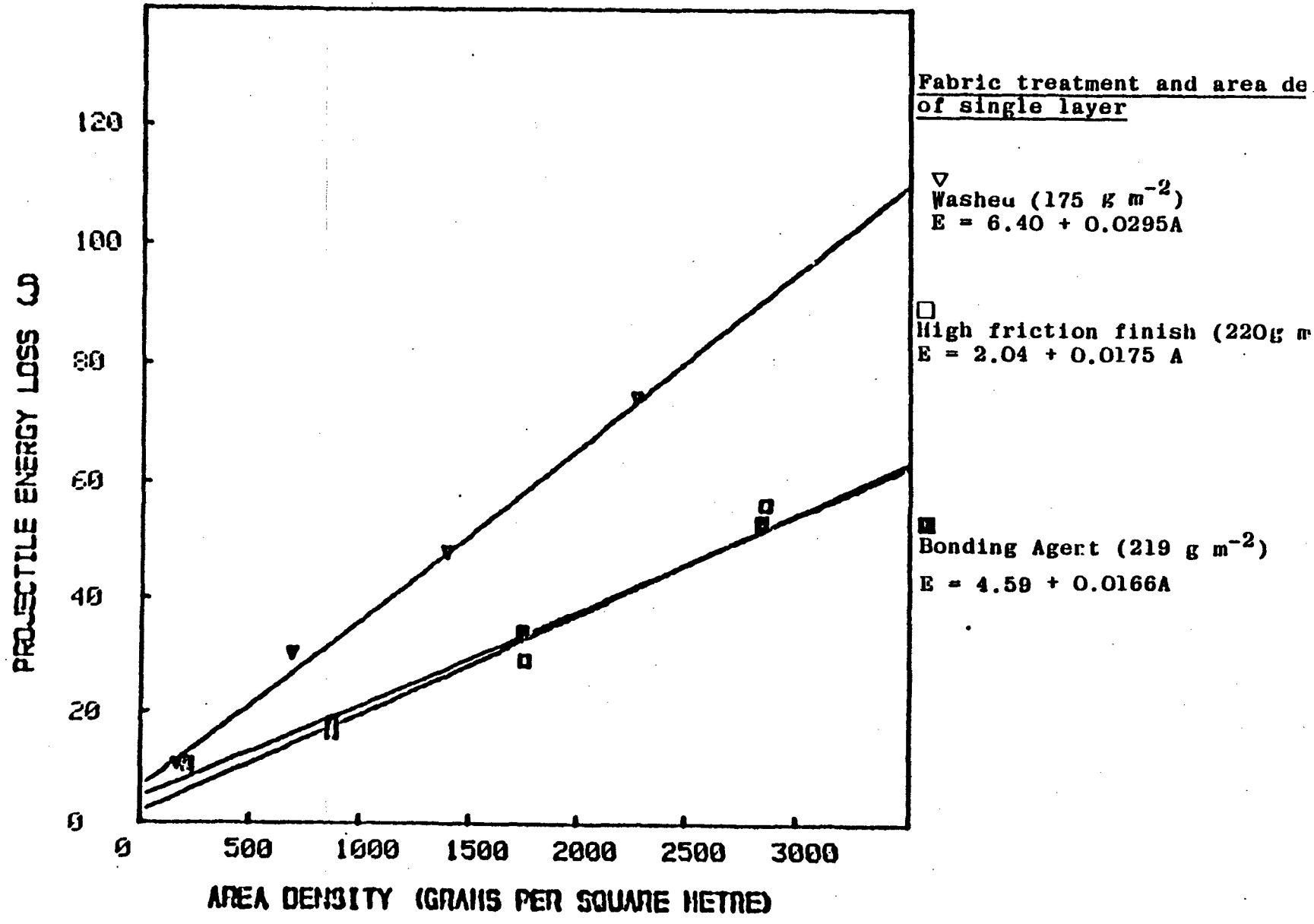

Projectile energy loss (E) against the combined area density (A) of multilayered Kevlar. Effect of fabric treatments on Kevlar 49.

FIG. 18

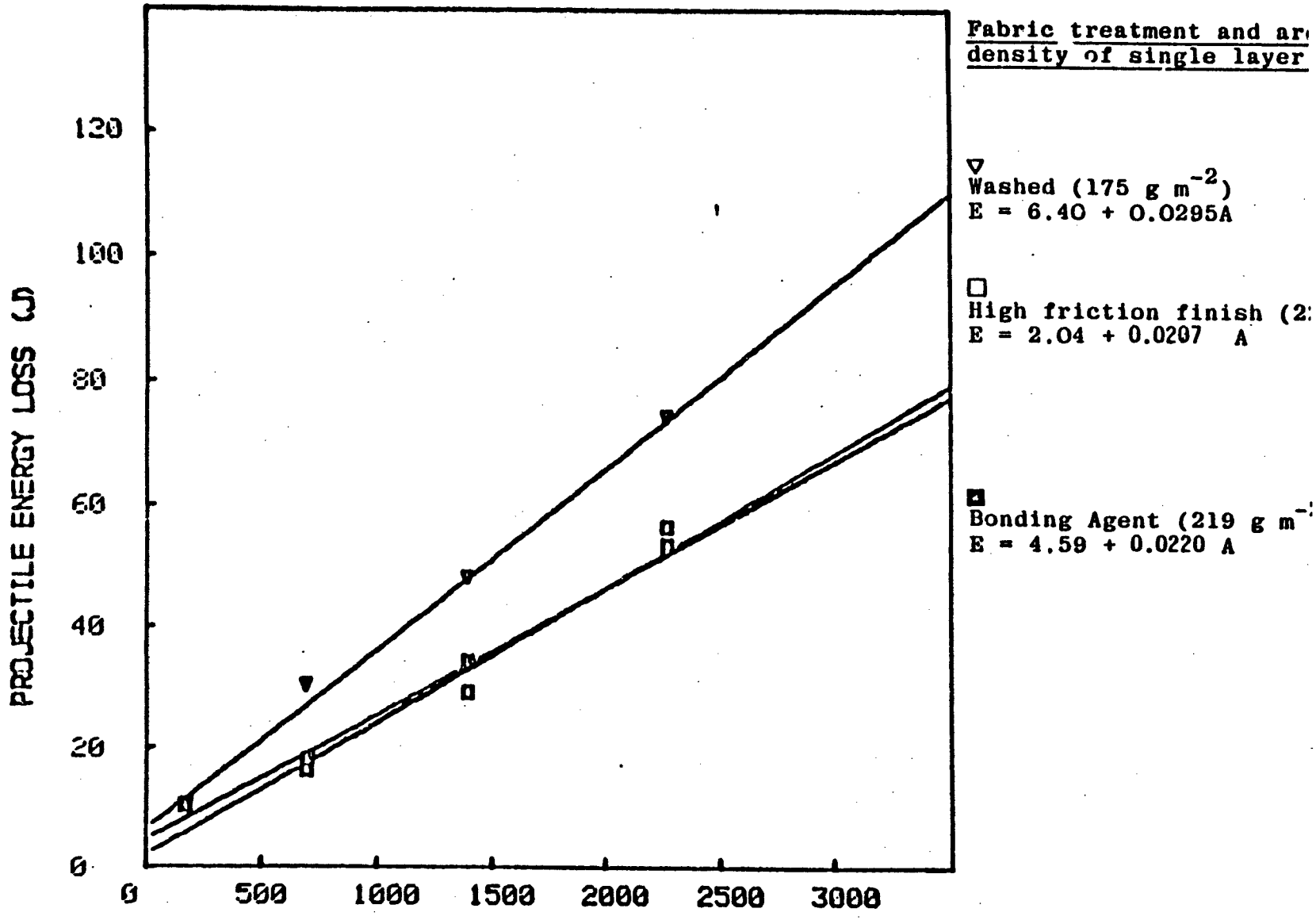

- Based on untreated weight

Projectile energy loss (E) against the combined area density (A) of multilayered Kevlar. Effect of fabric treatments on Kevlar 49.

FIG. 19

a finite difference model for the ballistic impact onto textile structures. Using these quasi-static fibre parameters, Roylance predicts that Kevlar 29 is superior to Kevlar 49. However, Roylance refers to experimental results which seem to indicate a similarity in ballistic resistance.

In order to provide our own data a Kevlar 29 and a Kevlar 49 fabric of similar construction were compared on the ballistic test range. Both fabrics were treated with the high friction finish as the results were also used to provide data on the effect of finishers.

Results of Tests on Kevlar 49 and Kevlar 29

No significant difference was found between the ballistic resistance of Kevlar 29 and Kevlar 49. Figures 20 and 21 are plots of projectile energy loss against combined area density of the multilayer fabric for these two fabrics. In Figure 21 the results have been renormalised to reflect the untreated weight of the fabrics (175 gm^{-2}). The B.P.I's are shown in Table 5 .

It is of interest to compare the author's results with those of Figucia (ref. 4) who found B.P.I's in the range of 22.6 to 31.5 $J/kg/m^2$. The two untreated Kevlar samples tested by the author were found to have B.P.I's of 29.6 and 33.6 $j/kg/m^2$. Thus the results for Kevlar are in good agreement even though the authors results were obtained using a blunt cylindrical projectile instead of the fragment simulator and a 6" rather an a 1" diameter fabric sample size.

Model of Multilayer Impact

A simple computer model was used to calculate and display graphically the multilayer performance from single layer data. The model assumed no physical interaction between layers. The exit

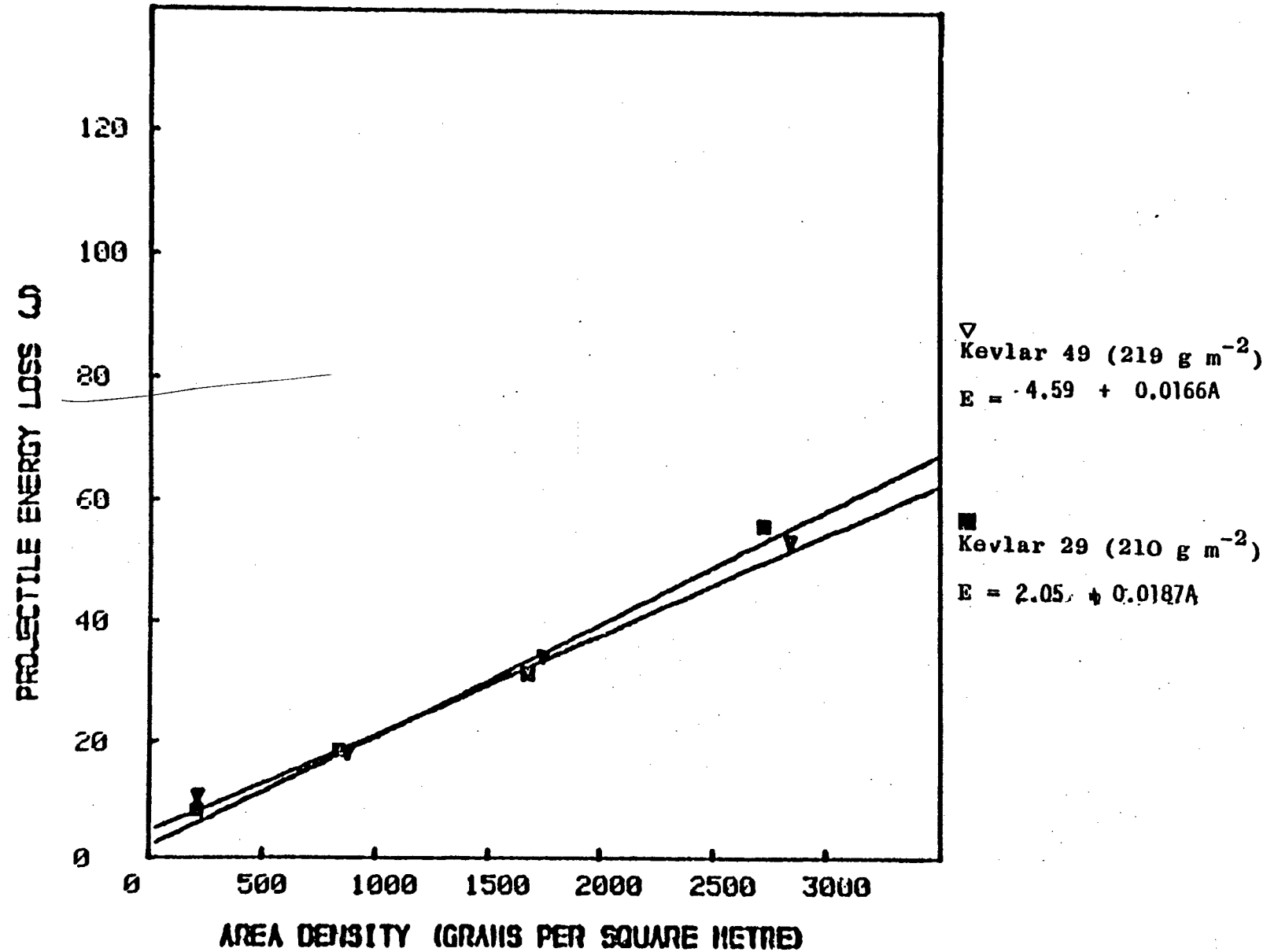

Projectile energy loss (E) against the combined area density (A) of multilayered samples. Comparison between the ballistic performance of Kevlar 29 and Kevlar 49 Both fabrics had been treated with a high friction finish. FIG. 20

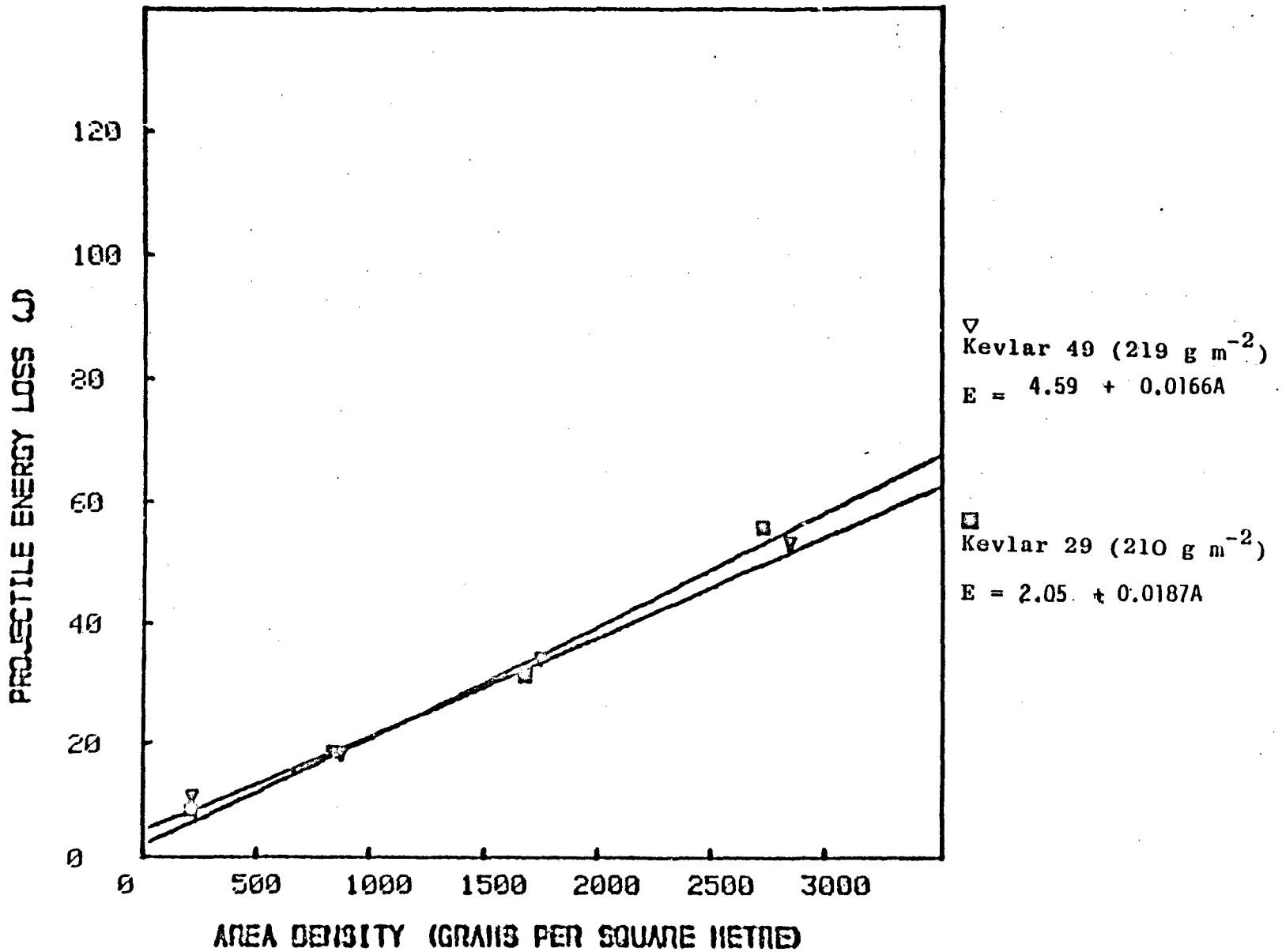

Projectile energy loss (E) against the combined area density (A) of multilayered samples. Comparison between the ballistic performance of Kevlar 29 and Kevlar 49 Both fabrics had been treated with a high friction finish.. FIG 20

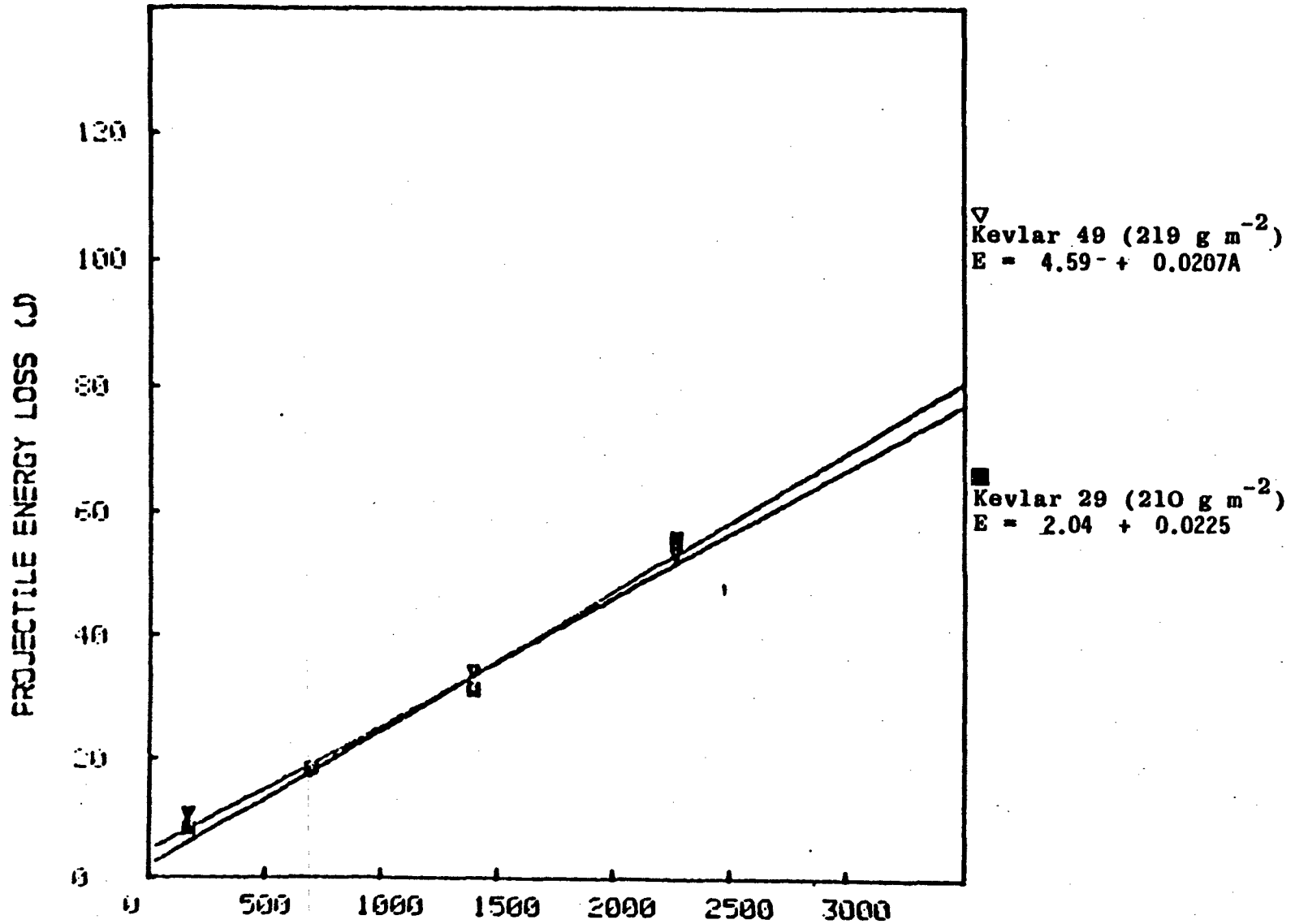

- Based on untreated weight.

Projectile energy loss (E) against the combined area density (A) of multilayered samples. Comparison between the ballistic performance of Kevlar 29 and Kevlar 49 Both fabrics had been treated with a high friction finish.

FIG. 21

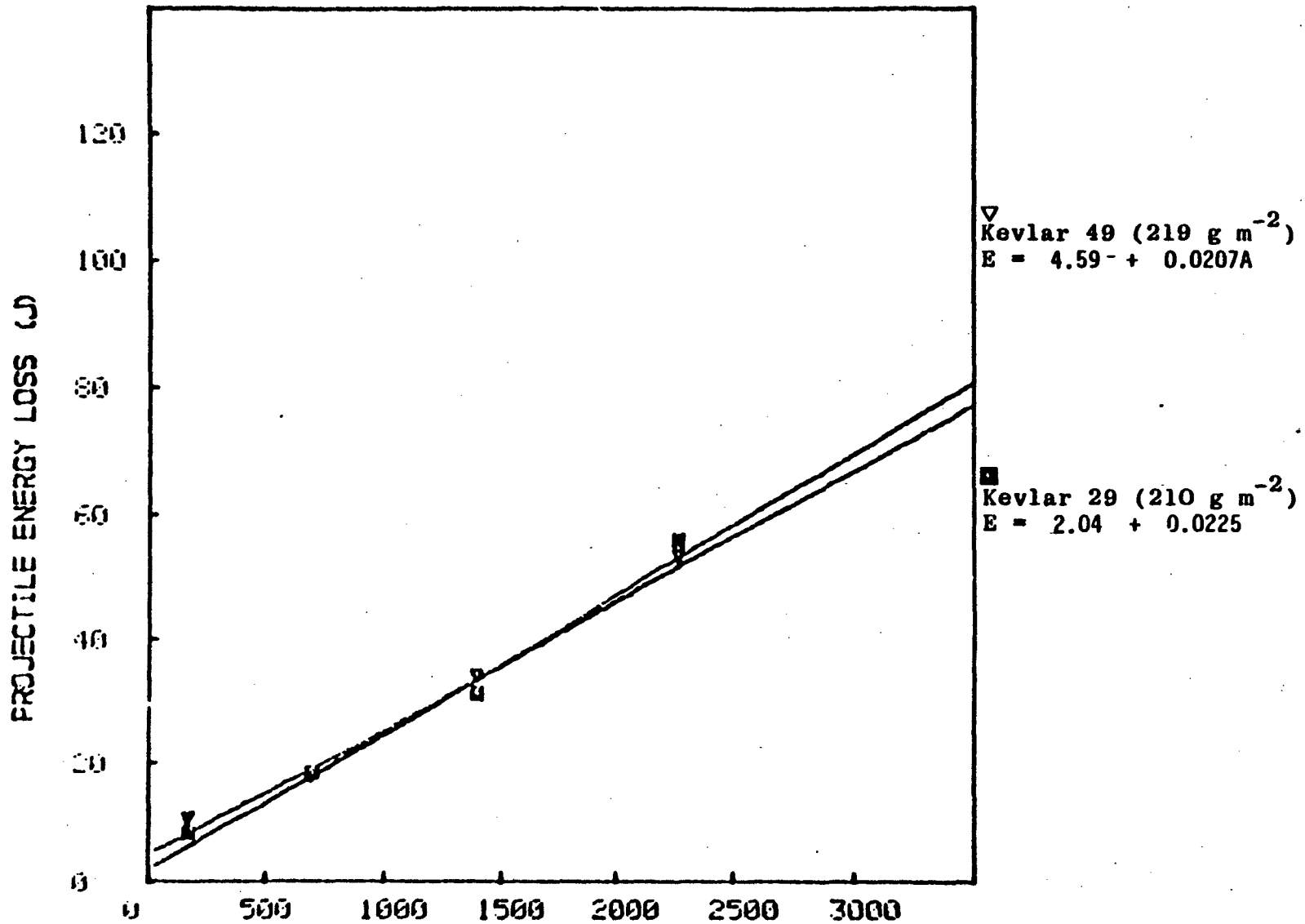

- Based on untreated weight.

Projectile energy loss (E) against the combined area density (A) of multilayered samples. Comparison between the ballistic performance of Kevlar 29 and Kevlar 49 Both fabrics had been treated with a high friction finish.

FIG. 21

FABRIC	TREATMENT	1st MAXIMUM kgf	2nd MAXIMUM kgf	% decrease in maximum from 1st to second	BALLISTIC PERFORMANCE INDICATOR $J/kg/m^2$
KEVLAR 49 $175gm^{-2}$	Water	0.125	0.107	14.4	29.5
KEVLAR 49 $219\ gm^{-2}$	High friction	0.590	0.490	16.9	17.5
KEVLAR 49 $220\ gm^{-2}$	Bonding agent + high friction	6.14	2.04	66.8	16.6
KEVLAR 29 $210\ gm^{-2}$	High friction	0.406	0.343	15.5	18.7

Table 5. Results of yarn pull test and the Ballistic Performance Indicator for a set of Kevlar fabrics.

velocity (v_e) from each layer is calculated from the single layer relation ($E=f(v_I)$) of energy loss against impact velocity (v_I). Thus

$$v_e = \tfrac{1}{2} m v_I^2 - f(v_I)$$

where m = projectile mass.

This velocity is then taken to be the impact velocity onto the next layer. This iteration is continued until penetration of all the layers, or until the projectile is arrested. This routine is repeated for initial impact velocities in the range 0 to 550 m s^{-1} in order to obtain the multilayer related ($E + f'(v_I)$).

This routine was applied to single layer data which had earlier been obtained for nylon and Kevlar treated with high and low fabric finishes. Experimental data from the multilayer tests was then compared to that predicted by calculated. The original data points, the corresponding least squares curve fits, together with the predicted curves of energy loss against impact velocity are shown in figures (11) to (16).

It can be seen that generally the experimental results show that the maximum energy absorption occurs at the V_{50} limit. In addition the calculated energy losses (shown by a broken line) are generally higher than those found experimentally at the high velocities. The one exception to this is the Kevlar treated with Siligen E, where the three layer curves are similar.

The above results are replotted as graphs of projectile energy loss at the V_{50} limit against the combined area density of the multilayered sample. These are presented in fig. 22 to 27. It is concluded that in the range of these tests, the calculated V_{50} limit agrees with the experimental results.

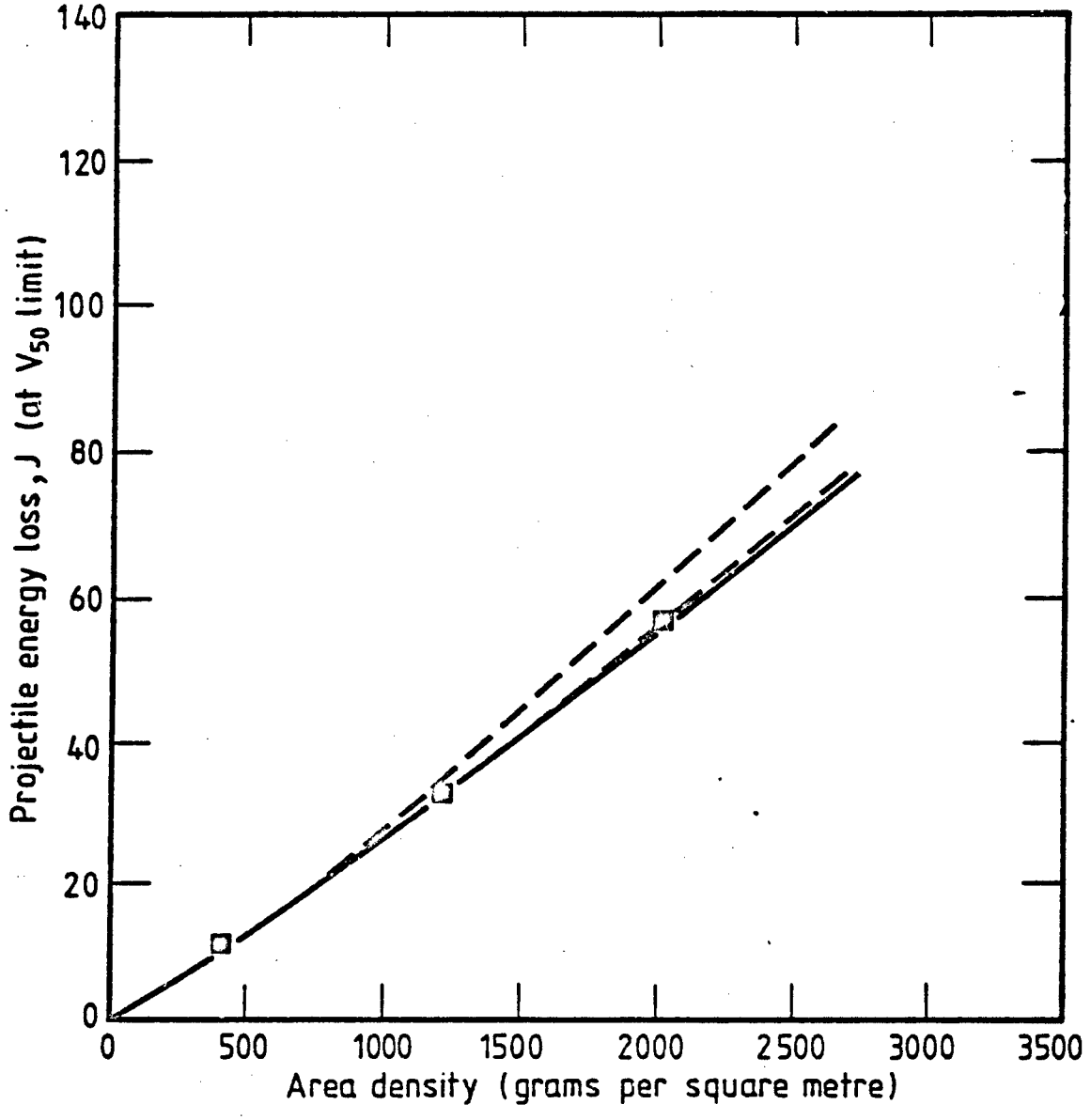

Fig. 22 V_{50} energy loss against area density of multilayered sample for a nylon fabric treated with a low friction finish.

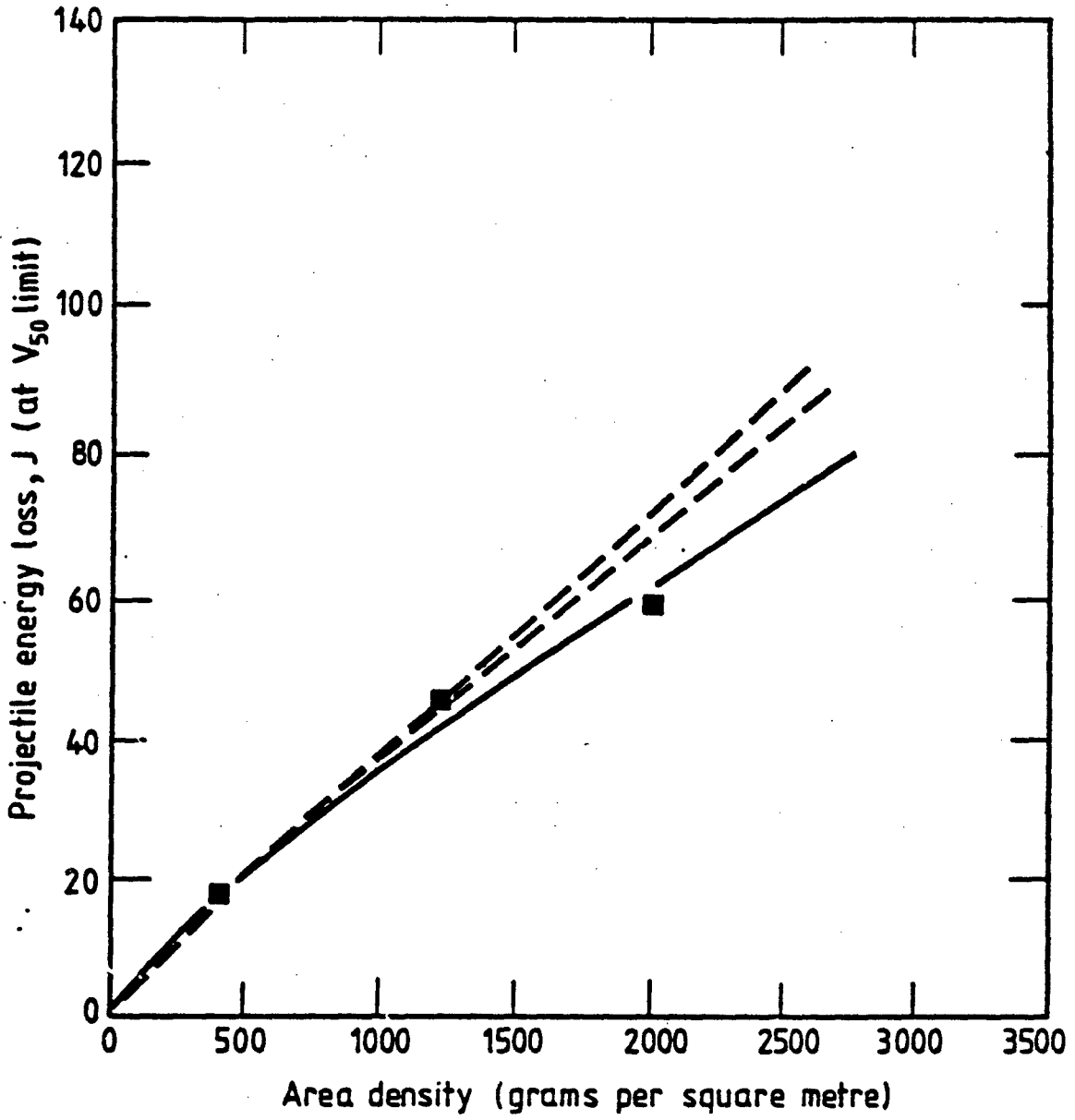

Fig. 23 V_{50} energy loss against area density of multilayered sample for a nylon fabric treated with a high friction finish.

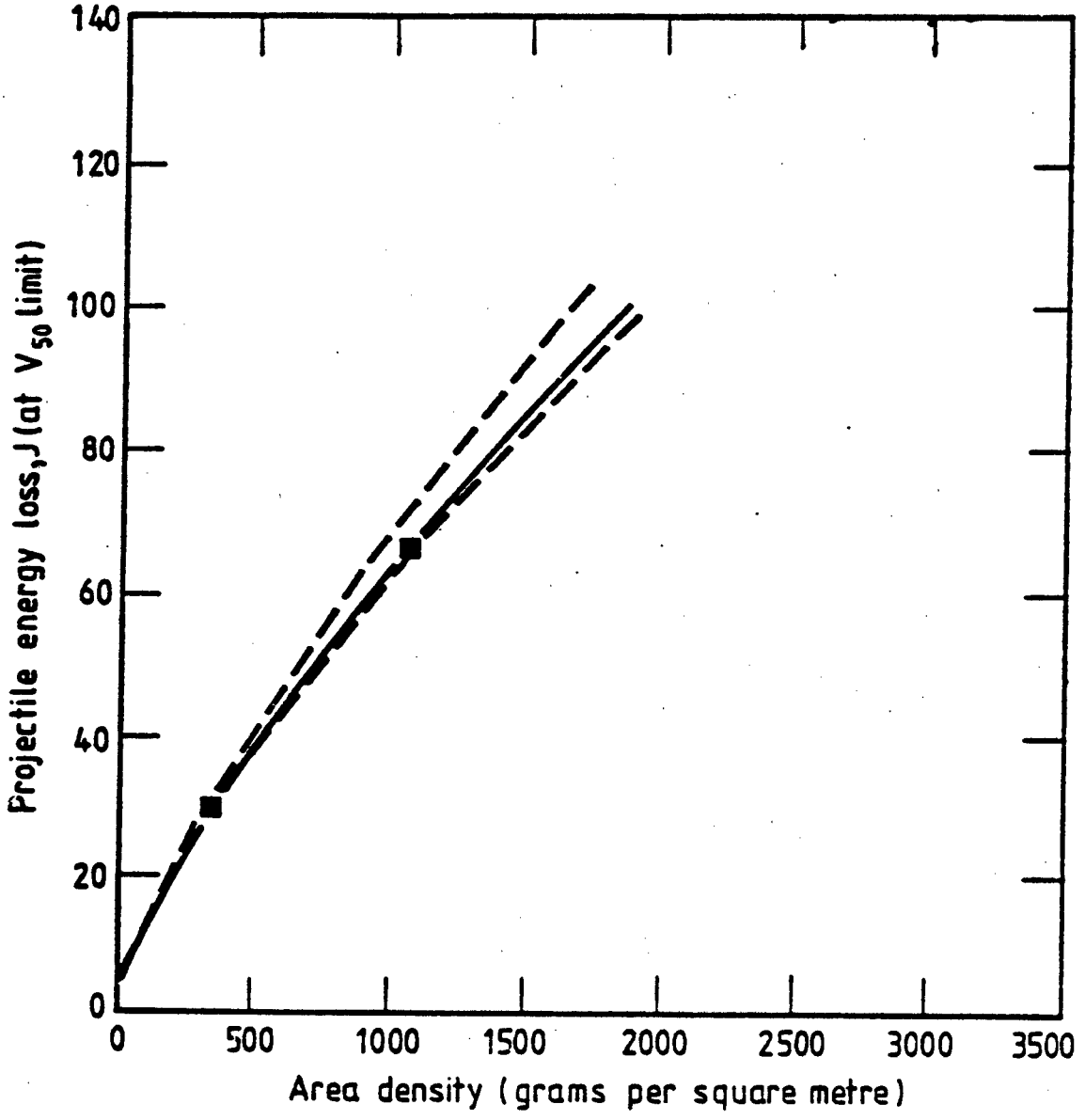

Fig. 24 V_{50} energy loss against area density of multilayered sample for a Kevlar fabric (as received).

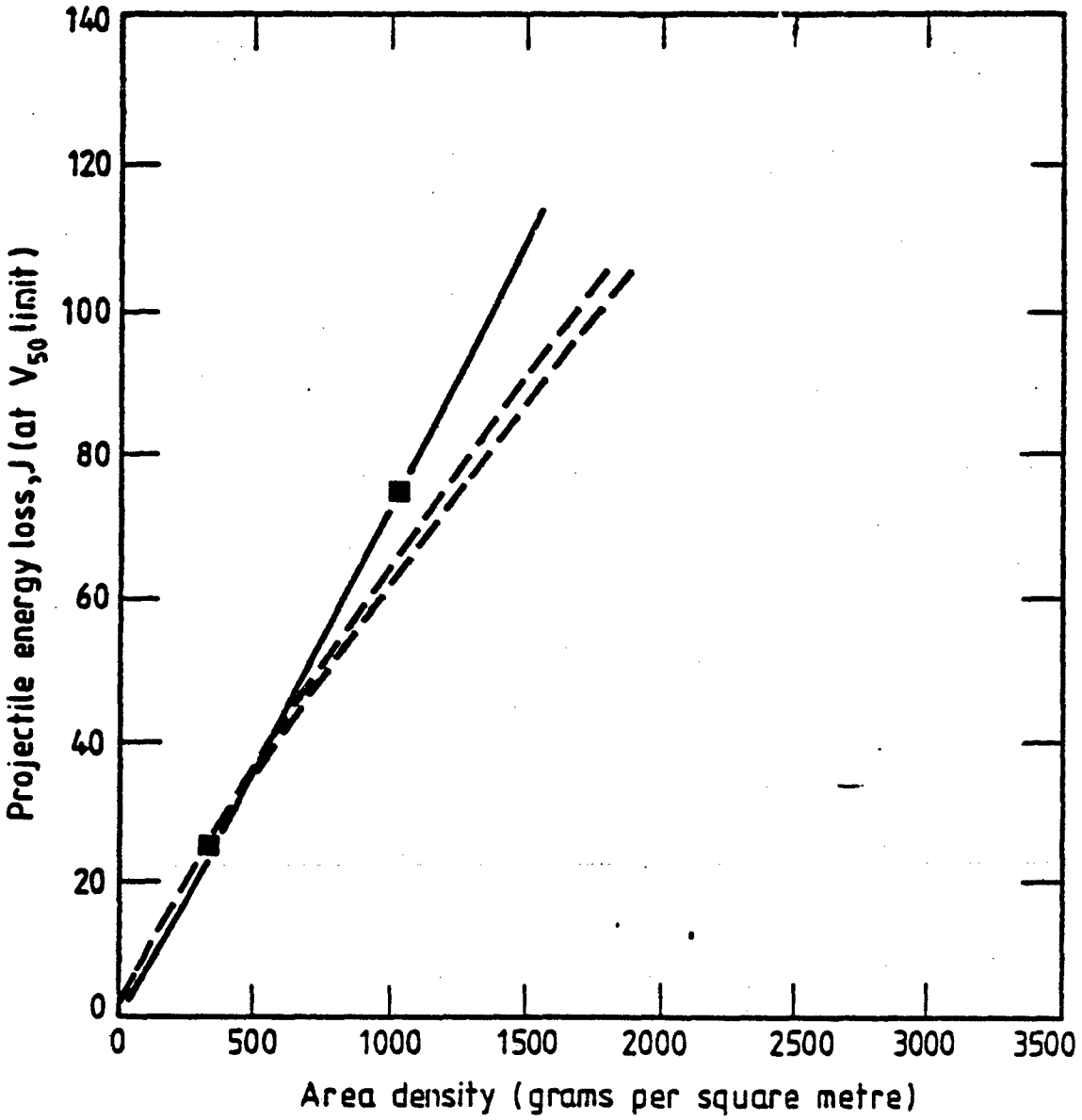

Fig. 25. V_{50} energy loss against area density of multilayered sample, for a Kevlar fabric after washing and heating to 110°C.

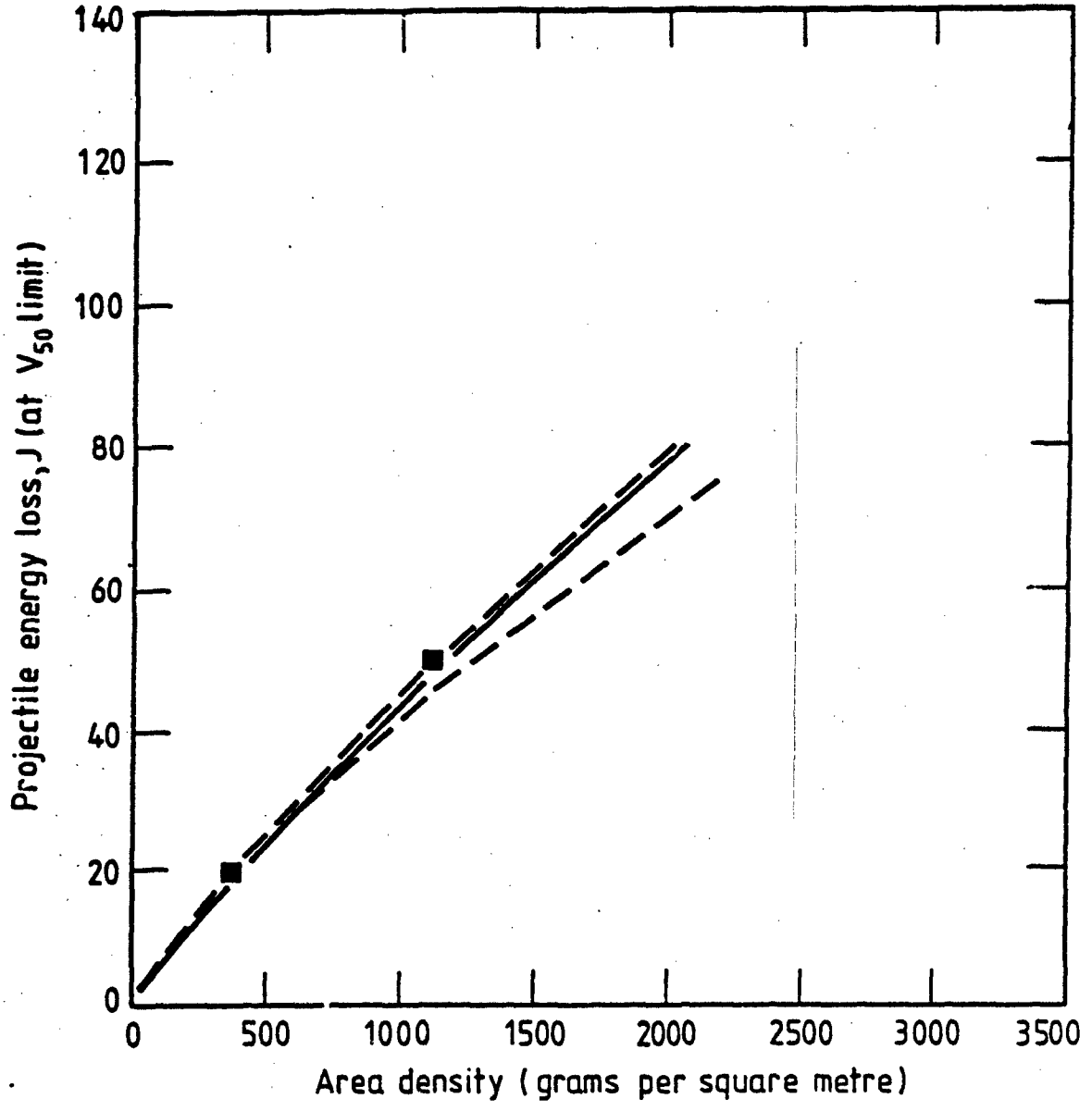

Fig. 26 V_{50} energy loss against area density of multilayer sample for a Kevlar fabric treated with Siligon E.

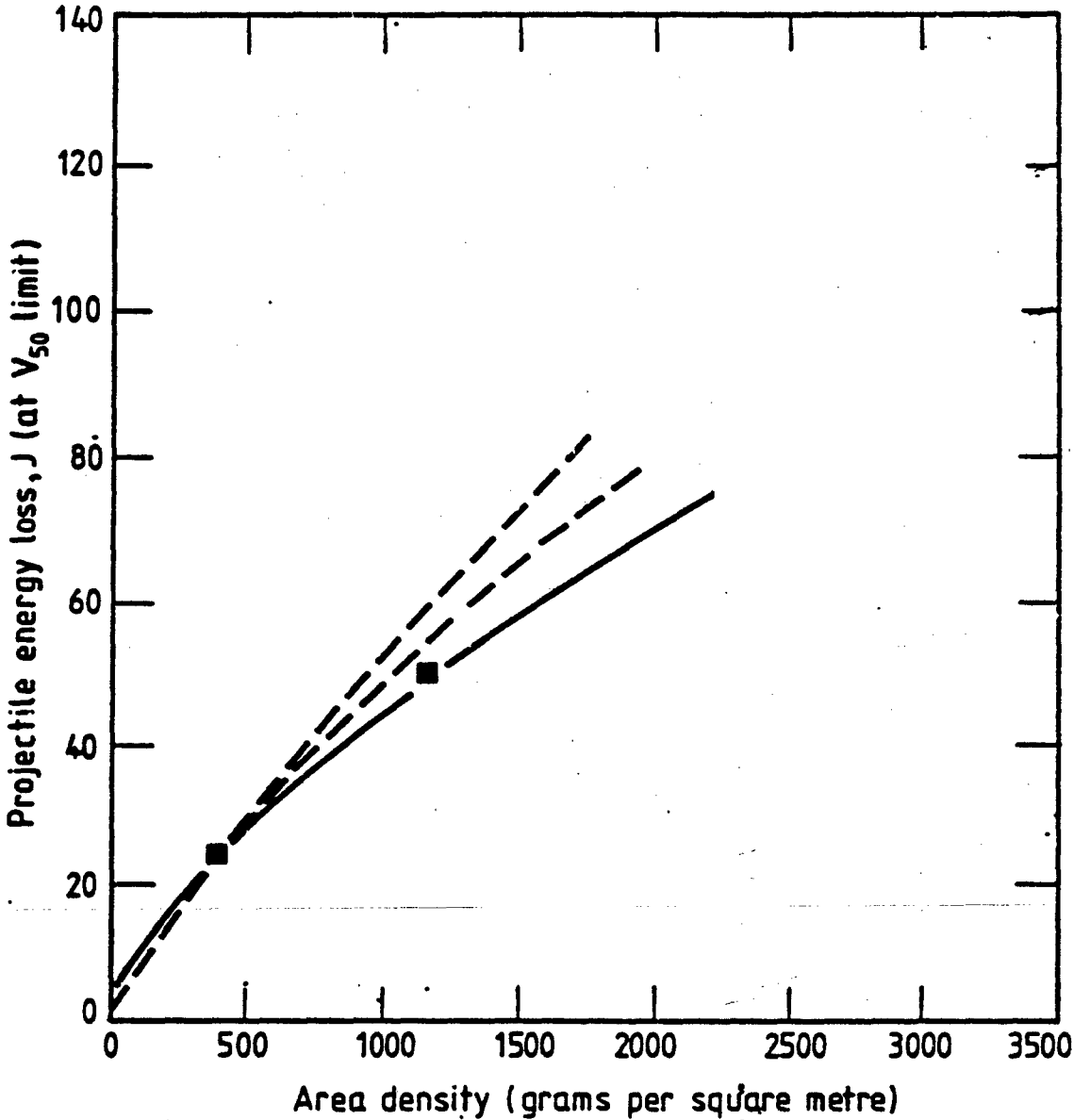

Fig. 27 V_{50} energy loss against area density of multilayer sample for a Kevlar fabric treated with a high friction finish.

General Results and Conclusions

A ballistic rig has been designed and constructed by the author in order to:

1) impact 1 gm cylindrical steel projectiles onto a fabric samples;

2) measure the impact velocity electronically;

3) measure the exit velocity photographically;

4) provide single or multiflash photographs of the fabric under impact;

5) measure the arrival of stress waves at the fabric boundary.

Tests on fabrics have produced the following results:

1) the shape of the transverse wave front is octagonal for a two ply fabric, if the yarn directions of each layer are set at 45° to each other;

2) the shape of the transverse wave front is hexagonal for triaxial fabrics;

3) two triaxial fabrics have been shown not to be ballistically superior to biaxial fabrics.

4) a Kevlar 29 and a Kevlar 49 fabric of similar weight and construction were found to have similar ballistic resistances.

The following conclusions can be drawn:

1) the octagonal form of the transverse wave in the bilayer impact indicates that there is some degree of interlayer interaction and that any computer model must not assume a rhomboidal form as a starting condition unless the fabric in each layer is similarly orientated;

2) the hexagonal shape of the transverse wave for a triaxial fabric indicates that more energy should be absorbed as kinetic

energy of transverse motion, however as empirical data shows that triaxial fabrics are in fact inferior to biaxial weaves other effects such as the parting of yarns at the impact zone must be predominant;

3) the high friction finish probably improved the ballistic performance of the nylon fabric by a reduction in lateral mobility of yarns at the impact zone or due to the influence of the degree of yarn to yarn friction on the strain distribution during impact;

4) a lightweight nylon fabric was shown to be ballistically inferior to a heavyweight nylon fabric and although these results could be partly attributable to the stress-strain relations of the constituent yarns, it is postulated that the mode of penetration (plugging in the case of the lightweight close weave fabric) is also a contributory factor;

5) a high friction finish conferred a greater ballistic performance on a nylon fabric than the same fabric treated with a low friction finish;

6) both the high friction and the bonding agent proved seriously detrimental to the ballistic performance of the Kevlar fabrics tested;

7) a simple energy model, designed to simulate impact onto separate layers, agrees well with empirical results of the V_{50} energy where the number of layers is low, but overestimates the ballistic performacne when penetration occurs at high velocities;

8) the reduction in ballistic performance of Kevlar due to the addition of high friction or bonding agents could be because the level of friction is already idealised in the natural state, unfortunately no finish was found to confer a lower friction on

Kevlar. Another possible effect is that the add-on weight could influence the mechanics of impact and penetration and therefore mask any effects of friction;

9) as the energy models for multiple impact do not consider interlayer interaction, yet generally agree with empirical data of V_{50} energy, it seems that interlayer interactions are second order effects, where the number of layers is small.

It is proposed that

1) no major work on the ballistic properties of triaxial fabrics alone should be undertaken. However the use of triaxial fabrics in hard composites should not be dismissed as in such materials, yarn mobility will be reduced and penetration due to the pushing aside of yarns will be precluded;

2) the multilayer impact models should be compared with data from multilayer impact where the number of layers is greater, in order to determine whether there is a need for more sophisticated models.

	CALCULATED FROM SINGLE LAYER DATA (Joules)	EXPERIMENTAL RESULT (Joules)
KEVLAR As Received	62.4	62.8
Siligen E (high friction)	40.8	43.9
Lurapret (high friction)	48.3	44.4
Nylon Siligen E (low friction	27.8	26.6
Lurapret (high friction)	37.5	35.6

Table 4. V_{50} Energy at an Area Density of $1000 g.m^{-2}$

References

1 LAIBLE, R.C., The Mechanical Properties of Polypropylene as Related to Ballistic Applications, Proc. Symp. on Polypropylene Fibres, Sept. 17-18, 1967, p.61.

2. MORRISON, C.E., BOWYER, W.H., Factors Affecting Ballistic Impact Resistance of Kevlar 49 Reinforced Composites, Palmer Research Laboratories Ltd., Stoke Poges, Slough, England, Contract No. A 93 B/189, (1980).

3. LEECH, HEARLE and MANSELL, Some Aspects of Wave Propagation in Orthogonal Nets, Int. J. Mech. Sci., Vol. 19, 93.102, (1979).

4. FIGUCIA, F., Energy Absorption of Kevlar Fabrics Under Ballistic Impact, United States Army Natick Research and Development Command, Natick, Massachusetts (1980).

5. CUSICK, G., DOGLIOTTI, L.M., WRIGLEY, A.S., Microscopial Study of a Multilayer Nylon Body Armour Panel After Impact, Text. Res. J., 28, 360 (1958).

6. CORK, C.R., 'The Response of Woven Textile Materials to Transverse Ballistic Impact' M.Sc, Thesis, Dept. of Textiles, University of Manchester Institute of Science & Technology, Manchester, England.

7. MINER, L.H., The Ballistic Resistance of Fabrics of Kevlar Aramid Fibre their Core and Use, Report of E.I. du Pont de Nemours Co., Inc., Wilmington, Delaware, U.S.A. (1980).

8. ROYLANCE, D., WANG, Su Su, Chapter 12, "Ballistic Materials and Penetration Mechanics", Ed. Laible, R.C., Elsevier Scientific Publishing Company, Amsterdam-Oxford-New York, (1980).

PART II

THEORETICAL

Introduction

Textile materials in the forms of fabrics, webbings and felts are widely used in energy absorbing systems such as automobile seat belts, parachute lines, and personnel protection. The particular problem reported here . . . is an investigation of the behaviour of single-layer and multiple-layer assembles of woven fabric used in protective clothing worn in the vicinity of medium velocity (500 ms^{-1}) particle hazards.

These protective clothings are made by sewing together many layers of fabrics, each of which may have been subjected to various surface treatments. Usually for easy mobility, the fabrics are not bonded together and can therefore slip relative to one another. The materials most commonly used in the manufacture of these fabrics are Nylon and Kevlar. The yarns are bundles of thin, long, fibers, held together by friction.

The mechanics of the behaviour of the clothing is complex and various simplications are made to render the problem tractable. The projectile is taken to be rigid, blunt, and travelling perpendicularly to the fabric assembly without spinning. Each yarn is assumed to completely lie in a plane, initially. Under these conditions, it is no longer possible for the projectile to penetrate the fabric simply by pushing aside the yarns in its path without breaking them. Yarn rupture occurs when a given maxiumum strain is exceeded and visco-elastic effects are not investigated.

Different mathematical methods are used to investigate the mechanics of the fabric assemblies with the aim of developing numerical methods for evaluating the effectiveness of various fabric parameters.

Before the details of these methods are given, a brief review of publications by previous investigators of this and related problems, is given in Chapter 1.

In Chapter 2, a variational model is described. In this model, only the out-of-plane transverse motion of the fabric(s) is considered. The shape of the indentation is first predicted from the given weave pattern and the equation of motion is then derived. Next, the effect of yarn crossovers (nodes) on the transmission and reflection of the strain waves which are initiated at, and propagate away from, the impact area are investigated. The well-known equation for the propagation of waves along a string forms the basis of this enquiry. Assuming rigid connections at the nodes, equations are derived for the impedance of a node for any fabric geometry. Numerical examples are obtained to compare various geometries.

In Chapter 3, a description is given of an application of the method of characteristics to the investigation. The characteristic equations of the three types of waves travelling along the yarns (no twist) are obtained. The motion of the fabric assembly is obtained by following the characteristics entering each of the nodes. A quasi-linear model is also developed in which only the out-of-plane motion is considered: an attempt to reduce the amount of computation effort. In each of the models based on the method of characteristics, it is necessary to give the fabric a non-zero prestrain to prevent numerical instability.

The application of the finite element method to the development of different models of a fabric is described in Chapter 4. Attempts were made to investigate the significance to overall fabric structural behaviour of; crimp, inter-yarn slip, and inter-fabric slip.

In Chapter 5, the numerical results are discussed and compared with the available experimental results.

Chapter 6 is the conclusion and some suggestions are also included for those interested in pursuing the investigation.

The impacting particle is always a blunt cylinder, mass 1.0003g, diameter 5.56 mm.

CHAPTER 1 LITERATURE SURVEY

The geometrical structure of the arrangements of yarns in a fabrics significantly affects some of the fabric properties. This fact makes a brief review of publications on the geometry of fabrics of relevance here. Pierce(1) made an important contribution to study of the geometry of the plain orthogonal weave consisting of two families of yarns interlaced at right angles. The yarns, in that investigation, were considered as thin rods of circular cross section. Allowance was made for the effect of the finite radius of the yarns, at the cross overs, that is, crimp was included. The deformation characteristics of the model was not considered in his analysis. Since, geometric-mechanical models have been developed for various fabrics (18), (19). Olofson(2) developed a model and analysed the tensile deformation of a fabric. Kawabata et al, in a series of papers (3), (4) and (5), developed the 'stereo' model and applied it to the study of uniaxial extension, biaxial extension and of a plain weave shear. They showed that the compressive strength of the yarn significantly affects its mechanical properties under these loading cases. In the case of uniaxial extension, localised bending at the yarn cross overs was introduced to prevent straightening out of the yarn. This bending resistance was produced by the frictional resistance against inter-fiber slip. In the analysis of biaxial extension, perfectly flexible yarns were assumed. The resistance of the fabric to shear was predicted to be due to the torsional resistance to the rotation of the yarns relative to one another at the cross-overs. The magnitude of the shear stiffness was therefore dependent on the reaction between crossing yarns.

In another publication, Olofsson(6) investigated the rheology of a frictional-elasto-plastic model and derived expressions for the extensional, shearing, bending and buckling, and creasing modulii in terms of the yarn bending stiffness, its crimp, its extensional stiffness and the effect of sliding friction between the yarns. There are many publications of studies into the mechanics of fabric under static conditions by the researchers associated with Leeds University, Grosberg and Kedia(7) reported that the initial extension of a fabric can only be analysed successfully by including the bending resistance of the yarns, and that the assumption of perfect flexibility leads to large discrepancies between theoretical and experimental results. MacRoy, McGraith and McNamara(8), and Hearle and Grosberg(9) have analysed the mechanical behaviour of knitted fabrics. Skelton and Freeston(10) reported that the effect of a decrease of the pitch of a fabric, that is an increase of the pick per length, is greater interyarn force and poorer translation of yarn strength to fabric strength. The efficiency of translation, however, remains above 90% in most cases at both low and high strain rates for all conditions of finish. Shanahan and Postle(11), and Hearle(12) have also reported analyses of the mechanics of knitted fabrics.

The mechanics of triaxially woven fabrics was investigated by Skelton(13). The results showed that the use of this weave pattern improves the shear strength of a fabric over that of a biaxially woven fabric of the same area density. It has subsequently been reported(14) that a triaxial weave is superior to a biaxial not only in resistance to shear but also in resistance to uniaxial and biaxial extensions.

Huang(15) analysed the finite biaxial and uniaxial extension of a completely set plain-woven fabric in which the yarns have a non-zero flexural stiffness. The flexural resistance sharply decreases when the

change of curvature exceeds a fixed, limiting, value. This reduction in flexural resistance is due to slipping of the fibers in the yarn. The results show that the stress-strain relation for the yarn is non-linear even for a Hookean or linear fiber material.

Genensky and Rivlin(16) developed a theory for the deformation of a network of orthogonal cords, assuming a stress-free shear deformation model. They analysed different deformations. Recently Christoffersen(17) published an analysis of the mechanics of the in-plane deformation of fabrics. The fabric was treated as an orthotropic plane which behaves elastically in stretching along two orthotropic directions and is capable of stress-free deformation in shear. No slippage of the yarns was allowed. Results were published for stress concentration at a crack in the fabric.

Another line of investigation, different from all those reported above, was adopted by Leech(20) in the analysis of nets. Fourier representation of the thickness changes was used to obtain expressions for: the natural frequency of the net, the conditions for travelling waves, and, the ray and front theories for propagation.

There have been few publications of the analysis of the dynamic response of uncoated fabrics and dense nets to impact loading. Most publications on the mechanical behaviour have been for statical loading while there have been reports on the dynamics of the response of individual yarns to impact. The paucity of publications in this field is reflected in the fact that only 2 of the 278 references cited in the review of the mechanics of penetration, by Jonas and Zukas (21), are on the penetration of uncoated fabrics. Mansell(22) compiled an up-to-date list of publications on the response of single layers of uncoated fabrics and has reported some new experimental work and finite element analysis.

In the analysis of the mechanics of multilayer of fabrics, new factors, either negligible in, or unconnected with, the analysis of single layers now have to be considered. These include the influence of slip between layers, the frictional properties of the fabric surfaces, the pattern of laying the layers and the significance of the compressive stiffnesses. A relevant investigation is the study by Marom and Bodner(23) in which results show that a multilay assembly of thin aluminium plates has a higher resistance to ballistic impact than either a monolithic plate of the same total thickness or seperated thin plates. The different modes of shear and compression are cited as causes of the different resistances.

The publications on the response of composite plates to impact are also relevant. Daniel and Liber(24) reported that the primary deformation appeared to be a flexural wave. Cristescu et al(25), on the other hand, concluded from experimental results, that, even for composite plates, the projectile energy is absorbed mostly by extensional deformation. While it mostly occurs after heavy delamination, extension is the major energy absorption mechanism, but that the delamination serves to spread the deformations, thus involving more of panel in the energy absorption. The sequence of delamination is also reported.

FINITE ELEMENT ANALYSIS OF FABRICS

A bibliography of most of the published finite element analyses of fabrics are listed in Ref (22). Henghold and Russel(26) developed a formulation for a cable element which is directly applicable to the modelling of individual yarns. Ozdemir(27) modified the strain formulation in the last-mentioned model. In the new formulation, the cable length at any time is specified as a function of the lengths from

the origin to the nodes. The formulation avoids the inconsistencies in some formulations which lead to non-zero strains when the shape of the cable distorts without a change of length. The equations of motion obtained by this formulation were shown to coincide with those obtained by the simple rod elements, for two-node elements. The 3-node, and 4-node elements tend to be overstiff compared with other published results. de Lynch(28) analysed the dynamics of both yarns/fibers and fabrics. Rod elements were used to represent the yarns while semi-annuli membrane elements were used for fabric analysis. In the fabric analysis, circumferential buckling was reported to occur during the propagation of waves prior to reflection at the boundaries. The accuracy of the modelling of buckling was said to need further study.

Shanks and Leech(29) published results on the influence of weave pattern on the transient response of coarse nets and cloths to impact. Zero crimp was assumed in the model, an assumption which, while realistic enough for coarse nets may lead to inaccuracies in the analysis of dense fabrics. Stubbs and Fluss (18) developed a space-truss model for a plain-weave, coated fabric. The model incorporates crimp. Each element has 6 nodes and is a combination of 7 straight rods. The formulation allows for large deformation and non-linear material properties to be investigated. While results were not published for dynamic loading, this model is considered here as it is easily used in such an analysis. A similar model developed by Torbe(19) involves shear resistance and has the nodal variables at the yarn crossovers condensed out, leaving only 4 nodes for element. This crucifix element was used in the analysis of coated airballons. It should make a more efficient use of computer storage than the 6-node element of Ref 18. However, the latter model allowed for yarn flattening, or yarn compression, which the former neglected.

MEMBRANE MODELS

Leech, Hearle and Mansell(30) developed a membrane model to analyse the arrest of projectiles by pretensioned cloths and nets. All in-plane motions were neglected while the shape of the front of the out-of-plane transverse motion was based on earlier work by Leech and Mansell(31) on the prediction of wave fronts in orthogonal fabrics. It was shown the shape assumed for the cross section of the indent does not significantly affect the numerical results. Already mentioned is the use of semi-annulii membrane elements in the finite element of fabrics by de Lynch. There was no comparison given between the numerical results and experimental results and as such it is difficult to specify the extent to which the wave front could be predicted using annulii elements. Annulii elements may be most appropriate in the analysis of the dynamics of knitted fabrics for which experimental results show a circular front for out-of-plane transverse motion. Oden, Kay and Fost(32) published results on an analysis of the non-linear response of an incompressible membrance using constant strain, triangular, elements with a Green's deformation tensor formulation for strain. The loading was provided by a constant force which was applied for a short time and then removed. Benzley and Kay(33) obtained numerical results for the vibration of a pretensioned membrane and reported that these results compare well with analytical results. The nonlinearities caused by large deformation were shown while the derivation of the equations of motion of the nodes of the elements involve the determination of Cauchy stresses. The formulation allows for the initial orientation of yarns to be specified and allows for their rotation during motion. Computationally, the disadvantage of this formulation results from the fact that the directional cosine of the yarns are defined relative to the initial shape of each element, and therefore has to be recalculated

for each element shape. This is except when a membrane is divided into square, rectangular, or similar triangular, elements. Another method of accounting for the rotation of yarns was adopted by Tabaddor and Stafford(34) in their study of the vibration of a cord-reinforced tyre. The constitutive equations were defined to incorporate the relation between yarn rotation and strains.

Leonard and Verma(35) used a double curved element to analyse the properties of a Mooney-Rivlin membrane. Coons geometry was used to obtain accurate representation of points on the curved surface. The paper contains a useful bibliography.

The only study, known to this author, of the use of three-dimensional finite element analysis to model a single layer of a fabric is that by Lloyd(36). In this analysis, 20-Node, three dimensional parallelpiped elements were used and the deformed shape of a knitted fabric was successfully predicted. However the model fails at large strains.

MULTILAYER SYSTEM OF UNCOATED FABRICS

The only publication encountered in this literature survey, on the response of layered, uncoated fabrics to impact, by Flaherty (37), is based on experimental work. The results show that the order of arrangement of the fabrics affects their combined strength, at least, for the 2-layer system reported. There are, however, reports of numerical, and even analytical, studies of the responses of layered beams or plates made from aluminium and wood. Some of these studies are briefly mentioned later.

Some of the phenomena such as slipping, which may significantly affect the overall structural behaviour of a multilayer system of fabrics have already been investigated in the study of metal

deformation of Wilkins(38). The method used in that study to model separation is also relevant.

Thompson, Goodman and Vanderbilt(39) studied the effect of interlayer slip on the deflections and stressed in a statically loaded layered system of wooden beams. The slip was related to the shear across the thickness of each layer. With the assumption of negligible friction, resistance against interlayer slip only occurs when the layers are glued together. Suzuki and Chang(40) showed that interlayer slip may significantly affect the overall structural behaviour of layered wooden structures, in a study of bonding failure during the bending of a laminated cantilever. Analytical expressions were derived to relate deflection and loading force, and the movement of the slip/no-slip boundary, with increasing load, was demonstrated. It was concluded that; interlayer slip due to debonding, if it occurs. will reduce the overall stiffness of the cantilever. This conclusion can be compared with that of Refs (24) and (25) on the significance of the delamination process in spreading an impact load over a large area of composite sheet.

There are other publications, which are not on the analysis of fabrics, but which are relevant to this study because they suggest possible approaches to the finite element analysis of multilayers(41), (42), (43).

The study of fluid motion in containers also involve the modelling of slip. An outline of the problems and prospects of the methods currently used in that analysis are given in a book on structural mechanics which is edited by Donea (44). One of the most important sections in the book is the description of an extension of Wilkins's work on the concept of 'slave' line, 'slave' nodes and 'master' elements which are defined at the interface between two materials which can slide

relative to one other during motion. Other important contributions have also been made to the modelling of slip in finite element analyses(45) - (51).

CHAPTER 2 SIMPLE MODELS

2.0 Introduction

In this chapter, two aspects are considered; firstly the variational model used by Leech, Hearle and Mansell(30) in analysing the response of an orthogonally woven cloth to transverse impact is extended to the case of an impacted triaxially woven fabric. The equations for the two fabrics are then used to predict their relative effectiveness in retarding a projectile.

The second aspect considered here relates to nodal impedances; the relationship between yarn angular arrangement and the rates at which different incidents disturbances are transmitted.

2.1 Wave front Variational Model

In this model only the out-of-plane motion is considered, with all in-plane yarn motions neglected.

Firstly, the shape of the transverse wave front is predicted and the size of the disturbed area expressed as a function of time and a similarity coordinate, η , which measures the perpendicular distance behind the wave front, the magnitude of η at the wave-front being 1. The deflection at any point in the disturbed area, $W(\eta, t)$, is represented by a trial function which satisfied the kinematic conditions at the point of impact and at the boundary between the excited zone and the quiet zone.

The total energies, (kinetic and strain) are calculated and Hamilton's principle introduced to obtain the dynamics of the system. Hamiltion's principle states that between times t_1 and t_2,

$$\int_{t_1}^{t_2} \delta(T-U)dt + \int_{t_1}^{t_2} \delta W dt = 0 \qquad 2.1$$

for any dynamic system, where the kinetic variables vanish at t_1 and t_2. T is the Kinetic co-energy of the system and W is the virtual work associated with slippage and internal friction. In this case, an ordinary 2nd order differential equation results and can be solved numerically using Runge-Kutta methods.

2.1.2 Application to a Triaxially woven Fabric

Leech and Mansell (31) showed that the wave front in a transversely impacted orthogonal fabric is rhomboical. This prediction is confirmed by experiments. The equation of motion they obtained is given by $t = \frac{x}{C_x} + \frac{y}{C_y}$, where t is time; Cx and Cy are respectively the wave velocities in the x- and y-directions. The triaxially woven fabric consists of three families of strands each of which makes a 60 degree angle with the adjacent yarn, Fig 2.7(c). In the first instance, the wave fronts separating the 'quiet' region from the transversely displaced region is necessarily deduced.

Consider the fabric shown in Fig 2.1 and let it be transversely impacted at any point, I.

The axes, s1, s2, s3, are as shown in Fig 2.1 along the strand directions. The fabric is then divided into six sectors. Now consider one of these sectors.

On impact, disturbances travel along Ia' and Ib' respectively. At b', the disturbance along Ib' is partly reflected, partly diverted along b'a' and partly transmitted along $b'b^2$, similarly for the disturbance along Ia' when it reaches a'.

A strand parallel to s3, such as a $'b'$ is disturbed at both ends.

After the two waves have passed through it, it would become horizontal and unstrained for the rest of the motion. Considering only the tranmission of out-of-plane transverse waves, it is clear that, at time t after signal initiation, the stress front in this section is given by:

$$t = \frac{s1}{\bar{C}1} + \frac{s2}{\bar{C}2} \qquad 2.2a$$

similarly, the wave front equations in the 5 other sectors are:

$$t = -\frac{s1}{\bar{C}1} - \frac{s2}{\bar{C}2} \qquad 2.2b$$

$$t = \frac{s2}{\bar{C}2} + \frac{s3}{\bar{C}3} \qquad 2.2c$$

$$t = \frac{s3}{\bar{C}3} - \frac{s1}{\bar{C}1} \qquad 2.2d$$

$$t = \frac{-s2}{\bar{C}2} - \frac{s3}{\bar{C}3} \qquad 2.2e$$

$$t = \frac{-s3}{\bar{C}3} + \frac{s1}{\bar{C}1} \qquad 2.2f$$

where C1, C2, C3 are the transverse wave velocities in the directions of s1, s2, and s3 respectively. The fronts whose equations are given in equations (2.2,a-f) form the sides of an hexagon. The predicted indentation is shown in Fig.10A and is confirmed by the experimental photograph, Fig. 10B (PART I)

2.1.3 Equation of Motion for small deformation

In Appendix 1, the derivation of the equation of motion for an impacted triaxial fabric is given, using the wave front predicted in section 2.1.2. The equation relating the displacement at the impact point, Wo and the non-dimensionalised time, $\bar{t}$, is given by:

$$(1 + r^2)Wo'' + 2\,r\,Wo' + \frac{\lambda I3+(I1-I2)}{I1} W_o = 0, \qquad 2.3$$

where r is related to the real time, t, by the equation

$$r = t\,a_t; \quad a_t^2 = \frac{\sqrt{3}m(C1C2+C2C3+C1C3)}{12M_p} ;$$

M_p = mass of projectile; m = area density of fabric;

$$\lambda = \frac{C1C3\left(\frac{\sigma 1}{c_1^2} + \frac{\sigma 3}{c_3^2}\right) + C_2C_1\left(\frac{\sigma 1}{c_1^2} + \frac{\sigma 2}{c_2^2}\right) + C_2C_3\left(\frac{\sigma 3}{c_3^2} + \frac{\sigma 2}{c_2^2}\right)}{m(C_1C_3 + C_1C2 + C_3C_1)}$$

and $(\;)' = \frac{\partial(\;)}{\partial r}$

I1, I2, and I3 are integrals whose values depend on the assumed shape (trial function) of the sides of the indent. The equation, corresponding to equation (2.3), for an orthogonal fabric, is given in Ref (30) as: $(1+r^2)W_o'' + 2rW_o' + \delta W_o = 0$ 2.4

where $r = a_b xt$; $a_b^2 = \frac{mC_xC_y}{3M_p}$, $\delta = \frac{I3+I1-I2}{Ii}$;

and Cx and Cy are the respective transverse wave speed along the two orthogonal strands. For comparison of the two fabrics, let C1=C2=C3=Cx=Cy and the following simplified expressions are now obtained:

$$a_t^2 = \frac{3mC1^2}{4M_p} \; ; \quad \text{and} \quad \lambda = 2/3$$

Also, equation 2.3 could be written as:

$$(1+r^2)Wo''+2rWo'+\left(\frac{\frac{2}{3}I3+I1-I2}{I1}\right)Wo = 0 \qquad 2.5$$

and equation 2.4 as

$$(1+r^2)Wo''+2rWo'+\frac{I3+I1-I2}{I1}Wo = 0 \qquad 2.6$$

Equation 2.5 is only different from 2.6 in that in equation 2.5 the term I3 is multiplied by 2/3, while in equation 2.6 it is multiplied by 1. The last expression of the left hand side of equation 2.5 (or equation 2.6) was obtained from strain energy considerations and the factor of 2/3 in equation 2.5 represents a reduction in strain energy per unit area in the triaxial weave case due to the fact that in each of the six slanted faces of the pyramid, one family of strands remain horixontal and unstrained. The material utilisation factor for the triaxial weave, relative to the biaxial, in absorbing projectile energy by strand straining, is 2/3.

The ratio of the displaced areas is 1.3:1, to the advantage of the triaxially woven fabric, which is less than 1:2/3 or (1.5:1), the ratio of material utilisation factors. It is reasonable, therefore, to conclude that more strain energy may be absorbed, in a given time, by an orthogonally woven fabric than by a triaxially woven fabric of the same area density.

The ratio of the time factors, $a_t / a_b = 1.30$,

since $a_t = \sqrt{\frac{3mC1^2}{4M_p}}$ and $a_b = \frac{mC1^2}{3M_p}$

This ratio results from the fact that in a given time, the transversely displaced area is larger in the fabric with 0-60° -120° arranged strands than in another fabric of equal area density in which the yarn directions are perpendicular. It is reasonable to suppose that the kinetic energy of the triaxial fabric is higher at any time after impact than that of the biaxial fabric. This combination of these two generally produces a difference between the performances of the two fabrics of equal area density, one with orthogonally woven yarns and the second with triaxial weave.

2.1.4 Equation of Motion for Large Deformation

Equation 2.3 and 2.4, above, are only applicable for small strains. For large strains the full, non-linear strain expressions are needed.

It was shown in Appendix 1 that the equation of motion for the triaxial fabric then becomes:

$$(1+r^2)Wo''+2rWo'+6Wo\left(\frac{k1b1}{\varepsilon_1}\left(1+\varepsilon_1-\frac{1}{\sqrt{(1+(W_oa/C_1r)^2)}}\right)(1+\varepsilon_1)\right.$$

$$+\frac{k2b2(1+\varepsilon_2)}{\varepsilon_2}\left(1+\varepsilon_2-\frac{1}{\sqrt{(1+(Woa/C2r)^2)}}\right)+$$

$$\left.\frac{k3b3(1+\varepsilon_3)}{\varepsilon_3}\left(1+\varepsilon_3-\frac{1}{\sqrt{(1+(Woa/C3r)^2)}}\right)-1/3\right)=0, \qquad 2.7$$

where $k1 = \frac{C1C3+C1C2}{C1C3+C1C2+C2C3}$;

$k2 = \frac{C1C3+C1C2}{C1C2+C1C3+C2C3}$;

$$k3 = \frac{C2C3+C1C3}{C1C2+C2C3+C3C1}$$; and b1, b2, and b3 are the mass fraction of the s1, s2, and s3 strands.

For an orthogonally woven fabric, the corresponding equation is:

$$(1+r^2)Wo''+2r\,Wo'+6Wo\left(\left(\frac{1+\varepsilon_x}{\varepsilon_x}\right)\left(1+\varepsilon_x-\frac{1}{\sqrt{\left(1+(Woa/C_x r)^2\right)}}\right)\right.$$

$$\left.+\left(\frac{1+\varepsilon_y}{\varepsilon_y}\right)\left(1+\varepsilon_y-\frac{1}{\sqrt{\left(1+(Woa/Cy r)^2\right)}}\right)-1/3\right)=0 \qquad 2.8$$

Putting the wave velocities equal, as before, equation 2.7 and equation 2.8 respectively become:

$$(1+r^2)Wo''+2r\,Wo'+6Wo\left(2/3\frac{1+\varepsilon}{\varepsilon}\left(1+\varepsilon-\frac{1}{\sqrt{(1+(Woa/Cr)2)}}\right)-1/3\right)=0 \qquad 2.9$$

and

$$(1+r^2)Wo''+2rWo'+6Wo\left(\frac{1+\varepsilon}{\varepsilon}\left(1+\varepsilon-\frac{1}{\sqrt{(1+(Woa/Cr)2}}\right)-1/3\right)=0 \qquad 2.10$$

Comparing equation 2.9 with equation 2.10, it is clear that, again, the triaxial arrangement of the strands leads to a larger time factor, a_t, and, at the same time, causes an underutilisation of a third of the fabric as far as the absorption of energy by strain is concerned.

The above observations suggest that in a multilayer ply, there might be some improvement in performance if the direction of the yarns in two orthogonally woven fabrics are set at 45° to one another so as to gain the advantages of the two different weaves.

This possibility may be examined in details by more accurate methods.

2.2 NODAL IMPEDANCE METHOD

2.2.0 Introduction

The absorption of impact by fabrics is accomplished by the propagation of the input energy away from the directly impacted zone. Energy is dispersed into connecting members in the fabric via the node connections. In general three types of signals are generated in the yarns of a fabric on impact. These are, in the plane of the yarns; the transverse signal and the extensional signal, and, perpendicular to the plane, the out-of-plane transverse signal. At the nodes, each type of signal may generate one or more of the three types of signals in the connecting yarns, depending on the fabric weave.

The yarns normally undergo large deformations and consequently the complete non-linear string equations would be employed to model the response of such systems. The string equations have been developed by various investigators; for example see Ref 30. They form a non-linear hyperbolic system with two distinct propagation speeds, namely, the propagation speed of extensional (fast) and transverse (slow) disturbances. The nonlinearities arise from considerations of gross deformation of the string (yarn) and from the admission of nonlinear constitutive relations.

In this section, the propagation of disturbances through fabrics of various weaves is considered, the linearised decoupled string equations are employed and coupling between extensional and transverse waves is initiated when nodes are encountered.

The effectiveness of the weaves is assessed by comparing the percentages of the incident disturbed signals which are reflected at a node.

2.2.1 Linearized string Theory

The linearized equations of motion of the strings are easily derivable and are summarised in this section.

(a) Extensional motion

The equation of motion is

$$\rho \frac{\partial^2 u}{\partial t^2} - E \frac{\partial^2 u}{\partial x^2} = 0 \qquad 2.3.1$$

where ρ is the material density, E is the modulus of elasticity, X is a running co-ordinate along the string, t is time and u(x,t) is longitudinal displacement of the string. The material strain is simply given by

$$\varepsilon = \frac{\partial u}{\partial x} \qquad 2.3.2$$

The equation of motion admits the following characteristic solution

$u = Fe\ (x - C_e t)$ and $u = G_e(x + C_e t)$

where $C_e (= \sqrt{(E/\rho)})$ is the propagation speed of extensional signals. The two characteristic solutions represent outgoing (right-travelling) and ingoing signals (left-travelling) and they suggest that there is no attenuation or dispersion of the wave front.

(b) Transverse motion

The equation of motions, in this case, is

$$\rho A \frac{\partial^2 v}{\partial t^2} - T \frac{\partial^2 v}{\partial x^2} = 0, \qquad 2.3.3$$

where A is the string cross-sectional area, T is the pre-tension and $V(X, t)$ is the transverse displacement of the string. The equation of motion for transverse disturbances, admits characteristic solutions

$$V = F_t(X - C_t t) \text{ and } V = G(x + C_t t),$$

where $C_t (= \sqrt{(T/\rho A)})$, is the propagation speed of transverse signals.

The material strain induced by the transverse motion is, for small motions:

$$= \tfrac{1}{2} \left(\frac{\partial v}{\partial x} \right)^2 \qquad 2.3.4$$

Although this is a second order quantity, it will propagate ahead of the transverse signal with the extensional propagation speed, C_e.

2.2.2 NODE EFFECTS NEAR IMPACT ZONE

When a disturbance propagating through a yarn encounters a node, only part of the signal will pass through the node, while another part of the signal is reflected. The attenuation will be dependent upon the type of disturbance (extensional, in-plane transverse or out-of-plane transverse), upon the material characteristics of the yarns meeting at the node, and upon the weave pattern. This node, as well as transmitting part of the signal, will cause a reflection back towards the signal source and a diversion along the branch yarns and for in-plane motions, a change of mode along the connecting yarns.

In an impact zone, energy is continuously provided by the projectile as it is retarded. Three types of signals are propagated along the impacted yarns. The signals are consequently partly transmitted, partly diverted to other yarns beyond the impact zone, and

partly reflected back into the zone. At a rate of energy input, the chances of yarn failure increases as the percentage reflection of signals back into the directly impacted yarns. The influence of yarn arrangement on this percentage is an indicator of weave efficiency.

In the first instance, the passage of an out-of-plane transverse input disturbance through a node is considered. Only two weave patterns, the orthogonal and the (0 - 60° - 120°) triaxial are considered. The general equations for the passage of in-plane signals are then derived and expressions obtained for a few weave patterns.

2.3.1 Out-of-plane Transverse Signals

The discussion refers to Fig. 2.4(a), 2.4(b), 2.5(a) and 2.5(b).

In an orthogonal weave, a disturbance along IM, the incident at I, creates signals in the three other yarns connected to I, that is in IK, IL and IJ. The input signal in IM, $f_1(\xi - C_{xt}t)$, gives rise to a transmitted signal $f_2(\xi - C_{tx}t)$, a reflected signal $g(\xi + C_{tx}t)$ and signals in the cross elements $h(\xi - C_tgt)$ where ξ is a coordinate along a yarn.

Referring to Fig 2.5, it can be shown that

$$g^1 = \frac{2}{3} f_1^1, \quad f_2^1 = \frac{1}{3} f_1^1, \quad h_1^1 = p_1 = \frac{1}{3} f_1 \qquad 2.3.5$$

and

$$h_2^1 = p_2^1 = \frac{1}{3} f_1^1 \qquad 2.3.6$$

where $(\ )^1 = \partial(\ )/\partial\xi$, the slope.

The sum of the amptitudes of the incident signal, f_1, and the reflected signal, g_1,

$= f_1 + g_1 = \frac{5}{3} f_1$ from equation 2.3.5

Leech and Mansell (31) showed that the corresponding equations for a biaxial fabric are:

$$f_2^1 = \frac{1}{2}f_1^1; \quad g_1^{11} = \frac{1}{2}f_1^1; \quad h^1 = \frac{1}{2}f_1^1, \qquad 2.3.7$$

where f_2, g_1 and h are the transmitted, reflected and diverted signals respectively.

Therefore, for a biaxial weave, the sum of the incident and reflected signals is given by

$$f_1 + g_1 = \frac{3}{2}f_1 \qquad 2.3.8$$

Since the sum is less for a biaxially woven fabric, failure due to overstraining might be expected to occur at a lower impact velocity in a triaxially woven fabric. A higher proportion of the incident signal is reflected in a triaxial fabric because the greater number of yarns poses a stiffer constraint to out-of plane motions.

The partitioning of the total input energy (kinetic and strain), Ii, into that transmitted, It, that reflected, Ir, and that diverted into the branch yarns, I_{b1}, and I_{b2}, can be shown to be given by

$$\frac{It}{Ii} = \frac{1}{9}; \quad \frac{Ir}{Ii} = \frac{4}{9}; \quad \frac{Ib1}{Ii} = \frac{Ib2}{Ii} = \frac{1}{9} \qquad 2.3.9$$

Hence the energy in the yarn carrying the incident wave, assuming continuous input of energy $= \frac{13}{9}$ Ii. $(I_r + I_i)$.

Under similar conditions for an orthogonal fabric, the energy in yarn $= \frac{5}{4}$ Ii.

2.3.2 NODAL IMPEDANCE FOR IN-PLANE SIGNALS: GENERAL EQUATIONS

The general equations for the influence of a node subjected to an in-plane incident wave along one of its connecting member will be derived. The percentage of the incident wave which is reflected along the disturbed yarn is of paramount importance, since, as mentioned earlier, a yarn arrangement which causes an high percentage of the incident wave to be reflected would produce yarn failure at [illegible] signal level.

Consider the node O in Fig 2.5 at which n + 1 yarns meet. The pretensions in the yarns are enough to prevent compression (or buckling) from occuring.

The yarn labelled 1 is subjected to an extensional wave $U(x-C_e t)$ and an in-plane transverse disturbance $V(X - C_t t)$, where the wave speeds are given by: $C_e = \sqrt{\frac{E}{\rho}}$ and $C_t = \sqrt{\frac{T}{\rho A}}$.

The reflected extensional wave is taken as $\beta U(x + C_e t)$, while the reflected in-plane transverse wave is $dV\ (x + C_t t)$. The fractions β and d are dependent on the yarn arrangement. The extensional, and the transverse disturbance generated in a typical yarn are respectively taken as $U_L(x - C_{eL} t)$ and $V_L(x - C_{tL} t)$ where the wave speeds are given by

$$C_{eL} = \sqrt{\frac{E_L}{\rho_L}} \quad \text{and} \quad C_{tL} = \sqrt{\frac{T_L}{\rho_L A_L}}$$

Compatibility at the node requires that (Fig 2.6)

$$\dot{U}_L = \dot{U}(1-\beta) \cos\alpha_L + \dot{V}(1-d) \sin\alpha_L, \qquad 2.3.10$$

resolving along the yarn, and perpendicular to the yarn:

$$\dot{V}_L = -\dot{U}(1 - \beta) \sin\alpha_L + \dot{V}(1-d)\cos\alpha_L , \qquad 2.3.11$$

where the dot denotes differentiation with respect to time and primes denotes derivatives with respect to x.

The equations can be rewritten in terms of derivatives with respect to axial length, x, as

$$C_{eL} U_L' = C_e U'(1-\beta) \cos\alpha_L + C_t V'(1-d) \sin\alpha_L$$

$$C_t V_L' = -C_e U'(1-\beta) \sin\alpha_L + C_t V'(1-d) \cos\alpha_L,$$

or

$$U_L' = \frac{Ce}{CeL} U'(1-\beta) \cos\alpha_L + \frac{Ct}{CeL} V'(1-d) \sin\alpha_L , \qquad 2.3.12$$

$$V_L' = \frac{Ct}{CtL} V'(1-d) \cos\alpha_L - \frac{Ce}{CtL} U'(1-\beta) \sin\alpha_L . \qquad 2.3.13$$

The equations 2.3.10 and 2.3.11 holds for each yarn connected to node 0.

From equilibrium considerations:

along disturbed yarn,

$$EAU'(1+\beta) = \sum (E_L A_L U_L' \cos\alpha_L - T_L V_L' \sin\alpha_L) \qquad 2.3.14$$

Substituting for U_L' and V_L' from equations 2.3.12 and 2.3.13, equation 2.3.14 becomes

$$EAU'(1+\beta) = \sum (E_L A_L \cos\alpha_L (\frac{Ce}{CeL} U'(1-\beta)\sin\alpha_L + \frac{Ct}{CeL} V'(1-d)\sin\alpha_L)$$

$$- T_L \sin\alpha_L (\frac{Ct}{CtL} V'(1-d)\cos\alpha_L \frac{Ce}{CtL} U'(1-\beta)\sin\alpha_L))$$

The terms involving the fractions β and d are all put on one side and the final equation is:

$$\beta U' \left[EA + \sum (E_L A_L - \frac{C_t}{C_{eL}} \cos^2\alpha_L + T_L \frac{Ce}{CtL} \sin^2\alpha_L)\right]$$

$$- d.V' \sum \frac{\sin 2\alpha_L}{2} \quad (E_L A_L \frac{C_t}{C_{eL}} + T_L \frac{Ct}{CtL})$$

$$= -EAU' + U' \sum (E_L A_L \cos^2\alpha_L + T_L \frac{Ce}{CtL} \sin^2\alpha_L)$$

$$- V' \sum (E_L A_L \frac{Ct}{CeL} + T_L \frac{Ct}{CtL}) \frac{\sin 2\alpha_L}{2} \qquad 2.3.15$$

Similarly, consideration of equilibrium in a direction perpendicular to the disturbed yarn gives the following:

$$TV'(1+d) = \sum (E_L A_L U_L' \sin\alpha_L + T_L V_L' \cos\alpha_L) \qquad 2.3.16$$

Upon substitution for U_L^1 and V_L^1,

$$TV^1(1+d) = \sum E_L A_L \sin\alpha_L (U_1^1 \frac{Ce}{CeL} (1-\beta)\cos\alpha_L)$$

$$+ \quad T_L \cos\alpha_L (V^1 \frac{Ct}{CtL}(1-d)\cos\alpha_L - \frac{Ce}{CtL} U^1 (1-\beta)\sin\alpha_L) +$$

$$\frac{Ct}{CeL} V' (1-d) \sin\alpha_L$$

The final form of this expression is

$$d_1 V^1 \left[T + \sum (E_L A_L \frac{Ct}{CeL} \sin^2\alpha_L + T_L \frac{Ct}{CtL} \cos^2\alpha_L \right.$$

$$- \beta U^1 \quad (ELA_L \frac{Ce}{CeL} - T_L \frac{Ct}{CtL} \frac{\sin 2\alpha_L}{2}$$

$$= - TV^1 + U^1 \sum (E_L A_L \frac{Ce}{CeL} + T_L \frac{Ce}{CtL} \quad \frac{\sin 2\alpha_L}{2}$$

$$+ V^1 \sum (T_L \frac{Ct}{CtL} \cos^2\alpha_L \quad E_L A_L \frac{Ct}{CeL} \sin^2\alpha_L) \qquad 2.3.17$$

The summation is over all the yarns connected to the node, apart from the initially disturbed yarn.

Given the number of the yarns connected to a node and the angle with a fixed direction, equations 2.3.15 and 2.3.17 would give the values of the fractions of the proportions of an in-plane disturbance which are reflected along the disturbed yarn. The expressions for the general solutions of the two equations are long and were not very useful for numerical work. It is bette for any given fabric, to generate the values of the summed expressions from the given values of α_L, T_L, E_L and A_L, and then to solve the two resulting simultaneous equations.

Once the values of β and d are evaluated, the level of the signal (U_L and V_L) in the other yarns can be calculated using equations 2.3.12

2.3.3 IN-PLANE TRANSVERSE DISTURBANCES

The equations connected with this case are obtained by putting $U^1 = 0$ in equations 2.3.15 and 2.3.17. They are:

$$V'd \sum \frac{\sin 2\alpha_L}{2} \left(E_L A_L \frac{Ct}{CeL} + T_L\right) =$$

$$- V' \sum \left(E_L A_L \frac{Ct}{CeL} + T_L \frac{Ct}{CtL}\right) \frac{\sin 2\alpha_L}{2} \qquad 2.3.18$$

and,

$$V' \cdot d \left[T + \sum \left(E_L A_L \frac{Ct}{CeL} \sin^2 \alpha_L + T_L \frac{Ct}{CtL} \cos^2 \alpha_L\right)\right]$$

$$= - TV' + V' \sum \left(T_L \frac{Ct}{CtL} \cos^2 \alpha_L + E_L A_L \frac{Ct}{CeL} \sin^2 \alpha_L\right) \qquad 2.3.19$$

The expression in equation 2.3.10 shows that an incident in-plane transverse disturbance generates, in a branch yarn, an extensional wave, if

$\sin\alpha_L \neq 0$, that is if the yarn in question is not parallel to the disturbed yarn.

In the case when only two yarns are connected together at the mode ($\alpha_1 = 180^\circ$), Fig 2.7(a), the equations reduce to

$0 = 0$ and

$$V' \cdot d \left[T + T_L \frac{Ct}{CtL}\right] = V' \left[- T + T_L \frac{Ct}{CtL}\right] \qquad 2.3.20$$

If the yarns are made of the same material, the right hand side of equation 2.3.20 is zero since the tensions are the same. This is as could be expected, and the wave would pass through the yarn without reflection since the two yarns are equivalent to a single continuous yarn. If yarn 1 is denser than the disturbed yarn, that is $C_t > C_{tL}$,

some reflection occurs. The value of d increased with the ratio of the densities until the case of a rigid (yarn) ($C_t \gg C_{tL}$) when the whole signal is reflected.

On the other hand, a wave of the opposite sign is reflected in the case when yarn 1 is lighter than the disturbed yarn ($C_{tL} > C_t$). In the terminal case with the second yarn removed, d = - 1. This is as could be expected since the free end must be stress-free.

2.3.4 EXTENSIONAL DISTURBANCES

The governing equations are:

$$-EAU' + U' \sum (E_L A_L \cos^2 \alpha_L \frac{Ct}{Cel} + T_1 \frac{Ce}{CtL} \sin^2 \alpha_L)$$

$$= \beta . U' \left[EA + \sum (E_L A_L \cos^2 \alpha_L \frac{Ct}{CeL} + T_L \frac{Ce}{CtL} \sin^2 \alpha_L) \right], \quad 2.3.21$$

$$\beta . U' \sum (E_L A_L \frac{Ce}{CeL} - T_L \frac{Ce}{CtL}) \frac{\sin 2\alpha_L}{2}$$

$$= - U' \sum (E_L A_L \frac{Ce}{CeL} + T_L \frac{Ce}{CtL}) \frac{\sin 2\alpha_L}{2} . \quad 2.3.22$$

For the case $\alpha_1 = 180$, Fib 2.(a), equation 2.3.22 is trivial, while equation 2.3.21 gives

$$\beta = \left(-EA + E_1 A_1 \frac{Ce}{CeL} \right) / \left(EA + E_1 A_1 \frac{Ce}{CeL} \right) . \quad 2.3.23$$

For the same material, $\beta = 0$, no reflection. For a free end, $CeL \gg Ce$, $\beta = -1$. At the other extreme, when the yarn carrying, the disturbance is connected to an extremely dense yarn, $\beta = 1$, complete reflection occurs and any incident strain is doubled.

2.3.5 NODAL IMPEDANCE OF DIFFERENT YARN ARRANGEMENTS

The different patterns of yarn arrangement which are discussed are shown in Figs 2.7 (a - e)

(a) ORTHOGONAL PATTERN

Joint data

$$\alpha_1 = 90^\circ, \quad \alpha_2 = 180^\circ, \quad \alpha_3 = 270^\circ .$$

(Assume equal tensions and yarn materials)

Case 1, $V^1 = 1$, $U^1 = 0$ (in-plane transverse)

$$T + 2EA\frac{Ct}{Ce} + T = -T + 2EA\frac{Ct}{Ce} + T .$$

$$d = \frac{EA\frac{Ct}{Ce}}{T + EA\frac{Ct}{Ce}} = \frac{\frac{EACt}{TCe}}{1 + \frac{EACt}{TCe}} ,$$

$$= \frac{P}{1 + P} , \text{ where } p = \frac{EACt}{TCe} . \qquad 2.3.24$$

Case 2, $V^1 = 0$, $U^1 = 1$ (Extensional disturbance)

$$\beta . EA + \beta\left(EA + 2T\frac{Ce}{Ct}\right) = -EA + EA + 2T\frac{Ce}{Ct}$$

$$\beta = \frac{T_L\frac{Ce}{Ct}}{EA + T_L\frac{Ce}{Ct}} ,$$

$$= \frac{1}{P + 1} . \qquad 2.3.25$$

Case 3 V = 1, U = 1

The value of β is equal to that of case 2 while that of d equals that of ca-e 1..

(b) TRIAXIAL PATTERN (60°-120°-180°)

Case 4 Incident extensional wave, $U' = 1$, $V' = 0$

$$\beta = \frac{EA + 3T\frac{Ce}{Ct}}{3EA + 3Tc\frac{Ce}{Ct}} = \frac{1 = P/3}{1 + p} . \qquad 2.3.26$$

Case 5 Incident in-plane disturbance $V' = 1, U' = 0$

$$d = \frac{T + 3EA\ Ct/Ce}{3T + 3EA\ Ct/Ce} = \frac{\frac{1}{3} + P}{1 + P} \qquad 2.3.27$$

Case 6 Combined incident disturbance $V' = U' = 1$

The values of β and d are given by 2.3.26 and 2.3.27

(c) SPECIAL TRIAXIAL (45°-135°-180°)

$$\alpha_1 = 45^{\circ},\ \alpha_2 = 135,\ \alpha_3 = 180,\ \alpha_4 = 225,\ \alpha_5 = 315$$

Case 7 Incident extensional signal

$$\beta\, EA + \beta\left[EA\ (\tfrac{1}{2}+\tfrac{1}{2}+1+\tfrac{1}{2}+\tfrac{1}{2}) + T_L\frac{Ce}{Ct}(\tfrac{1}{2}+\tfrac{1}{2}+0+\tfrac{1}{2}+\tfrac{1}{2})\right]$$

$$- d(EA\ \frac{Ct}{Ce} + T_L)\ (\tfrac{1}{2}-\tfrac{1}{2}+\tfrac{1}{2}-\tfrac{1}{2})$$

$$= - EA + 3EA + 2T_L\frac{Ce}{Ct} .$$

$$= \frac{2EA + T_L \frac{Ce}{LCt}}{4EA + 2T_L \frac{Ce}{LCt}} = \frac{1 + P}{1 + 2P}$$

$$= \frac{(1 + P)^2}{1 + 2P} \cdot \frac{1}{1+P} \cdot \qquad 2.3.28$$

Case 8

Incident in-plane transverse signal, $V^1 = 1$, $U^1 = 0$

$$d \left[T + EA \frac{Ct}{Ce} (\tfrac{1}{2}+\tfrac{1}{2}+0+\tfrac{1}{2}+\tfrac{1}{2}) + T \ (\tfrac{1}{2}+\tfrac{1}{2}+1+\tfrac{1}{2}-\tfrac{1}{2}) \right]$$

$$- \beta \ (EA - T \frac{Ce}{Ct}) \ (\tfrac{1}{2}-\tfrac{1}{2}+\tfrac{1}{2}-\tfrac{1}{2})$$

$$= - T + T \ (\tfrac{1}{2}+\tfrac{1}{2}+1+\tfrac{1}{2}+\tfrac{1}{2}) + EA \frac{Ct}{Ce} (\tfrac{1}{2}+\tfrac{1}{2}+0+\tfrac{1}{2}+\tfrac{1}{2}) \cdot$$

$$d \left[4T + 2EA \frac{Ct}{Ce} \right] = 2T + 2EA \frac{Ct}{Ce}$$

$$d = \frac{2T + 2EA\frac{Ct}{Ce}}{4T + 2EA\frac{Ct}{Ce}} = \frac{1 + P}{2 + P}$$

$$= \frac{(1 + P)^2}{2 + P} \cdot \frac{1}{1 + P} \cdot \qquad 2.3.29$$

(d) LIMIT PATTERN WITH LARGE NUMBER OF YARNS

In the limit when the number of yarns are large and uniformly arranged, the summation signs of equations 2.3.15 and 2.3.17 are replaced by integration signs. This is how the result below is obtained. This limit case is practical with the regular 'fan' arrangement of yarns which are then held together in a matrix.

Case 9 Incident extensional disturbance, $U' = 1$, $V' = 0$

$$\beta\left[EA + (EA + T\frac{Ce}{Ct})\right] + d.o = -EA + \pi\left[EA + T\frac{Ce}{Ct}\right]$$

$$\beta = \frac{EA(\pi - 1) + \pi T\frac{Ce}{Ct}}{EA(\pi + 1) + \pi T\frac{Ce}{Ct}} = \frac{0.6819P + 1}{1.318P + 1}$$

$$= \frac{(\pi - 1)P + \pi}{(\pi + 1)P + \pi}(1 + P) \quad \frac{1}{1 + P} \qquad 2.3.30$$

$$= \frac{0.6819P + 1}{1.318P + 1} \cdot (1 + P) \cdot \frac{1}{(1+P)}$$

Case 10 Incident in-plane transverse disturbance $V = 1$, $U = 0$

$$d\left[T + \pi\left(EA\frac{Ct}{Ce} + T\right)\right] = -T + (T + EA\frac{Ct}{Ce})\pi$$

$$d = \frac{T(\pi - 1) + \pi EA\frac{Ct}{Ce}}{T(\pi + 1) + \pi EA\frac{Ct}{Ce}} = \frac{\frac{\pi - 1}{\pi} + P}{\frac{\pi + 1}{\pi} + P} \qquad 2.3.31$$

$$= \frac{(0.6819 + P)}{1.318 + P}(1 + P) \quad \frac{1}{1 + P}$$

2.3.6 ENERGY PARTITIONING

In order to compare the 4 different yarn arrangement patterns, the rates at which energy is reflected are calculated.

The energy dissipated in time t are

$$\text{Incident energy} = \frac{C_t t T(V')^2}{2} + \frac{C_e EA t (U')^2}{2}$$

$$\text{Reflected energy} = C_t t \frac{T d^2 (V')^2}{2} = C_e t \frac{EA \beta^2 (U')^2}{2}$$

The percentage energy reflected is proportional to β^2 and d^2. The values of β^2, d^2 are compared for the different yarn patterns.

In Fig 2.8, the values of β^2 and d^2 are each plotted against values of $^1/P$. The range of values of $\frac{1}{p}$ used is 0 - 1. This range corresponds to values of p from ∞ to 1.0 and the range of strain from 0.0 to 1.0.

Note that for a yarn made of Hooken material:

$$P = \frac{EACt}{TCe} = \frac{EA\sqrt{\frac{T}{PA}}}{T\sqrt{E/\rho}} = \sqrt{\frac{EA}{T}} = \frac{1}{\sqrt{\varepsilon}} \qquad 2.3.32$$

$$p^2 = \frac{1}{\varepsilon}, \quad \frac{1}{p^2} = \varepsilon \qquad 2.3.33$$

It is the region of low values of prestrain, ε, which are of practical interest. This region, as the graphs show, is also the region where the percentage of incident signal which is reflected is highest.

The most "efficient" yarn arrangement is the orthogonal, since this arrangement produces the lowest percentage of reflected energy both in-plane transverse disturbance and extensional disturbance. At very low prestrains, the percentage of input in-plane transverse signal which is reflected in case 8 is less than that in case (1).

The graphs for the different yarn arrangements are very close to one another at low prestrains, for in-plane transverse disturbances; which means that the arrangement of the yarns would not appreciably affect the performance of the fabrics. At zero pretension, in Ref (61), a very low reflection coefficient (approximately 0.01) is estimated for typical fabrics.

The optimum condition occurs at p = 1, or when the prestrain equals unity. Most yarns would fail long before this strain is attained so this condition cannot be realised. Even if such prestrains could be attained, the practical difficulty of designing rigid anchors necessary to maintain the fabric under the high strain remains.

2.4 SUMMARY

In these simplified analyses, slip, friction and geometric nonlinearities were not considered.

The results show that a biaxially woven fabric may fail at a higher impact velocity for a given area density, than another fabric of a different weave pattern. This is true for out-of-plane disturbances, and in-plane disturbances.

CHAPTER 3

CHARACTERISTIC THEORY

3.0 Introduction

In this chapter, an application of the method of characteristics to the analysis of the dynamic response of densely woven fabric is described. The fabric is analysed as a network of the yarns. The expressions for the kinetic and strain energy in a yarn are stated and both the equation of motion of the yarn and the compatibility equations for the yarn crossovers are obtained. A technique using the theory of characteristics is then employed in a discrete fashion to determine the motion of each crossover or node. The motion of the fabric is then defined by the motion of each node.

The method has, computationally, advantages over a finite element model with consistent mass formulation in that, for the same discretisation, the rank of the largest matrix to be inverted in the solution by the method of characteristics is 3 against n^2 (where n is the number of nodes in the finite element model). It is also better suited for wave front predictions. This is because the positions of the waves fronts, even then they are between nodes, could be determined directly with the characteristics equations. Whereas in the finite element solution, the wave-front is not usually sharp, but smoothened and spread out.

3.1 THEORY

The following assumptions are made;

1) the centreline of the yarns are initially straight.

ii) The yarns are rigidly fixed at the nodes, slip and separation of the yarns are not allowed.

iii) the yarns are completely flexible and the energies associated with bending or twist is negligible.

3.1.1 FIBRE/YARN DYNAMICS

For a hyperelastic yarn material, there is a work or strain energy functional W which is a function of only the extensional Green strain E; the dependency of this functional on the other components of strain is assumed to be very weak since the yarn is stiff in tension but weak in flexure and shear.

the extension Green strain E is written as

$$E = u' + \tfrac{1}{2}(u'^2 + v'^2 + w'^2), \qquad 3.1.1$$

where u, v, w are the motions of the yarn in the extensional and two transverse directions, Fig. 3.1. the strain energy functional is thus

$$W = W(E) \equiv W(u', v', w'). \qquad 3.1.2$$

The kinetic energy of the yarn is simply obtained and the Lagrangian $\mathcal{L}$ for a complete yarn, length L, density ρ and rosette area A is thus

$$\int_0^L \left\{ \frac{\rho A}{2}(\dot{u}^2 + \dot{v}^2 + \dot{w}^2) - W A \right\} ds, \qquad 3.1.3$$

where $\dot{u} = \dfrac{\partial u}{\partial s}$

and $\dot{u} = \frac{\partial u}{\partial t}$,

and t and s are time and position along the yarn.

Now by applying Hamilton's principle to each yarn, and ignoring for a moment the end conditions, then the following equations hold with the span of the yarns.

$$\rho\ddot{u} - \left\{\frac{d^2W}{dE^2}(1+u')^2 + \frac{dW}{dE}\right\}u'' - \frac{d^2W}{dE^2}(1+u')v'v'' - \frac{d^2W}{dE^2}(1+u')w'w'' = 0 \qquad 3.1.4(a)$$

$$\rho\ddot{v} - \frac{d^2W}{dE^2}(1+u')v'u'' - \left\{\frac{d^2W}{dE^2}v'^2 + \frac{dW}{dE}\right\}v'' - \frac{d^2W}{dE^2}v'w'w'' = 0 \qquad 3.1.4(b)$$

$$\rho\ddot{w} - \frac{d^2W}{dE^2}(1+u')w'u'' - \frac{d^2W}{dE^2}v'w'v'' - \left\{\frac{d^2W}{dE^2}w'^2 + \frac{dW}{dE}\right\}w'' = 0 \qquad 3.1.4(c)$$

These three coupled non-linear partial differential equations form a hyperbolic set with three pairs of characteristic equations. One of these pairs is associated with the propagation of extension waves and propagates with the velocity

$$C_e = \sqrt{\left(T + (1+2E)\frac{dT}{dE}\right)/\rho} \qquad 3.1.5$$

where T, the 2nd Piola-Kirchhoff stress, is given by $\frac{dW}{dE}$

and $\frac{d^2W}{dE^2} = \frac{dT}{dE}$ is the modulus of elasticity of the yarn. The remaining pairs of characteristics propagate with the common velocity

$$C_t = \sqrt{T/\rho}$$

where C_t is the propagation velocity of transverse waves.

At this point, a set of parameters is substituted solely for simplicity and ease of development;

let $p = \dot{u}$, $q = \dot{v}$, $r = \dot{w}$ 3.1.6

and $\theta = u'$, $\phi = v'$, $\psi = w'$. 3.1.7

Then $E = \theta + \frac{1}{2}(\theta^2 + \phi^2 + \psi^2)$, 3.1.8

and the equations of motion become

$$\rho\dot{p} - \left\{\frac{d^2W}{dE^2}(1+\theta)^2 + \frac{dW}{dE}\right\}\theta' - \frac{d^2W}{dE^2}(1+\theta)\phi\phi' - \frac{d^2W}{dE^2}(1+\theta)\psi\psi' = 0, \quad 3.1.9(a)$$

$$\rho\dot{q} - \frac{d^2W}{dE^2}(1+\theta)\phi\theta' - \left\{\frac{d^2W}{dE^2}\phi^2 + \frac{dW}{dE}\right\}\phi' - \frac{d^2W}{dE^2}\phi\psi\psi' = 0, \quad 3.1.9(b)$$

$$\rho\dot{r} - \frac{d^2W}{dE^2}(1+\theta)\psi\theta' - \frac{d^2W}{dE^2}\phi\psi\phi' - \left\{\frac{d^2W}{dE^2}\psi^2 + \frac{dW}{dE}\right\}\psi' = 0, \quad 3.1.9(c)$$

and

$$\dot{\theta} - p' = 0, \quad 3.1.9(d)$$

$$\dot{\phi} - q' = 0, \quad 3.1.9(e)$$

$$\dot{\psi} - r' = 0. \quad 3.1.9(f)$$

This set of six first order, non-linear, partial differential equations will be referred to in the later section on the application of characteristics.

3.1.2 Node Conditions

In the previous section, the end conditions associated with each yarn have been ignored. They will now be considered for each yarn intersecting a node and a compatibility condition for each node will be applied.

Firstly, the end variation for each yarn can be shown to be

$$\frac{dW}{dE_i}\left\{\frac{\partial E}{\partial u'}\delta u + \frac{\partial E}{\partial v'}\delta v + \frac{\partial E}{\partial w'}\delta w\right\}$$

applied at each end of the yarn.

Now let each yarn originate from the node under consideration and now label each yarn. The natural boundary condition then becomes

$$\sum_{i=1}^{m} A_i \frac{dW_i}{dE_i}\left\{\frac{\partial E_i}{\partial u_i'}\delta u_i + \frac{\partial E_i}{\partial v_i'}\delta v_i + \frac{\partial E_i}{\partial w_i'}\delta w_i\right\}_{s=0} = 0 \quad 3.1.10$$

where there are m yarns meeting at the node.

Now let the joint movement be u, v, w, and since each yarn end must respond with the node, the following compatibility equations result

$$Ui = U\cos\chi_i + V\sin\chi_i, \qquad 3.1.11(a)$$

$$Vi = -U\sin\chi_i + V\cos\chi_i, \qquad 3.1.11(b)$$

$$Wi = W, \qquad 3.1.11(c)$$

where χ_i is the initial angle orientation to the frame axis. Fig 3.3

It then follows that the constraint equations apply

$$\delta u_i = \delta u\cos\chi_i + \delta v\sin\chi_i, \qquad 3.1.12(a)$$

$$\delta v_i = -\delta u\sin\chi_i + \delta v\cos\chi_i, \qquad 3.1.12(b)$$

$$\delta w_i = \delta w, \qquad 3.1.12(c)$$

and the node equations then become

$$\delta u\sum_{i=1}^{m} A_i\frac{dW_i}{dE_i}\{(1+\theta_i)\cos\chi_i - \phi_i\sin\chi_i\} = 0,$$

$$\delta v\sum_{i=1}^{m} A_i\frac{dW_i}{dE_i}\{(1+\theta_i)\sin\chi_i + \phi_i\cos\chi_i\} = 0, \qquad 3.1.13$$

$$\delta w\sum_{i=1}^{m} A_i\frac{dW_i}{dE_i}\psi_i = 0,$$

since δu, δv and δw are independent; however, since they are also arbitrary as they are virtual displacements, it must follow that their multipliers are zero and the node equations then become

$$\sum_{i=1}^{m} A_i\frac{dW_i}{dE_i}\{(1+\theta_i)\cos\chi_i - \phi_i\sin\chi_i\} = 0,$$

$$\sum_{i=1}^{m} A_i\frac{dW_i}{dE_i}\{(1+\theta_i)\sin\chi_i + \phi_i\cos\chi_i\} = 0, \qquad 3.1.14$$

$$\sum_{i=1}^{m} A_i\frac{dW_i}{dE_i}\psi_i = 0.$$

If there is a point mass located at the node then these equations have to be re-written to take account of the kinetic energy of the mass located at the node. They now become

$$M\dot{p} - \sum_{i=1}^{m} A_i \frac{dW_i}{dE_i}\{(1+\theta_i)\cos\chi_i - \phi_i \sin\chi_i\} = 0,$$

$$M\dot{q} - \sum_{i=1}^{m} A_i \frac{dW_i}{dE_i}\{(1+\theta_i)\sin\chi_i + \phi_i \cos\chi_i\} = 0, \qquad 3.1.15$$

$$M\dot{r} - \sum_{i=1}^{m} A_i \frac{dW_i}{dE_i}\psi_i = 0.$$

3.1.3 Solution Strategy

The solution to the fabric dynamics problem, as has been stated, is defined by the deflections of each node or crossover. In woven fabrics the free span of yarn is small since the material is an array of closely packed yarns, it is sensible to consider the node equations as equally important as the yarn equations.

Consequently, the yarn equations are written in characteristics form, and more specifically as backward going characteristics, and meeting the node all at the same time; they now become, in difference form,

$$(1+\theta_i)\Delta p_i + \phi_i \Delta q_i + \psi_i \Delta r_i + C_e\{(1+\theta_i)\Delta\theta_i + \phi_i \Delta\phi_i + \psi_i \Delta\psi_i\} = 0, \qquad 3.1.16(a)$$

$$\phi_i \Delta p_i - (1+\theta_i)\Delta q_i + C_t\{\phi_i \Delta\theta_i - (1+\theta_i)\Delta\phi_i\} = 0, \qquad 3.1.16(b)$$

$$\psi_i \Delta p_i - (1+\theta_i)\Delta r_i + C_t\{\psi_i \Delta\theta_i - (1+\theta_i)\Delta\psi_i\} = 0. \qquad 3.1.16(c)$$

Equation 3.1.16(a) is the backward going extensional wave and the difference operator is applied between point d and point a along the I characteristic, Fig. 3.2 Equation 3.1.16(b) and 3.1.16(c) are applied along the backward going transverse characteristics, II, and the operator Δ in this case, is the difference between the values at point d and point b. The time step Δt and hence the point d is dictated by the condition that all of the characteristics shall originate from a point in the free span in the yarn and not from beyond the neighbouring nodes.

Given the point d or the time step Δt, the points a and b, the origin of the relevant characteristic is found by projecting backwards from point d with the appropriate slopes C_e and C_t; however, these slopes do change since they depend on the local strain and hence the

local deflections. An iterative process is then used to account for this curvature, the procedure being as follows: First, using the conditions at the node (d^1) which are known and at node c, an estimate is made for points a and b. The values of strain and hence propagation velocities at these points is then evaluated and averaged with those of point d. These average quantities are then used to find a new estimate of points a and b and the process is repeated a number of times (approximately five) to ensure a reasonably accurate location of the points a and b. the iteration scheme is shown in Fig. 3.4 and Fig. 3.5

The equations 3.1.16(a), (b), (c) can then be used to search for the six unknowns of the yarn, namely pi, qi, ri and θ_i, ϕ_i, ψ_i at the point d. However, the velocities are constrained by the node compatibility equation to the global node velocities.

That is

$$\begin{aligned} p_i &= p\cos\chi_i + q\sin\chi_i, \\ q_i &= -p\sin\chi_i + q\cos\chi_i, \\ r_i &= r. \end{aligned} \qquad 3.1.17$$

Thus, at each node there are three velocity unknowns (p, q, r) and three deformation gradients (θ_i, ϕ_i, ψ_i) for each connecting yarn. There are three backward going characteristic equations for each connecting yarn and, finally, there are the three node equations to complete the solution.

Two approaches for the incorporation of these nodal equations are now considered. Firstly, if the problem is solely concerned with fabric dynamics without any impacting masses, the equations are firstly differentiated and then numerically integrated.

The differentiated equations are

$$\sum_{i=1}^{m} A_i \frac{dW}{dE}\left\{\dot\theta_i\cos\chi_i - \dot\phi_i\sin\chi_i\right\} + A_i \frac{d^2W}{dE^2}\left\{(1+\theta_i)\cos\chi_i - \phi_i\sin\chi_i\right\}(1+\theta_i)\dot\theta_i + \dot\phi_i\phi_i + \psi_i\dot\psi_i\} = 0$$

$$\sum_{i=1}^{m} A_i \frac{dW}{dE}\left\{\dot\theta_i\sin\chi_i + \dot\phi\cos\chi_i\right\} + A_i \frac{d^2W}{dE^2}\left\{(1+\dot\theta_i)\sin\chi_i + \phi_i\cos\chi_i\right\}(1+\theta_i)\dot\theta_i + \phi_i\dot\phi_i + \psi_i\dot\psi_i\} = 0$$

m . . . .

or in matrix form

$$\sum_{i=1}^{m} [E_i] \{\underset{\sim}{\theta}\}_i^{\cdot} = 0 \qquad 3.1.19$$

where

$$\underset{\sim}{\theta}_i \equiv \{\theta_i, \phi_i, \psi_i\} . \qquad 3.1.20$$

this matrix equation can be written in difference form

$$\sum_{i=1}^{m} [E_i] \{\underset{\sim}{\theta}_i\}_i^{D} = \sum [E_i] \{\underset{\sim}{\theta}_i\}_i^{O} \qquad 3.1.21$$

where the superscripts D and O refer to the positions, Fig, 3.5.

Using this approach, the problem is then well posed for numerical evaluation using simple matrix algebra. For each joint, the problem to be solved is the following matrix inversion:

$$\begin{bmatrix} 0 & E_1 & E_2 & - & - & - \\ A_1 & B_1 & 0 & - & - & - \\ A_2 & 0 & B_2 & - & - & - \\ | & | & | & - & - & - \\ | & | & | & - & - & - \\ | & | & | & - & - & - \end{bmatrix} \begin{bmatrix} p \\ q \\ r \\ \theta_1 \\ \phi_1 \\ \psi_1 \\ \theta_2 \\ \phi_2 \\ \psi_2 \\ | \\ | \\ | \end{bmatrix} \quad \begin{bmatrix} \underset{\sim}{F} \\ \underset{\sim}{C}_1 \\ \underset{\sim}{C}_2 \\ . \\ | \\ | \end{bmatrix} \qquad 3.1.22$$

where the matrices A, B and C are obtained from the characteristic equations. The rank of the above system is 3m + 3 where there are m connecting yarns into that joint. Each joint can be solved, for that time, independently of the neighbours, and a march through the structure will complete the solution for one time step.

The problem above can be reduced by noting that

$$A_i \underset{\sim}{P} + B_i \underset{\sim}{\theta}_i = \underset{\sim}{C}_i \quad \text{for} \quad i = 1, 2, \ldots m, \qquad 3.1.23$$

$$\text{and} \sum_{i=1}^{m} E_i \underset{\sim}{\theta}_i = F_i . \qquad 3.1.24$$

$$\text{Then} \quad \underset{\sim}{\theta}_i = B_i^{-1} [\underset{\sim}{C}_i - A_i \underset{\sim}{P}] , \qquad 3.1.25$$

$$\text{and hence} \sum_{i=1}^{m} E_i B_i^{-1} [\underset{\sim}{C}_i - A_i \underset{\sim}{P}] = \underset{\sim}{F} . \qquad 3.1.26$$

Solving then for $\underset{\sim}{P}$ gives

$$\underset{\sim}{P} = \left(\sum_{i=1}^{m} E_i B_i^{-1} A_i\right)^{-1} \left[\sum_{i=1}^{m} E_i B_i^{-1} \underset{\sim}{C}_i - \underset{\sim}{F}\right] . \qquad 3.1.27$$

The problem has thus been reduced to that of finding the inverses of matrices, rank 3, rather than matrices, rank 3m + 3.

In the case where there are impacting masses, the differentiation of the joint equation leads to rates of change of acceleration and there is no improvement in this formulation; instead a finite difference formulation of the joint equation is used; they thus become

$$P^d - \frac{\Delta t}{2M} \sum_{i=1}^{m} A_i \frac{dW}{dE} \{\cos\chi_i \theta_i^d - \sin\chi_i \phi_i^d\} = P^c + \frac{\Delta t}{2m} \sum_{i=1}^{m} A_i \frac{dW}{dE} \{(2+\theta_c)\cos\chi_i - \phi_i^c \sin\chi_i\} ,$$

$$q^d - \frac{\Delta t}{2M} \sum_{i=1}^{m} A_i \frac{dW}{dE} \{\theta_i^d \sin\chi_i + \phi_i^d \cos\chi_i\} = q^c + \frac{\Delta t}{2m} \sum_{i=1}^{m} A_i \frac{dW}{dE} \qquad 3.1.28(a)$$

$$+ \phi_i^c \cos\chi_i\} , \qquad 3.1.28(b)$$

$$r^d - \frac{\Delta t}{2M} \sum_{i=1}^{m} A_i \frac{dW}{dE} \psi_i^d = r^c + \frac{\Delta t}{2M} \sum A_i \frac{dW}{dE} \psi_i^c , \qquad 3.1.28(c)$$

and in this case the matrix form is

$$[I] \underset{\sim}{P}^d - \sum_{i=1}^{m} E_i \underset{\sim}{\theta}_i^d = [I] \underset{\sim}{P}^c + \sum_{i=1}^{m} E_i \underset{\sim}{\theta}_i^c = \underset{\sim}{F} . \qquad 3.1.29$$

A similar mode of solution is employed to that previously described and, in this case,

$$\underset{\sim}{P} = \left[I + \sum_{i=1}^{m} E_i B_i^{-1} A_i\right]^{-1} \left[\sum_{i=1}^{m} E_i B_i^{-1} \underset{\sim}{C}_i + \underset{\sim}{F}\right] . \qquad 3.1.30$$

In this latter approach, improved approximation $\frac{dW}{dE}$, the intermediate values of θ, ϕ and ψ and the propagation velocities C_e and C_t are obtained by performing a two pass system at each joint. The first pass finds approximate values for the joint motion and yarn deformation gradients at point . These are then used to improve the approximation

for the above and these improved values are then used to find better values for the joint movements and yarn deformation gradients.

3.2 LINEAR OUT-OF-PLANE TRANSVERSE WAVE MODEL

This model involves only the out-of-plane transverse wave, as all in-plane motions were neglected. This model was developed to overcome the buckling of the yarns which may occur when the equations developed in Section 3.1 are applied to the analysis of a fabric under low prestrain. The minimum prestrain above which no yarn of a fabric will buckle increases with the velocity of impact.

The model is applied to a highly stressed fabric where

$$\frac{dW}{dE} \gg \frac{dw}{dE}, \quad \frac{dW}{dE} u^2{}_{,s}, \quad \frac{dw}{dE} v^2{}_{,s} \text{ or } \frac{dw}{dE} w^2{}_{,s} \text{ and}$$

the product terms are small, Equation 3.1.4(c) then reduces to

$$\rho\ddot{w} - T.w'' = 0, \qquad 3.2.1$$

where $T = \frac{dW}{dE}$, the tension which is taken as constant. The corresponding characteristic equation is:

$$\Delta r_i - C_t \Delta \psi_i = 0, \qquad 3.2.2$$

$$C_t = \sqrt{(T/\rho)} \qquad 3.2.3$$

The nodal equilibrum equation is:

$$M\ddot{r} - \sum_{i=1}^{m} A_i T_i \psi_i = 0. \qquad 3.2.4$$

The solution is obtained with the strategy described in Section 3.1.3

3.3 QUASI-LINEAR OUT-OF-PLANE TRANSVERSE WAVE MODEL

In order to maintain the accuracy of the linear model described in Section 3.2 without losing much of its simplicity, the condition that the tension in the yarn remain constant during motion was remcved. The relevant equations are:

$$\Delta r_i - C_t \Delta \psi_i = 0, \text{ where } C_t = \sqrt{\left(\frac{1}{\rho}\frac{dW}{dE}\right)}$$

and the equilibrum equation

$$M\ddot{r} - \sum_{i=1}^{m} A_i \frac{dW_i}{d\varepsilon_i} \psi_i = 0 .$$

CHAPTER 4

FINITE ELEMENT MODELS

4.0 Introduction

The theory of the finite element method has been described in many books and publications and would therefore not be repeated here.

Interested readers are referred to either the book by Zienkiewicz (57) or the book by Irons and Ahmed (58).

There are many possible approaches to the formulation of the equations of state of the finite elements. Some involved only one independent field while others involve two or more independent fields. The variational statements used in the work reported here involve displacement as the only independent field.

A short theoretical background to the equations of motion is given.

Four different models are described. Each was developed for the investigation of the significance of specific fabrics parameters to the overall structural performance. The four models are:

1) A space-truss model - with crimp, slip and shear in single layers.
2) A membrane model for single layers, as well as multilayers.
3) A combination of membrane elements and three dimensional elements to model compression and slip.

4) A two-dimensional, layered membrane model which allows slip between layers, called the master-slave layer model.

4.1 GENERAL BACKGROUND THEORY

In the finite element approach to the analysis of a body its volume is divided into a finite number of subregions called elements. Within each element (subregion) the unknown variables are represented by simple functions of their values at points on (or within) the subregion called nodes. The nodal variables are calculated in a manner that leaves the corresponding variational statement stationary.

Consider a volume V in a space defined by cartesian coordinate system (x_1, x_2, x_3). Let the nodal displacement vector $\underline{U}^{(n)} = \underline{U}^{(n)}(U_1, U_2, U_3)$ for node n

The general field displacement $\underline{U} = \sum_{n=1}^{P} \underline{U}^{(n)} N^{(n)}$ where there are P such nodes and,

the matrix $N^{(n)}$ is the shape function for the nth node.

The Cartesian components, ε_{ij}, of the Green's strain tensor are defined as

$$\underline{\varepsilon}_{ij} = \frac{1}{2}\left(\frac{\partial u_i}{\partial x_j} + \frac{\partial u_j}{\partial x_i} + \frac{\partial u_k}{\partial x_i} \cdot \frac{\partial u_k}{\partial x_j} \right), \quad i,j,k = 1,2,3. \qquad 4.1.1$$

It is assumed that there exists a strain energy density function, $\underline{\Phi}$, referred to the undeformed state of the body which depends only on the components of strain tensors: $\underline{\Phi} = \underline{\Phi}(\varepsilon_{11} .. \varepsilon_{12} .. \varepsilon_{33})$.

To define the state of stress in the body, the second Piola-Kirchhoff stress tensor is used, given by

$$S_{ik} = \frac{\partial \underline{\Phi}}{\partial \underline{\varepsilon}_{ik}} \qquad 4.1.2$$

As in the classical theory of elasticity, it can be shown that

$$\underline{\Phi} = \frac{1}{2} C_{ikjl} \varepsilon_{ik} \varepsilon_{jl}. \qquad 4.1.3$$

and that

where Cikjl are the components of a fourth-order tensor of material properties.

The total potential energy of the system consists of

1) the strain energy, given by $U = \int_V \Phi \, dV$

2) the energy due to the body forces. $\int_V \rho \underline{F} \cdot \underline{u} \, dV$

(ρ is mass per unit undeformed volume)

3) the energy due to surfaces forces (these forces may be non-conservative)

$$= \underline{X} \cdot \underline{U}$$

Applying the principle of virtual displacement, after summing up for all the elements of the body, the variational expression is:

$$\sum_{\text{elements}} \int_V \delta \Phi \, dV - \delta \int_V \rho \underline{F} \cdot \underline{u} \, dV - \underline{X} \cdot \delta \underline{u} = 0 . \qquad 4.1.4$$

The strain field, $\underline{\varepsilon} = [\varepsilon_{11}, \varepsilon_{12} \cdots]^T$ is then related to the nodal point displacement vector as $\underline{\varepsilon} = [B_1, B_2 \cdots B_n]\underline{u} = [\bar{B}]\underline{u}$, and the virtual nodal displacement $\delta \underline{u}$ can be expressed as $\delta \underline{\varepsilon} = [B] \delta \underline{u}$ and eqtn. 4.1.4 as

$$\sum_{\text{elements}} \left(\int_V [B] S_{ij} \, dV + \int_V \rho \underline{F} \, dV - \underline{X} \right) \delta \underline{u} = 0 \qquad 4.1.5$$

($\dot{}$) denotes differentiations with respect to time)

Since the expression within the brackets must always be zero for any arbitrary variation of displacement,

$$\sum \left(\int_V [B] S_{ij} \, dV + \int_V \rho \underline{F} \, dV - \underline{X} \right) = 0$$

Equations (4.1.6) can be written in matrix form as

$$[M]\ddot{\underline{u}} + \underline{F} = \underline{R} \qquad 4.1.7$$

the column vector $\underline{F}$ is dependent on the strain and therefore changes as the volume deforms, while the column of externally applied forces $\underline{R}$ may also vary with time.

The original mass matrix, $[M]$, obtained by integrations, was consistent. Thereafter, all the non-diagonal elements in a column were lumped with the diagonal. All the results presented later were therefore obtained using a diagonalised mass matrix.

To obtain the displacement vector at a time $t+\frac{\Delta t}{2}$, the central difference scheme is used given by

$$\dot{\underline{u}}^{t+\Delta t} = \Delta t\,[\underline{R} - \underline{F}][M]^{-1} + \dot{\underline{u}}^{t} \qquad 4.1.8$$

$$\underline{u}^{t+\frac{\Delta t}{2}} = \tfrac{1}{2}\Delta t\,(\dot{\underline{u}}^{t+\Delta t} + \dot{\underline{u}}^{t}) \qquad 4.1.9$$

4.2 THE SPACE-TRUSS MODEL

Introduction

Photographs of impacted fabrics show that yarn strain distribution in an uncoated fabric may vary discontinuously from yarn to yarn. This evidence points to the possibility that better results might be obtained by modelling a fabric as an assembly of yarns, appropriately arranged, than as a thin ctontinuum. A model of fabric as an assembly, of yarns whose relative motions follow a pattern determined by the fabric weave is described. The model is designed to allow the

influence of the initial distribution of impact load can also be investigated.

4.2.1 KINEMATICS AND STRAINS

The basic element of this model is the cable element which may be a simple two-node rod or a higher order element. The element may have all the nodes lying on a straight line, or the equations of its centre line may be described by a specified polynomial (or transcedental) expression. By the appropriate choice of the shape of the centre line, crimp is modelled.

Fig. 4.1 (b) shows an arrangement of four, 2-node, straight elements, to reproduce plain-weave while Fig. 4.2(b) shows the combination of two 3-node elements to model the same weave. Fig 4.2(c) shows a model of a triaxial weave, and Fig. 4.2(d) shows a knitted fabric model. The nodes numbered (5) and (6) are actually vertically above one another but were separated in Fig. 4.2(d) only for illustration purposes. The same is true of nodes (7) and (8). Only one strain is of interest, that along the yarn.

Following Ozdemir, the distance along a yarn from the origin to any point is expressed as a function of the distances from the origin to the nodes. The values of the Green Strain of the yarn based on such nodal length is reported to be more consistent than that obtained by the usual methods (27).

For a 2-node element, the equation obtained by this formulation coincides with those obtained using the usual rod formulation.

4.2.2 MODELLING OF SLIP AT YARN CROSSOVERS

The discussion will be restricted to a plain-weave fabric with orthogonal yarn directions.

In the space-truss model assembled from 3-node elements, slip was allowed at yarn crossovers.

To simplify the calculations, it is assumed that the two nodes representing the crossover points lie on top of one another throughout the motion of the fabric. This approximation is reasonable in cases where yarn pull-through does not occur, and the total slip is small relative to yarn length.

At the beginning of a time step, both the magnitude and direction of the frictional force opposing slip are unknown. To overcome this difficulty a two-pass step was adopted.

At the beginning of the first pass, the frictional resistance is set equal to zero, and, the transverse velocities of the two overlapping nodes and a first estimate of the direction of the relative motion are calculated. The frictional force is put equal to the product of the normal reaction and the corresponding coefficient of sliding friction. In the second pass, the frictional force is applied as an external force each node, acting along the slip direction estimated above, but opposed to it. Better estimates are then calculated for the magnitude and direction of the slip and hence of the components of the frictional resistance. The second-pass is repeated a few times until convergence. See Fig. 4.3

Let the relevant equations of motion of the nodes, assembled as in equation (4.3.7) be

$$M_5\ddot{U}_{z5} + F_{5z} = R_{5z} \qquad (a)$$

$$M_6\ddot{U}_{z6} + F_{6z} = R_{6z} \qquad (b)$$

$$M_5\ddot{U}_{x5} + F_{5x} = {}^{K}R_{5x} \qquad (c) \qquad 4.2.1$$

$$M_6\ddot{U}_{x6} + F_{6x} = {}^{K}R_{6x} \qquad (d)$$

$$M_5\ddot{U}_{y5} + F_{5y} = {}^{K}R_{5y} \qquad (e)$$

$$M_6\ddot{U}_{y6} + F_{6y} = {}^{K}R_{6y} \qquad (f)$$

where the prefix $({}^{K})$ denotes the K^{th} estimate.

The significance of an approximation mentioned briefly before will be stated. This was the approximation involving in putting the node (5) and node (6) of each element of the fabric vertically above one another at the beginning of each time step, despite the cummulative slip during the earlier time steps. This approach obviates the need to determine:

(a) the actual points where the orthogonal yarns cross.

(b) the nodal equivalents of the normal reaction and the frictional resistance which act at the points which would otherwise have been calculated in (a).

If this approximation were not made, then the value of the normal reaction would also have had to be recalculated at every pass.

4.2.3 FABRIC SHEAR

Shear deformation, at a node, is defined as the relative rotation at that node between a yarn and an orthogonal yarn which overlaps it at that node. The shear resistance, T, is related to the relative rotation, θ, and the normal reactions at the crossover, F_z, by the equation:

$$T = C_1 + (C_2 + C_3 . F_z)\,\theta \qquad 4.2.2$$

where C_1, C_2 and C_3 are material and weave properties. The equation is adopted from the work by Kawabata et al. and discussed in greater details in the next section.

4.3 THE MEMBRANE MODEL

Introduction

In this model, the fabric is treated as a thin membrane made from densely woven yarns. The yarn are thin, perfectly flexible, incompressible rods. The weave pattern is modelled by the "stereo model" described by Kawabata et al. and shown in Fig. 4.4 and Fig. 4.5.

4.3.1 KINEMATICS AND STRAINS

The relevant strains are (Exx, Eyy, Exy, Eyx), given by:

$$Exx = \frac{du}{dx} + \frac{1}{2}\left[\left(\frac{du}{dx}\right)^2 + \left(\frac{dv}{dx}\right)^2 + \left(\frac{dw}{dx}\right)^2\right],$$

$$Eyy = \frac{dv}{dy} + \frac{1}{2}\left[\left(\frac{du}{dy}\right)^2 + \left(\frac{dv}{dy}\right)^2 + \left(\frac{dw}{dy}\right)^2\right] \qquad 4.3.1$$

$$Eyx,\ Exy = \frac{1}{2}\left(\frac{dy}{dy} + \frac{dv}{dx}\right) + \frac{1}{2}\left[\frac{dv}{dx}\cdot\frac{dv}{dy} + \frac{du}{dx}\cdot\frac{du}{dy} + \frac{dw}{dx}\cdot\frac{dw}{dy}\right]$$

4.3.2 CONSTRAINTS AND GEOMETRY OF WEAVE

In order to satisfy the weave pattern, both force and geometrical constraints have to be satisfied for each element. This mathematically means an addition of extra terms to the variational statement of equation 4.1.4. Fig. 4.6 shows the initial geometry of the centrelines of the intersecting yarns before deformation and Fig. 4.7 show the same lines after deformation.

Let Exx be the strain in the plane of the fabric in the plane of yarn 1, and the Eyy the strain along the perpendicular direction. These strains are calculated using equations (4.3.1). Let e_1 be the actual strain in yarn 1. which lies in the xz plane. If the pitches in the x and y directions are P_1 and P_2 respectively, the equations

$$l_1^2(1 + e_1)^2\sin^2\theta_1 = P_1^2(1 + Exx)^2 + h,^2, \qquad 4.3.2$$

$$l_2^2(1 = e_2)^2\sin^2\theta_2 = p_2^2\ (1 + Eyy)^2 + h_2^2, \qquad 4.3.3$$

arise from the assumption of no slip.

Also from the incomprassibility assumption

$$\begin{aligned} & l_1(1 + e_1)\cos\theta_1 + l_2(1 + e_2)\cos\theta_2 \\ &= l_{10}\cos\theta_{10} + l_{20}\cos\theta_{20} \qquad 4.3.4 \\ &= h_1 + h_2 = h_{10} + h_{20} \end{aligned}$$

Let the tensions in the yarns be T_1 and T_2 respectively, then, from consideration of equilibrum at the crossover (see Fig.4.7)

$$T_1\cos\theta_1 = T_2\cos\theta_2 \qquad 4.3.5$$

At any given time, Exx and Eyy, the strains in the plane of the fabric can be calculated using equations 4.3.1. then, using the Newton-Ralphson method, equations (4.3.2) to (4.3.5) are solved iteratively to obtain e_1, e_2 and therefore T_1 (e_1) and T_2 (e_2). The values of T_1 and T_2 can now be used for the integration of equations (4.1.6) to obtain the equations of motion.

4.3.3 SHEAR EQUATIONS

Until the shear force is increased beyond a limiting value, relative rotations between the yarn, in other words, shear, would not occur. Beyond this limit, the shear strain, Exy or Eyx, increases in a complex way which depends on the magnitude of shear force as well as the reaction between the yarns, and on the direction of rotation.

The model was developed by Kawabata et al (3) and could be written as

$$T_{12} = \pm C_1 \pm (C_2 + C_3 * T_1 \cos\theta_1)\, Exy \qquad 4.3.6$$

where T_{12} is the shear force, C_1 is the frictional constraint, while C_2 and C_3 represent the effect of elastic behaviour of the contact area.

4.4 THREE-DIMENSIONAL MODEL

Experiments show that in a multilayer of fabric, the layers closest to an impacting projectile fail first even when the layers are identical and slip is negligible. Such a sequence of perforation cannot be easily predicted if the layers are treated as thin plates. Otherwise, a failure criterion which involves the magnitude of the reactional forces on the surface of each layer may be necessary. Apart

from this observation, it has be suggested by Marom and Bodner (23) that compressive resistance is significant to the overall structural mechanics of layers of comparatively thin 1100-H16 aluminium sheets and beams.

The three-dimensional model is therefore designed to investigate the significance of the yarn compressive strength, and, at the same time, the significance of inter-layer slip.

Under impact, some layers may be penetrated and separated from the forward, unpenetrated layers. This model allows such separation to occur. there is also a check for when a previously separated layer re-establishes contact.

The in-plane resistance of a fabric is provided by a two-dimensional membrane element. The interface between two layers is modelled by three-dimensional parallelpiped elements which also provide resistance against shear and compression. Each three-dimensional element has zero mass, and its thickness equals half the sum of the thicknesses of the fabrics on either side of the interface it represents.

Fig. 4.8 shows the combination of elements to model three fabric layers.

4.4.1 STRAINS AND STRESSES

For the two dimensional membrane elements, the relevant strains are:

$$Exx = \frac{du}{dx} + \frac{1}{2}\left[\left(\frac{du}{dx}\right)^2 + \left(\frac{dv}{dx}\right)^2 + \left(\frac{dw}{dx}\right)^2\right]$$

$$Eyy = \frac{dv}{dy} + \frac{1}{2}\left[\left(\frac{dw}{dy}\right)^2 + \left(\frac{dv}{dy}\right)^2 + \left(\frac{dw}{dy}\right)^2\right] \qquad 4.4.1$$

$$Exy = Eyx = \frac{1}{2}\left(\frac{du}{dy} + \frac{dv}{dx}\right) + \frac{1}{2}\left[\frac{du}{dx}\cdot\frac{du}{dy} \;\; \frac{dv}{dx}\cdot\frac{dv}{dy} \;\; \frac{dw}{dy}\cdot\frac{dw}{dx}\right]$$

From experiments, the in-plane stiffness coefficients of a fabric, along and perpendicular to the weft direction, are measured. They could be expressed in a relation between stresses and strains as:-

$$\begin{bmatrix} Sxx \\ Syy \\ Sxy \end{bmatrix} = \begin{bmatrix} D_{11} & D_{12} & 0 & Exx \\ D_{12} & D_{22} & 0 & Eyy \\ 0 & 0 & D_{33} & Exy \end{bmatrix} \qquad 4.4.2$$

During the arrangement of fabrics into a multilayer assembly, the warp direction of a layer may be laid at an angle θ to that of the reference layer. This angle may be different from layer to layer. It is necessary to transform the constitutive relations so as to relate the force in each layer and the strain in the reference directions.

The terms Dij of the constitutive relations in equations 4.4.2. is then replaced by Dij (θ), which are given by the expressions:

$$D_{11}{}^1 = D_{11}\cos^4\theta + D_{22}\sin^4\theta + (2D_{12} + 4D_{33})\sin^2\theta\cos^2\theta$$

$$D^1{}_{22} = D_{11}\sin^4\theta + D_{22}\cos^4\theta + (2D_{12} + 4D_{33})\sin^2\theta\cos^2\theta$$

$$D_{12}{}^1 = D_{21}{}^1 = D_{12} + (D_{11} + D_{22} - 2D_{12} - 41)_{33})\sin^2\theta\cos^2\theta$$

$$D^1{}_{23} = D^1{}_{32} = (D_{11} - D_{12} - 2D_{33})\sin\theta\cos^3\theta + (D_{12} - D_{22} + 2D_{33})\sin^3\theta\cos\theta$$

$$D_{33}{}^1 = D_{33} + (D_{11} - D_{12} - D_{33})\sin^3\theta\cos\theta - (D_{12} - D_{22} + 2D_{33})\sin\theta\cos^3\theta$$

4.4.3

4.4.2 STRAIN AND STRESSES FOR INTERFACE ELEMENTS

The nodal displacements are the same as for the two-dimensional fabric elements. The important strains are: (Exx, Eyy, Ezz, Exz, Eyz) which are defined as:

$$Exx = \frac{du}{dx} + \frac{1}{2}\left[\left(\frac{du}{dx}\right)^2 + \left(\frac{dv}{dx}\right)^2 + \left(\frac{dw}{dx}\right)^2\right],$$

$$Eyy = \frac{dv}{dy} + \frac{1}{2}\left[\left(\frac{du}{dy}\right)^2 + \left(\frac{dv}{dy}\right)^2 + \left(\frac{dw}{dy}\right)^2\right], \qquad 4.4.4$$

$$Ezz = \frac{dw}{dz} + \frac{1}{2}\left[\left(\frac{du}{dy}\right)^2 + \left(\frac{dv}{dz}\right)^2 + \left(\frac{dw}{dz}\right)^2\right],$$

$$Exy = \frac{1}{2}\left(\frac{du}{dz} + \frac{dw}{dx}\right) + \frac{1}{2}\left(\frac{du}{dz} \cdot \frac{du}{dx} + \frac{dw}{dx} \cdot \frac{dw}{dz}\right),$$

$$Eyz = \frac{1}{2}\left(\frac{dv}{dz} + \frac{dw}{dy}\right) + \frac{1}{2}\left(\frac{dv}{dz} \cdot \frac{dw}{dy} + \frac{dw}{dy} \cdot \frac{dw}{dz}\right),$$

The derived stresses which are of interest are Sxx, Syy, Szz, Sxz, Syz. they are related to the strains in equations 4.4.4 by the expressions of the form:

$$\begin{bmatrix} Sxx \\ Syy \\ Szz \\ Sxz \\ Syz \end{bmatrix} = \begin{bmatrix} C_{11} & C_{12} & C_{13} & 0 & 0 \\ C_{21} & C_{22} & C_{23} & 0 & 0 \\ C_{31} & C_{32} & C_{33} & 0 & 0 \\ 0 & C_{44} & 0 & C_{44} & 0 \\ 0 & 0 & 0 & 0 & C_{55} \end{bmatrix} \begin{bmatrix} Exx \\ Eyy \\ Ezz \\ Exz \\ Eyz \end{bmatrix} \qquad 4.4.5$$

Where the stiffness coefficients C_{11}, C_{22}, depend on both strain and strain rates.

For unbonded, layered fabrics, C_{11}, C_{12}, C_{13}, C_{21}, C_{22}, C_{31}, C_{32} are made very small and C_{33} put equal to the average compressive modulus of the fabrics on either side of the interface. When Ezz is positive, that is separation occurs, C_{33} and the other coefficients are set to a very small number (10^{-4}). When the interlayer is compressed, that is Ezz is - ve, C_{33} is set to the value stated earlier.

The stresses are integrated through the volume to obtain the nodal load vector (Fx, Fy, Fz). In cases where the layers are free to slip, the resultant in-plane force, $(Fx^2 + Fy^2)^{\frac{1}{2}}$ is adjusted, if necessary, so that

$$(Fx^2 + Fy^2)^{\frac{1}{2}} \leq \mu\, Fz \qquad 4.4.6$$

where μ is the coefficient of friction.

In a bonded interface, the stiffnesses in the xx, yy, and zz directions are set equal to that of the binding resin.

4.5 THE MASTER-SLAVE LAYER METHOD

4.5.0 Introduction

The model iiscussed in the last section involved the use of three-dimensional elements to simulate the compressive resistance of the yarns and the slip between layers. The thickness of each fabric is however very small compared with its in-plane dimensions: 0.5mm to 150mm by 150mm. Very many elements are necessary to keep the aspect ratio of the three-dimensional elements low and to ensure accurate stress results. This requirement drastically restricts the number of

layers which could be modelled. A solution to the problem is to avoid the use of three dimensional interface elements altogether. The master-slave layer method is an attempt to achieve this end, and at the same time allow for slip between layers.

The computational procedure is similar to that used in fluid-structure dynamic analysis to investigate the motion of two contacting materials which have a relative tangential motion along their interface, but which remain in contact throughout this motion. See Ref 44. The material lying on one side of the plane of contact is designated as the 'master' material, while the material on the other side is the 'slave' material. Generally the stiffer, or the denser material, is chosen as the 'master' material. Both materials are divided into elements as usual, the nodes of the elements of the master material lying on the interface are given different numbers from the nodes of the slave elements lying on the same surface even when some nodes are initially coincident. The values of the variables at the nodes of the slave elements which lie on the interface are fixed by those of the nodes of the master elements on which they lie. In turn, the slave nodes are deemed to exert forces on these master elements.

In the application of such a scheme to the investigation of the dynamic response of a multilayer system, many modifications are necessary. For example, the master layer at any time is the layer directly in contact with the projectile at that time. Since, during motion, layers may get penetrated and separate, the layer designated as the master layer must be upgraded at the beginning of each time step to be the layer just below the last penetrated layer. To satisfy this requirement, a check is carried out at the start of each time step for elements which have failed. If elements in the top layer have failed,

then the projectile is assumed to be in contact with the next layer. The check is continued until the projectile is in contact with an unpenetrated layer.

Once the master layer has been identified, as above, the next step is to calculate the acceleration during the time step. First the nodal loads (Vector $\underline{F}$ in equation (4.16)) are determined for the nodes of each layer not yet penetrated. The external forces acting at the nodes of the elements of the master layer, due to inertia and strains in the other layers, are determined. The layers are assumed to be constrained against slip and the accelerations of the master nodes are calculated. From the accelerations of the master nodes, an estimate can be obtained of the acceleration of a node on any slave layer. This is only possible because it was assumed that slip did not occur. The reaction force between the layers is calculated at each node, and modified, if necessary, to satisfy the frictional properties of the interface. The acceleration of each node (master or slave) is recalculated with the modified values of reactions.

4.5.1 BASIC PRINCIPLES : MASTER-SLAVE LAYERS

Consider the membrane elements T and S in Fig. 4.9. The element S lies on element T.

Let the element T be the master element and the element S the slave element. The velocities of the nodes A, B, C and D of the element S are therefore determined by their positions on the element T. This statement is true as long as contact is maintained between the elements without slip.

The equation of motion of the nodes of element T, following equation (4.1.17) can be written as

$$M_I \ddot{\underline{U}}_I + \underline{F}_I = \underline{R}_I . \qquad 4.5.1$$

The equation of motion of the nodes of element S is similarly written as

$$M_i \ddot{\underline{U}}_i + \underline{F}_i = \underline{R}_i , \qquad 4.5.2$$

Where the externally applied force vector Ri is assumed to be only due to the reaction of element T on element S.

The velocity vector of A, B, C or D is given by

$$\dot{\underline{U}}_i = \sum N_I \dot{\underline{U}}_I , \qquad 4.5.3$$

where N_I is the value of the shape function of the Ith node of element T, evaluated at the position of node i of element S.

Using the approximation

$$\dot{\underline{U}}^{t+\Delta t} = \dot{\underline{U}}^{t} + \Delta t \ddot{\underline{U}} ,$$

and assuming that slip is small we can rewrite the expression (4.5.3) in terms of accelerations as:

$$\ddot{\underline{U}}_i = \sum N_I \ddot{\underline{U}}_I . \qquad 4.5.4$$

$$M_I \sum N_I \ddot{\underline{U}}_I + \underline{F}_i = \underline{R}_i \,. \qquad 4.5.5$$

By virtual work considerations it can be shown that the force $\underline{H}_I$ at node I of element T due to the action of external force $\underline{R}i$ at A is given by

$$\underline{H}_I = - N_I \underline{R}_i = - N_I M_i \sum N_J \ddot{\underline{U}}_J - N_I \underline{F}_i \,. \qquad 4.5.6$$

The total external force $\underline{R}_I$ at node I is the sum of the equivalent nodal forces, $\underline{H}_I$, due to the reactions on elements which share node I a common node, that is

$$\underline{R}_I = \sum \underline{H}_2 = - \sum N_I \underline{R}_i \,. \qquad 4.5.7$$

Equation 4.5.1 can now be rewritten as

$$M_I \ddot{\underline{U}}_I + \underline{F}_I + N_I \sum^{L} \left(M_i \sum^{Q} N_J \ddot{\underline{U}}_J + \underline{F}_i \right) = 0 \,, \qquad 4.5.8$$

the summation variable L refers to the number of slave nodes which lie on master elements to which node I is common, while the variable Q refers to the number of nodes, J, of the particular master element on, or within, which the slave node, i, lies.

By this procedure, the number of unknowns has been reduced, and only the acceleration vectors of the master nodes need to be calculated. The acceleration of the slave nodes are later evaluated using equation (4.5.4).

It can be shown that the expression 4.5.8 is correct even when the

slave layer (on which node i) lies is not in direct contact with the master layer, but is in contact with another slave layer which is in contact with the master layer. The expression is correct for as long as the velocity vector of the slave nodes satisfies equation (4.5.3), that is, for as long as there is no slip between the fabrics or the separation of one fabric from the rest.

4.5.2 APPLICATION TO MULTI-LAYER ANALYSIS

The layers are identically divided into elements, so nodes on the lower layers are vertically below nodes on the top, master, layer. Once impact occurs, slip generally takes place, and a node on a lower layer may no longer be vertically below any node in the top layer. Therefore, in order to calculate the acceleration vector of a slave layer node from those of master layer nodes (using equation 4.5.3) the following steps have to be taken:

1. the identification of the element in the top layer within which horizontal projection the slave layer node lies.

2. the calculation of the values of the parametric coordinates of the point in the master layer element (identified in 1) which is vertically below the slave layer node.

4.5.3 IDENTIFICATION OF MASTER LAYER ELEMENT BELOW A GIVEN SLAVE LAYER NODE

The search scheme described here is, strictly speaking, only suitable for elements bounded by straight edges. It can however be

easily modified for use with other shapes.

Referring to Fig 4.10, the problem is to determine whether or not a given point N lies on, or within, an area bounded by straight sides. See Fig 4.11, also.

The nodes of the elements are numbered in an anticlockwise sense.

The coordinates of the rectangle 1234 which envelopes the master element is found. If the coordinates of N, (Xp, Yp), do not satisfy the conditions

$$Xmin \leqslant Xp \leqslant Xmax \qquad 4.5.9$$

and $$Ymin \leqslant Yp \leqslant Ymax \qquad 4.5.10$$

then the search procedure is terminated.

If both conditions are satisfied, then the distance from the node N to each of the sides of the element IJLK is calculated.

If point (Xp, Yp) lies within the element whose sides have end points (X_1, Y_1) and (X_2, Y_2) respectively, then

$$(Y_1 - Y_2).Xp + (X_2 - X_1).Yp + (X_1.Y_2 - X_2.Y_1) > 0 \qquad 4.5.11$$

If this inequality is not satified by any side of the element, the point (Xp, Yp) does not lie within the element. The condition given by equation (4.5.11) follows from the choice of node numbering system.

Once it has been shown that a node lies above an element, the next step is to calculate the parametric coordinate of the vertical projection of this node on the master element. This is the object of the next section.

4.5.4 CALCULATION OF THE PARAMETRIC COORDINATES OF A POINT, GIVEN ITS CARTESIAN COORDINATES

The cartesian coordinate of a general point, A(X, Y, Z), on an element can be calculated from the nodal values using the expression

$$A = \sum^{K} A^{(n)} N^{(n)} (\xi, \eta), \qquad 4.5.12$$

where the nodal shape functions $N^{(n)}$ are evaluated at this point. (Note that the slave node and its vertical projection on a master element have the same x and y coordinates).

The parametric coordinates (ξ_I, η_I) of point I (X_I, Y_I), are obtained from the solution of the equations

$$X_I = \sum^{K} x^{(n)} N^{(n)} (\xi, \eta) \qquad 4.5.13$$

and

$$Y_I = \sum^{K} y^{(n)} N^{(n)} (\xi, \eta) \qquad 4.5.14$$

The equations can respectively be rewritten as

$$F_1 (\xi, \eta) = X_I - \sum^{K} x^{(n)} N^{(n)} (\xi, \eta) \qquad 4.5.15$$

and

$$F_2 (\xi, \eta) = Y_I - \sum^{K} y^{(n)} N^{(n)} (\xi, \eta) \qquad 4.5.16$$

The solution procedure used to solve functions F_1 and F_2 are based on the Newton's method for non-linear equations.

4.5.5 ORGANISATION OF COMPUTER PROGRAM

The diagonalised mass matrix is stored in an array MASS.

At the beginning of a time step, the coordinates of all the nodes (slave and master nodes) are known. The vector of internal nodal forces, $\underline{F}$, due to strains are evaluated by numerical integration and stored in an array FOR (NNODS, NVAR) where, NNODS = total number of nodes in the active system, that is, the nodes of all the layers that have not been penetrated or separated, and NVAR = number of variables at each node.

Next the element in the master layer, above which a node on a slave layer lies, is identified as described in Section (4.5.3). Let the master element be called E. The contribution of the slave node to the equation of motion of each of the nodes of element E, given by $\underline{H}_I$, (see equation 4.5.6 of Section 4.5.1) is then summed. The coefficient of the acceleration term of this contribution (first term in bracket, eqtn. 4.5.8) is added into the corresponding position of an initially null array CONTR(NNOLA, NNOLA), where

NNOLA = number of free (unfixed) nodes in a layer.

The second term within the bracket (eqtn. 4.5.8) is added to the corresponding location in an array RHS (NNOLA, NVAR).

Note that $\underline{F}i$ in equation (4.5.6) is the transpose of the terms stored in the i^{th} column of array FOR(NNODS, NVAR).

The equations obtained after summing up the contributions of all the slave layer nodes and completing the summation of equation (4.5.8)

$$[\bar{M}]\ \ddot{Q} + [G] = 0 \qquad 4.5.17$$

where

$[\bar{M}]$ = the modified mass matrix, no longer diagonal but sparce (equivalent to array CONTR).

$\ddot{Q}$ = Vector of the acceleration of master layer nodes (= NNOLAxNVAR).

$[G]$ = vector of modified generalised forces at master layer nodes (= NNOLAxNVAR).

The equation is then solved for Q.

4.5.6 NODAL ACCELERATIONS WITHOUT SLIP RESTRICTION

This last part of the procedure involves the calculation of the accelerations of each active (both master and slave nodes) with the no-slip restriction relaxed. The acceleration vectors for the master layer nodes, Q, calculated in equation 4.5.17 are used.

Two arrays are set up: RETOP (NNOLA, NVAR) and REBOT (NNOLA, NVAR). the first array contains the vector of forces externally applied to the top surface of the layer under consideration, while the array REBOT (NNOLA, NVAR) contains the forces externally applied to the lower surface of the array. Initially all the elements of each of the two arrays is set to zero.

The steps taken in order to calculate the acceleration of an

unfixed node in any layer, starting from the top (master) layer are:

Note: The master layer is the topmost layer.

Two column vectors $[\underline{R}_t]$ and $[\underline{R}_b]$ are set up. $[\underline{R}_t] = [R_{xt}, R_{yt}, R_{zt}]^T$ contains the external reactions at the node due to the effect of the layer just above.

$[\underline{R}_b] = [R_{xb}, R_{yb}, R_{zb}]^T$ is the external reaction at the node due to the reaction between the layer under investigation and the one below it.

The total external force at node I, $[\underline{R}]_I = [\underline{Rt}]_I + [\underline{Rb}]_I$ 4.5.18

For a slave layer, $[\underline{R}_b]_I$ is calculated using the expression

$$[\underline{Rb}]_I = -\sum [\underline{R}_J] N_I(J) \qquad 4.5.19$$

where R_J are force vectors read from the array REBOT which must have been earlier calculated for the layer above that of node I. $N_J^{(I)}$ is the shape function of node J with respect to the element above which node I lies. Generally, the node I lies within one element, but it may lie on the boundary between elements. In the second case, node I could be assumed to lie on any of the elements sharing the boundary.

For the master layer, $[\underline{Rt}]_I$ is null since its top surface is assumed free.

The components of $[\underline{Rt}]_I$ are now stored in the I^{th} column of array RETOP.

The forces at node I, on the lower surface of the layer, is calcul ated using equations 4.1.17 and 4.5.8 are

$$\left[\underline{Rt}\right]_I = M_I \ \ddot{\underline{U}}_I + \underline{F}_I - \left[\underline{Rb}\right]_I \qquad 4.5.20$$

For a slave node I, the acceleration vector $\ddot{\underline{U}}_I$ is determined by using equation 4.5.4 and the values of vector $\underline{Q}$ which were evaluated in equation 4.5.17.

A check is now performed to see if the reaction vector $\left[\underline{Rt}\right]_I$ satisfies the frictional properties of the interface between the layer on which I lies and the one above it.

The directional cosines of the normal at I, (l, m, n), are calculated. The normal component, R_N of $\left[\underline{Rt}\right]_I$ is given by

$$R_N = l.R_{xt} + m.R_{yt} + n.R_{zt} \qquad 4.5.21$$

and the components of the in-plane part of the vector Rt_I are:

$$\begin{bmatrix} Rxt - l.R_N \\ Ryt - m.R_N \\ Rzt - n.R_N \end{bmatrix} = \mu \begin{bmatrix} r_x \\ r_y \\ r_z \end{bmatrix}$$

If the value of the normal reaction, R_N, obtained from equation 4.5.21 is negative, then separation has occurred and the program is terminated. Else, the satisfaction of the no-slip assumption is checked:

The resultant in-plane reaction,

$$Rr = \sqrt{r_x^2 + r_y^2 + r_z^2} \quad , \qquad 4.5.22$$

while the maximum allowed in-plane reaction is $\mu \underline{R}_N$.

If $Rr \leqslant \mu R_N$ then no adjustment is needed to the vector $\left[\underline{Rt}\right]_I$ and there was no slip at the node I in that interval. If, however, this condition is violated, the components of the in-plane reaction are adjusted to the values:

$$R_N \cdot r_x/Rr$$

$$R_N \cdot r_y/Rr \qquad 4.5.23$$

$$R_N \cdot r_z/Rr$$

The corrected reaction at the node I, on the top surface, $\left[\underline{R}_t\right]_{IC}$, becomes:

$$\left[\underline{R}_t\right]_{IC} = \begin{bmatrix} R_N \cdot r_x/Rr + 1.R_N \\ R_N \cdot r_y/Rr + m.R_N \\ R_N \cdot r_z/Rr + n.R_N \end{bmatrix} \qquad 4.5.24$$

The acceleration of node I is recalculated with the vector $\left[\underline{R}_t\right]_I$ in equation 4.5.18 replaced by $\left[\underline{R}_t\right]_{IC}$.

the vector $\left[\underline{R}_t\right]_{IC}$ is now stored in the I^{th} row of the array RETOP.

After these calculations have been completed for all the free nodes in a layer, the contents of array REBOT are now replaced with those of array RETOP in preparation for the repetition of the same calculations for the nodes in the next layer. This completes the solutions for one time step.

CHAPTER 5

RESULTS AND DISCUSSION

5.0 Introduction

In this chapter the numerical results obtained using the models described earlier will be presented and discussed. The potential use of the different models in the accurate analysis of fabric mechanics will also be discussed and finally the results will be compared with those of other investigations. Of paramount interest is the prediction of the velocity of impact at which a given fabric fails, for a given projectile mass. Many models have been proposed for fabric, yarn and fiber failure, some of which are based on the strain energy absorbed by a unit length of the yarn while others are based on the strain history of the yarn. In Ref (54) and (55) models of load shearing between the constituent fibers of a yarn under tension were proposed. The loading to which the yarns in a fabric are subjected are mainly due to extension, although as suggested in Chapter 2, failure may occur due to local overstressing at a node. The overstressing may be due to nodal constraints or wave reflection. In order to minimise the complexity of the analysis, a simple failure criterion was chosen. This condition is that when the strain at a point in the fabric exceeds the maximum value allowed, the yarn breaks. The magnitude, of course, varies from material to material. A fabric is penetrated when a yarn in the region of impact is broken. Results were only obtained for materials whose mechanical properties were independent of strain rates. This decision was taken because earlier reports (22) indicate that the significance of such strain rate dependency on the mechanical response of fabrics is minimal.

Only two yarn materials are investigated. They are Nylon and Kevlar. This choice was based on the fact that these two materials are the most commonly used for weaving protective clothing and sheaths. Different types of nylon yarns were investigated. Some had linear stress strain relations, while the complex constitive relations of others are represented by three linear sections. Only Kevlar 29 was modelled.

Input Data

Projectile

Radius	2.76 mm
Mass	1.1 g

The projectile is assumed to be rigid and the effect of its shape was not modelled.

Impact Velocity

Impact takes place normal to the plane of the fabric panel. A velocity range of 100 m/s to 500 m/s was investigated.

Fabrics

Size The in-plane size of the fabric panel investigated in each case was approximately 154 mm by 154 mm. This size was chosen to correspond with that of the specimen used in some fabric penetration experiments in UMIST.

The thickness of the fabric was assumed to be at 0.5 mm for purposes of numerical work.

Yarn Materials:

For convenience, the units of the yarn modulus is Newton/strain/Tex.

Kevlar 29

Modulus : 48.56

Breaking strain : 3.23 per cent

Nylon

Type A

Strain Range	Modulus
0.0 - 0.05	1.75
0.116 - 0.20	4.16
0.20 - 0.24	1.75

Breaking strain 24.0 per cent

Type B

Strain Range	Modulus
0.0 - 0.1	0.629
0.1 - 0.1475	1.14
0.1475 - 0.27	1.43

Breaking strain 24.0 per cent

Fabric Weight

Fabric No	Area Density units g/mm^2	Yarns per cm			Tex of Yarns			Weave
Nylon D305	240	11.4		12.3	103		10.1	Biaxial
Nylon D322	386	9.8		9.1	181		170	Biaxial
Kevlar D236	351	10.8		9.2	175		175	Biaxial
Nylon	221	3.63	3.75	3.77	200	205	201	Triaxial
Nylon	483							Biaxial

5.1 SIMPLE MODEL RESULTS

Linear Model

The strain expression used in the linear model (appendix 1) for fabric with high prestrain is

$$\varepsilon = (1 + \varepsilon_p) \frac{dWo}{ds}, \qquad 5.1.1$$

where ε_p is the prestrain, Wo the transverse deflection at the point of impact and s the length along the yarn.

It can be shown that the maximum value of the slope, $\frac{dW}{ds}$, occurs immediately after impact. This fact can be observed from the graph of the indentation against time, Fig. 5.1.

The maximum value of $\frac{dW}{ds} = \frac{Vp}{Cs}$ where Vp is the velocity of impact and Cs is the wave speed along the yarn.

Equation 5.1.1 can therefore be written as:

$$= (1 + \varepsilon_p) \frac{Vp}{Cs} \qquad 5.1.2$$

For a linear Hooken material, $Cs = \sqrt{\frac{\varepsilon_{p.E}}{\rho}}$ where ρ is the yarn density and E is the modulus, hence:

$$\varepsilon = (1 + \varepsilon_p) \frac{Vp}{\sqrt{\frac{\varepsilon_{p.E}}{\rho}}} \qquad 5.1.3$$

In other words, the value of the maximum strain developed in the yarn is directly proportional to the impact velocity for a given prestrain.

The impact velocity, V_f, required to produce fabric (yarn) failure at strain ε_s is given by:

$$V_f = \frac{\varepsilon_s . c_s}{(1 + \varepsilon_p)} = \varepsilon_s \cdot \frac{\sqrt{\varepsilon_p}}{1 + \varepsilon_p} \sqrt{\frac{E}{\rho}} \qquad 5.1.4$$

This velocity increases as the yarn material modulus, E, increases, which means that fabrics made of strong materials are more efficient.

Fig. 5.2 shows the deceleration diagrams for three different fabric densities at an impact velocity of 150 m/s. In Fig. 5.3 the initial slopes of the indentation time curves are all the same for the three fabrics, which is as expected. Fig. 5.4 shows the deceleration diagrams at a lower prestrain, 0.002, for 2 nylon fabrics and one of Kevlar. As expected, the deceleration is higher for Case (3). Fig. 5.5 shows that the use of a heavier fabric, Case (2), does not lead to a reduction in the value of the maximum strain developed in the yarns, although it leads to a smaller value for the maximum indentation, and a shorter projectile arrest time than case (1).

The results obtained for the response of two fabrics of similar area densities, Fig. 5.2 for a 240 gm^{-2} orthogonally woven nylon fabric, and Fig. 5.3 for a 221 gm^{-2} triaxially woven nylon fabric, predict that the orthogonal weaving pattern provides a better translation of yarn strength to fabric dynamic stiffness.

Non-linear Model

The expression for strain valid for large deflections which are expected to occur in fabrics with low prestrains is given by:

$$\varepsilon = (1 + \varepsilon_p)\sqrt{\left(1 + \left(\frac{Wo}{C_s t}\right)^2\right)} - 1 \qquad 5.1.5$$

It can also be shown that the ratio $\left(\frac{W_o}{C_s t}\right)$ attains its maximum value of $\frac{V_p}{C_s}$, just immediately after time t = 0. Note that the magnitude of the slope of the line from the origin to the curve at time t is $\frac{W_o}{C_s t}$. See Fig. 5.1.

Hence the maximum strain, ε_{max}, is given,

$$\varepsilon_{max} = \left((1 + \varepsilon_p)\sqrt{\left(1 + \left(\frac{V_p}{cs}\right)^2\right)} - 1\right) \qquad 5.1.6$$

The impact velocity, V_f, above which failure of the fabric occurs, is given by

$$V_f = \varepsilon_{p.E.}((1 + \varepsilon_s)^2/(1 + \varepsilon_p)^2 - 1) \qquad 5.1.7$$

The optimum value of prestrain, corresponding to the stationary value of the variation of V_f with respect to ε_p, is given by:

$$\varepsilon_p = w - (1 + \varepsilon_s)/3w, \text{ where}$$

$$w = \left[(1 + \varepsilon_s) + \sqrt{(1 + \varepsilon_s) + (1 + \varepsilon_s)^3/27} \right]^{\frac{1}{3}}$$

This optimum conditions corresponds to a high prestrain which would be higher than the breaking strain, ε_s, for most yarn materials and is therefore not practically realisable.

The general equation for strain (eqtn. 5.1.6) predicts that:

1 the velocity at which failure occurs is independent of the density (mass per area) of the fabric. This follows because the highest strain occurs immediately after impact, that is before part of the projectile energy is absorbed by the fabric as kinetic energy,

2 The value of the strain is independent of the geometry of the weave. This is true for any weave in which the yarns through the point of impact are straight (neglecting crimp).

3 For equal prestrains, the value of the maximum strain is lower in a fabric made out of the material of higher modulus since the value of C_s is higher. Protective clothing are, therefore, more effective if made of high tensile modulus materials.

Fig. 5.6 shows indentation of 240 g/m^2, orthogonally woven, fabric as predicted by the non-linear model. The variation of impact velocity at failure with prestrains is displayed in Fig. 5.7 for Kevlar and Nylon. Very low values of prestrain which may, somehow, be easily produced in cloths are used in the calculations.

5.2 Characteristic Model results

A property of the characteristic solutions described in Chapter 3 is that it can only be succesfully applied to the analysis of prestrained fabric. At low prestrains, buckling occurs and the solutions goes unstable. The level of prestrain required to prevent buckling increases with the impact velocity. It was noticed that in cases when the initial velocity of the transverse wave (which is proportional to the root of the prestrain) is less than the velocity of impact, compressive strains are developed at some points in the fabrics and the solution routine fails. The results which are discussed are obtained with the smallest prestrains necessary to prevent buckling.

The effect of prestrain is indicated by the differences in the graphs in Fig. 5.8. The results obtained by the finite element method (membrane model) almost exactly coincides with experimental results (56). Until approximately 160μs after impact, the deflection of a fabric with 1% prestrain obtained by the method of characteristics is indistinguishable from the finite element results. Zero pretension was assumed in the finite element solution. Since fabric failure, when it occurs, takes place early during motion, it may be predictable by a method of characteristics solution with small prestrains.

Results obtained by using this method was successfully applied to predict the maximum velocity at which layers of nylon can be impacted before failure occurs.

Two schemes were used to model the impact. In one scheme, the velocity of each impacted node was put equal to that of the projectile at time t = 0, and the same

the deceleration of the projectile. This corresponds to putting the acceleration of those nodes equal to infinity at time t = 0.

In this second scheme, a period of acceleration of 10μs was assumed, and,in this period,normal velocity of each node in the impacted zone was put equal to

$$\left(= V_p \sin\frac{\pi}{2} (t/\ 0.00001) \right),$$

where Vp is the velocity of impact. Beyond this period, deceleration occurs. The second scheme was successful, except in the high velocity cases, when some of the yarns attached to an impacted node failed during the period of acceleration. The first scheme was used on such occasions to determine the correct residual velocity, and thence, the energy absorbed by the fabric before failure.

Apart from the high velocity cases mentioned above, there was no difference in the results obtained by using either scheme with the same input data. While most of the results were obtained from solutions involving the use of the first scheme, others were obtained using the second. The solution converges as the number of nodes was increased. The results reported below were obtained using a 39 x 39 grid. For most fabrics, this means a representation of about every 4 yarns by a single yarn.

Fig, 5.9 (a) shows the sequence of the deformation of a 386 g/m^2 nylon fabric on impact by a 1.1 gm projectle at 150 m/s. The arrest of the projectile took place in 262 μs during which the maximum strain in the yarns through the impact zone was 21.7%. The initial fabric

prestrain was 3%. Is is evident, Fig. 5.9 (b) that the out-of-plane transverse wave reached the fixed edge of the panel before the projectile came to rest. This can also be deducted from the velocity profile. the absence of a second 'hump' in the curve of the strain history shows that the reflected out-of-plane transverse wave did not arrive back at the point of impact before the projectile was stopped. Fig. 5.10 shows similar graphs for a projectile velocity of 160 m/s. The maximum strain in the yarn for an impact velocity of 170 ms^{-1}, Fig. 5.11, is quite close to the breaking strain of 24% and the fabric will be penetrated at a slightly higher velocity.

MULTI-LAYERS

In order to model the dynamics of layered fabric panels, by the method of characteristics, the yarn and fabric properties of a single layer are multiplied by the number of layers. This method involves the implicit assumption that the deformation of each fabric in a panel of layers is the same as the next. Slip is presumed not to occur between layers.

The prestrain required to prevent yarn buckling during motion was found to increase with the number of layers in a panel. This makes the analysis of the results more complex.

The results obtained for a simulated panel of two layers of 351 g/m^2 Kevlar fabrics are plotted in Fig. 5.12 (a) and (b). The impact velocity is 290 m/s. The two layers absorbed 33.0 J before penetration. This amount of energy is close to the experimental results

obtained in UMIST when a panel of these two layers of Kevlar fabric, free of prestrain, was impacted. With a prestrain of 0.0025, three layers of Kevlar, modelled as described above absorbed 36.1J when impacted by a projectile moving at 300 ms^{-1}. Again this amount of energy falls within the range of experimental results obtained for the three layers, under zero prestrain at impact.

The results obtained from the model of a panel made up of two layers of 240 gm^{-2} Nylon fabrics, with an initial prestrain of 3%, impacted at 235 ms^{-1}, predict a maximum strain of 26.8 per cent -about the average breaking strain for the size of the yarns. See Fig. 5.13. For a panel made up of three-layers of fabrics, a maximum strain of 26 per cent is predicted, with the same prestrain, when the impact velocity is increased to 245 ms^{-1}. Fig 5.14 shows the profiles for the out-of-plane transverse velocity along a yarn through the point of impact at five different times after impact. Also shown are the deformed shapes of this yarn at these same times. From the graph of the out-of-plane transverse velocity, the speed for the out-of-plane transverse wave can be estimated, the wave being assumed to have just reached the point on the yarn where the graph becomes horizontal.

Some results were also obtained for multi-layer panels made up of higher density nylon fabric. The maximum strain developed in a panel of three 386 gm^{-2} Nylon fabrics, due to an impact at 255 ms^{-1} was 18 per cent. The panel was under a uniform prestrain of 3 per cent. The combined area density of the panel, 1158 gm^{2} is almost half as much again as that of the panel in the last case, while the maximum strain was reduced by only about 30 per cent.

Fig. 5.15 shows the shape, at different times after impact, of a 483 gm^{-2} Nylon fabric impacted at 150 ms^{-1}. An 11 x 11 grid was used. Fig. 5.16 shows the velocity variation along a yarn through the single impacted node and the shape of the yarn at different times. It could be noted that the out-of-plane transverse wave did not reach the edge of the panel before the projectile was stopped. The results shown in Fig. 5.15 are for the case in which the projectile was fixed to the central node throughout the motion.

Fig. 5.17 shows the response of a 966 gm^{-2} fabric, (2x483), to a similar impact. The arrest of the projectile, as could be expected, occurred earlier than in the last case, and with a smaller out-of-pane indentation.

Fig. 5.18 shows a typical variation of boundary force with time.

QUASI-LINEAR CHARACTERISTICS METHOD: RESULTS

The values of prestrain, above which numerical results could be successfully obtained for Nylon fabrics, is 10 per cent. Below this prestrain, wild velocity fluctuations occurred. For Kevlar fabrics, prestrains greater than 0.02 per cent were required. This fact makes this approximate model only useful for the analysis of highly prestrained fabrics. For a given fabric prestrain, the quasi-linear model is much stiffer than the fully nonlinear model. For example, the former predicts that a projectile fired at 150ms^{-1} into a 240gm^{-2} Nylon fabric would be arrested 100μs after impact while the nonlinear model predicts that a much heavier fabric, a 483gm^{-2} fabric with the same prestrain value of 10% would bring the project to rest only 140μs after impact.

Fig. 5.19 and Fig 5.20 show respectively the results obtained using the quasi-linear model to analyse the response of a 240 gm^{-2} and a 386gm^{-2} Nylon fabric to impact at 150ms^{-1}.

5.3 FINITE ELEMENT METHOD RESULTS

5.3.1 Introduction

In this section, some examples of the descretisations used in the various finite element codes are mentioned and examples are given of the results obtained. Comparison is also made with a few experimental results.

5.3.2 THE MEMBRANE MODEL

Firstly, the results obtained using constant strain, three-node, triangular elements are described.

Fig 5.21 (a) and 5.21 (b) show the two patterns of descretisations investigated. With the pattern in Fig. 5.2 (a), compressive strains are generated in some elements for all impact velocities when the yarn directions are chosen to be parallel to the perpendicular sides of the elements. The descretisation pattern was therefore abandoned and that Fig. 5.21 (b) used subsequently. The results obtained with this mesh was then compared with the experimental values of deformation obtained in Ref (56). Even for this coarse mesh the predicted formation results were close to the experimental. The need for a finer division of the panel was found necessary in order to obtain accurate strain values. The model was found to converge and the final mesh chosen for generating results is the 800 element, 441 node mesh shown in Fig. 5.22

The membrane model involving constant strain triangluar elements was used to investigate the significance of:

1 Initial distribution of impact load

2 Shear resistance and jamming

3 Multilayer panels

It was found that for some values of input data, there were wild oscillations in the value of strain at the point of impact. These oscillations were suppressed by the addition of a damping factor $k\underline{M}\ddot{\underline{U}}$ to the assembled equation of motion. The equation (equation 4.17) then becomes

$$[M]\ddot{\underline{U}} + k[M]\ddot{\underline{U}} + \underline{F} = \underline{R} \qquad 5.3.1$$

where k is a fraction chosen to lie in the range .01 - .1.

1 Two starting procedures were used. In the first, a single node which was considered to be directly hit by the projectile was given an initial displacement. In the second procedure, the impact was shared between 5 nodes each of which is given the velocity of the projectile.

2 The fabric stiffness against shear, as explained earlier, is assumed to be mostly due to torsional resistance against the rotation of one yarn against another at their crossover. By changing the weft, or warp, pitch it was possible to change the number of crossovers in a given area and therefore the shear stiffness of the fabric. Using the 351gm^{-2} Kevlar fabric, and also the 386 gm^{-2} Nylon fabric, as test fabrics, both the pitch and the tex of the yarns were halved (area

density maintained constant). The results did not show any appreciable change. This was inevitable as the shear stiffness of the fabric was very low compared with the stiffness in tension in either the weft or warp directions. In fact there was hardly any change in the strain history at the point of impact when the shear stiffness was removed. The value of the parameters C_1 and C_3 in eqtn. 4.3.6 are respectively 3.5×10^{-8} and 0.0002. These values are taken in Ref. (3).

For values of shear strains less than $\pm$ 0.174 rad (10%), the value of the parameter C_2 in the Kawabata equations relating shear torque and shear strain was set to 1.948×10^{-5}gm. Above this value of shear strain, C_2 was increased to 1.0gm, that is by a factor of about 5×10^4. By this means, it was possible to prevent shear strain from exceeding 0.20. However the system as a whole became much stiffer than the physical system. This method of modelling jamming was therefore abandoned.

3 To model the response, to impact, of a panel made of a number of fabrics, the panel is replaced by a single layer but the tex and the modulus of each yarn in this model layer is put equal to that of the yarn of a single fabric multiplied by the number of fabrics in the panel. Of course, this approach is only possible when the fabrics are all identical, and laid one over another with the weft yarns parallel.

Fig. 5.23 (a) shows deceleration of a projectile fired into a 483 gm^{-2} Nylon Fabric at 150 ms^{-1}. The experimental results are from Ref. (56). There was also remarkable closeness between the experimental and the finite element model results for the transverse deformation at the point of impact. In the experimental set up, the top edge of the fabric is fixed while the lower edge is loaded by hanging

weights. The prestrain produced in the yarn is estimated to equal 0.0022. In the finite element model, the prestrain is put equal to zero.

At the same impact velocity of 150 ms^{-1}, the projectile was stopped by a 351 gm^{-2} Kevlar fabric in 170 μs. The maximum strain developed at the impact point was 2.7 percent 135 μs after impact. The maximum transverse deflection of the fabric was 1.6 cm. It is instructive to compare the response of this Kevlar fabric with that of a Nylon fabric of similar density, a 386 gm^{-2} fabric. The Nylon fabric brought the projectile to rest in 353 μs. The transverse deflection at the impacted node was 2.97 cm. The maximum strain in the fabric was 0.17 which is about 70 percent of the breaking strain of the yarns. See Fig. 5.24. This maximum strain is a smaller percentage of the breaking strain of the yarn than in the previous case where maximum strain attained was about 84 per cent of the breaking strain of the Kevlar 29 yarns. It can be noticed from the shape of a quarter of the fabric, displayed at different times, that the faster in-plane wave was reflected from the boundary before the projectile was stopped. Experimental results show that the shape of the transverse indentation is rhomboidal, this is reasonably in agreement with the results, especially in the first 200 μs after impact.

Fig. 5.25 (a) show the deformed shape of two layers of 240 gm^{-2} Nylon fabric impacted at 200 ms^{-1}. Again, it can be noticed from the distortion of the grille drawn on the fabric that the in-plane waves have been reflected from the boundary before this time. The strain at the point of impact, Fig. 5.25 (b) shows the second 'hump' when this reflected wave arrives back at the impact point.

The model predicts that a panel of two layers of 351 gm^{-2} Kevlar fabric will fail if impacted at 270 ms^{-1}. This is an underestimation, most likely, of the impact velocity at which failure occurs, as a single layer is penetrated only above 250 ms^{-1}. However, the energy which is predicted to be absorbed before failure, 34.7 J is close to the experimental values for the energy absorbed by the 2-layer panel at high velocities.

Finally, a comparison is made between the results obtained with the membrane model involving constant strain, triangular elements and another model involving 8 mode quadratic elements. As will be shown later, the results obtained using the quadratic elements are generally very close to the experimental results. Fig. 5.26 (a) shows the variation of normal strain with time, at the single impacted node, using the two different elements, for a 351 gm^{-2} Kevlar fabric impacted by a 1.003 g projectile at 350 ms^{-1}. The calculations involving rectangular elements were stopped immediately the yarn exceeded its breaking strain of 3.2 per cent, while that involving the triangular elements were continued. There was appreciable difference between the variation of strain in the two models. In Fig. 5.26 (b) the two set of results for projectile displacement were almost coincident. These results typify the general behaviour of the membrane model with triangular elements. While it predicts the central deflection of the fabric with reasonable accuracy, the strain values are poor. The poor strain values result from the requirement that the strain does not vary within an element.

A second disadvantage of this model is the spurious oscillations which have to be supressed by the addition of damping. Its advantage is that, relative other codes, particularly the program based on the method of characteristics, it uses very little computer running time.

5.3.3 CABLE ELEMENTS: RESULTS

Introduction

The results obtained using either the 2-node element or the 3-node element showed oscillations which were damped as described in the section on the membrane model. Only few results are therefore presented.

The 2-node elements were used to model different fabrics of size 152 mm by 152 mm. A standard 39 x 39 orthogonal representation was used.

A circular piece of fabric 152 mm diameter was modelled using the 3-node cable elements.

Single-point and multiple-point impacts were simulated.

The simulations of crimp effect was found difficult as the numerical oscillations increased rapidly when the magnitude of the crimp is increased from zero.

An attempt to allow yarn slip when using 2-node elements was abandoned due to too numerical instability.

Fig. 5.27 shows the strain history at the centre of the 240 gm^{-2} fabric impacted at 150 ms^{-1}. The projectile came to rest 305μs after impact, showing that the model is stiffer compared with the membrane model. The out of plane deflection at the time of arrest was predicted

impact of the two layers of a 152 mm x 152 mm square piece of Kevlar 29 fabric. In either model, the fabric was under a prestrain of 0.005. While the values for the central out-of-plane deflection predicted by the two methods are reasonably close, Fig. 5.28 (b), there are large differences in the predicted strains. It however has to be remembered that the yarn strain plotted in Fig. 5.28 (a) for the 2-node model is for the maximum strain in the yarn at any given time. This maximum value may occur in the weft yarn through the centre at one instant and occur in the warp yarn at the next instant. However the fact that no crimp was included in the characteristic model ensures that the equal strain occur in the four yarns connected to the impacted node.

The results shown in Fig. 5.29 (a) and Fig. 5.29 (b) are obtained using the 3-node cable element. Only a quarter of the fabric is modelled, and the model has 1592 nodes. The oscillation of the strain values could be noticed in both cases. Slip was allowed in the first fabric, and a coefficient of frictions of 0.5 was used. The percentage of an incident wave which is reflected from a node is maximum when the yarns are rigidly connected. The percentage which is reflected for any given value of friction coefficient lies between this maximum value and zero. This is why the strain at the point of impact is higher when rigid crossover connections are assumed. Yarn failure and fabric penetration is therefore likely to occur at a lower impact velocity when the yarns are rigidly connected.

On the whole, the rod elements are stiffer compared with either the membrane (triangular element) model or with experimental results.

5.3.4 THREE-DIMENSIONAL ELEMENTS: RESULTS

Fig. 5.30 shows the descretisation used in a model involving the use of 3-dimensional, 8-node parallelopiped interface elements and 4-node membrane elements. Only a quarter of the fabric is investigated because of the symmetry of the problem. Fig. 5.31 shows the discretisation used in another model in which the 4-node membrane elements of the former model were replaced by 9-node rectangular elements. The details of the interface elements in this second model are shown in Fig. 5.32. There are four interface elements covering the surface of each membrane element such that the nodes of the membrane element coincide with those of the interface elements. During motion, interpenetration of the curved membrane surface by the straight edges of the interface element will occur away from the nodes. This approximation should not affect the results sugnificantly as the interface elements are only introduced to produce a resistance and do not correspond to any physical material. A single point integration point is used for the 3-dimensional elements; which means the generalised reaction forces on the nodes on the top surface are equal and opposite to those of the nodes on the lower surface. 2 x 2 Gaussian integration scheme is used for the membrane elements.

It was not possible to successfully obtain results when any of the three dimensional models are used to model a multilayer assembly for impact velocities higher than 160 ms^{-1}, even in this range the numerical results obtained are not reliable. The numerical difficulties arise from the critical nature of the compressive resistance of the interface elements to a successful code implementation. Experimental data of the relationship between the yarn

not available, and therefore arbitrary values were used. If the assumed compressive modulus is too high, the projectile is prematurely arrested. If the modulus is too low, on the other hand, the downstream layers do not provide any resistance, and some interface elements will flip over, that is, their depths become negative. However, the difficulty may not totally stem from the non-availability of experimental data.

A solution to this problem would be to make the marching step iterative and treat the nodal forces due to the compression of the interface elements as a sort of 'reaction' forces. At the beginning of the step, a first estimate is made of the nodal acceleration at the beginning of that step and the new nodal position vector and nodal force vector are calculated. Generally the forces at the nodes would not balance. The requirement that the upward reaction on a layer above an interlayer element be equal to the downward reaction vector exerted by the same interlayer element only the lower layer would not be satisfied, in other words. The nodal acceleration vector is then adjusted until the magnitude of the difference between the vectors falls below a fixed limit. This modification of the code was made unnecessary by the success of the master-slave method, described next, is modelling the mechanics of multilayer panels.

5.3.5 MASTER-SLAVE LAYER METHOD: RESULTS

Initialy, the method was tested in a model involving 4-node rectangular elements. Each layer was divided identically and the central node in a layer is given the same displacement to stimulate

impact. The method was found to converge with an increase in the number of elements into which a layer is divided. A test run was carried out with a panel of two layers. One layer is a 240gm^{-2} Nylon fabric while the second is a 351 gm^{-2} Nylon fabric. The panel was impacted at 500 ms^{-1}. In the first run, the lighter fabric was put in front (nearer to the projectile) and in the second, the position of the fabrics were reversed. In each run, the projectile penetrated the panel, 24 μs after impact, with a residual velocity of 457 ms^{-1}. The coincidence of the results of the two runs confirms the stability of the procedure.

The influence of the frictional resistance between the layers was checked for values of coefficients of dynamic friction between 0.0 - 0.03. Frictional resistance against interlay slip, or the surface treatment of the fabrcs, did not significantly affect the overall structural behaviour of the panel for this range of frictional coefficient.

For a single layer of fabric, it was found, that the membrane model based on 4-node element always predicts that fabric failure occurs earlier than experimentally observed. The difference is, partly, because the linear nature of the variations of variables within the 4-node element prevents an adequate variation of strains. The assumed strain variation pattern which results from the differentations of the displacements cannot accurately model the rapid change of strains which occurs in the fabric; especially in the area close to the impact point. The model therefore predicts higher yarn strains. The result is that the breaking strain is reached too early during motion and failure occurs at low impact velocities, for example, a projectile striking a 351 gm^{-2} Kevlar fabric at 500 ms^{-1} is predicted to have penetrated with

To improve the prediction of fabric strains, 8-node elements were subsequently used to obtain results comparable to the available experimental results. Nodal strains were calculated from strains at integration points by the use of a least square smoothing routine (59).

Still using 4 -node elements, the ability of the procedure to model the seperation of layers during motions was tested. A two-layer panel of a 386 gm^{-2} Nylon fabric and a 351 gm^{-2} Kevlar fabric was modelled. The resistance to interlayer slip was put at zero. In the first run, the Kevlar fabric was put nearer to the impacting projectile. The Kevlar fabric was penetrated 10μ s after the start of motion when the projectile speed has been reduced to 492 ms^{-1}. For the remaining part of the motion, the projectile was in contact with the Nylon fabric which then moved away from the penetrated fabric. The second layer was penetrated 14μ s later when the breaking strain of nylon was reached. The residual projectile velocity was 459 ms^{-1}. In the next run the nylon fabric was put nearer to the projectile so that seperation does not occur throughout the motion, although the Kevlar fabric failed when the strain at the centre of the panel exceeded 0.0323.

Fig. 5.33 shows the deceleration curve and the change of vertical displacement at the impacted node for a 240 gm^{-2} Nylon fabric impacted at 150 ms^{-1}. The 8-node rectangular elements were used. Although there are no comparable experimental results, the numerical results seem reasonable.

The strain values were improved by the use of 8-node rectangular elements. The residual velocity with which a 1.0 g projectile with an initial velocity of 500 ms^{-1} leaves a 351 gm^{-2} Kevlar fabric was

predicted to be 472 ms^{-1}. The energy absorbed by the fabric, 13.6 J, compares well with the value of 14.6 J which was obtained experimentally in UMIST for an impact velocity of 512 ms^{-1}. The variation of the energy absorbed with velocity is very weak at such high velocities.

The posibility of modelling multilayer panels as single layer panel was also investigated. This was achieved by multiplying the tex of the yarns and the fabric density of a single layer by the number of layers in panel. This implicity involves the assumption that each layer deforms identically to the other, which means that inter-layer slip is insignificant. This approximation is reasonable at high velocities. Experimental results obtained in UMIST (Textile Technology) (61) showed that while 9 layers of 240 gm^{-2} Nylon fabric are totally penetrated by a projectile travelling at 405 ms^{-1}, 10 layers are not penetrated even when the projectile velocity is increased to 407 ms^{-1}. With the approximate multilayer model just explained, it was predicted that whereas 10 layers of the fabric are totally penetrated at a velocity of 420 ms^{-1}, while the projectile is stopped when the velocity is reduced to 400 ms^{-1}.

Fig 5.34 shows the variation of the energy absorbed before penetration, for increasing numbers of 351 gm^{-2} Kevlar layers. Both the experimental results and the numerical predictions are shown.

In general it is observed that this approximate method of modelling multilayer panel produces results which are very close to the experimental results. However the difference between the numerical and experimental results increases as the residual energy approaches zero.

In this region, the size of fabric is just enough to absorb all the initial energy of the projectile. The contact time between the projectile and the fabrics, especially the last layers, is then relatively high and some factors, neglected in the approximation, become significant.

The master-slave layer method, with allowance for interlayer slip, that is the system described in section 4.5, was successfully implemented using 8-node rectangluar elements. However, solution time was found to be multiples of that required for the same problem when slipping was suppressed. Most of the extra time was taken in the search subroutine and in the calculation of the normal components of the reaction between the layers. Also, as explained in section 4.5, the modified mass matrix (eqtn. 4.5.17) is then no longer diagonal and has to be inverted. The only condition in which the original method need be used instead of this more efficient approximation is when the effect of fabric slip is under investigation or when panel is assembled from fabrics of different materials. Under these conditions, the panel may not be replaced by a single, equivalent, fabric.

Because of the storage and execution time advantages of the approximate method, it is to be preferred to the complete master-slave layer method, except under special conditions.

Experimental results (37) show that it is more effective, in a two layer panel, to put the denser layer upstream instead of downstream. the difference in effectiveness cannot be predicted by this model. This is possibly linked to the fact that influence of localised yarn compression on yarn rupture is neglected.

On the whole, this model can predict, with reasonable accuracy, the mechanics of the response of multilayer fabrics to impact.

CHAPTER 6

CONCLUSION

6.0 Introduction

The accuracy and usefulness of the different models in predicting the V_{50}, which is defined as the speed at which 50% of the projectiles fail to penetrate a test panel, is discussed in this chapter. The computer times required to obtain numerical methods by these methods are compared.

6.1 The Simple Variational Method

Although the computer units used in solving the equation is small, results are only obtainable for fabrics with high prestrains. While the method is useful for comparing different fabric weaves, it is not suitable for obtaining the V_{50} of a panel.

6.2 Nodal Impedance Analysis

This analysis may be useful in predicting the relative advantages of different fabric geometries, as far as their response to impact is concerned. However, the suggestion by two earlier investigations is that crossover effects may not significantly magnify strains as considerable slipping occurs (61), (62).

6.3 Method of Characteristics

This solution requires the maximum computer time, for a given fabric and projectile, of all the approaches and methods used in this investigation. Apart from this disadvantage, a high prestrain which increases with the impact velocity is required for its successful

implementation. The use of this method should be restricted to providing a basis for comparing different fabrics as it is too expensive for regular usage.

6.4 Finite Element Solutions

The various models are treated separately.

(a) Rod elements - (2 node and 3 node)

These produced well-conditioned results, with no oscillations for some fabrics. But oscillations occur, especially for Kevlar fabrics. This model provides a means of investigating the effect of rigidity of yarn connections at crossovers. However methods of supressing the strain oscillations have to be introduced before the model could be used in production. The model based on 2-node rod elements makes the most efficient use of computer time, compared with all the other models. They also provide an approximate approach to assessing the effect of crimp.

(b) The 3 node (triangular) membrane Element

This is an accurate model for investigating the mechanics of a single fabric layer. While the results are well-behaved for most input data, oscillations have to be supressed for some input data. The model is quite efficient in computer time usage. It is useful for different weaves of fabric and also for knitted fabric.

(c) The 3-Dimensional Model

Further work is required to render this model usable for routine design. The solution might be to replace the two-dimensional membrane elements by 20-node parallelopiped and remove the interface elements.

(d) The Master-slave layer method

This model involving 4-node rectangular elements produces poor predictions of V_{50} values. However it is useful as an inexpensive way of studying the effects of interlayer slip

Better results are obtainable by using 8-node rectangular elements. However the running times are high, compared with either that involving 3-node triangular elements or 4-node triangular elements. This code is useful for routine calculations.

6.5 Factors affecting overall behaviour of fabric

Only a description rather than a quantitative comparison of the significance of the various yarn and fabric properties would be given.

In-Plane Shear

Shear stiffeners seem to have little significance on fabric performance until its value is high enough to reduce the ability of the yarns to absorb the projectile kinetic energy as longitudinal strain energy. This will happen when a very stiff coating is applied to a fabric. Otherwise the change in fabric shear stiffness obtained by washing may not be significant.

Crimp interchange

The descretisation has not been fine enough for definite conclusions on the significance of crimp interchange. Its effect on fabric performance may vary with the impact velocity.

Friction

Increasing the friction of yarn crossovers will increase the percentage of reflections at nodes, and will therefore reduce fabric effectiveness. Friction between layers does not seem to be very significant close to the V_{50} since penetration occurs before appreciable movement of the panel can take place. The influence of friction-generated heat on modulus and breaking strain was not evaluated.

Size of yarn and pitch

The tex of a yarn seems to affect the value of its breaking strain

while its crimp varies with pitch, for a given tex. Apart from these indirect effects, neither the text of a yarn, nor the pitch in any direction, seem to significantly affect fabric performance.

Bending stiffness of yarn

Although some earlier investigations conclude that yarn bending cannot be neglected if the mechanics of fabric behaviour at low strains is to be accurately modelled, the results obtained show that the influence of bending may be of second order to the overall fabric effectiveness.

6.6 Future Work

(1) The condition for yarn failure which was adopted here is the simplest possible. Since the order of arrangements of two fabrics has been found to affect their efficiency in absorbing impact energy, it is likely that yarn compression affects the longitudinal strain at which a yarn ruptures. The relationship should be studied and incorporated into the failure condition used in any numerical method for predicting V_{50} values.

(2) The attempts to model a fabric with yarns which can slip during motion has not been very successful due to numerical oscillations of yarn strain. The development of an alternative method should be investigated.

BIBLIOGRAPHY

1 PIERCE, F.T.
The Geometry of Cloth Structure
J. of Tex. Inst. Vol 28, 1937, pp. 145-196.

2 OLOFSSON, B.
"A General Model of a Fabric as a Geometric-Mechanical Structure"
J. of Text. Inst., Vol 55, 1964, pp. T541-T557.

3 KAWABATA, S, NIWA, M., KAWAI, H.
"The Finite-Deformation Theory of Plain-Weave Fabrics Part I: The Biaxial-Deformation Theory"
J.Text. Inst., Vol 64. 1973, pp. 21-46.

4 KAWABATA, S., NIWA, M., KAWAI, H.
"The Finite Deformation Theory of Plain-Weave fabrics Part II: The Uniaxial Deformation Theory".
J. of Text. Inst. Vol 64, 1973, pp. 47-61.

5 KAWABATA, S., NIWA, M., KAWAI, H.
"The Finite Deformation Theory of Plain-Weave Fabrics, Part III: The Shear Deformation Theory".
J. of Text Inst. Vol 64, 1973, pp. 62-85.

6. OLOFSSON, B.,
"A study of Inelastic Deformation of Textile Fabrics",
J. Text. Inst., Vol. 58, No. 6, June 1967, pp. 221-241.

7 GROSBERG, P., KEDIA, S.,
"The Mechanical Properties of Woven Fabrics Part I: The Initial Load Extensoion Modulus of Woven Fabrics".
Text. Res.Jnr., Vol. 36, 1966, pp. 71-79.

8 MAcROY, B.M., McGRAITH, J.R., McNAMARA, A.B.,
"The Biaxial Load-Extension Properties of Plain Weft-knitted Fabrics - A Theoretical Analysis".
Text. Res. J., Vol 45, No. 10, Oct. 1975, pp. 746-759.

9 HEARLE, J W S., & GROSBERG, P.,
Chapter 14,
in Hearle, J W S, Grosberg, P, and Backer, S.
Structural Mechanical of Fibers, Yarns and Fabrics, Vol. 1, Wiley-Interscource 1969.

10 SKELTON, J., FREESTON
"The Tensile Behaviour of Woven Fabric at Low and High Strain Rates".
Text. Res. J., Vol. 41, No. 3, March 1971, pp. 187-196.

11 SHANHAN, W.J., POSTLE, R.,
"Jamming of Knitted Structures",
Text. Res.J. Vol. 43, No. 9, Sept 1973, pp. 532-538.

12 HEARLE, J W S
in "Mechanics of Flexible Fibre Assemblies", (ed), Hearle J W S, Thwaites, J J and Amirbayat, J. (Sijthoff and Noordhoff) 1979 NATO ASI Applied Science Series No. 38

13 SKELTON, J
"Triaxially Woven Fabrics: Their Structure and Properties"
Text. Res. J., Vol 48, No. 8, Aug 1971, pp. 637-647.

14 SCARDINO, F.L., KO, F.K.,
"Triaxial Woven Fabrics Part I: Behaviour Under Tensile, Shear and Burst Deformation".
Textile Res. J., Vol 51, No. 2, Feb 1981, pp. 80-89.

15 HUANG, N.C.,
"Finite Biaxial Extension of Completely Set Plain Woven Fabrics"
Tras. ASME (EM5) J. Appl.Mech. Vol46, Sept 1979, pp. 651-655.

16 GENENSKY, S.M., RIVLIN, R.S.,
"Infinitesimal Plane Strain in a Network of Elastic Cords",
Arch. Rational Mech., Vol 4, 1960, pp. 30-44.

17 CHRISTOFFERSEN, J.,
"Fabrics: Ortotropic Materials With a Stress-Free Shear Mode"
Tras. ASME E J. Appl. Mech. Vol 47, March 1980, pp. 71-74.

18 STUBBS, N., FLUSS, H.,
"A Space-Truss Model for Plain-weave Coated Fabrics",
J. Appl. Maths. Modelling, Vol 4, Feb 1980, pp. 51-58.

19 TORBE, I.,
"A Cruciform Element for the Analysis of Fabrics Structure" - in Mathematics of Finite Element and Applications. Vol. 1 (ed) Whiteman, J R, Academic Press, 1976.

20 LEECH, C.M.,
"The Modelling of Net and Cloth Dynamics",
J. of the Franklin Inst., Vol. 307, No. 6, June 1979, pp. 361-377.

21 JONAS, S.G.H., ZUKAS, J.A.,
"Mechanics of Penetration, Analysis and Experiment",
Inf. J. Engng. Sci., Vol 16, 1978, pp. 879-903.

22 MANSELL, J.,
"Ballistic Impact of Woven Fabrics",
Unpublished Ph.D. thesis submitted to the University of Manchester Institute of Science and Technology (1981).

23 MAROM, I., BODNER, S.R.,
"Projectile Perforations of Multilayered Beams",
Int.J. Mech. Sci., Vol. 21, 1979, pp. 489-504.

24 DANIEL, I.M. & LIBER, T.,
"Wave Propagation in Fiber Composite Laminates",
Final Report NASA CR-135086 IITRI D6073-III, III Research Institute, Chicago, Illinois, 1976.

25 CRISTESCU, N., MALHEIN, L E, SIERAKOWSKI, R.L.
"Failure Mechanisms in Composite Plates Imparted by Blunt-Ended Penetrators in Foreign Object Impact Damage to Composites ASTM STP 568, Philadelphia. American Society of Testing Materials (1975), pp. 159-172.

26 HENGHOLD, W.M., RUSSELL, J.J.,
"Equilibrium and Natural Frequencies of Cable Structures (A Non-linear finite element approach)",
Compt. and Struct., Vol. 6, 1976, pp. 267-271.

27 OZDEMIR, H.,
"A Finite Element Approach for Cable Problems"
Int. J. Solids and Struct. Vol 15, 1975, pp. 427-437.

28 des LINCH, F.,
"Dynamic Response of a Constrained Fibrous System Subjected to Transverse impact ", Part II, a mechanical model.

29 SHANKS, J.S., LEECH, C.M.,
"Dynamics of Reinforced Coarse Nets Using a Finite Element Analysis.
Int. J. Mech.Sci., Vol. 21 1979, pp. 131-138.

30 LEECH, C.M., HEARLE, J.W.S., MANSELL, J.
"A Variational Model for the Arrest of Projectiles by Woven Cloth and Nets",
J. Text. Inst., Vol 70, Nov 1979, pp. 469-477.

31 LEECH, C.M., MANSELL, J.,
"Some Aspects of Wave Propagation in Orthogonal Nets",
Int.J. Mech.Sci., Vol 19, 1977, pp. 93-102.

32 ODEN, J.T., KEY, J.E., FOST, R.B.,
"A Note on the Analysis of Non-linear Dynamics of Elastic Membranes by the Finite Element Method".
Comp. & Struct., Vol 4, 1974, pp. 445-452.

33 BENZLEY, S.E., KEY, S.W.,
"Dynamic Response of Membranes with Finite Elements",
Proc. ASCE J. Engng. Mech. (EM3), June 1976, pp. 447-60.

34 TABADDOR, F., STAFFORD, Y.J.R.,
"Nonlinear Vibration of Cord-Reinforced Composite Shells".
Comp. & Struct., Vol 13, 1981, pp. 737-743.

35 LEONARD, J., VERMA, V.,
"Double Curved Element for Mooney-Rivlin Membranes",
Proc. ASCE J. Engng. Mech., (EM3), Aug 1976, pp. 625-641.

36 LLOYD, D.
"Analysis of Complex Fabric Deformations", in "Mechanics of Flexible Fibre Assemblies" (ed) Hearle, J.W.S., Thwaites, J.J., and Amirbayat, J., (Sijthoff and Noordhoff) 1979, NATO ASI Applied Science Series No. 38.

37 FLAHERTY, R.E.,
"A Study of Low Velocity Impacts into Thin Sheet Aluminium and Nylon Cloth",
NASA TN D-6324 May 1971.

38 WILKINS, M.L.
"Calculation of Elastic-Plastic Flow",
UCRL-7322 Rev. 1, Lawrence Radiation Laboratory (Univ. of

39 THOMPSON, E.G., GOODMAN, J.R., VANDERBILT, M.D.,
"Finite Element Analysis of Layered Wood Systems",
Proc. ASCE, J. Structural Division, Vol 101, Dec 1975, pp. 2659-2671.

40 SUZUKI, H., CHANG, T-Y, P.,
"Bending of Laminated Cantilever Beams With Interface Slip",
Proc. ASCE, J. Structural Division, Vol 105, Feb 1979, pp. 269-281.

41. KHUTUA, T.P., CHEUNG, Y.K.,
"Triangular Element for Multilayer Sandwich Plates",
Proc. ASCE J. Engng Mech. EM5 Vol 98, Oct 1972, pp. 1225-1238.

42 HERZL, C., BAKCOCK, D., KNAUSS, W.G.,
"One Dimensional Modelling of Failure of Laminated Plates by Delamination",
Int. J of Solids and Struct. Vol 17, No. 11, pp. 1069-1083.

43 LEE, J.D.,
"3-Dimensional Finite Element Analysis of Layered Fiber-Reinforced Composite Materials",
Comp. & Struct., Vol 12, 1980, pp. 319-339.

44 DONEA, J. (ed),
Advanced Structural Dynamics (ISPRA)
Applied Science Publications (1978).

45 OHTE, S.,
"Finite Element Analysis of Elastic Contact Problems",
Japanese S.M.E. Bulletin, Vol 16, No. 95, May 1973.

46 TSUTA, T., YAMAJI, S.,
"Finite Element Analysis of Contact Problems", pp. 177-192 in Theory and Practice of Finite Element Structural Analyses. Proc. 1972 Tokyo Seminar on Finite Element Analyses (ed) Yamada, Y. & Gallagher, R.H. (Univ. of Tokyo Press).

47 HSU, T.R., BERTELS, W.M.,
"Application of Elasto-Plastic Finite Element Analysis to the Contact Problems of Solids",
AIAA J. Vol. 14, No. 1, Jan 1976, pp. 121-122.

48 JOHNSON, G.R.
"High Velocity Impact Calculations in Three Dimension",
Trans. ASME Series, E. J. Appl. Mech., Vol. 44, March 1977, pp. 95-100.

49 JOHNSON, G.R.,
"Three-Dimensional Analysis of Sliding Surfaces During High Velocity Impact",
Trans. ASME Vol. 99, Series E, J. Appl. Mech., Vol. 44, Dec 1977, pp. 771-773.

50 JOHNSON, G.R., COLBY, D.D., VAVRICK, D.J.,
"Three-Dimensional Computer Code for Dynamic Response of Solids to intense Impulse Loads",
Int. J. Num. Methods in Engng. Vol 14, 1979, pp. 1865-1871.

51 JOHNSON, G.R.,
"Dynamic Analysis of Explosive Metal Interaction in Three Dimensions",
Trans. ASME Vol. 103, Series E., J. Appl. Mech., Vol. 48, March 1981, pp. 30-34.

52 JEFFREY, A., TANIUTI, T,
Non-linear Wave Propagation (Academic Press) 1964.

53 CRISTESCU, N.,
Dynamic Plasticity (Series in Applied Mathematics and Mechanics), North Holland, 1967.

54 SMITH, R.L., PHOENIX, S.L.,
"Asymptotic Distribution for the Failure of Fibrous Materials Under Series - Parallel Structure and Equal Load-sharing",
Trans. ASME, Vol 103, Series E., J. Appl. Mech., Vol 48, 1981, pp. 75-82.

55 PITT, R.E., PHOENIX, S.L.,
"On Modelling the Statistical Strength of Yarns and Cables Under Localized Load-Sharing among fibers",
Text. Res. J., Vol 51, No. 6, June 1981, pp. 408-425.

56 MAHEUX, C.R., STEWART, G.M., PETTERSON, D.R., ODELL, F.A.,
"Dynamics of Body Armour Material under High Speed Impact", Part I,
US Army Chemical Warfare Laboratories, CNLR 2141, 1957.

57 ZIENKIEWICZ, O.C.,
The Finite Element Method (Third Edition), McGraw-Hill Book Co.

58 IRONS, B., AHMAD, S.,
Techniques of Finite Elements
(Ellis Horwood Series in Engineering Science).

59 HINTON, E., SCOTT, F.C., RICKETTS, R.E.,
"Local Least Squares Stress Smoothing for Parabolic Isoparametric Elements",
Int.J. Num. Meth. Engng. Vol 9, 1975, pp. 235-256.

60 HEARLE, J.W.S., LEECH, C.M., CORK, C., ADEYEFA, B.A.,
Ballistic Impact of Resistance of Multilayer Text. Fabrics",
Interim Report Oct 1981 (UMIST). Dept. of Textile Technology.

61 FREESTON, W.D., CLAUS, W.D.,
"Strain-Wave Reflections During Ballistic Impact of fabric panels"
Text. Res. J. Vol 43, No. 6, June 1973, pp. 348-351.

62 ROYLANCE, D.,
"Stress Wave Propagation in Fibres: Effect of Crossovers",
Fib.Sci. and Tech., Vol. 13, 1980, pp. 385-395.

APPENDIX 1

Wavefronts in Triaxial Weaves

Prediction of Wave-Front

Leech and Mansell (31) have shown that the wave front in a transversely impacted orthogonally woven fabrics is rhombiocal. Below, it is shown that for a plain triaxial weave the propagation front is hexagonal. The repeated cell of this fabric is shown in Fig. A1.1(a).

The equation of the sides of the hexagonal are

$$t = \frac{S_1}{C_1} + \frac{S_2}{C_2}, \qquad t = \frac{-S_1}{C_1} - \frac{SS_2}{C_2}, \qquad \text{A1.1a}$$

$$t = \frac{S_2}{C_2} + \frac{S_3}{C_3}, \qquad t = \frac{-S_2}{C_2} - \frac{S_3}{C_3}, \qquad \text{A1.1b}$$

$$t = \frac{S_3}{C_3} - \frac{S_1}{C_1}, \qquad t = \frac{-S_3}{C_3} + \frac{S_1}{C_1} \qquad \text{A1.1c}$$

where S_1, S_2 and S_3 are the coordinate in the directions of the yarns (Fig. A1.1b) and C_1, C_2 and C_3 are the transverse wave velocities in the respective directions.

A similarity type of solution $W(t_1 s_1, s_2, s_3) = Wo(t)W(\eta)$ is introduced where $\eta = \frac{S_1}{C_1 t} + \frac{S_2}{C_2 t}$ for the region where $S_1 \geq 0$, $S_2 \geq 0$, $S_3 \geq 0$ where Wo is the displacement at the point of impact. See Fig A1.2.

The coordinate η is perpendicular to the wavefront and $\eta = o$ at the impact and $\eta = 1$ at the wavefront Fig. A1.3.

The excited area $A = \sqrt{\frac{3}{4}}\, t^2 C_1 C_2\, \eta^2$ and the incremental area,

$$dA = \frac{\sqrt{3}}{2}\, t^2 C_1 C_2\, \eta\, d\eta \ .$$

T, the kinetic energy of the material in area dA behind the wave front, at any time t, is given by,

$$T = \int_A \frac{1}{2} m \left(\beta_1 + \beta_2 + \beta_3 \right) \left(\frac{\partial W}{\partial t} \right)^2 dA, \qquad \text{A1.2}$$

β_1, β_2, β_3 are the mass fractions of the yarn families (1, 2 and 3). The total kinetic energy for the whole deformed is

$$T = \sqrt{\frac{3}{2}} (C_1C_3 + C_2C_1 + C_2C_3)t^2 \left[Wo^2 I_1 + 2 \frac{\dot{W}o Wo}{t} I_1 + \frac{Wo^2}{t^2} I_2 \right] , \qquad \text{A1.3}$$

where $I_1 = \int_o^1 \bar{W} \eta\, d\eta$, and $I_2 = \int_o^1 W'^2\, \eta\, d\eta$.

Note (') denotes differentiation with respect to η and (˙) differentiations with respect to time.

The expression for the strain at one point in the yarn s, is

$$\varepsilon = \left\{ (1 + \varepsilon_s) \sqrt{1 + \left(\frac{\partial W}{\partial s}\right)^2} - 1 \right\} ,$$

where ε_s is the prestrain and $\frac{\partial W}{\partial s}$ is the slope along the yarn at that point.

For a linearly elastic material, the resulting strain energy =

$$\sum \frac{1}{2} \int_A E_s h_s \left\{ (1 + \varepsilon_s) \sqrt{1 + \left(\frac{\partial W}{\partial s}\right)^2} - 1 \right\} dA, \quad \text{A1.4}$$

Summed up for all the familiarty strands in the area. E is the Young's modulus of the sth strand and h_s is its average thickness.

Assuming highly stressed triaxial fabrics with small identation, the system is now linear $\left(\frac{\partial W}{\partial s} \ll 1\right)$ and the strain energy becomes,

$$U = \frac{\sqrt{3}}{2}\left[C_3C_1\left(\frac{\sigma_1}{C_1^2}+\frac{\sigma_2}{C_3^2}\right)+C_2C_3\left(\frac{\sigma_2}{C_2^2}+\frac{\sigma_3}{C_3^2}\right)+C_1C_2\left(\frac{\sigma_1}{C_1^2}+\frac{\sigma_2}{C_2^2}\right)\right]\int_0^1 W_0^2\bar{W}'^2\eta\, d\eta, \quad \text{A1.5a}$$

or

$$U = \frac{\sqrt{3}}{2} I_3 W_0^2\left[C_3C_1\left(\frac{\sigma_1}{C_1^2}+\frac{\sigma_2}{C_3^2}\right)+C_2C_3\left(\frac{\sigma_2}{C_2^2}+\frac{\sigma_3}{C_3^2}\right)+C_1C_2\left(\frac{\sigma_1}{C_1^2}+\frac{\sigma_2}{C_2^2}\right)\right], \quad \text{A1.5b}$$

where $I_3 = \int_0^1 (\bar{W}')^2 \eta\, d\eta.$

The initial kinetic energy of the projectile is $\frac{1}{2}$ MpẆo^2. When this is added to the total energy of the fabric and Hamilton's principle is applied, the result is the equation of motion:

$$\left[Mp + \sqrt{3m(C_1C_3+C_2C_1+C_3C_2)t^2 I_1}\right]\ddot{W}o + 2\sqrt{3m(C_1C_3+C_2C_1+C_3C_2)tI_1}\dot{W}o$$

$$+\sqrt{3}\left[\left(C_1C_3\left(\frac{\sigma_1}{C_1^2}+\frac{\sigma_2}{C_3^2}\right)+C_1C_2\left(\frac{\sigma_1}{C_1^2}+\frac{\sigma_2}{C_2^2}\right)+C_2C_3\left(\frac{\sigma_2}{C_2^2}+\frac{\sigma_3}{C_3^2}\right)\right)I_3 +$$

$$\sqrt{3m(C_1C_2+C_1C_3+C_2C_3)(I_1 - I_2)}\,\Big] Wo = 0, \quad \text{A1.6}$$

where $m = \frac{\sigma_1}{C_1^2} + \frac{\sigma_2}{C_2^2} + \frac{\sigma_3}{C_3^2}$.

The equations can be nondimensionalised by introducing the factor $\tau = \alpha t$ and λ, to get

$$(1 + \tau^2)\, Wo'' + 2\tau\, Wo' + \frac{\lambda I_3 + (I_1 - I_2)}{I_1} Wo = 0 \qquad A1.7$$

where $\alpha^2 = \frac{\sqrt{3}m(C_1C_2+C_2C_3+C_1C_3)}{12\,Mp}$ and

$$\lambda = \frac{C_1C_3\left(\frac{\sigma_1}{C_1^2}+\frac{\sigma_3}{C_3^2}\right)+C_1C_2\left(\frac{\sigma_1}{C_1^2}+\frac{\sigma_2}{C_2^2}\right)+C_2C_3\left(\frac{\sigma_2}{C_2^2}+\frac{\sigma_3}{C_3^2}\right)}{m(C_1C_2+C_1C_3+C_2C_3)}$$

Equation 3.7 is very similar to the expression $(I + \tau^2)Wo'' + 2\tau Wo' + \delta Wo = 0$ obtained for small indentation of an orthogonally woven fabric (31) where

$$\delta = \frac{I_3 + I_1 - I_2}{I_1}$$

The only parameter which affects the response of the orthogonal fabric for a nondimensional velocity of impact, is δ which is dependent only on the grouping of integrals while for the triaxial fabric λ also depends on the ratio of the yarn stresses.

Large Deformations

The equations of motion for large deformations of the triaxial fabric is obtained by the application of Hamilton's principle with the expressions A1.3 and A1.4 incorporated and is as follows

$$(1+\tau^2)W_o'' + 2\tau W_o' + 6W_o\left[\frac{k_1\beta_1(1+\varepsilon_1)}{\varepsilon_1}\left\{1+\varepsilon_1 - \frac{1}{\sqrt{1+(W_o/C_1\tau)^2}}\right\}\right.$$

$$\left. + \frac{k_2\beta_2(1+\varepsilon_2)}{\varepsilon_2}\left\{1+\varepsilon_2 - \frac{1}{\sqrt{1+(W_o/C_2\tau)^2}}\right\} + \frac{k_3\beta_3(1+\varepsilon_3)}{\varepsilon_3}\left\{1+\varepsilon_3 - \frac{1}{\sqrt{1+(W_o/C_3\tau)^2}}\right\} - \frac{1}{3}\right] = 0, \qquad \text{A1.8}$$

where $k_1 = \dfrac{C_1C_3 + C_1C_2}{C_1C_3 + C_1C_2 + C_2C_3)}$,

$$k_2 = \frac{C_1C_2 + C_2C_3}{C_1C_2 + C_2C_3 + C_3C_1}$$

$$k_3 = \frac{C_2C_3 + C_1C_3}{C_1C_2 + C_2C_3 + C_3C_1}$$, and β_1, β_2, β_3 are the

mass fraction of the s_1, s_2 and s_3 strands respectively.

APPENDIX 2

Theory of the Method of Characteristics

Theory

Consider a single filament, Fig. A2.1, with displacement functions, u, v, w relative to its initial constraint position. The displacements are functions of x, the running coordinate along the undisplaced length of the filament, and t the time.

To allow for large deformations, the strain, ε , is defined as

$$\varepsilon = \left\{ (1+u_{,x})^2 + v_{,x}^2 + w_{,x}^2 \right\}^{\frac{1}{2}} - 1. \qquad \text{A2.1}$$

(Note: $h_{,x}$ denotes the differentiation of h with respect to x).

The kinetic co-energy and the strain energy can be written as:

$$T = \frac{1}{2} \int_0^L \rho A (u_{,t}^2 + v_{,t}^2 + w_{,t}^2)\, dx , \qquad \text{A2.2}$$

$$U = \int_0^L \frac{AE\,\varepsilon^2}{2}\, dx ,$$

where A is the cross-sectional area of the yarn and E its Young's modulus, and ρ its density.

Applying Hamilton's principles, the differential equations of the motion of the string are:

$$u_{,tt} - \frac{E}{\rho}(1+\varepsilon)^2 \left\{ \varepsilon(1+\varepsilon) u_{,xx} + (1+u_{,x})\, \varepsilon_{,x} \right\} = 0 \qquad \text{A2.3(a)}$$

$$V,tt - \frac{E}{(1+\varepsilon)^2}\left\{(1+\varepsilon)V,_{xx} + V,_x\ \varepsilon,_x\right\} = 0 \qquad \text{A2.3(b)}$$

$$W,tt - \frac{E}{(1+\varepsilon)^2}\left\{(1+\varepsilon)W,_{xx} + W,_x\ \varepsilon,_x\right\} = 0 \qquad \text{A2.3(c)}$$

These equations are conveniently reduced to a system of six quasilinear hyperbolic equations by the introduction of the following terms:

$$P = U,_t \quad , \quad q = V,_t \quad , \quad r = W,_t \ ,$$

$$\Theta = U,_x \quad , \quad \Phi = V,_x \quad , \quad \Psi = W,_x \ .$$

Further at a point on the filament, the vectors $\underline{Z}$, $\underline{W}$, and $\underline{p}$ are defined as

$$\underline{Z} = \begin{bmatrix} p \\ q \\ r \\ \Theta \\ \Phi \\ \Psi \end{bmatrix} \quad , \quad \underline{W} = \begin{bmatrix} \Theta \\ \Phi \\ \Psi \end{bmatrix} \quad , \quad \underline{p} = \begin{bmatrix} P \\ r \\ q \end{bmatrix} \qquad \text{A2.4}$$

These 6 equations are now written in matrix form as

$$\underline{Z},_t + A\underline{Z},_x = 0, \qquad \text{A2.5}$$

where A is a 6 x 6 matrix.

Equations A2.3 are the equations of propagations of signals or disturbances along the filament.

Equation A2.3(a) models longitudinal wave motion while A2.3(b) and A2.3(c) are the equations of propagation of waves in the two transverse directions.

Characteristic theory is now applied to equation A2.5 to obtain the characteristic equations of the single yarn. These are:

$$\underline{\text{along}} \quad \frac{dx}{dt} = + C_e = \sqrt{E/\rho}$$

$$I^+ \qquad \underline{U}_1 (\underline{W})\, d\underline{Z} = 0, \qquad \text{A2.6(a)}$$

$$\underline{\text{along}} \quad \frac{dx}{dt} = - C_e = \sqrt{E/\rho}$$

$$I^- \qquad U_2 (\underline{W})\, d\underline{Z} = 0 \quad , \qquad \text{A2.6(b)}$$

$$\underline{\text{along}} \quad \frac{dx}{dt} = + C_T = \sqrt{E\varepsilon/\rho(1+\varepsilon)}$$

$$II^+ \qquad \underline{U}_3 (\underline{W})\, d\underline{Z} = 0 \quad , \qquad \text{A2.6(c)}$$

$$\underline{U}_4 (\underline{W})\, d\underline{Z} = 0 \qquad \text{A2.6(d)}$$

$$\underline{\text{along}} \quad \frac{dx}{dt} = C_T = -\sqrt{E\varepsilon/\rho(1+\varepsilon)}$$

$$II^- \qquad U_5 (W).d\underline{Z} = 0 \quad , \qquad \text{A2.6(e)}$$

$$U_6 (\underline{W}).d\underline{Z} = C. \qquad \text{A2.6(f)}$$

In each of the equations, $d\underline{Z}$ is the change in the vector $\underline{Z}$ along the characteristic curve see Fig A2.2, while

$\underline{U}_i$, i = 1,2 .....6 are the 6 left eigen vectors of the matrix A (equation A1.12).

It is to be noticed that the velocities of propagation of the transverse waves C_e, C_T are dependent on the strain and so vary with time. Also $C_e > C_T$ for all values of ε of interest.

The eigenvectors of the matrix A, equation A2.5 are:

$$U_1 = U_2 = \left[(1+\theta),\ \phi,\ \psi,\ \lambda_e(1+\theta),\ \lambda_e\phi,\ \lambda_e\psi\right]^T \qquad \text{A2.7}$$

$$U_3 = U_5 = \left[\phi,\ (1+\theta),\ 0,\ \lambda_t\phi,\ \lambda_t(1+\theta),\ 0\right]^T \qquad \text{A2.8}$$

$$U_4 = U_6 = \left[\psi,\ -(1+\theta),\ 0,\ \lambda_t\psi,\ -\lambda_t(1+\theta),\ 0\right]^T \qquad \text{A2.9}$$

The equations A2.6 are now rewritten as

$$(1+\theta)\Delta p_i + \phi\,\Delta q_i + \psi\Delta r_i + C_e(1+\theta)\Delta\theta_i + C_e\phi\Delta\phi_i +$$

$$C_e\psi_i\Delta\psi = 0 \text{ (I - extensional)} \qquad \text{A2.10}$$

$$\phi\cdot\Delta p_i - (1+\theta)\,\Delta q_i + C_t\,\phi\,\Delta\theta_i - C_t(1+\theta)\Delta\psi_i = 0 \qquad \text{A2.11}$$

(II^- characteristics-inplane transverse).

$$\psi\cdot\Delta p_i - (1+\theta)\ \Delta r_i + C_t\psi\,\Delta\theta_i - C_T(1+\theta)\,\Delta\psi_i = 0\,, \qquad \text{A2.12}$$

(II^- characteristics-out-of-plane transverse)

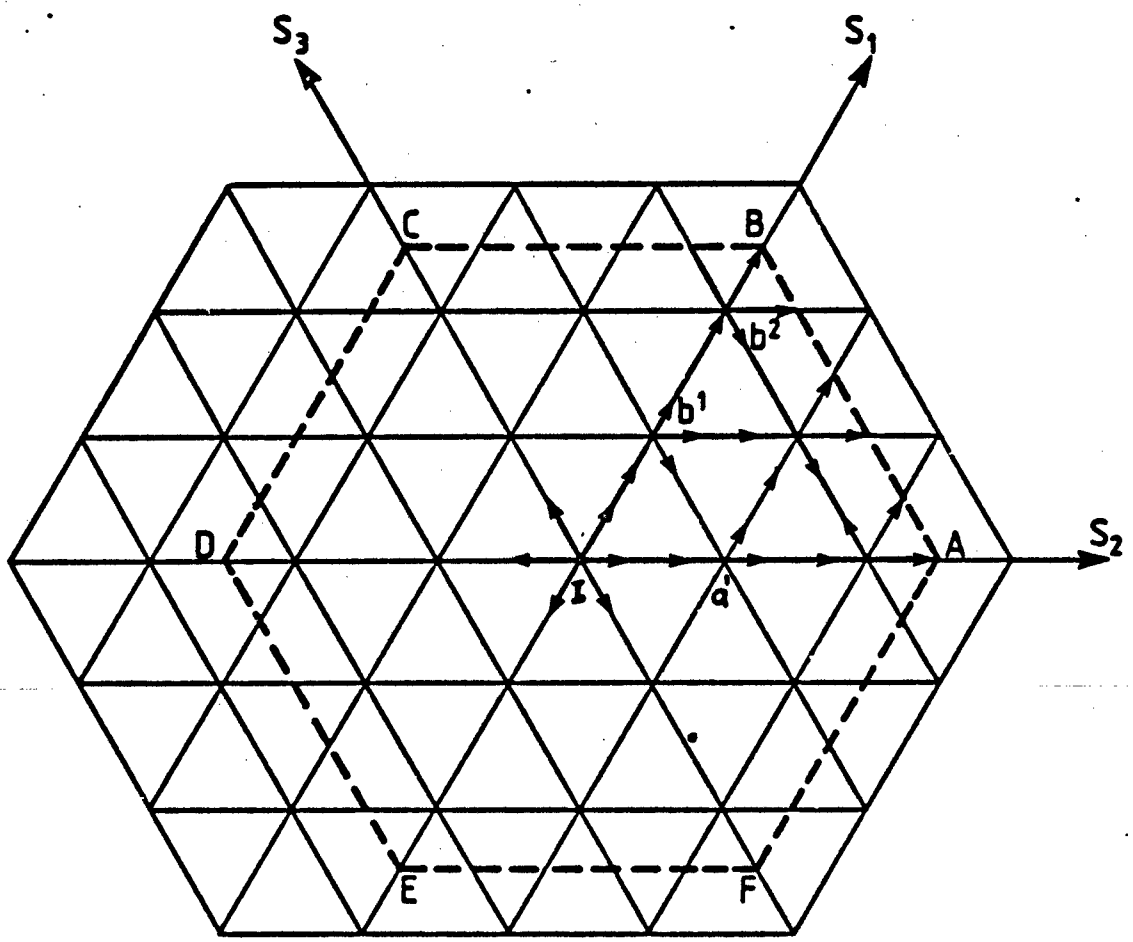

Fig. 2.1. Triaxial fabric

Front of out-of-plane waves (hexagon)

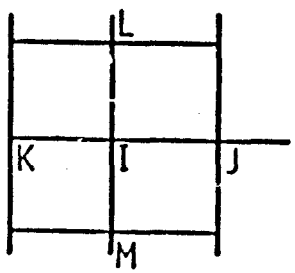

(a) Orthogonal weave

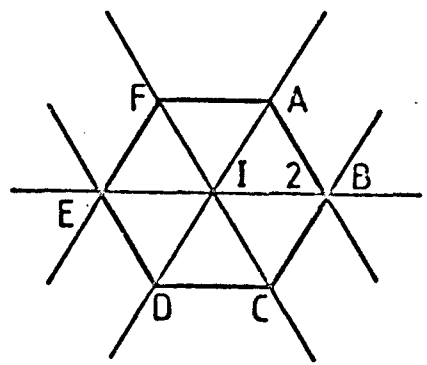

(b) Triaxial weave

Fig. 2.4.

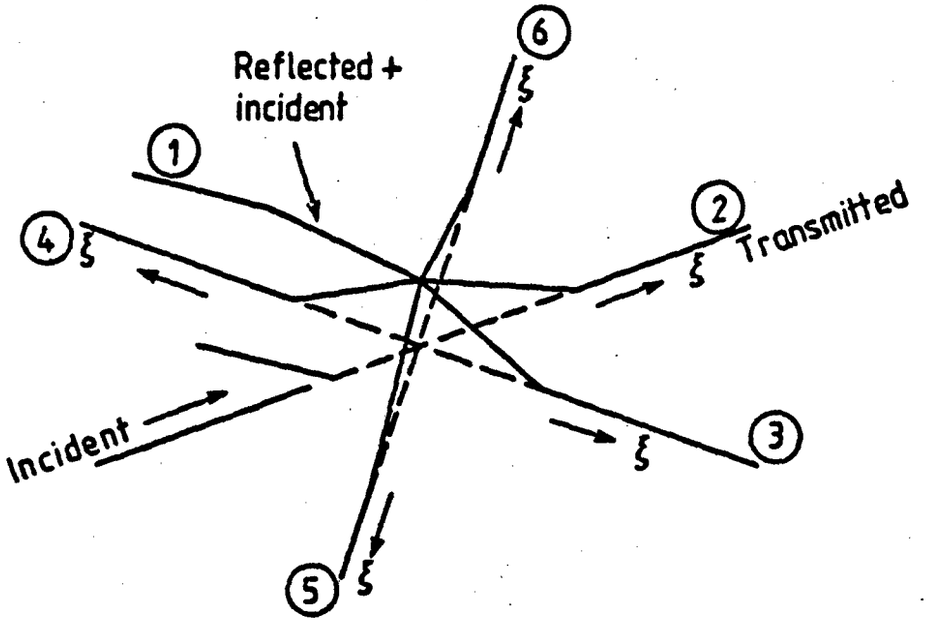

(a) Partitioning of wave incident on node

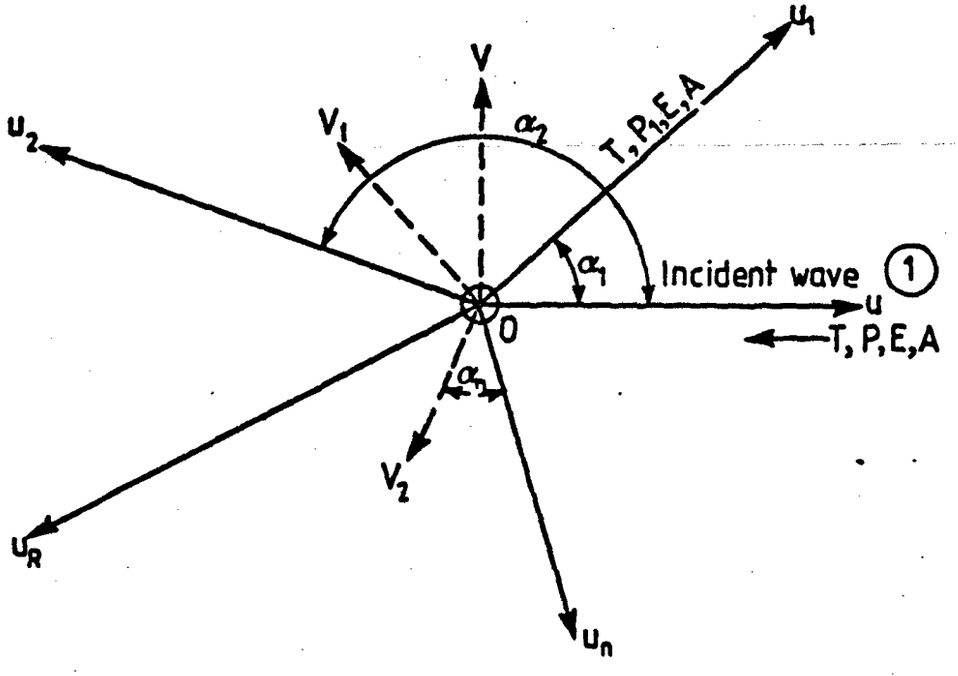

(b) Angular arrangement of waves associated

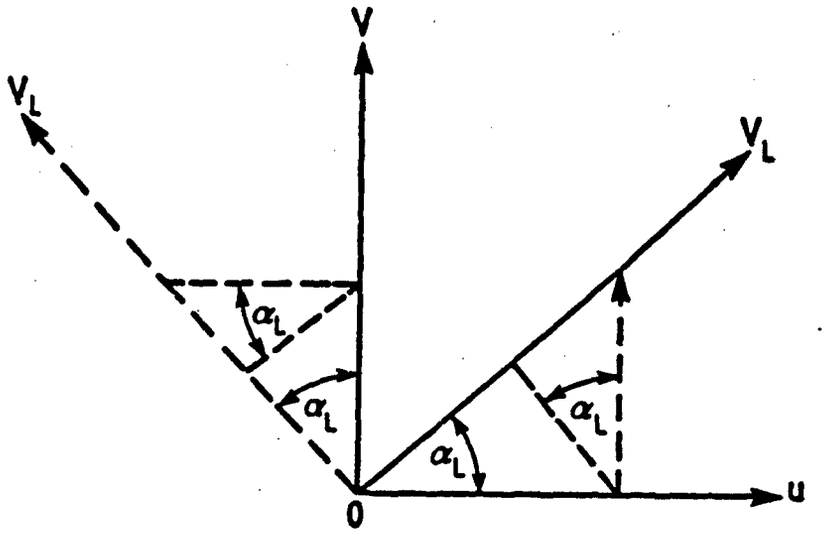

Fig. 2.6 Compatibility at node 0

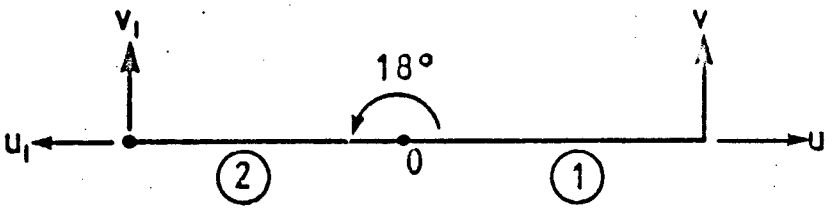

(a) Two yarns connected at a node 0

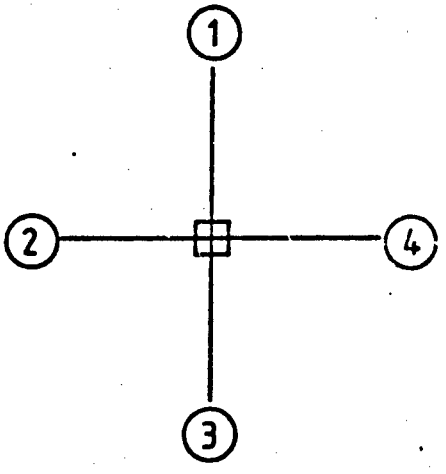

(b) Orthogonal

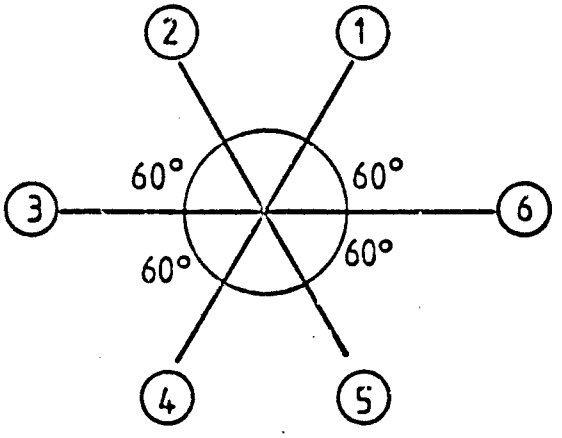

(c) Triaxial pattern

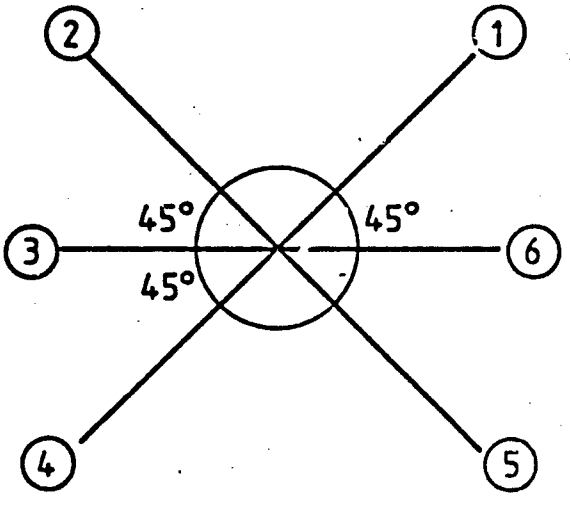

(d) Special triaxial

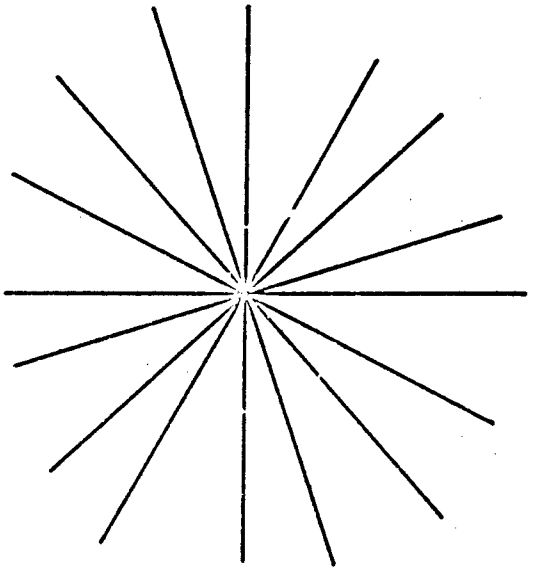

(e) Infinite number of yarns meeting at a node

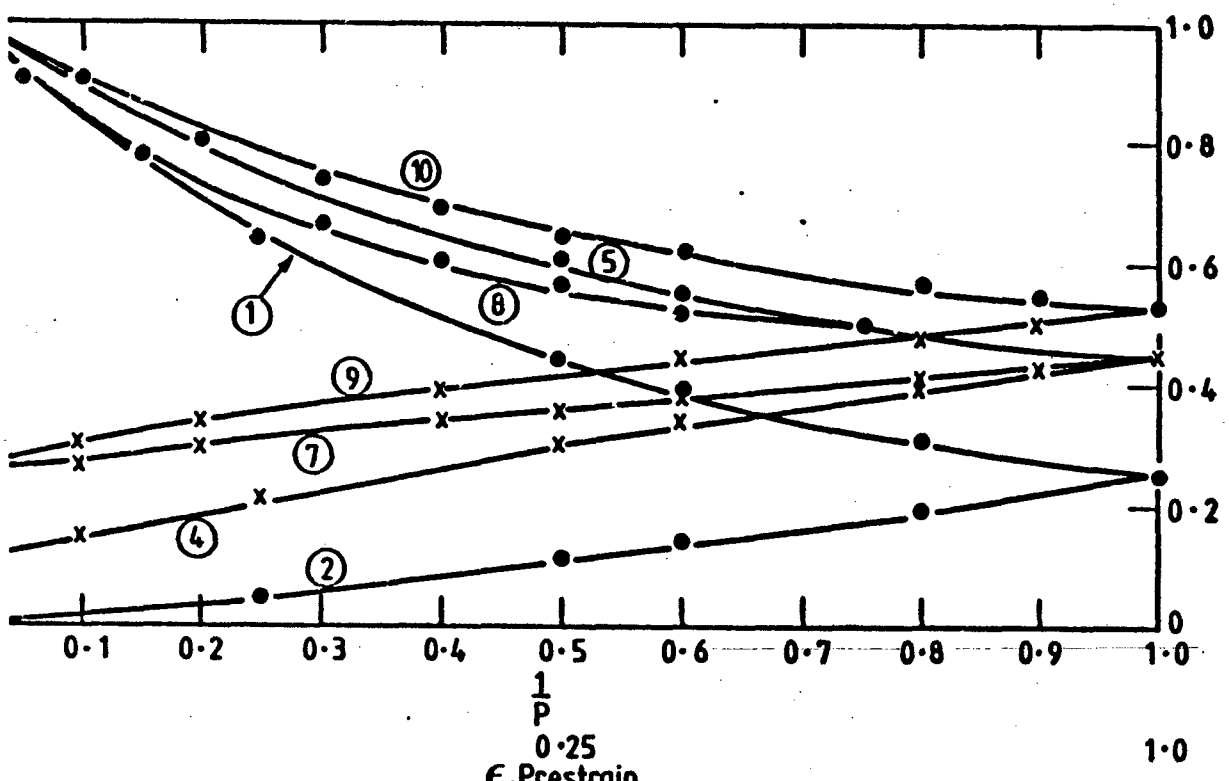

No.	Yarn arrangement	Input signal
1	Orthogonal	Transverse
2		Extensional
4	Triaxial	Extensional
5	(0 – 60 – 120)	Transverse
7	Triaxial	Extensional
8	(0 – 45 – 135)	Transverse
9	Infinite	Extensional
10		Transverse

$$P = \frac{EA_{ct}}{T_{ce}}$$

2.8 Percentage of in plane signal reflected for different yarn arrangements

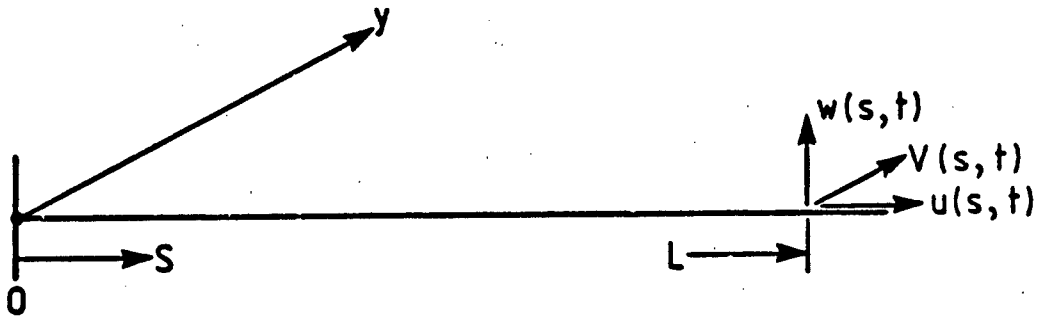

Fig.3.1. Typical yarn

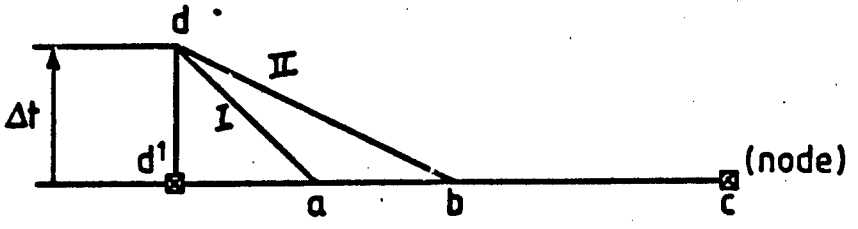

Fig.3.2. Characteristics entering a node and time increment

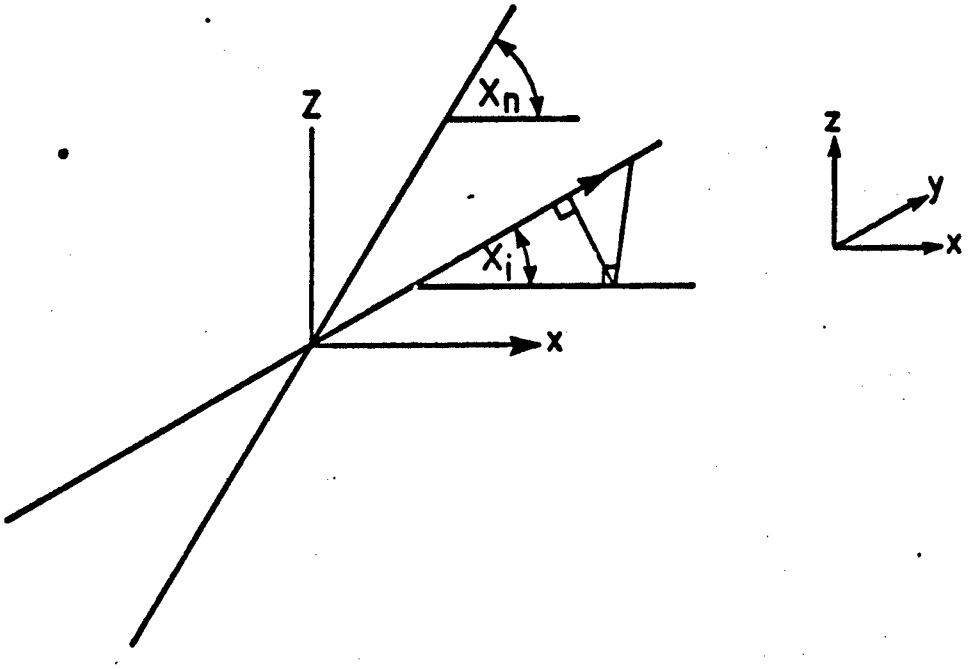

Fig.3.3 Orientation of element to global axes

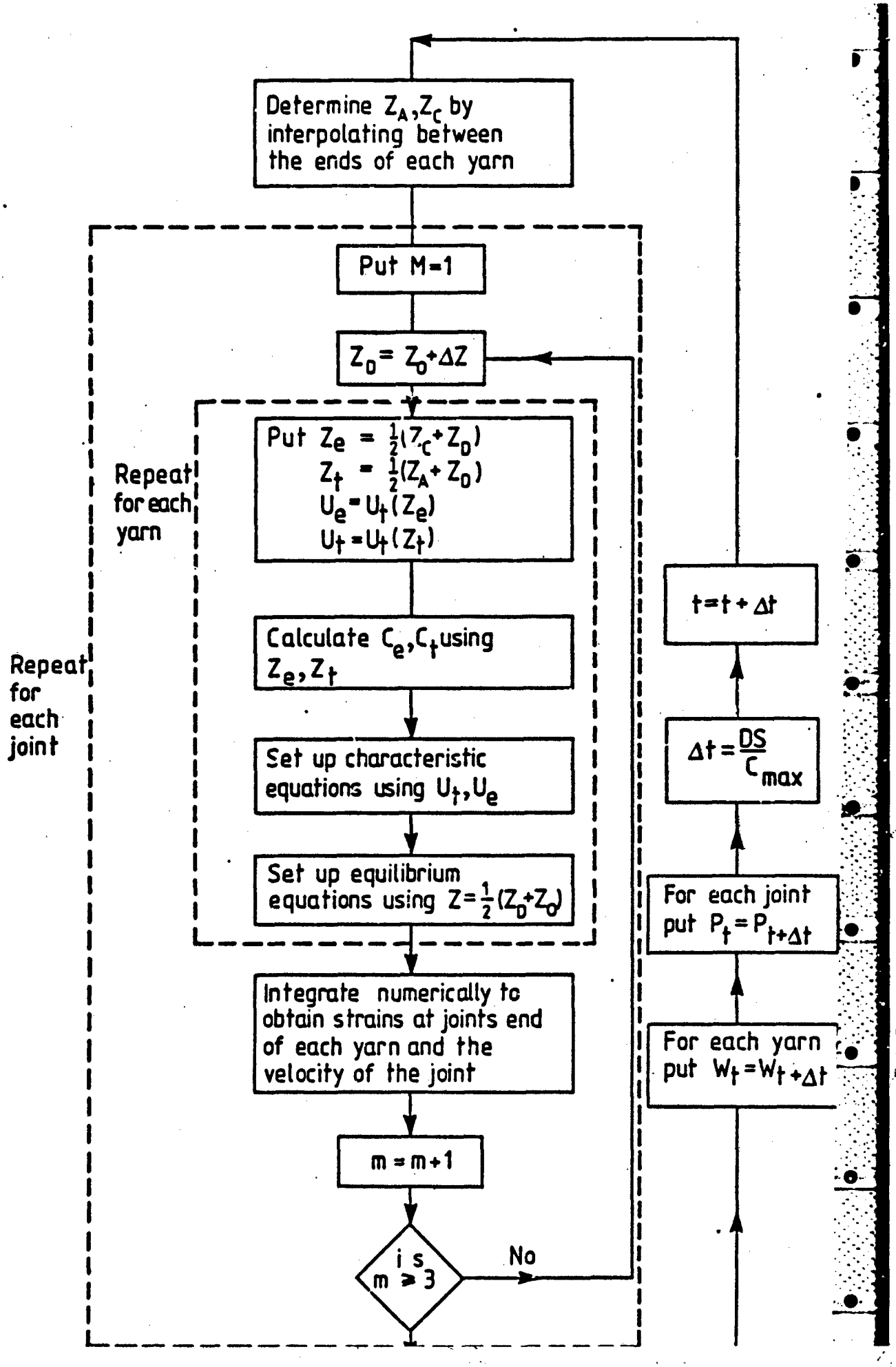
Determine Z_A, Z_C by interpolating between the ends of each yarn
Put M=1
$Z_0 = Z_0 + \Delta Z$
Repeat for each yarn
Put $Z_e = \frac{1}{2}(Z_C + Z_0)$
$Z_t = \frac{1}{2}(Z_A + Z_0)$
$U_e = U_t(Z_e)$
$U_t = U_t(Z_t)$
Calculate C_e, C_t using Z_e, Z_t
Set up characteristic equations using U_t, U_e
Set up equilibrium equations using $Z = \frac{1}{2}(Z_0 + Z_0)$
Repeat for each joint
Integrate numerically to obtain strains at joints end of each yarn and the velocity of the joint
m = m+1
i s m ≥ 3
No
$t = t + \Delta t$
$\Delta t = \frac{DS}{C_{max}}$
For each joint put $P_t = P_{t+\Delta t}$
For each yarn put $W_t = W_{t+\Delta t}$

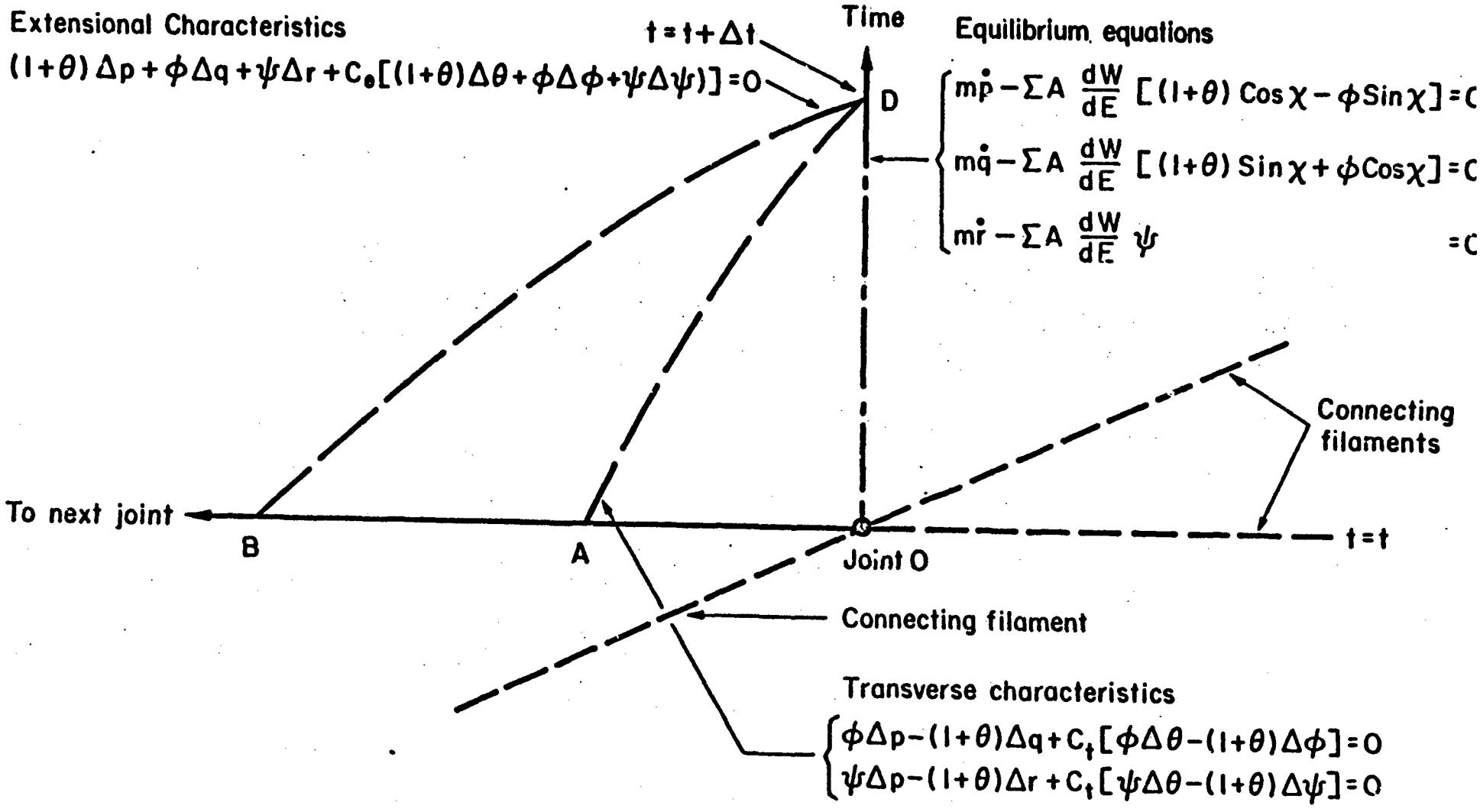
Extensional Characteristics
$(1+\theta)\Delta p+\phi\Delta q+\psi\Delta r+C_e[(1+\theta)\Delta\theta+\phi\Delta\phi+\psi\Delta\psi)]=0$
$t=t+\Delta t$
Time
D
Equilibrium equations
$m\dot{p}-\Sigma A\frac{dW}{dE}[(1+\theta)\cos\chi-\phi\sin\chi]=0$
$m\dot{q}-\Sigma A\frac{dW}{dE}[(1+\theta)\sin\chi+\phi\cos\chi]=0$
$m\dot{r}-\Sigma A\frac{dW}{dE}\psi=0$
Connecting filaments
To next joint
B
A
Joint O
t=t
Connecting filament
Transverse characteristics
$\phi\Delta p-(1+\theta)\Delta q+C_t[\phi\Delta\theta-(1+\theta)\Delta\phi]=0$
$\psi\Delta p-(1+\theta)\Delta r+C_t[\psi\Delta\theta-(1+\theta)\Delta\psi]=0$

Fig.3.5

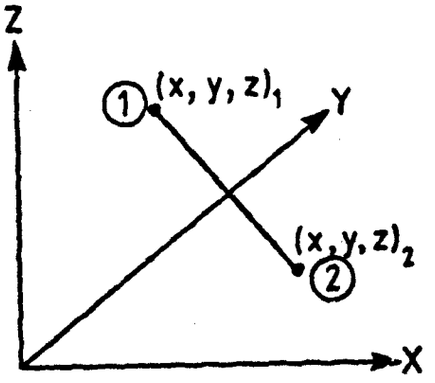

(a) Basic rod element in space

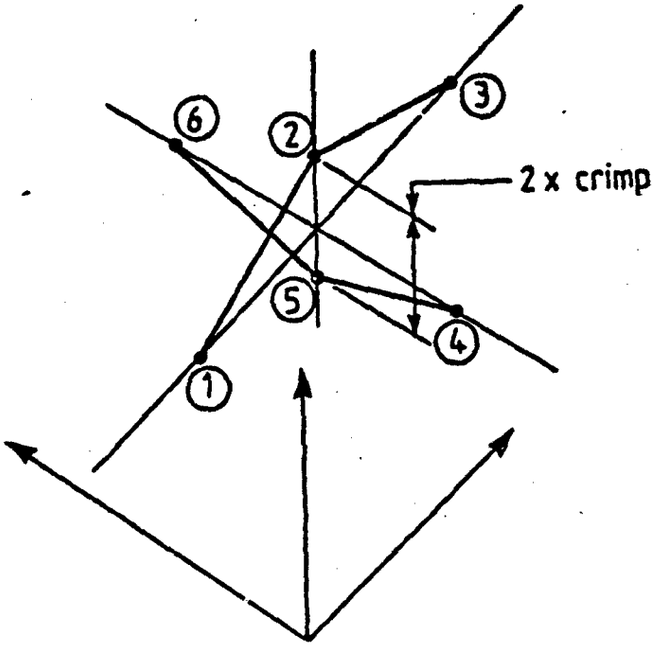

(b) Typical arrangementof rod elements reproduce weave with crimp (Orthogonal weave)

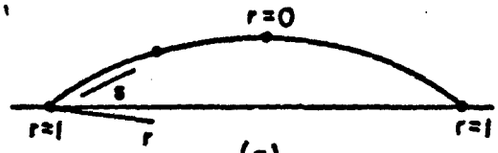

(a)
Basic cable element

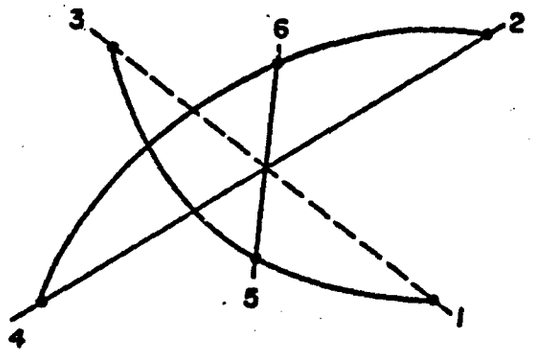

(b)
Orthogonal weave block

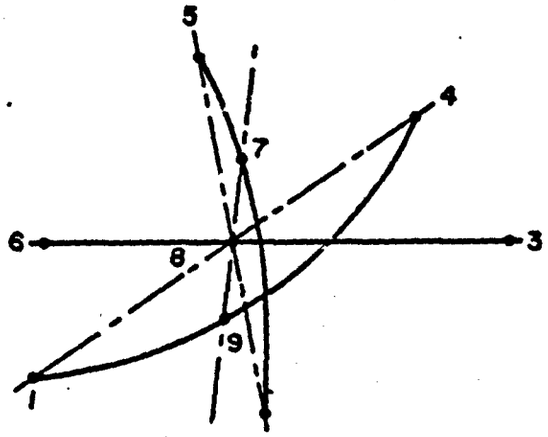

(c)
Triaxial weave block

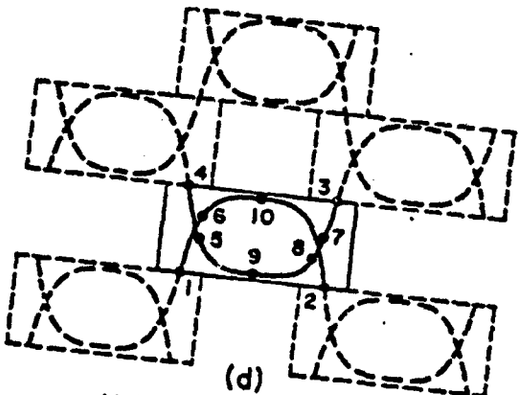

(d)
Knitted fabric blocks
(Assembled for 3-node elements)

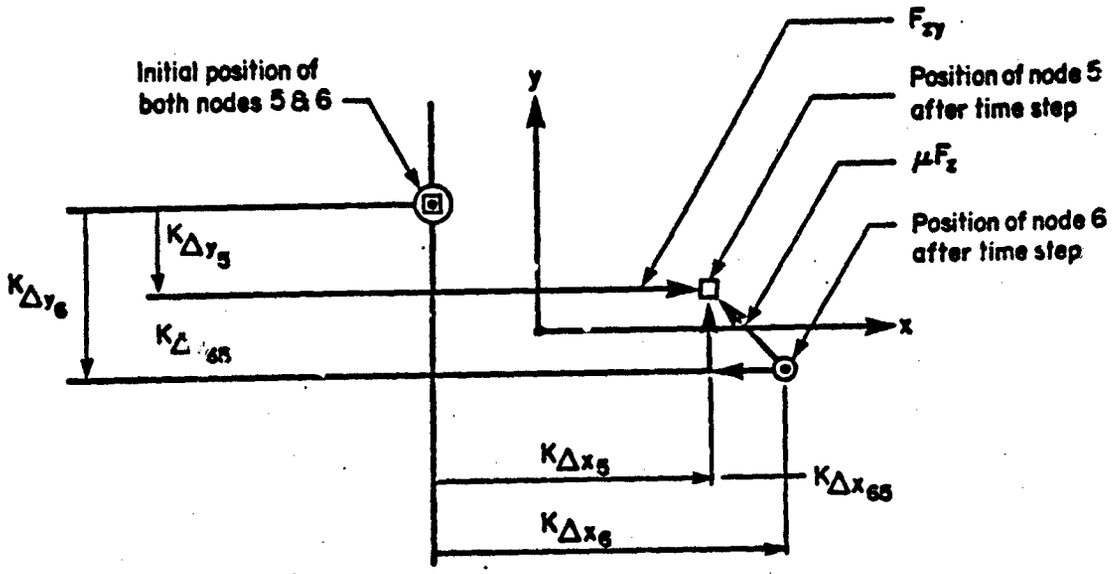

$$\overrightarrow{{}^{k}Slip} = \overrightarrow{{}^{k}\Delta x_{65}} + \overrightarrow{{}^{k}\Delta y_{65}}$$

$${}^{k}F_{yx} = \mu F_z \, {}^{k}(\Delta x_{65}/slip)$$

$${}^{k}F = \mu F_z \quad (\Delta y_{65}/slip)$$

Fig. 4.3 Direction of frictioncl force (K^{th} Estimate)

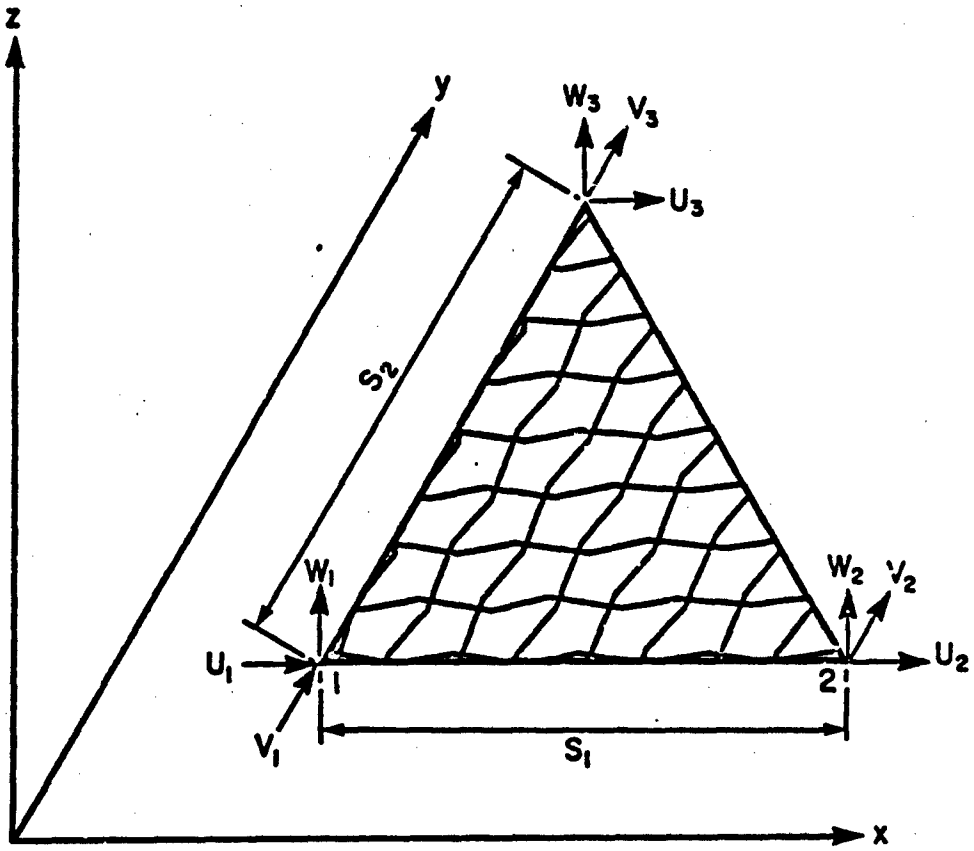

Fig. 4.4 Fabric showing crossing yarns

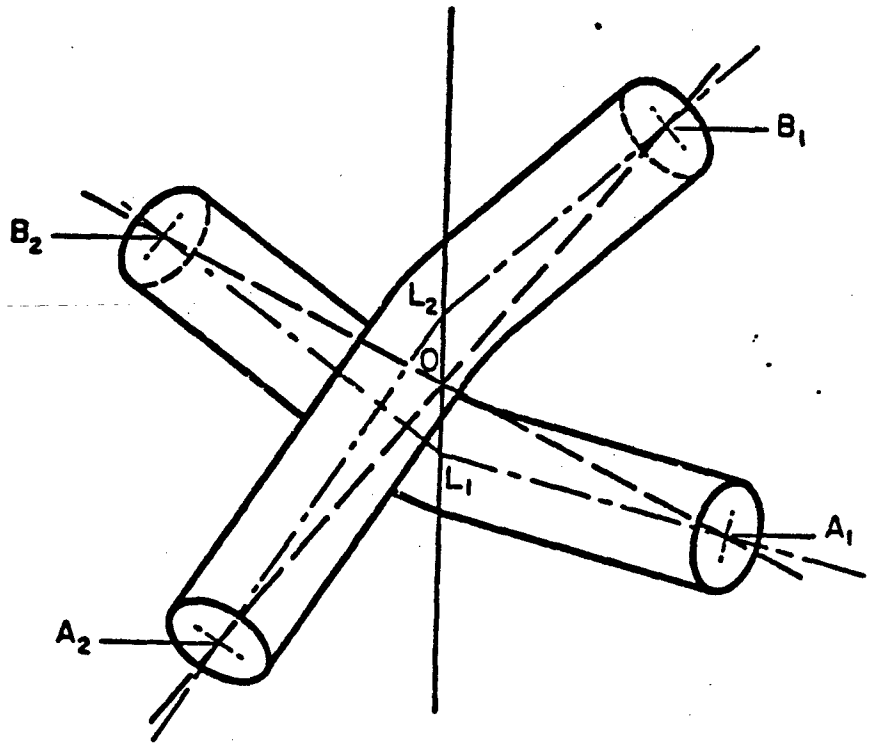

Fig. 4.5 Unit structure of weave

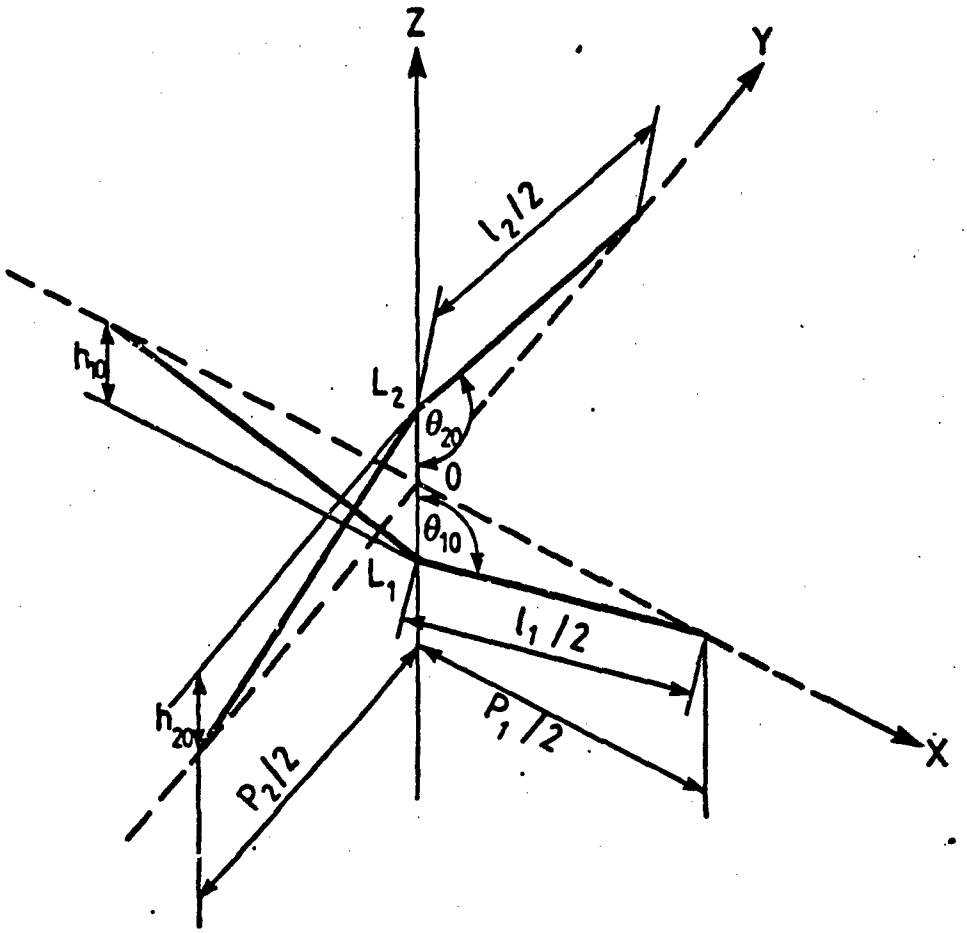

Fig. 4. 6 Geometry of undeformed yarn

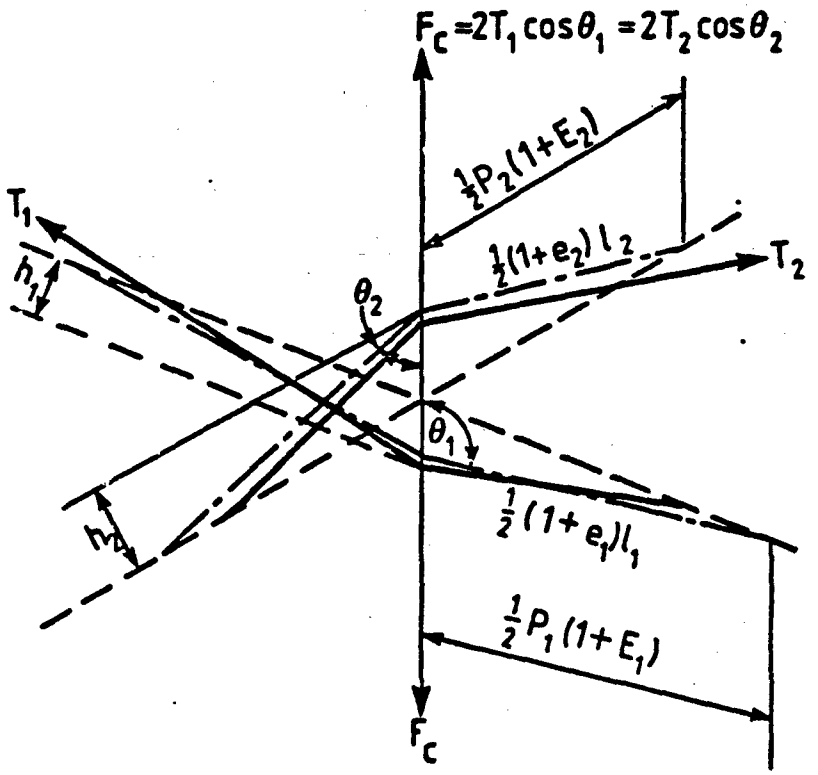

Fig. 4. 7. Geometry of deformed yarn

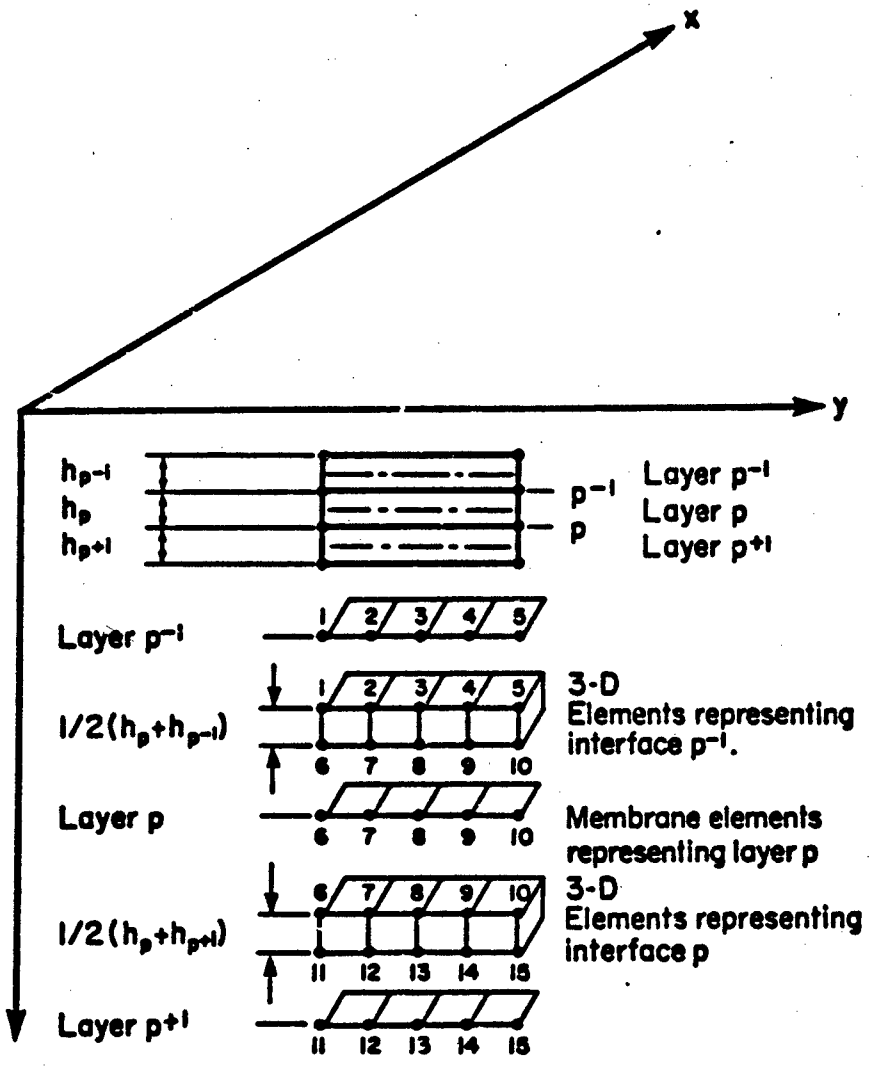

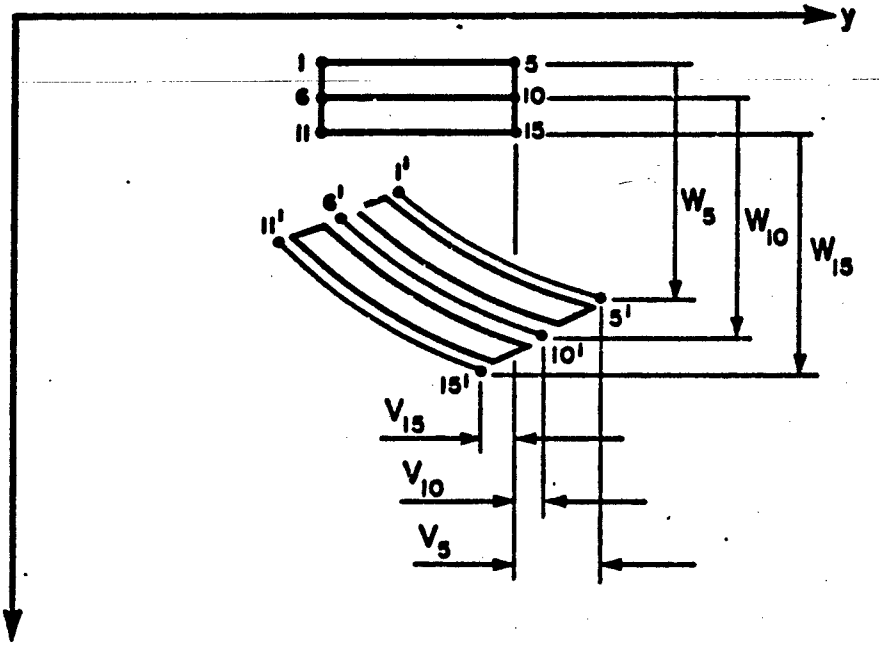

Fig. 4.8 Typical deformation of layers (with slip)

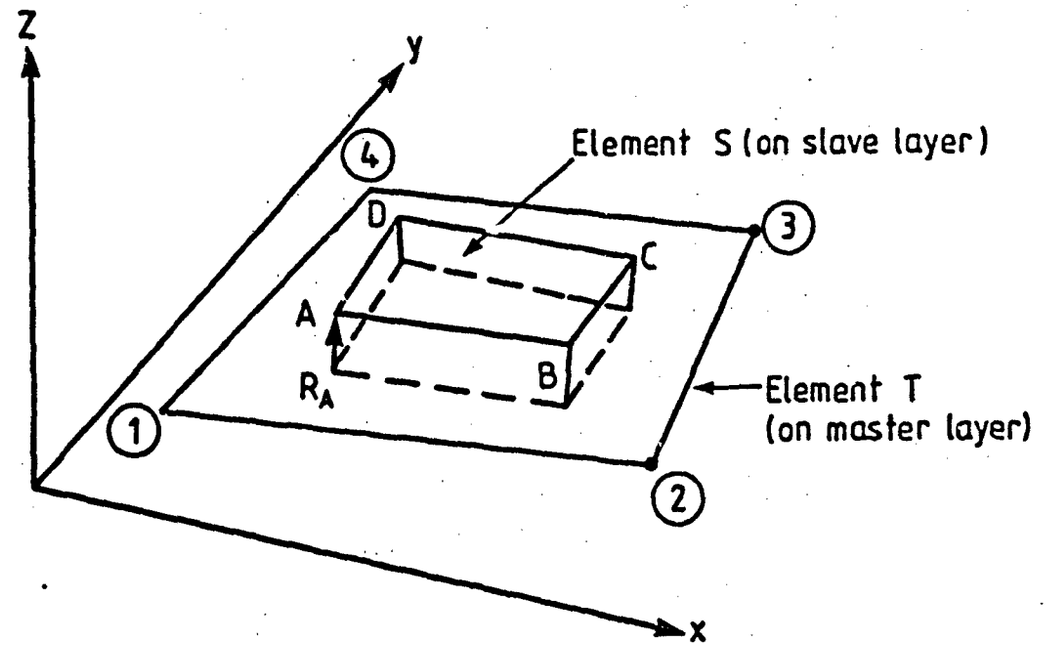

Fig.4.9 Reaction between master and slave layers

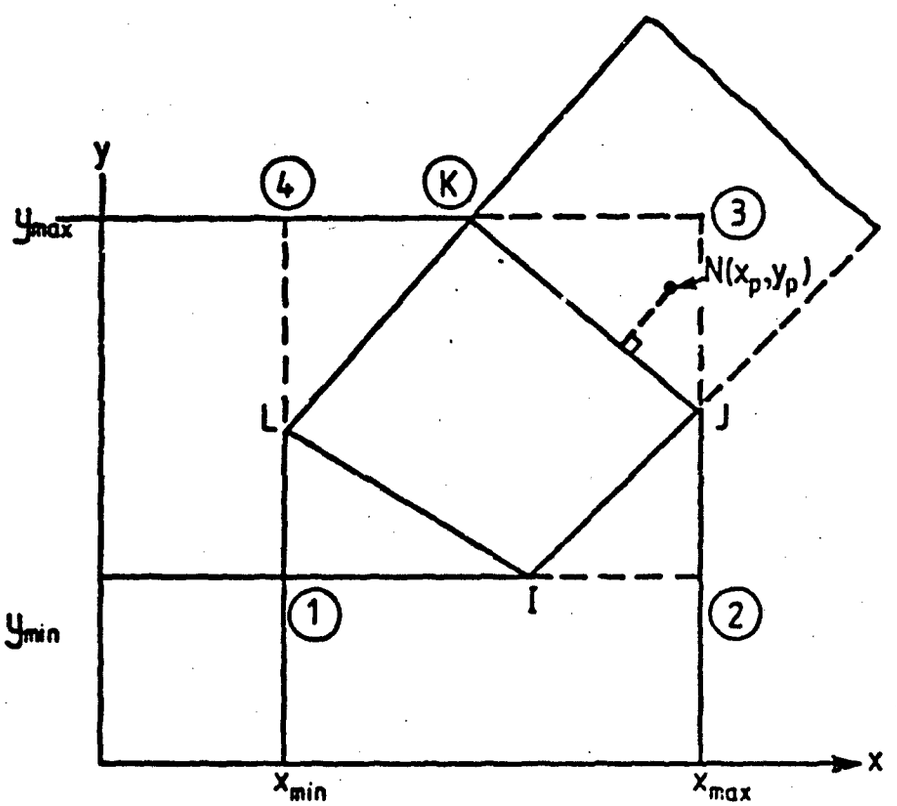

Fig.4.10 Identification of master layer element above node N

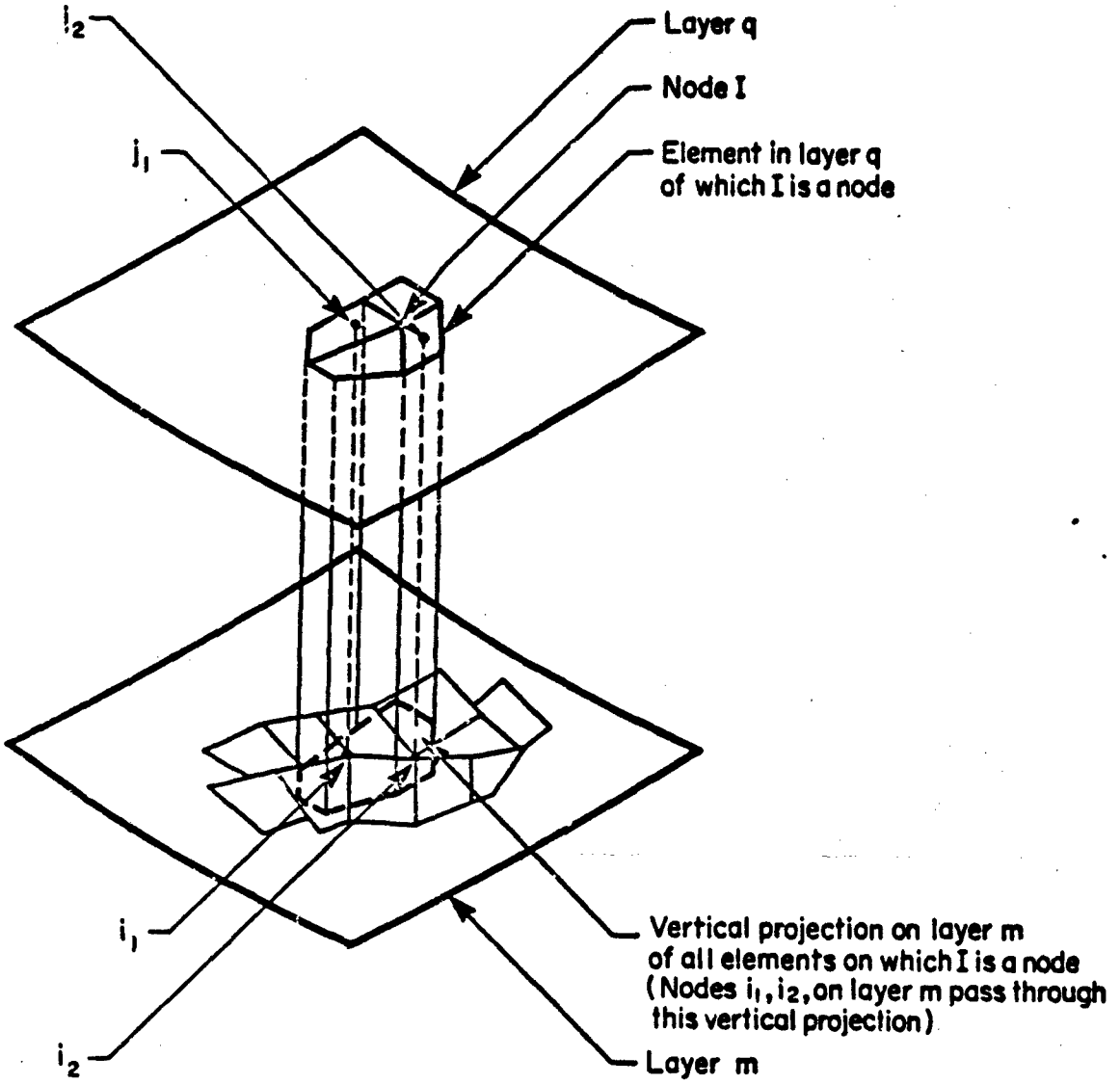

Fig. 4.11 Diagramatic representation of search procedure.

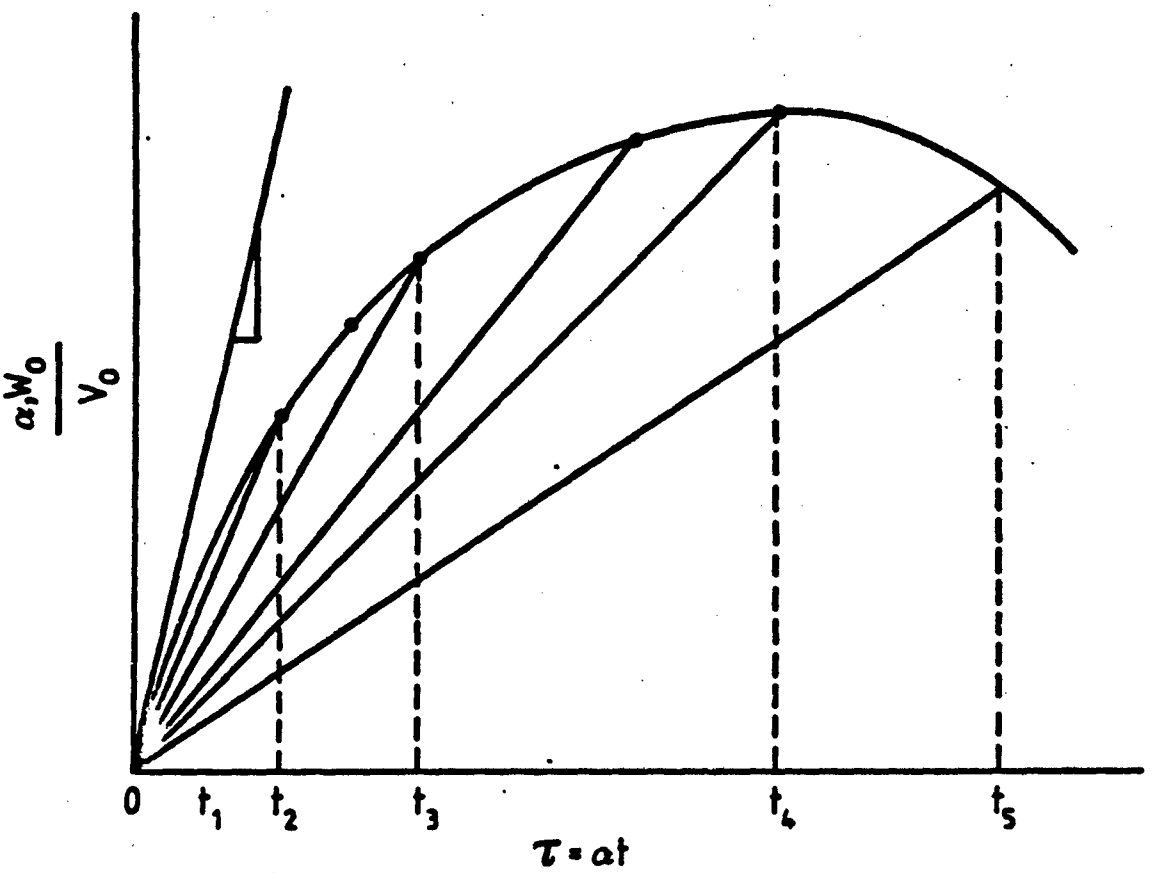

Fig. 5.1. Indentation vs. time. Typical curve

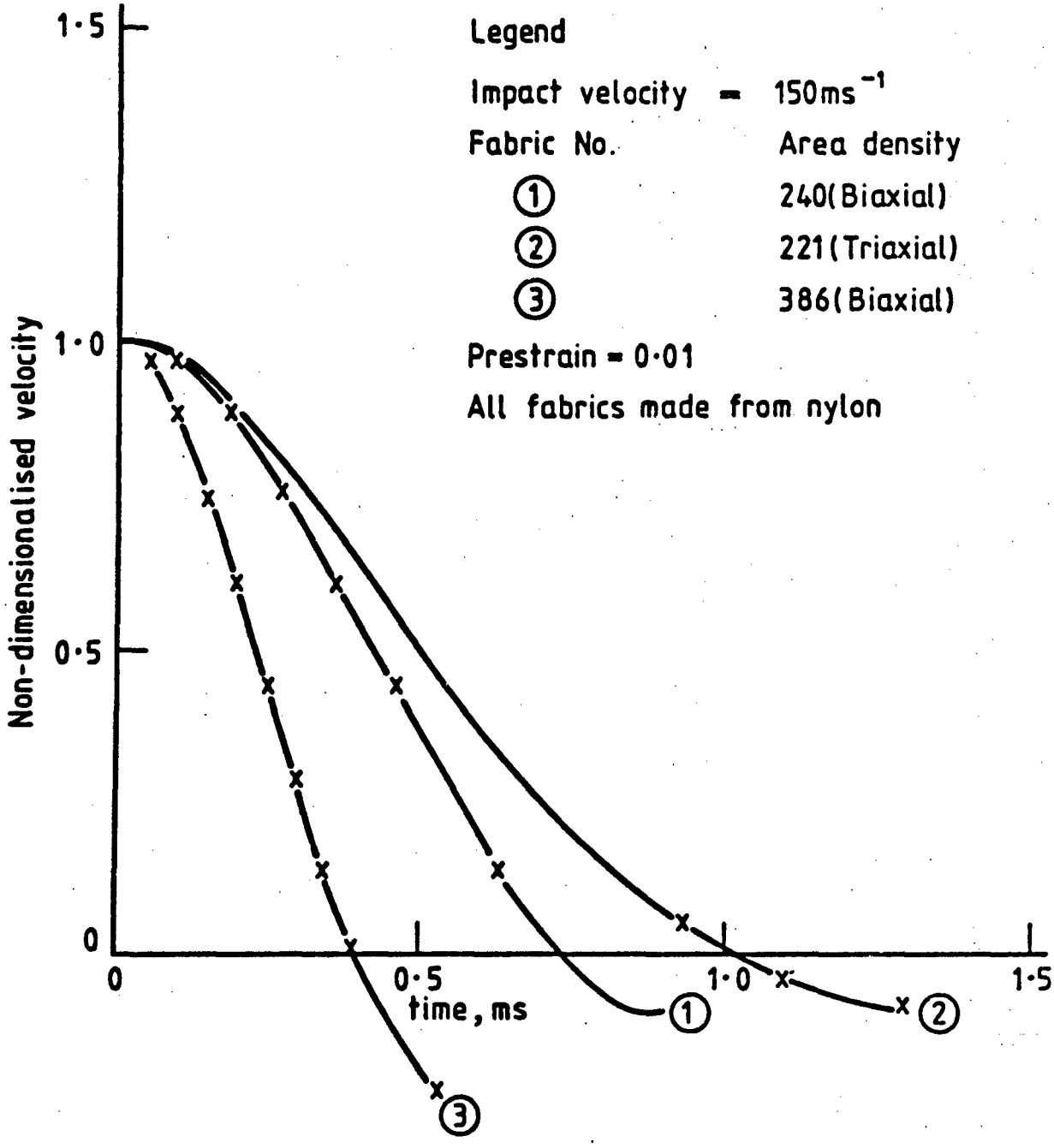

Fig. 5.2. Linear model: Deceleration graph: Different area densities.

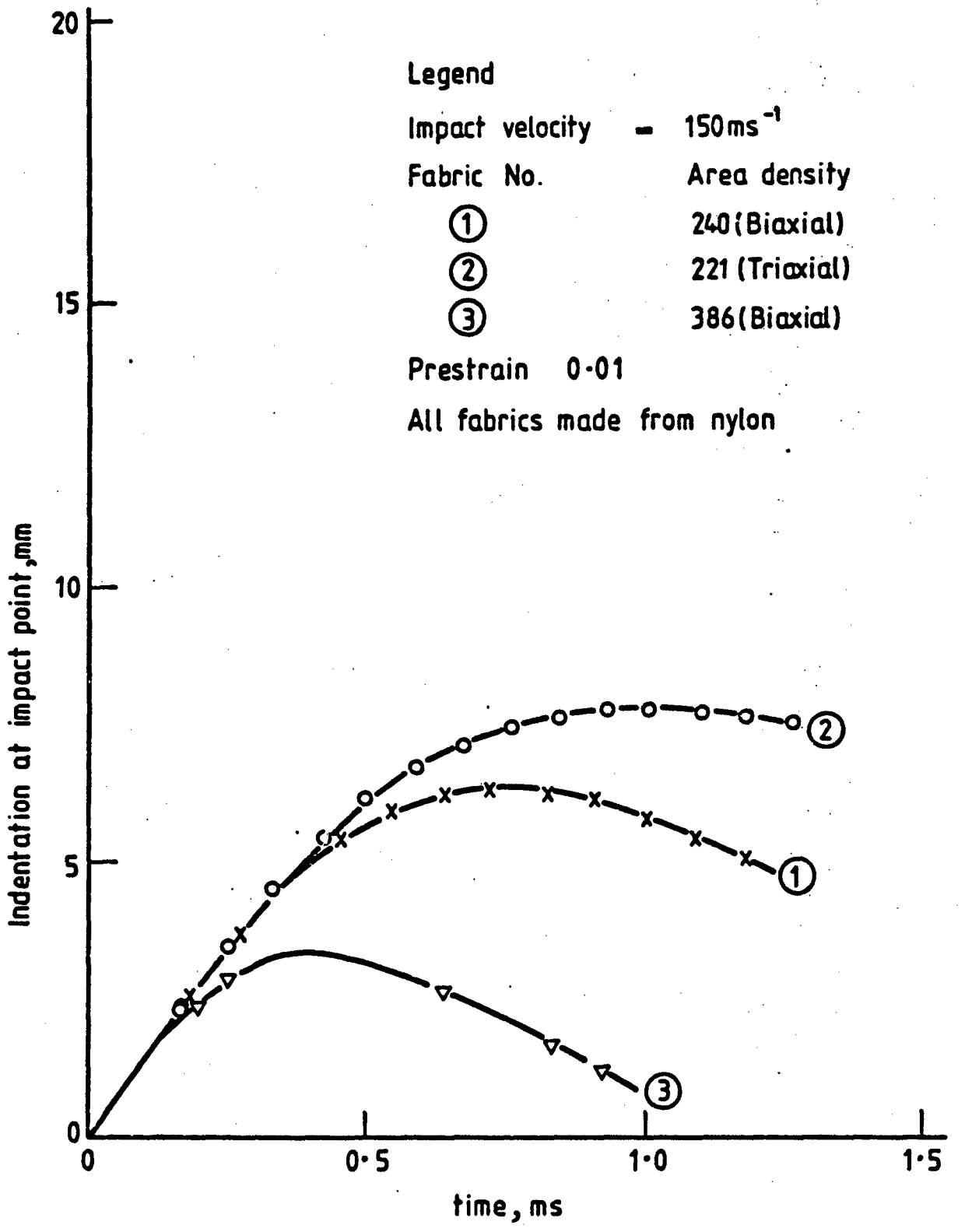

Fig. 5. 3. Linear model: Indentation: Different area densities.

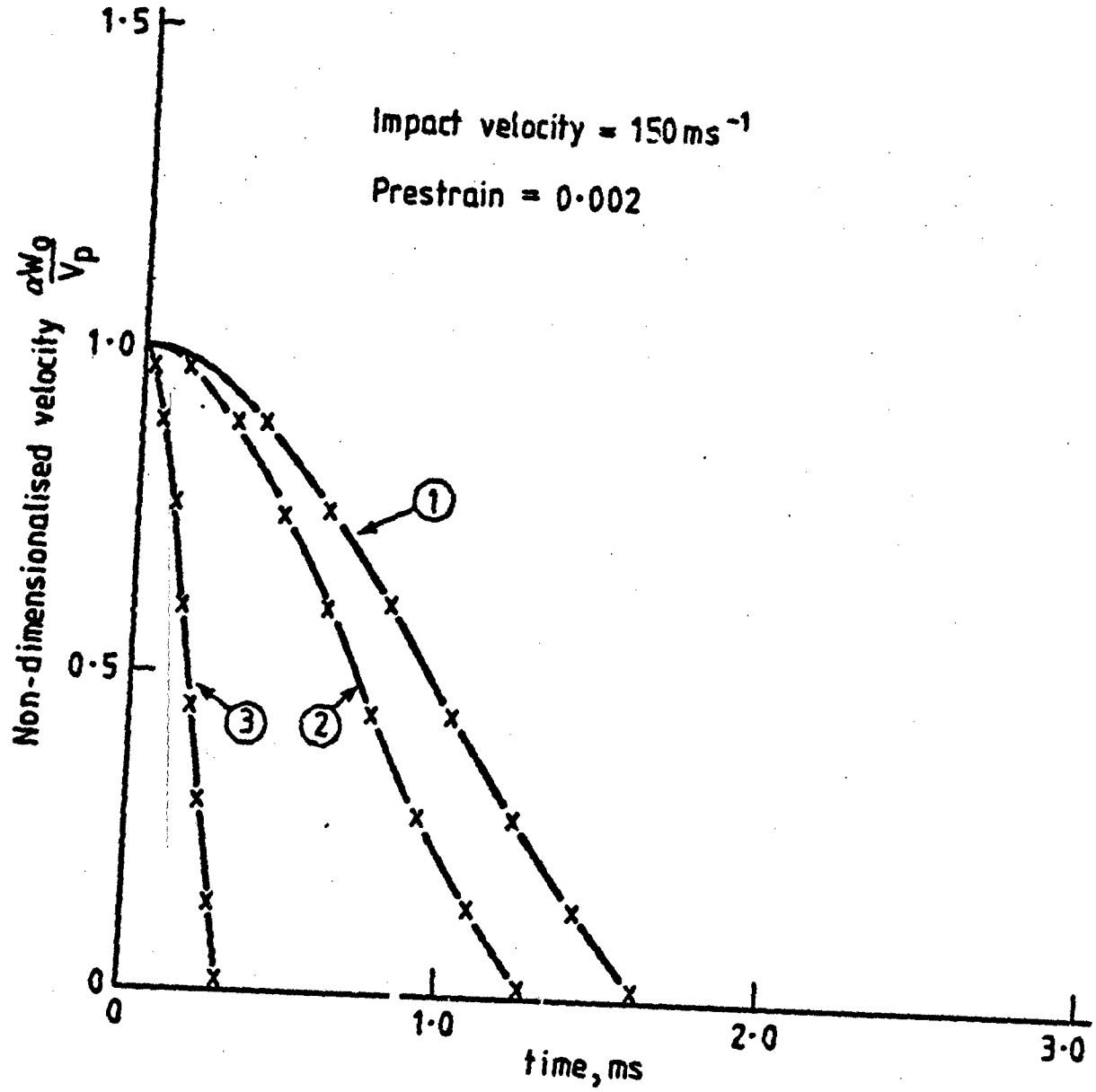

Fig. 5. 4. Linear model: Projectile velocity: Different fabrics.

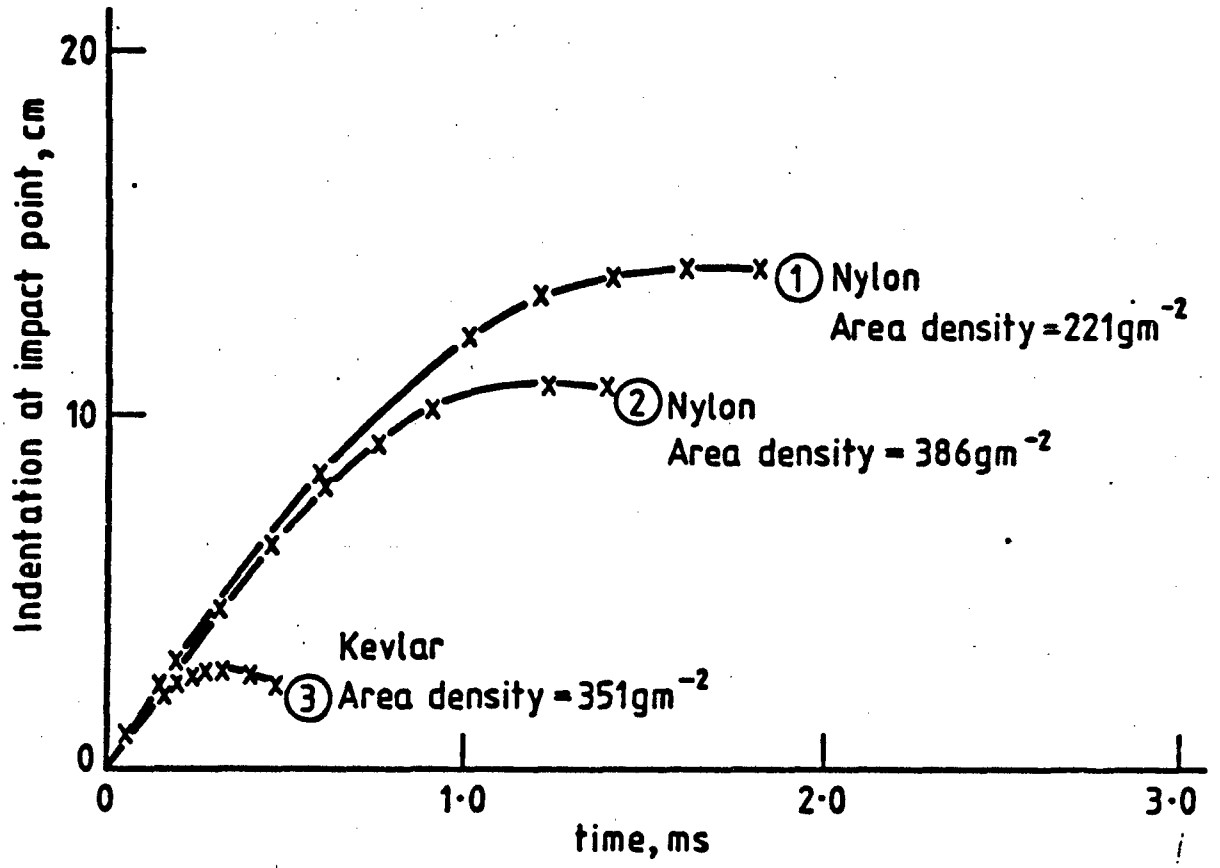

Fig. 5.5. Linear model: Indentation: Different fabrics

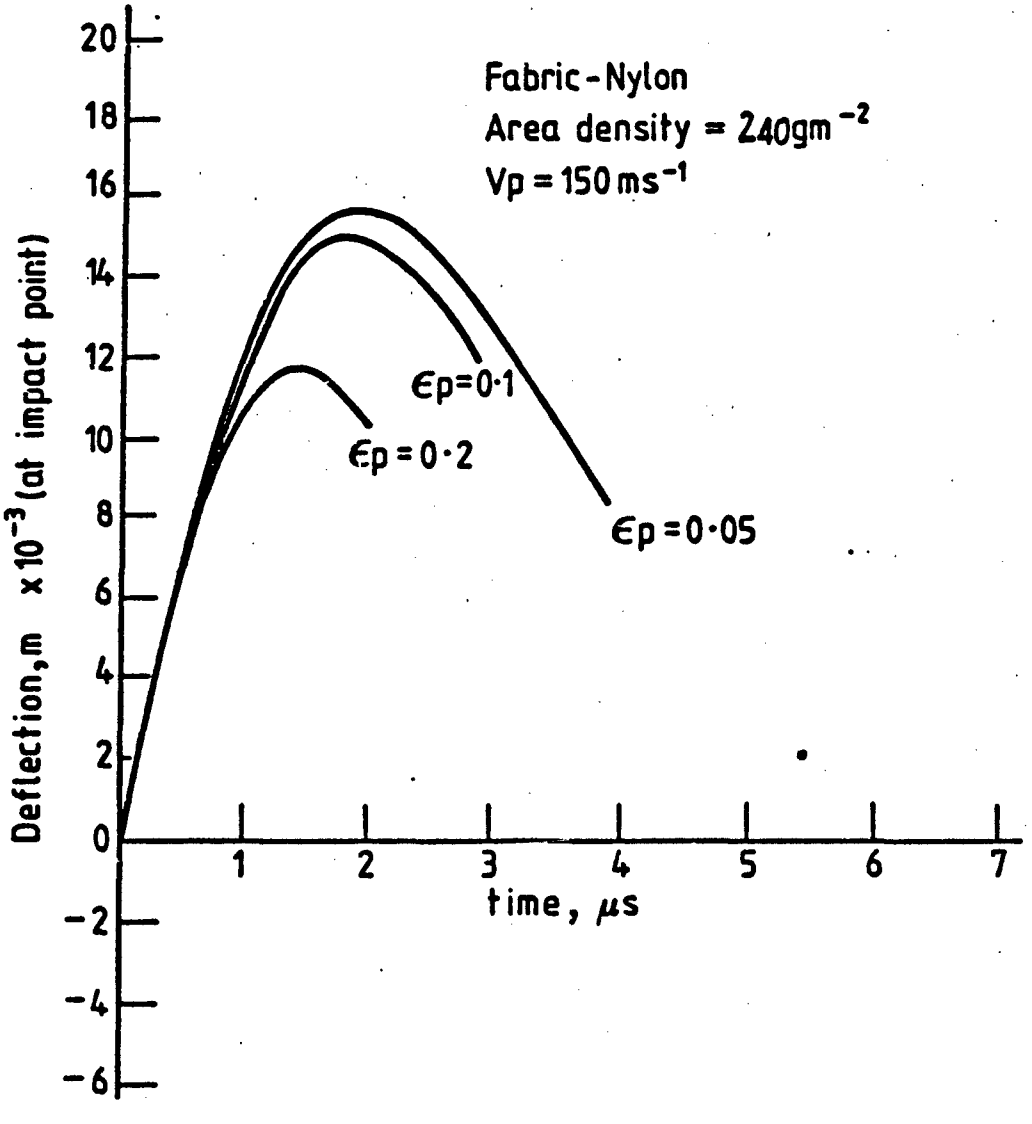

Fig. 5. 6. Deflection-time curve, non linear case.

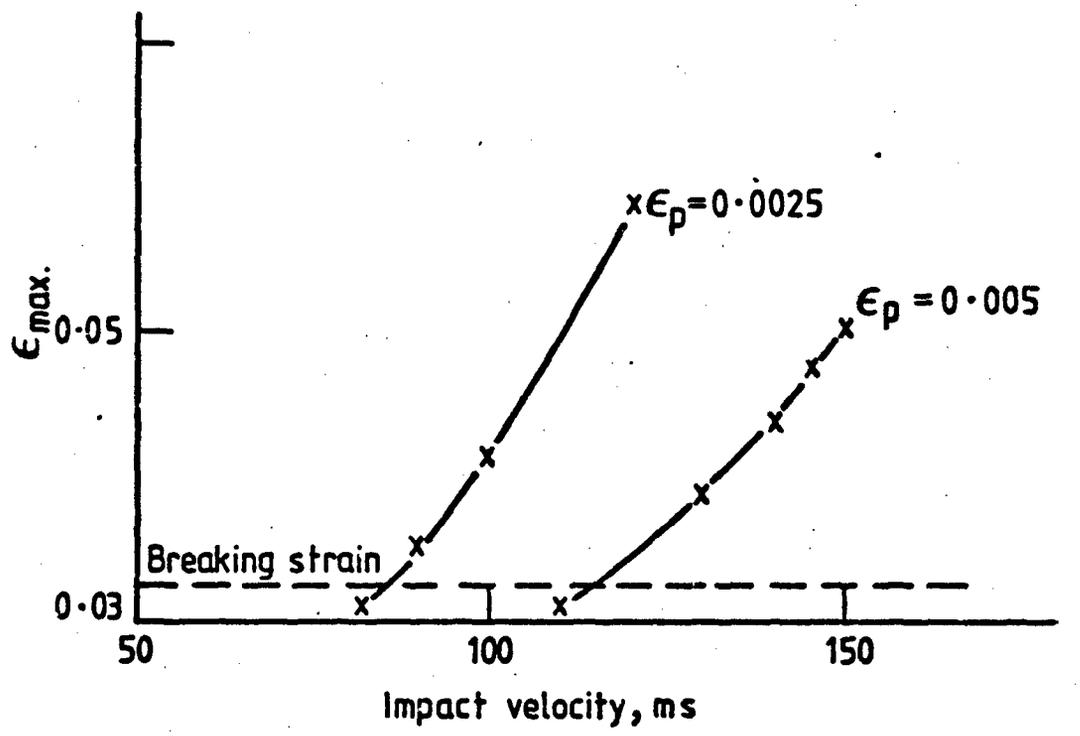

Max strain vs. Impact velocity: Kevlar

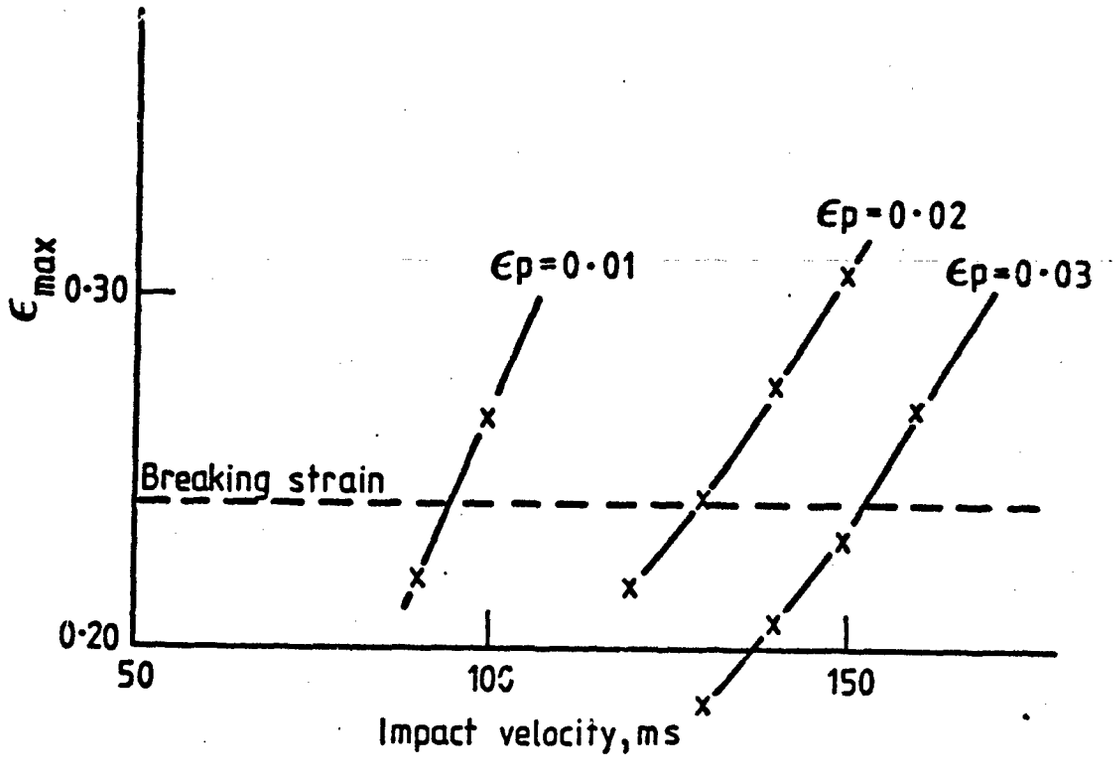

Max. strain vs. Impact velocity: Nylon

Fig. 5.7. Variation of strain with impact velocity. 2 materials

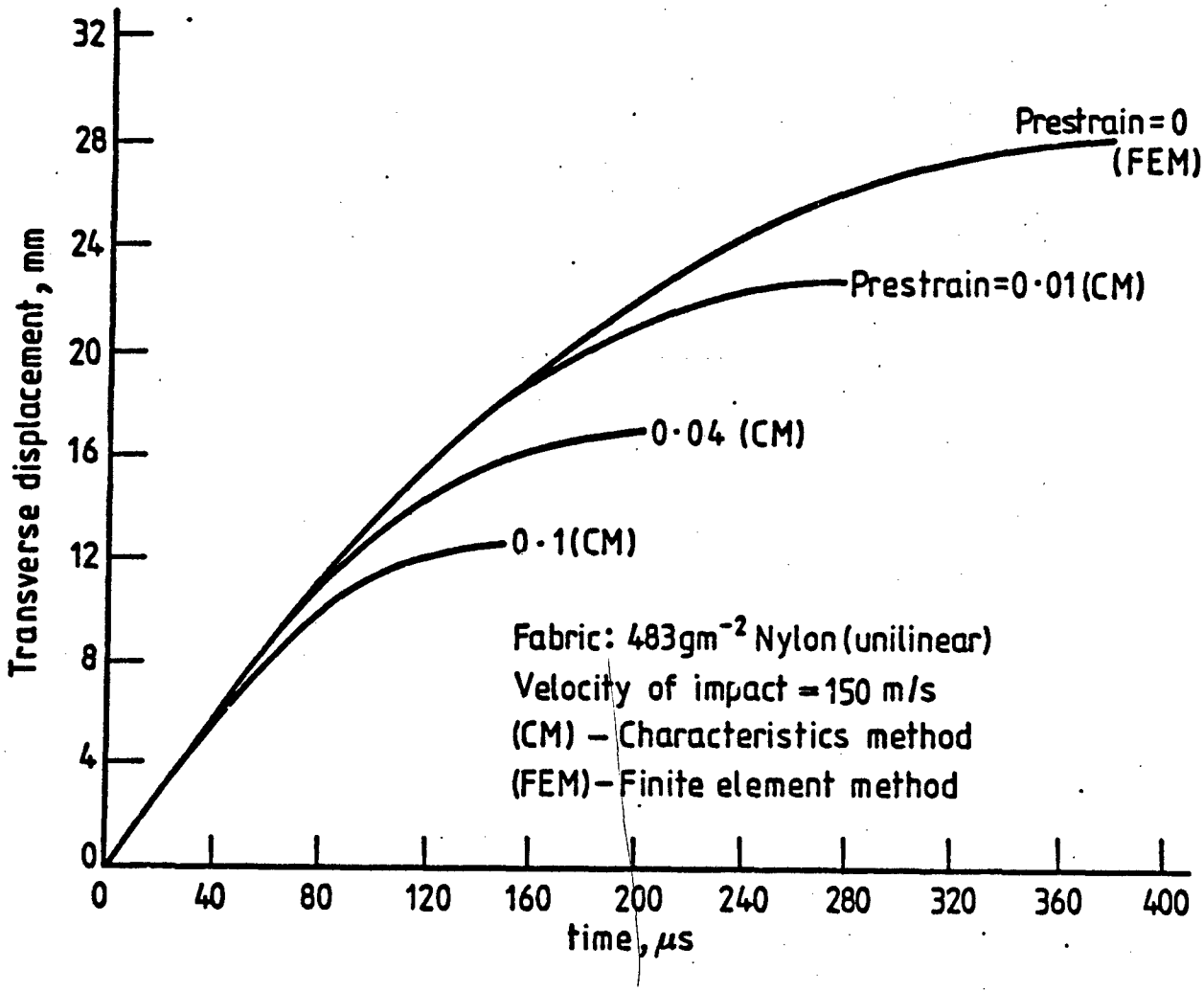

Fig. 5. 8. Transverse deformation against time

Data: Trilinear nylon – $\epsilon p = 0 \cdot 03$, $Vp = 150ms$, 1 layer
Area density = $386 g/m^2$

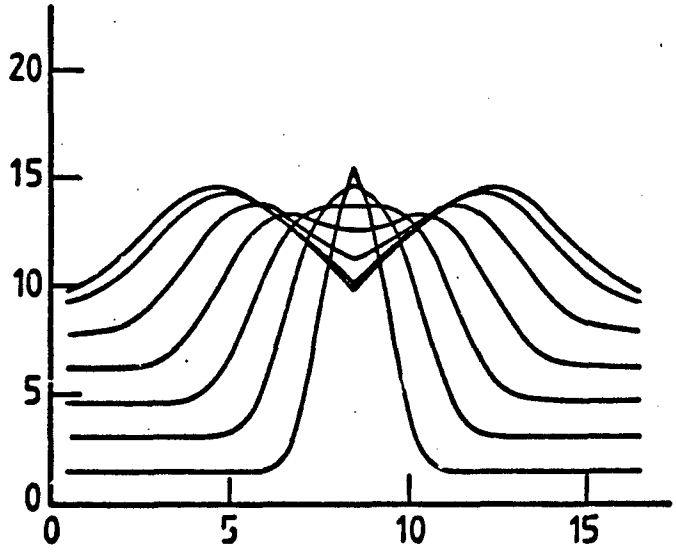

(a) Velocity profile along centreline

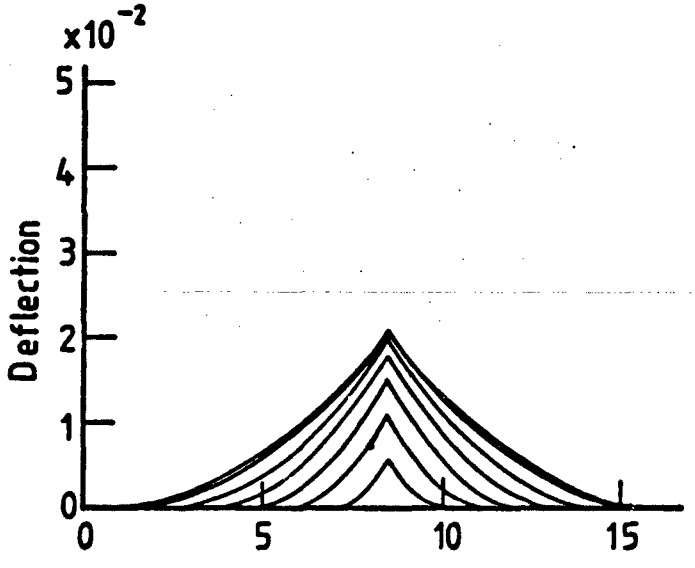

(b) Deformed shape of centreline

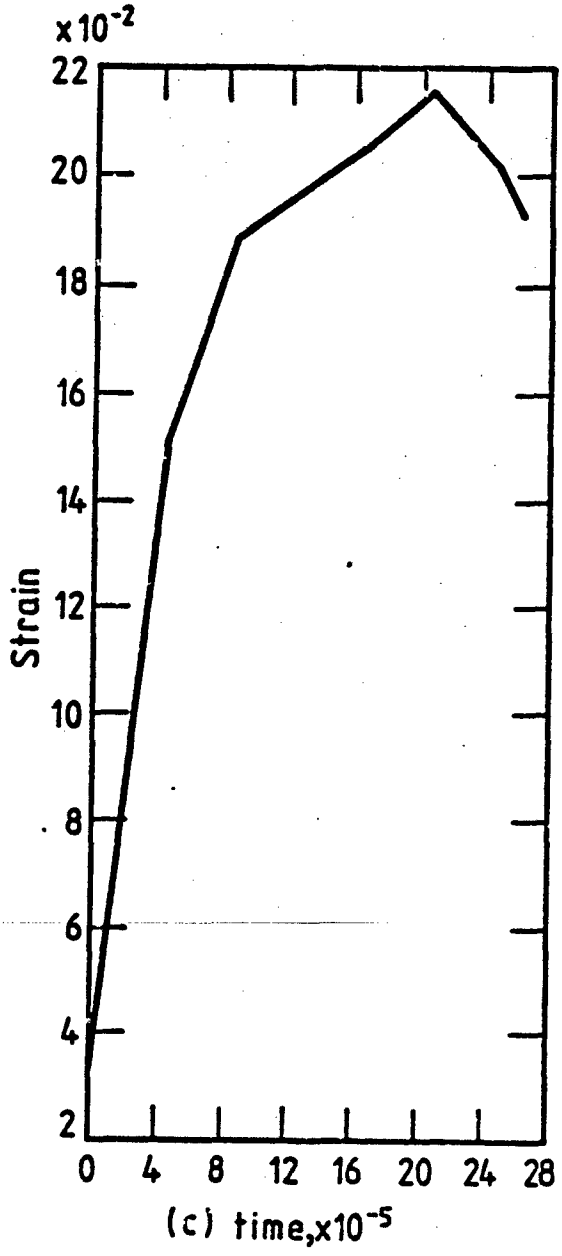

Fig. 5.9 Results obtained by method of characteristics

Data: Trilinear nylon - $\epsilon_p = 0{\cdot}03$, $V_p = 160$ ms, 1 Layer

Area density = 386 g/m^2

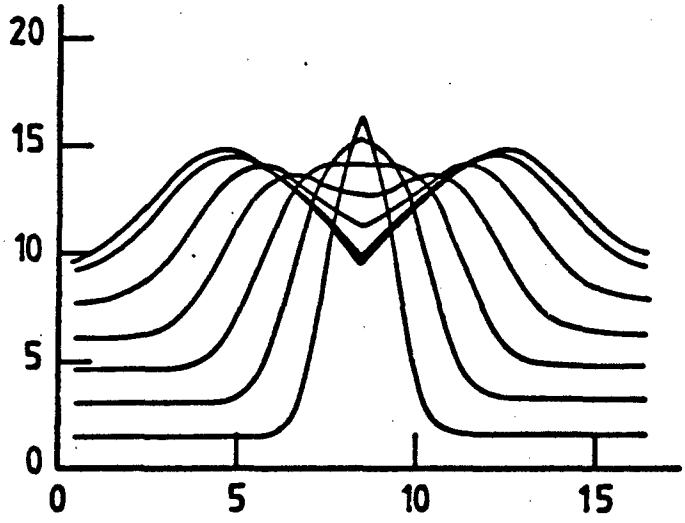

(a) Velocity profile along centreline

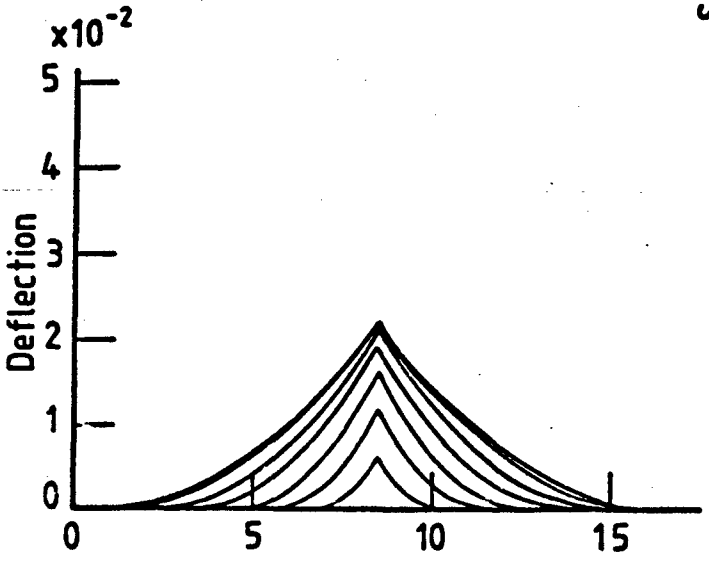

(b) Deformed shape of centreline

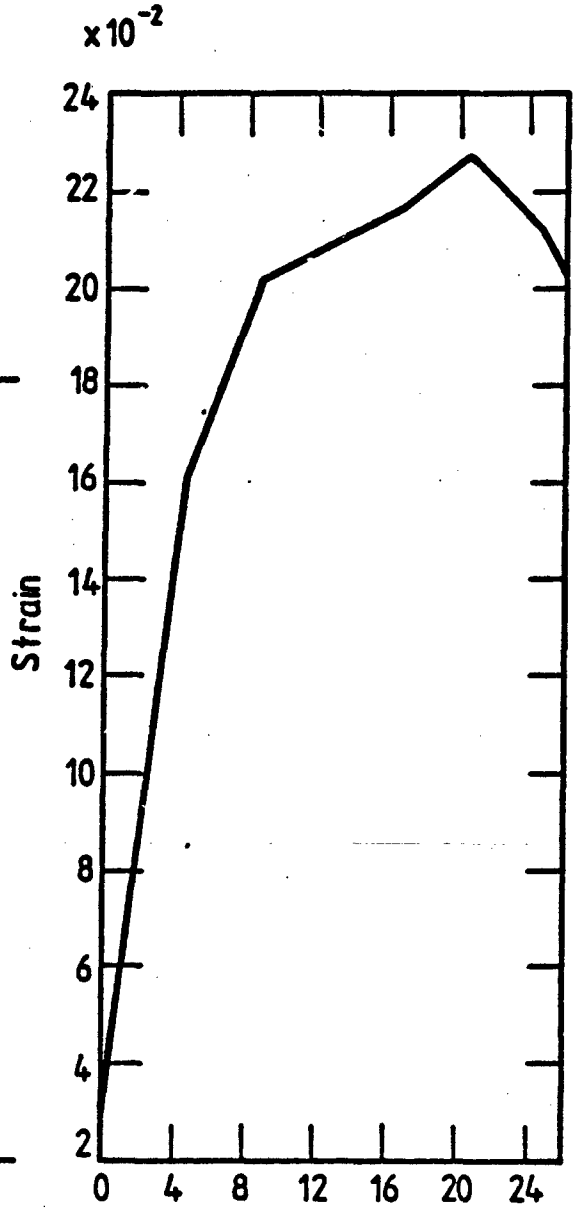

(c) time, x10^{-5}

Fig. 5.10 Results obtained by method of characteristics

Data: Trilinear nylon – $\epsilon p = 0{\cdot}03$, $Vp = 170ms$, 1 layer

Area density = $386 g/m^2$

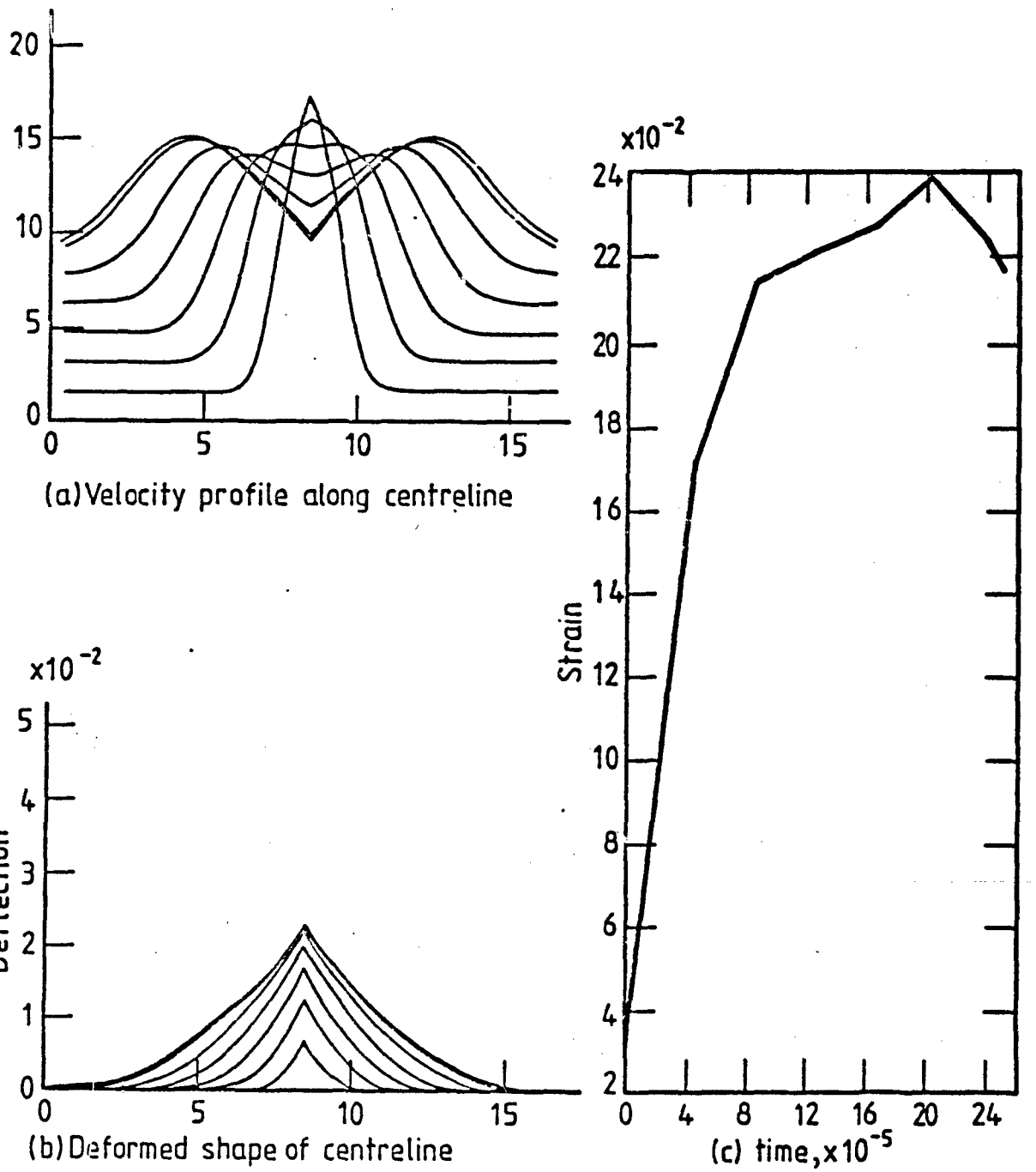

Fig. 5.11 Results obtained by method of characteristics

Data: linear kelvar. $\epsilon_p = 0{\cdot}0025$, $V_p = 290\,ms^{-1}$
2 layers. Area density $= 2 \times 351\ gm^{-2}$

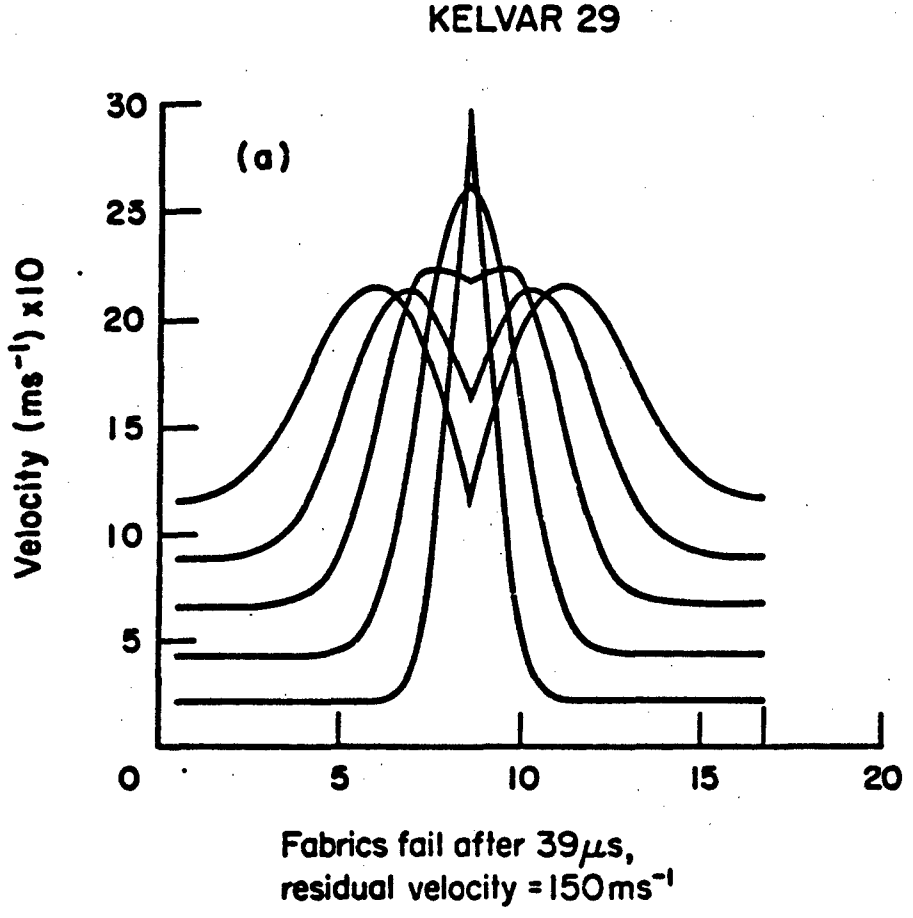

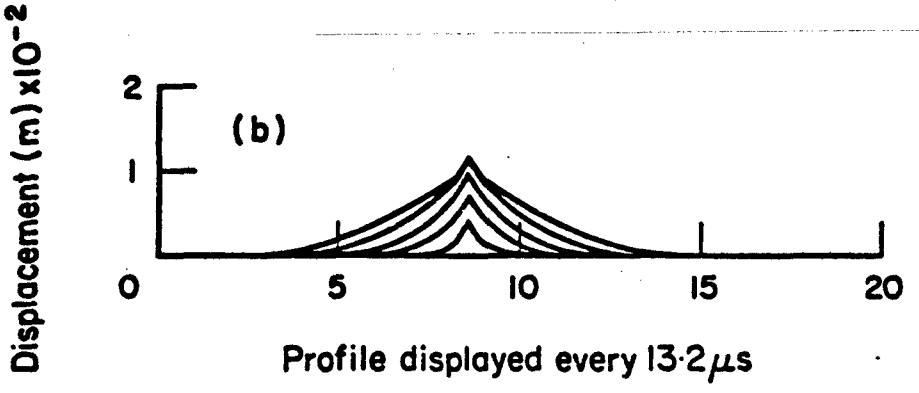

Fig. 5.12 Typical characteristic solution

Data : Trilinear nylon. $\epsilon_p = 0{\cdot}03$, $V_p = 235\,ms^{-1}$
3 layers. Area density = $3 \times 240\,gm^{-2}$

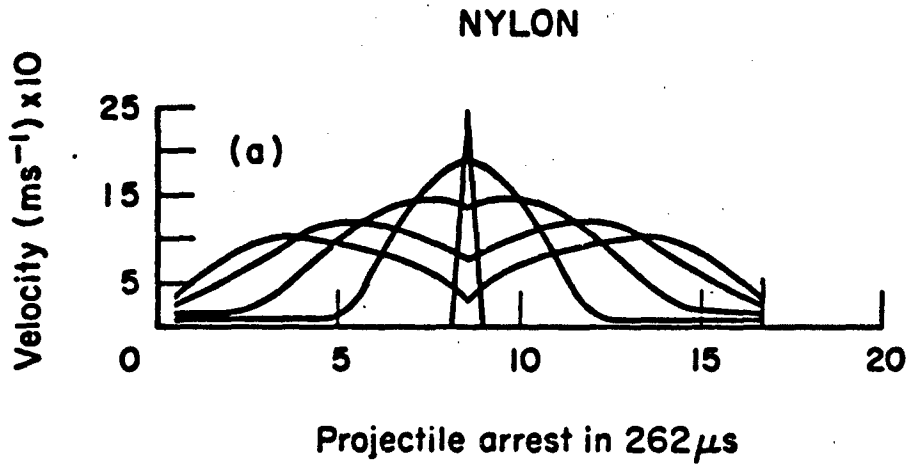

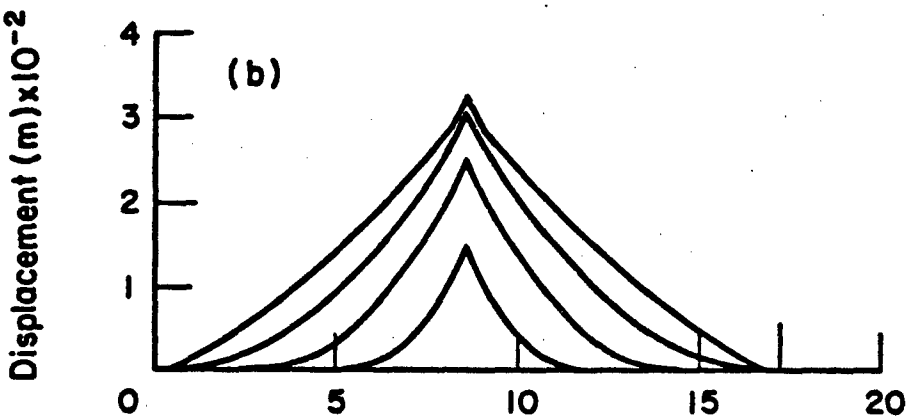

Profile displayed after:
68 μs, 132 μs, 196 μs, 262 μs

Fig. 5.13 Typical characteristic solution

Data : Trilinear nylon. $\epsilon_p = 0{\cdot}03$, $V_p = 245\,ms^{-1}$
3 layers. Area density = $3 \times 240\,gm^{-2}$

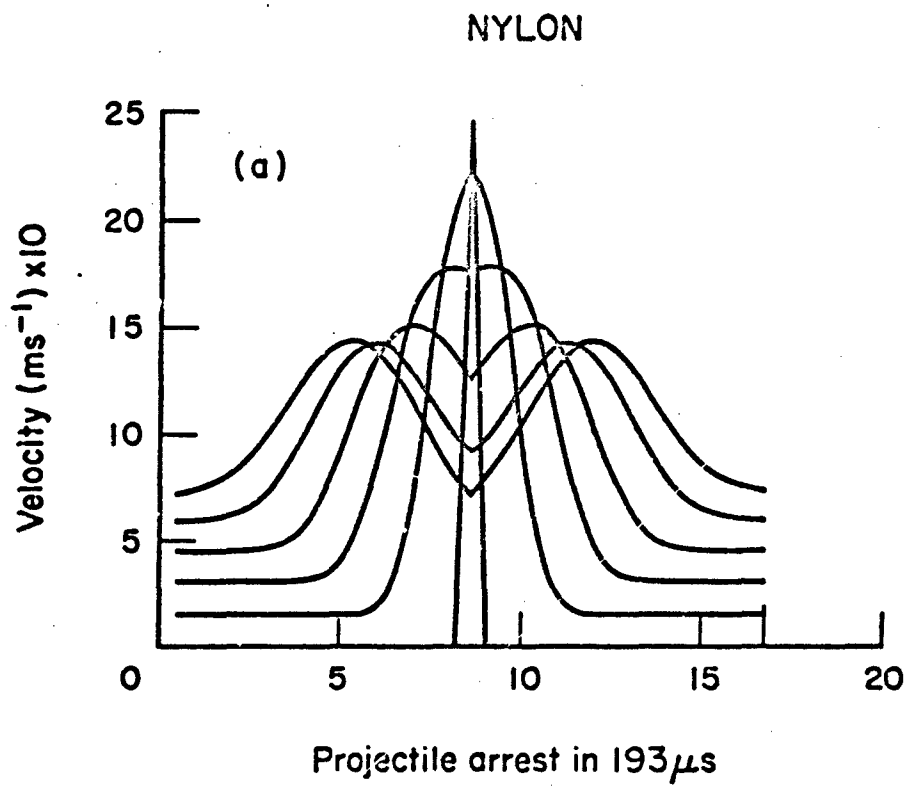

Fig. 5.14 Typical characteristic solution

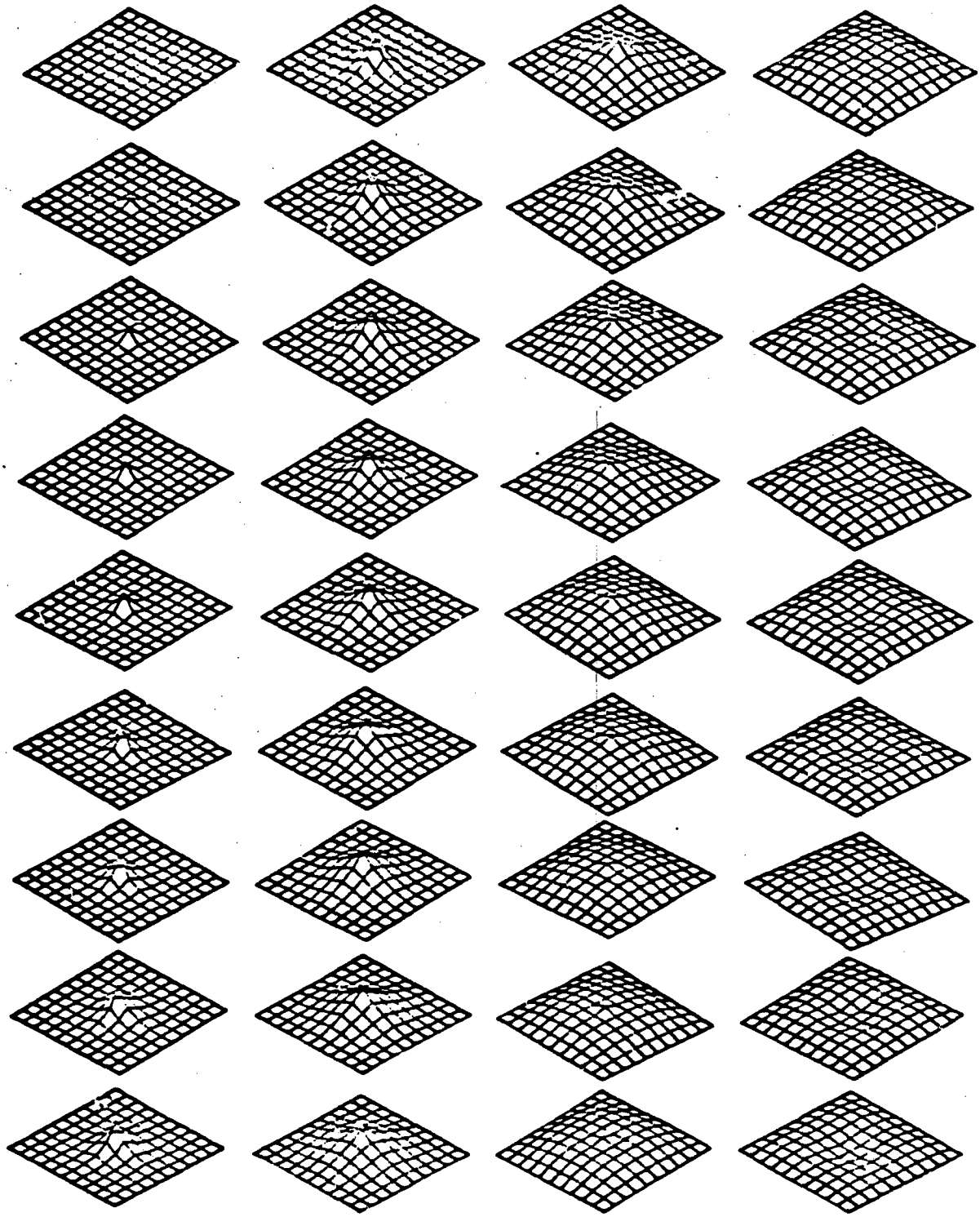

Time = 0·32 ms Time = 0·66 ms Time = 1·01 ms Time = 1·36 ms

Prestrain 10 % : Transverse displacement scaled by 2.
Impact Vel = 150 ms^{-1}

Fig. 5.15

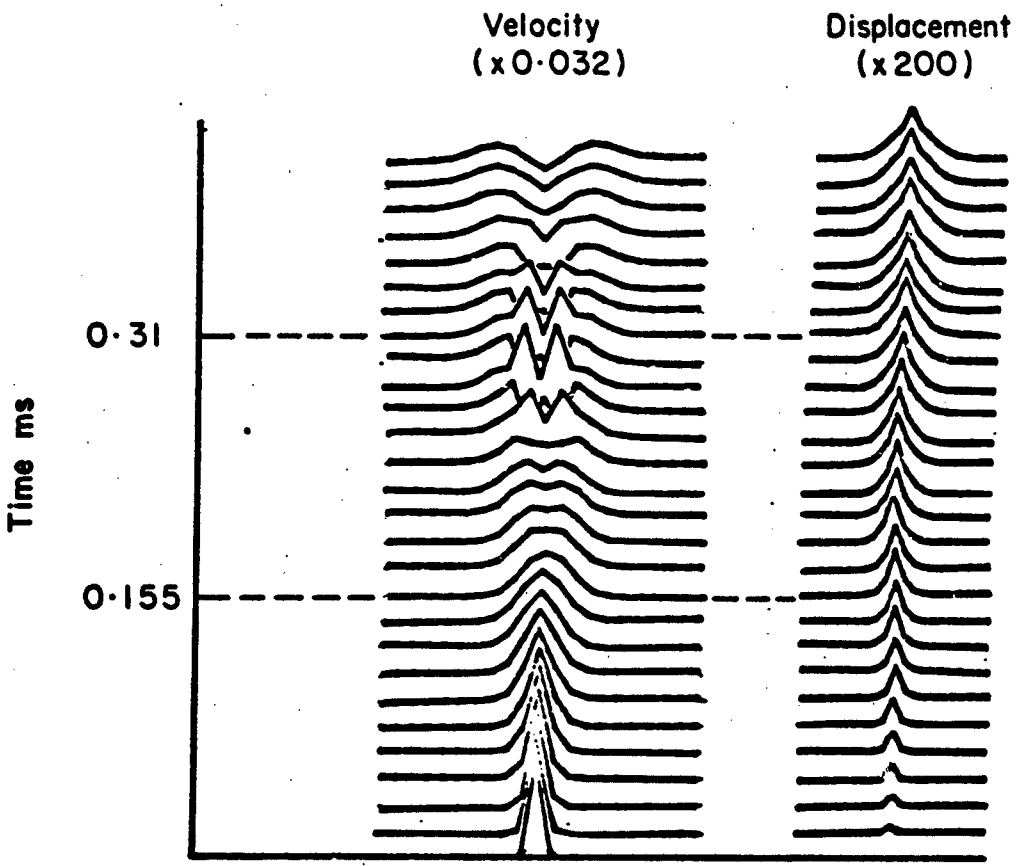

Fig. 5.16 Single weight fabric ($483 gm^{-2}$)

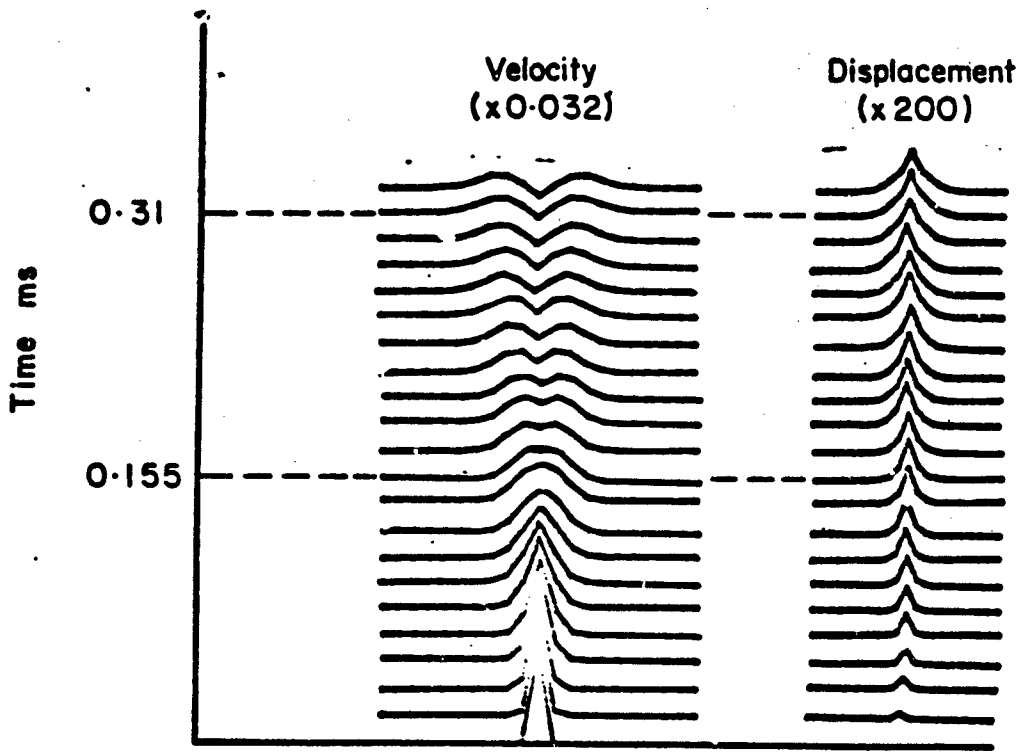

Fig. 5.17 Double weight fabric ($2 \times 483 gm^{-2}$)

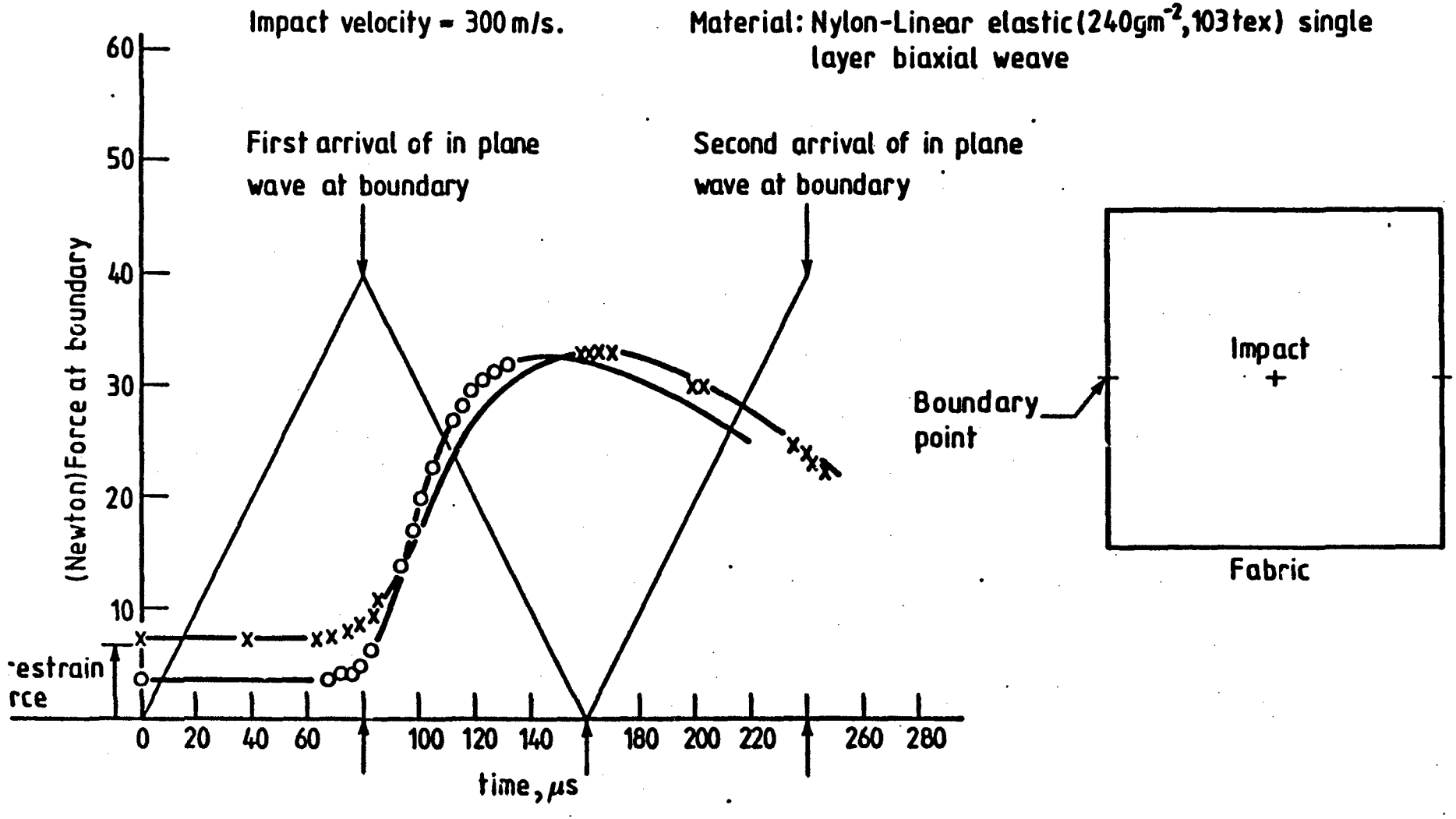

Fig. 5.18. Force at boundary against time for two values of prestrain.

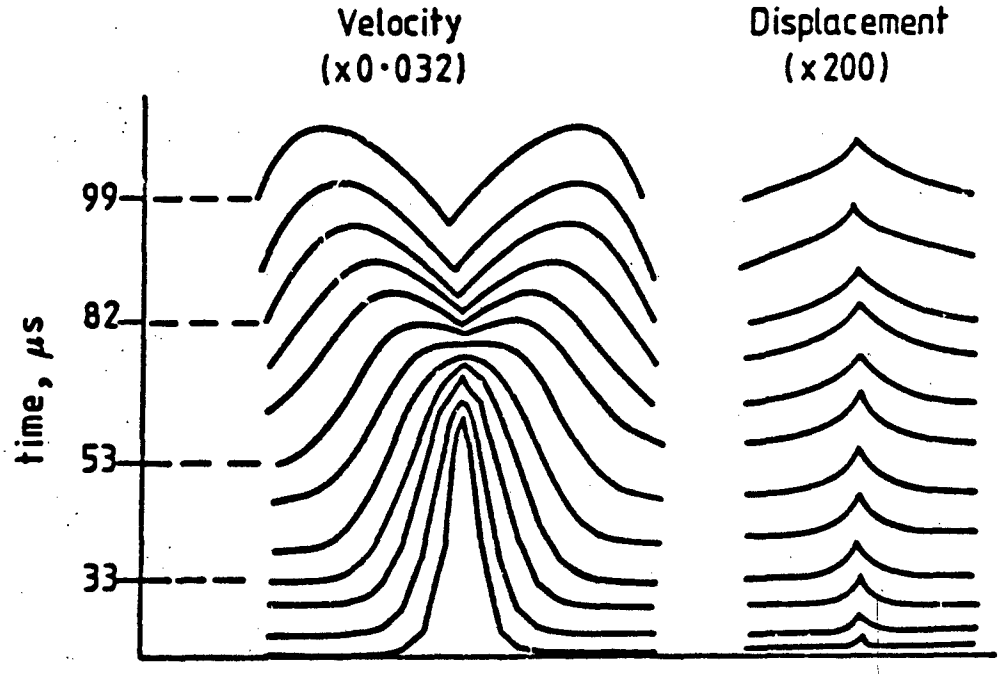

Fabric 1: 240gm^{-2} Nylon Fig 5.19

Prestrain 0·1

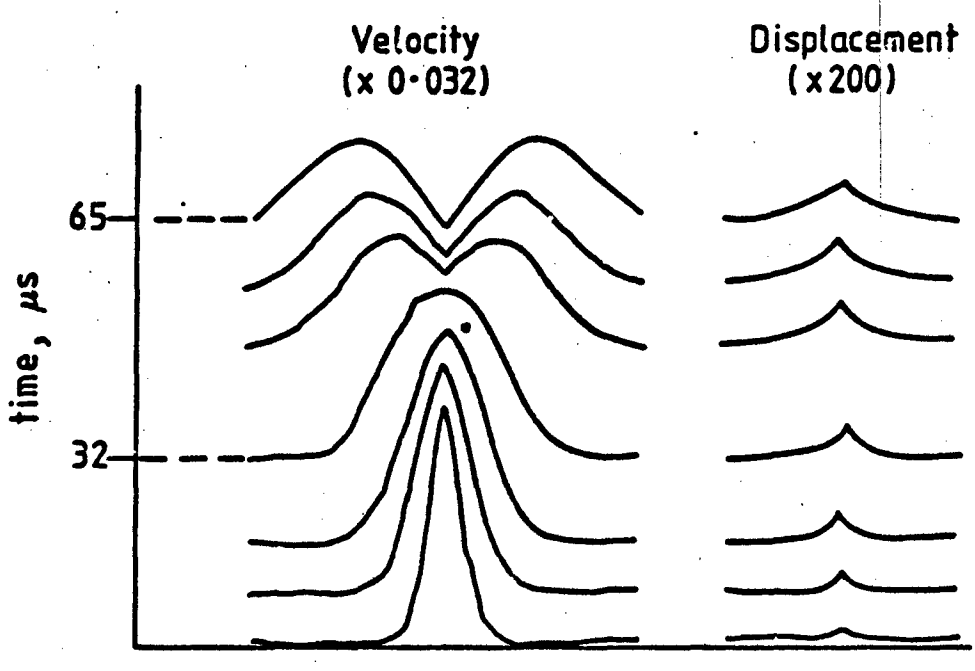

Fabric 2: 386gm^{-2} Nylon Fig 5.20

Prestrain = 0·1

Response of two weights of fabric to impact at

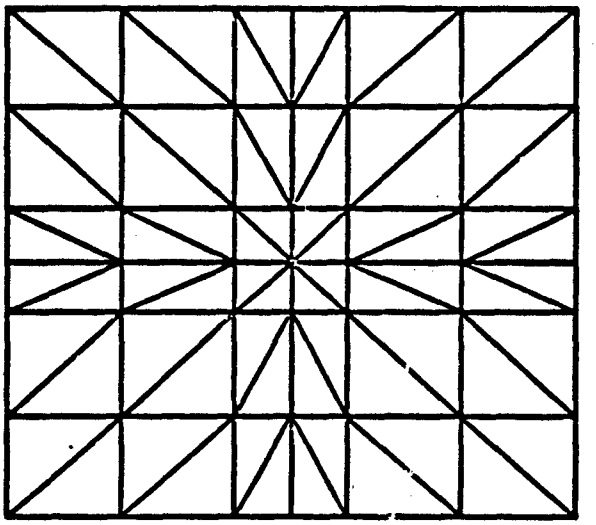

(a) First descretisation pattern

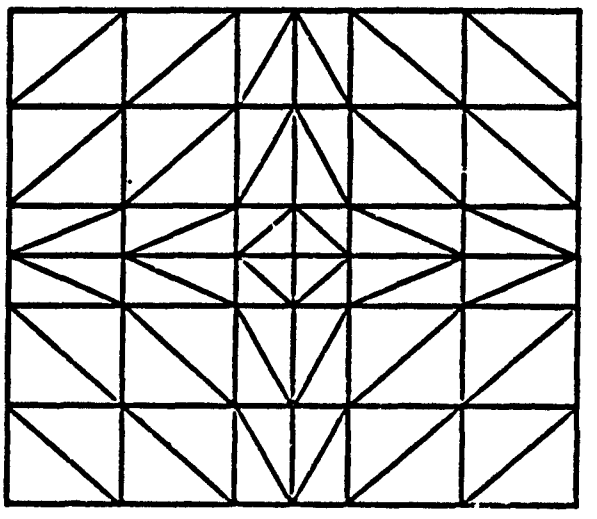

(b) Second descretisation pattern

Fig. 5.21

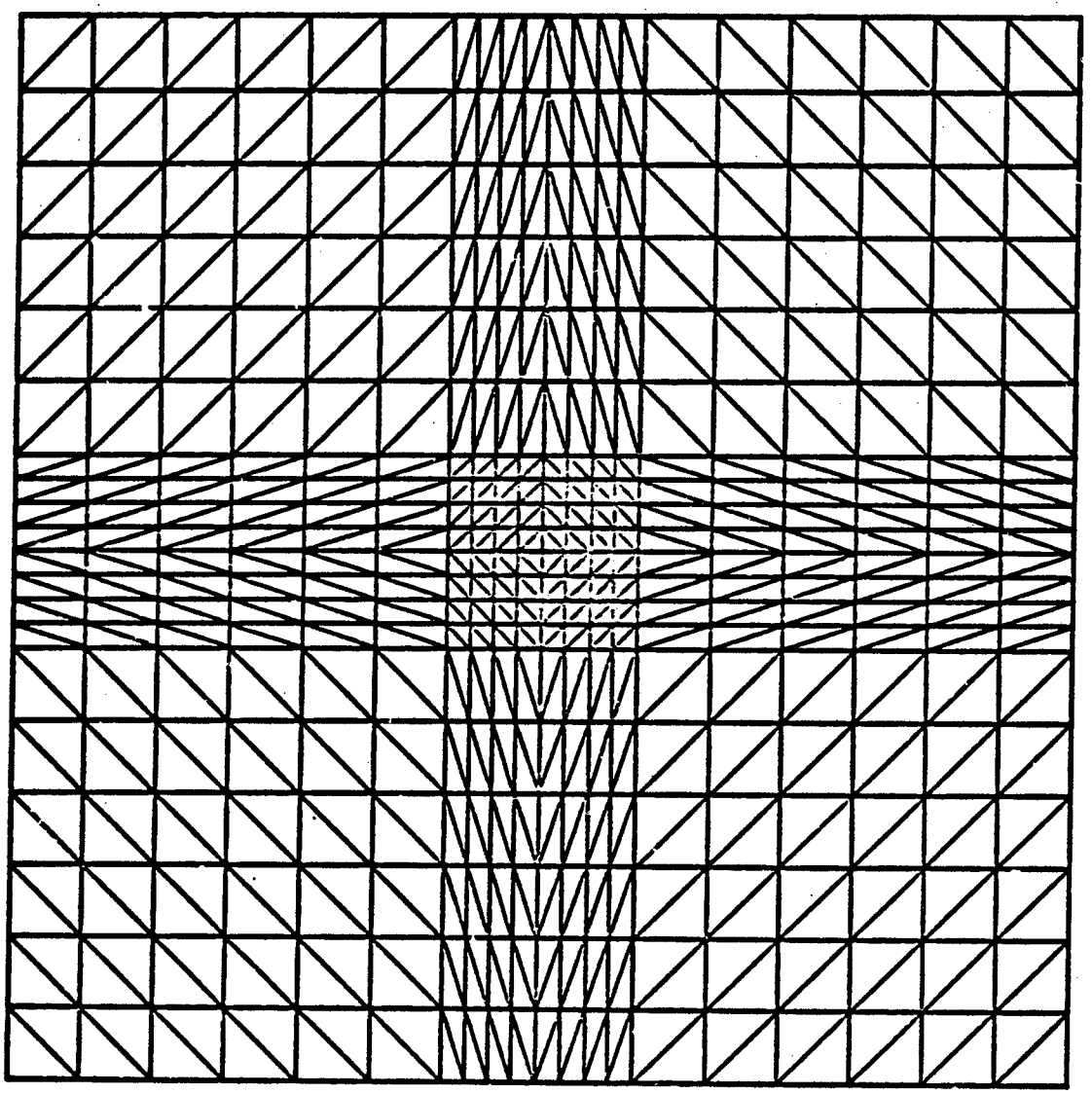

Fig. 5.22 Final mesh division

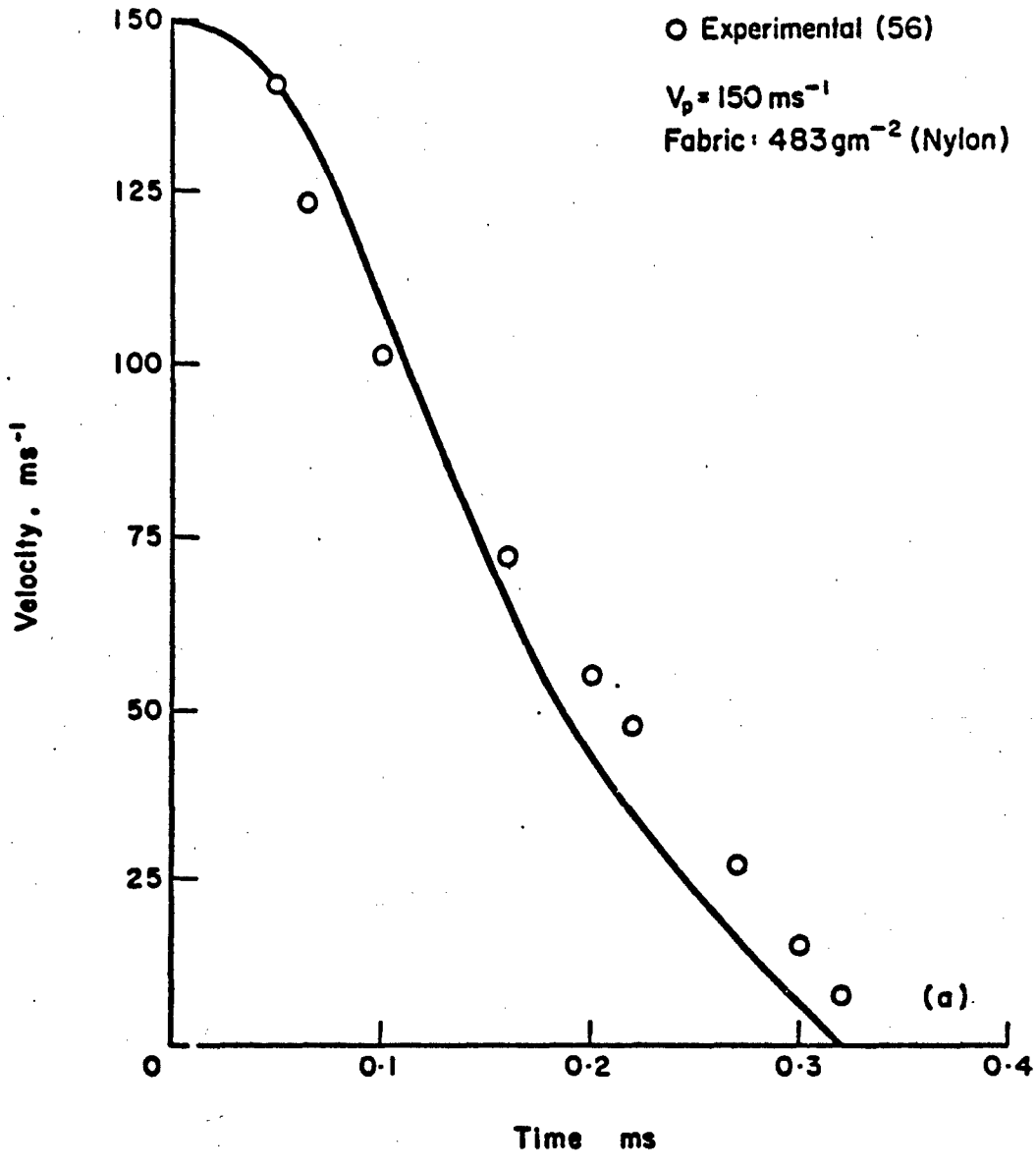
O Experimental (56)
$V_p = 150\ ms^{-1}$
Fabric : $483\ gm^{-2}$ (Nylon)
Velocity, ms^{-1}
150
125
100
75
50
25
0
0·1
0·2
0·3
0·4
Time ms
(a)

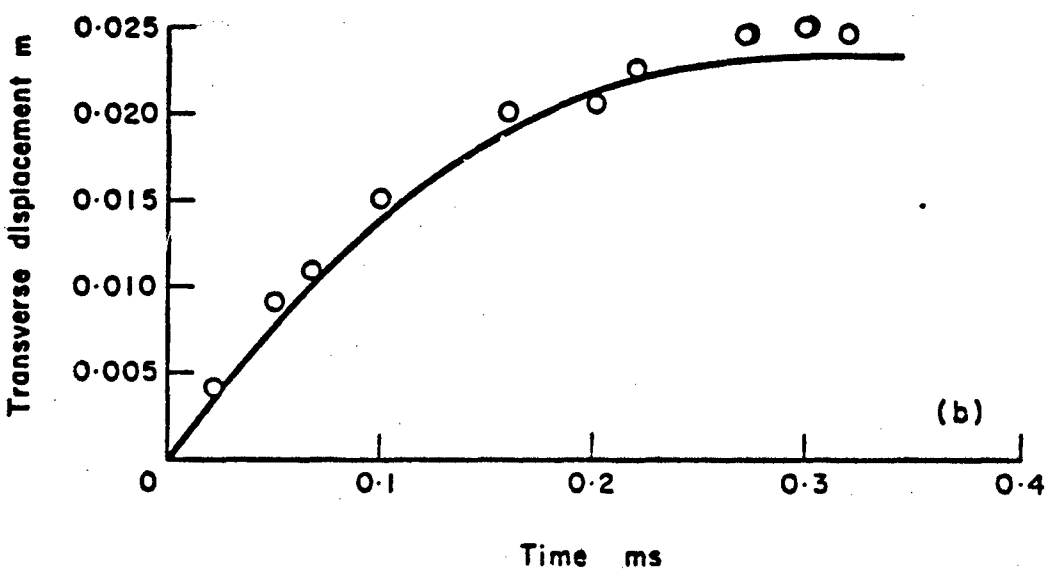
Transverse displacement m
0·025
0·020
0·015
0·010
0·005
0
0·1
0·2
0·3
0·4
Time ms
(b)

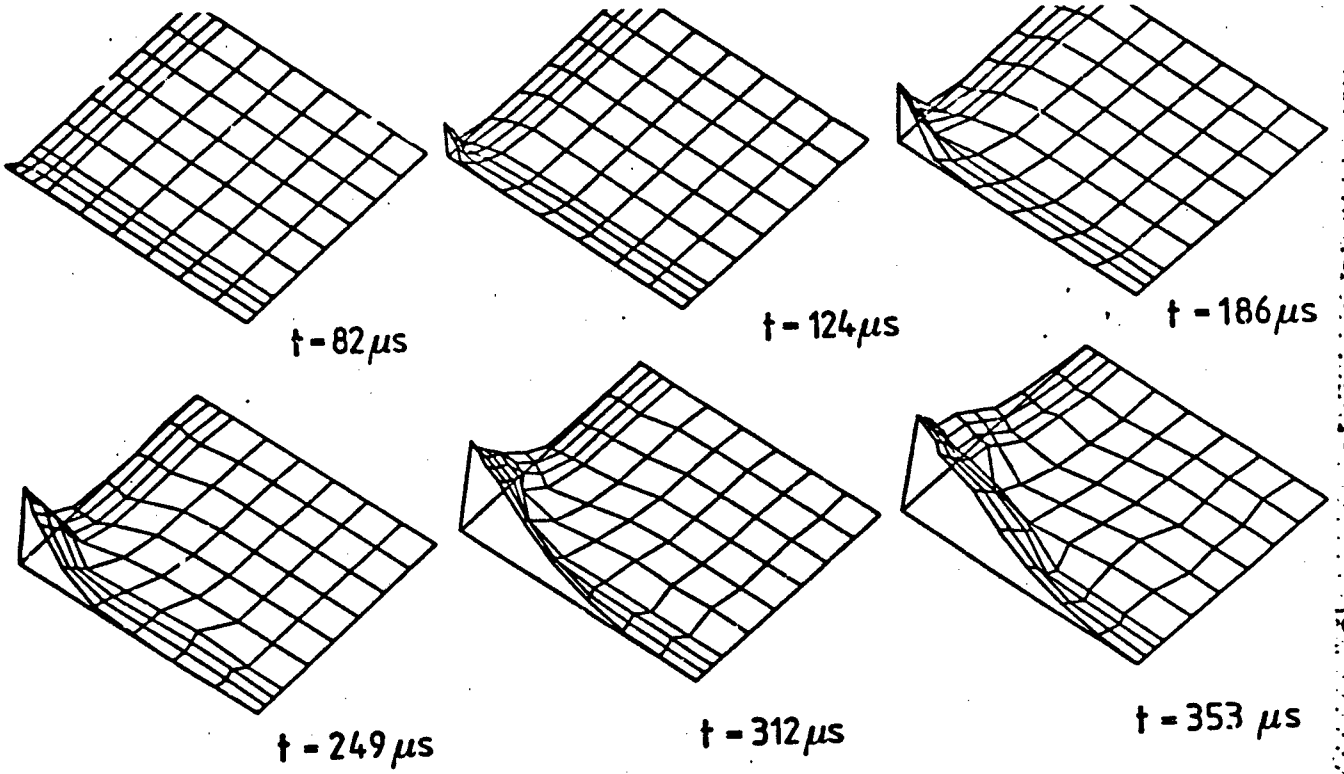

Deformation of impacted fabric

Fabric: 386 gm^{-2} Nylon

Projectile: 1.1g. Impact velocity = 150 ms^{-1}

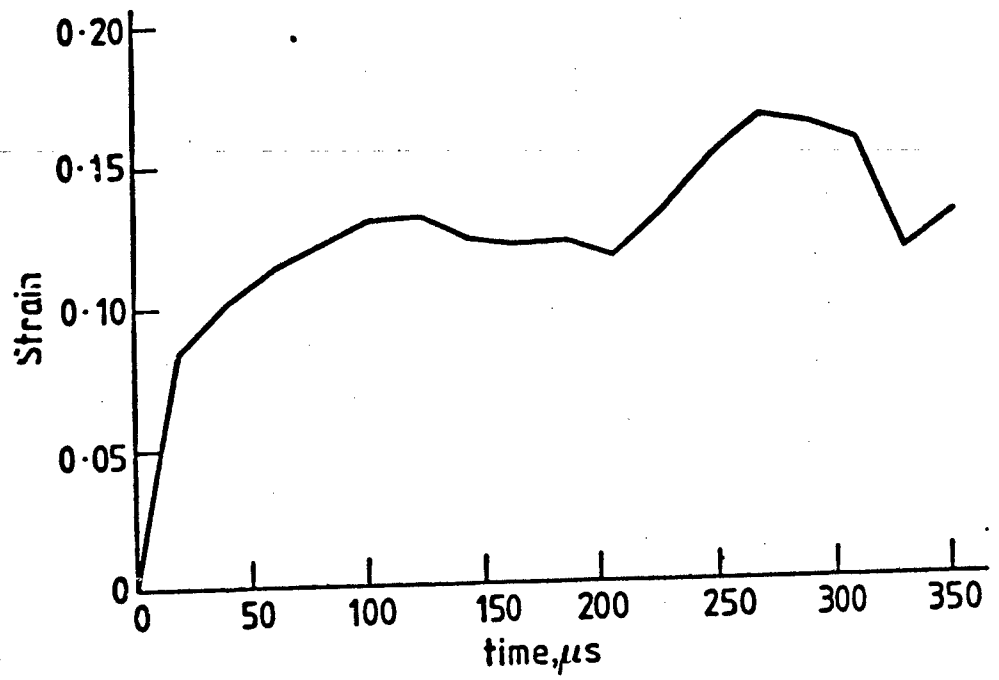

Strain history at impact point

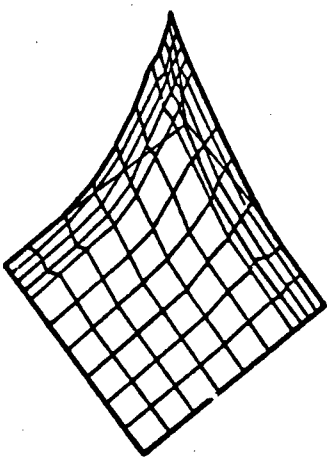

Fabric: Nylon $2 \times 240\ g/m^2$. Projectile 1.1g at $200\ ms^{-1}$

(a)

Fabric shape at time of projectile arrest

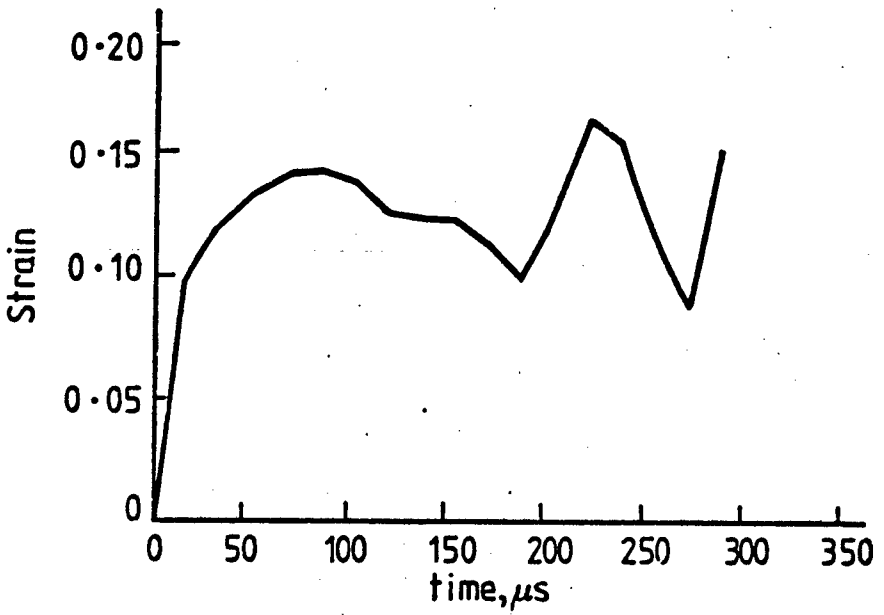

(b)

Strain history at impact point

Fig. 5.25. Impact response of nylon (2 layers)

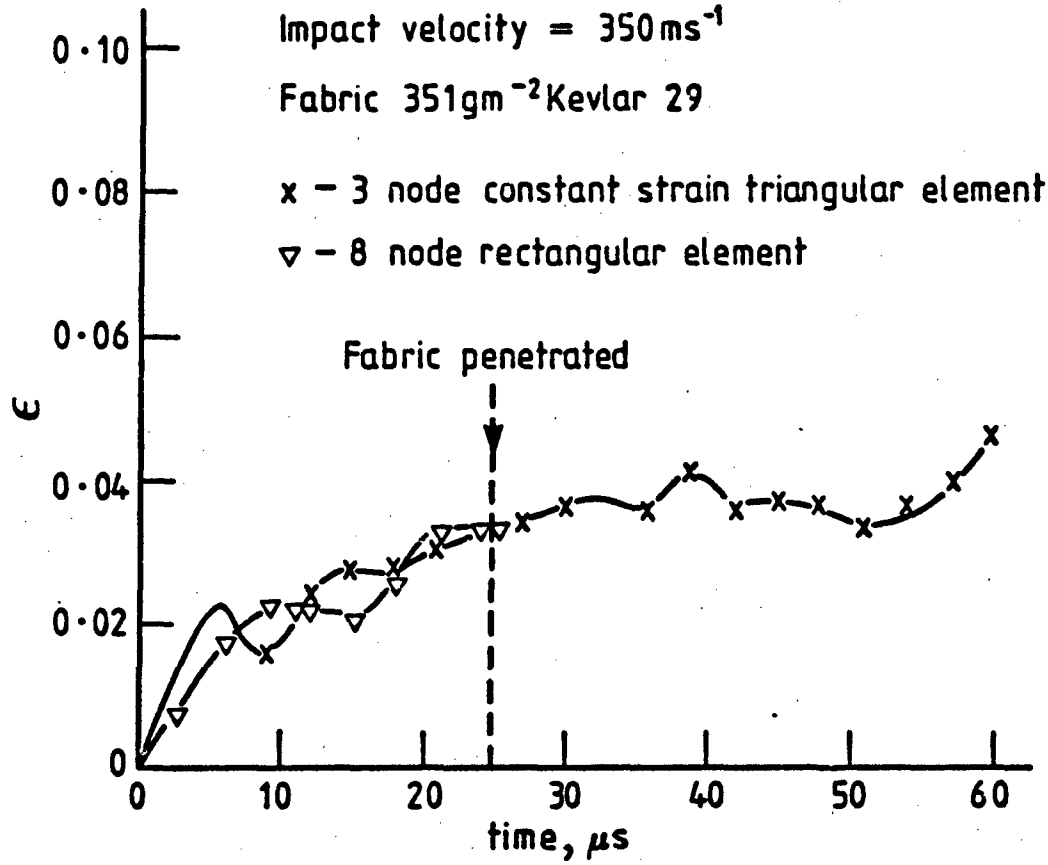

(a) Strain at impact point

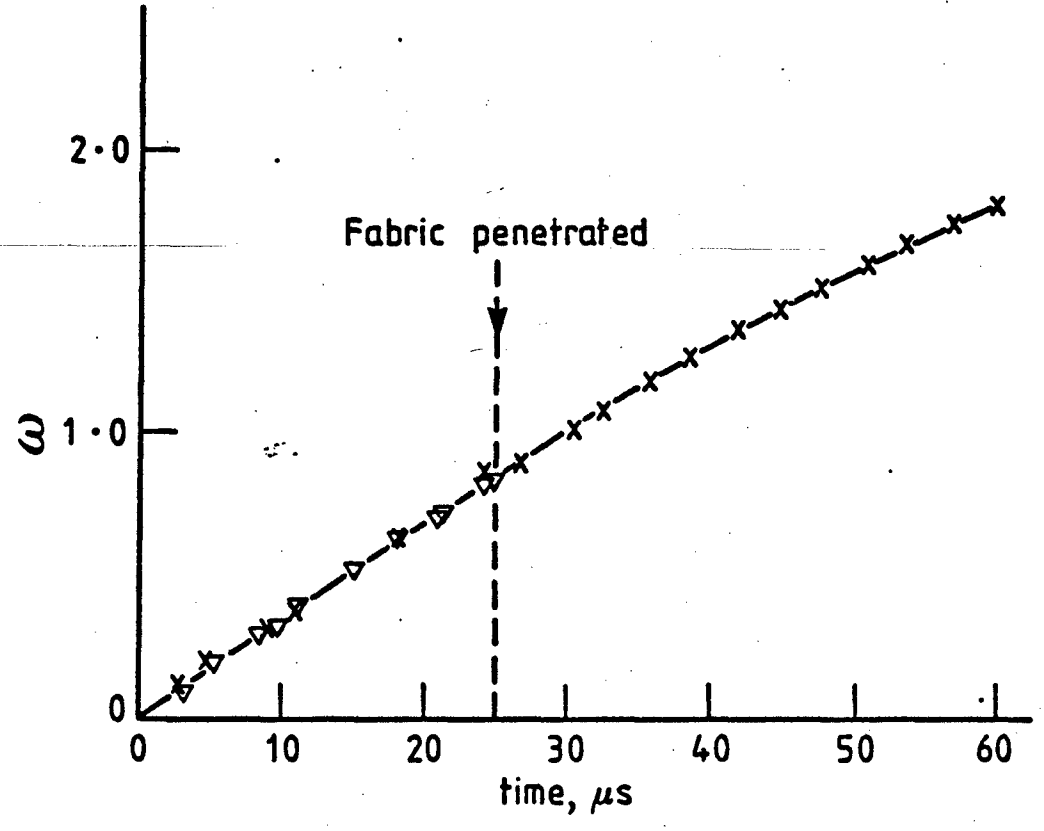

(b) Out of plane deflection at impact point

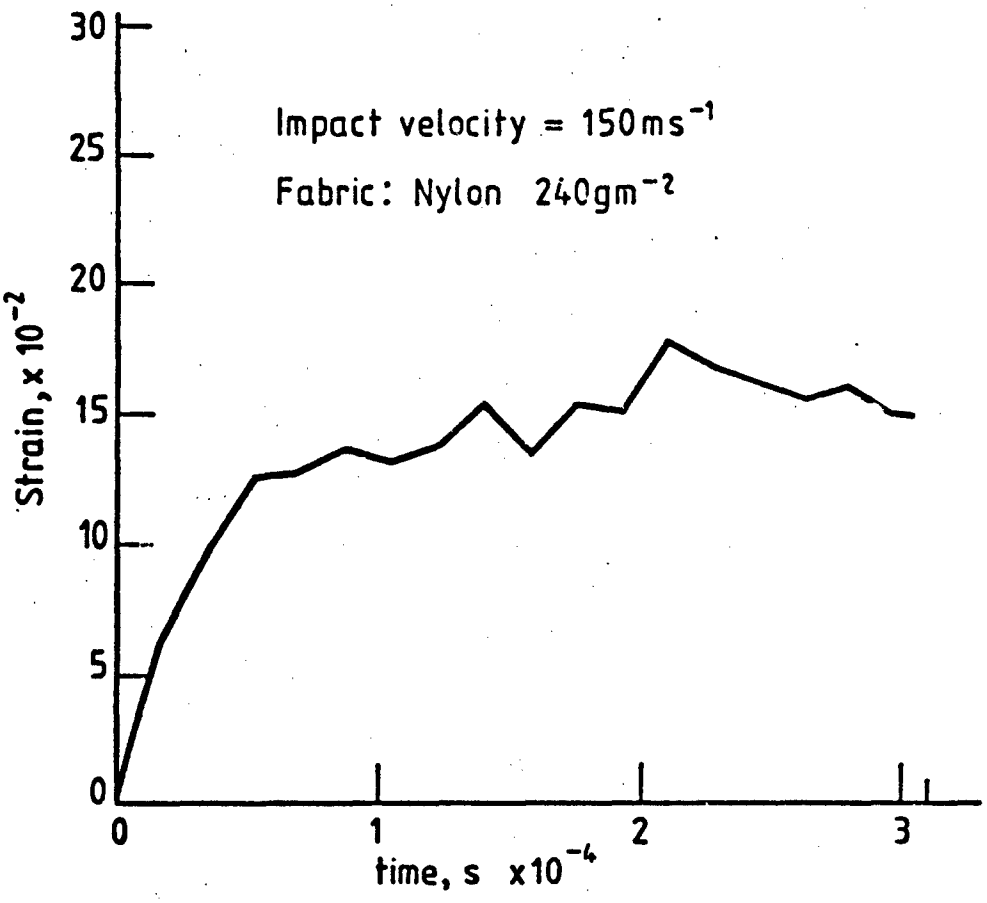

Strain at impact point

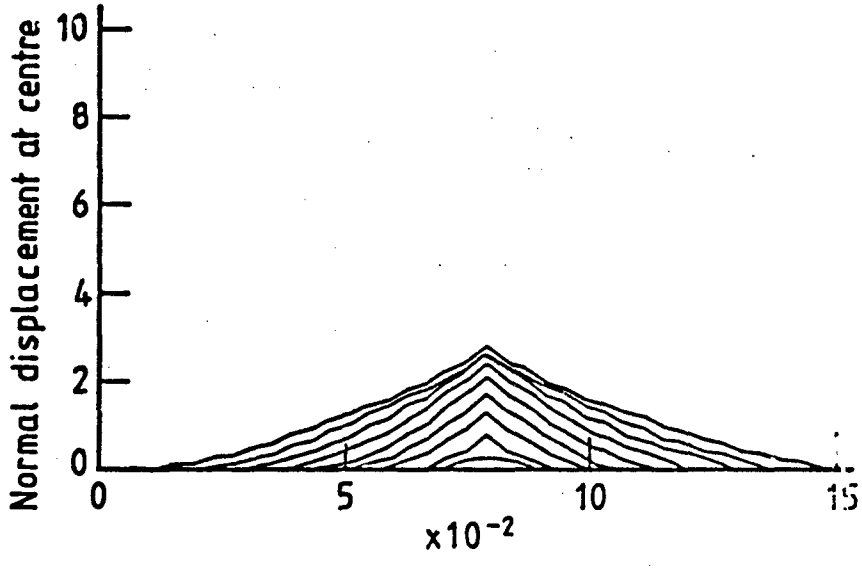

Shape of yarn through impact point at different times during motion

Fig. 5.27 Typical results obtained using 2-node rod elements

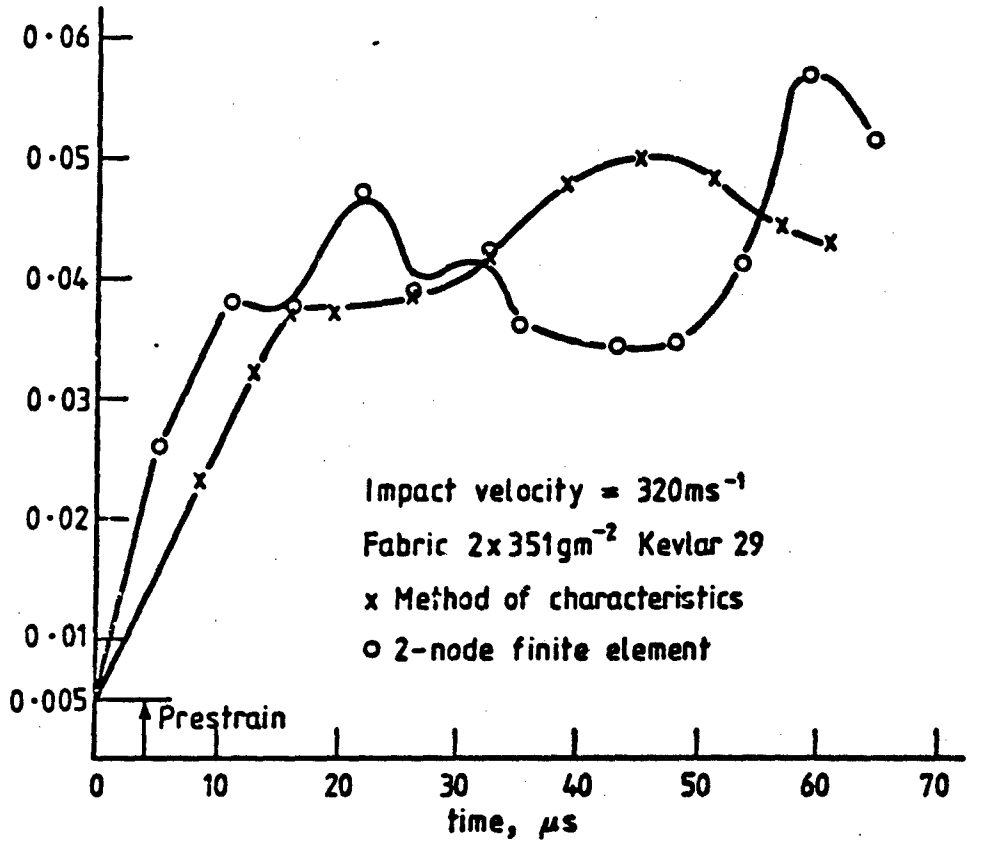

(a) Strain at impact point

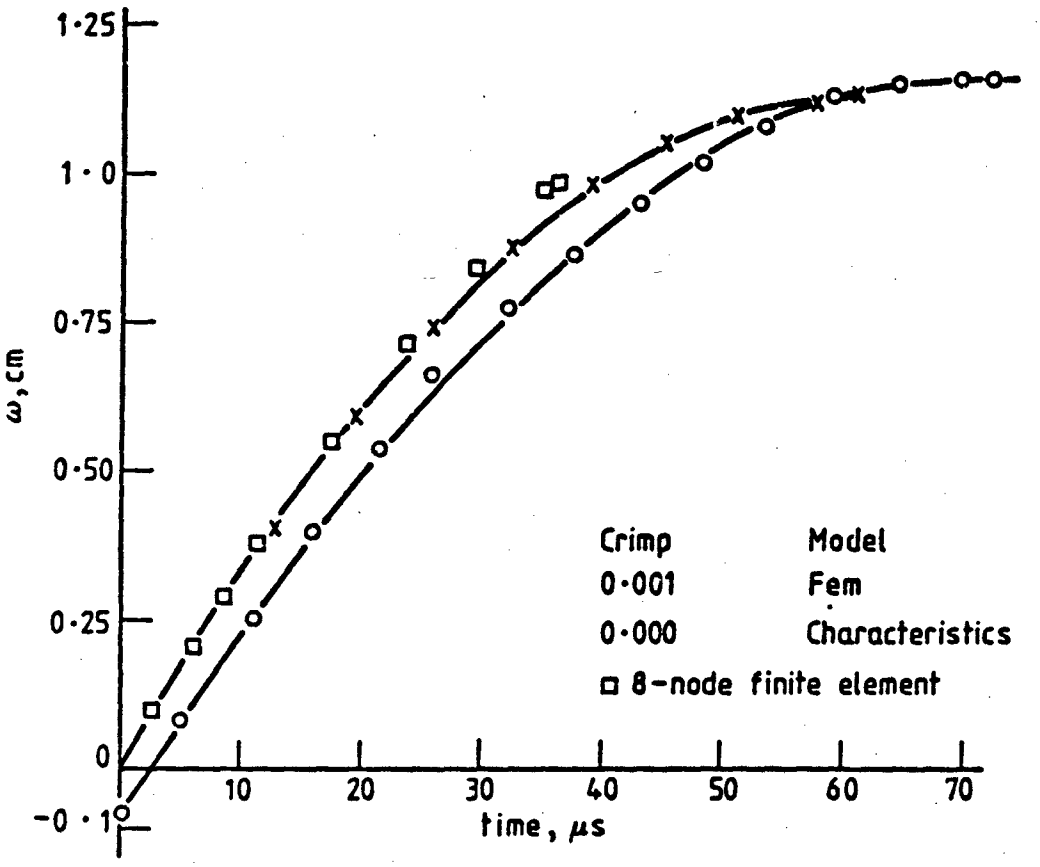

(b) Out of plane deflection at impact point

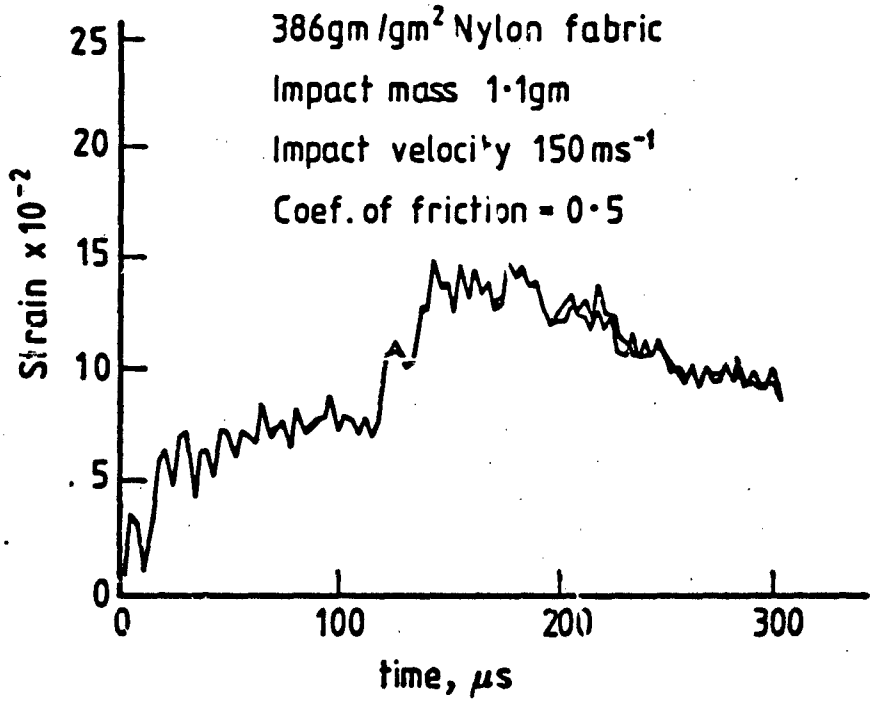

(a)

Slipping allowed at yarn crossovers

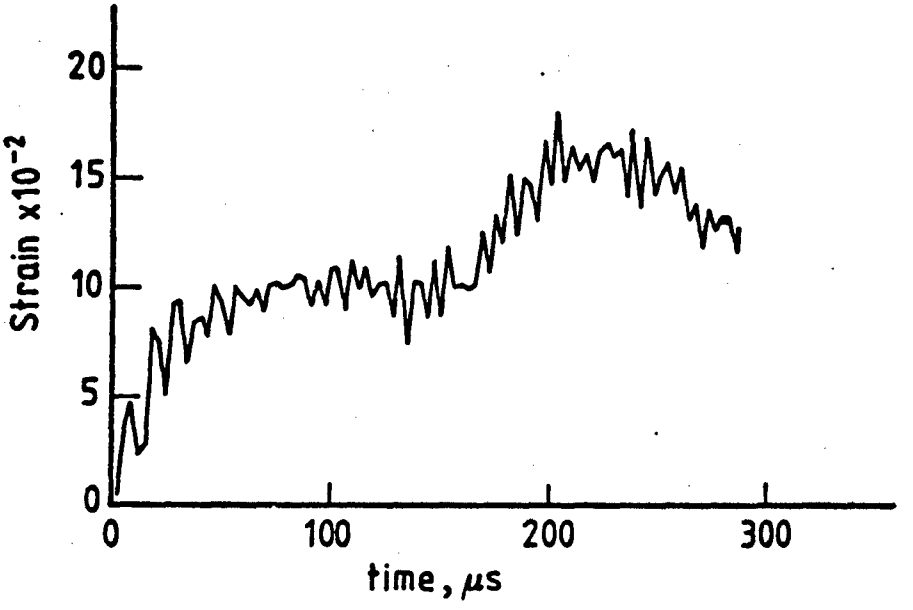

(b)

Yarns rigidly connected

Fig. 5.29. Strain history at impact point for two crossover

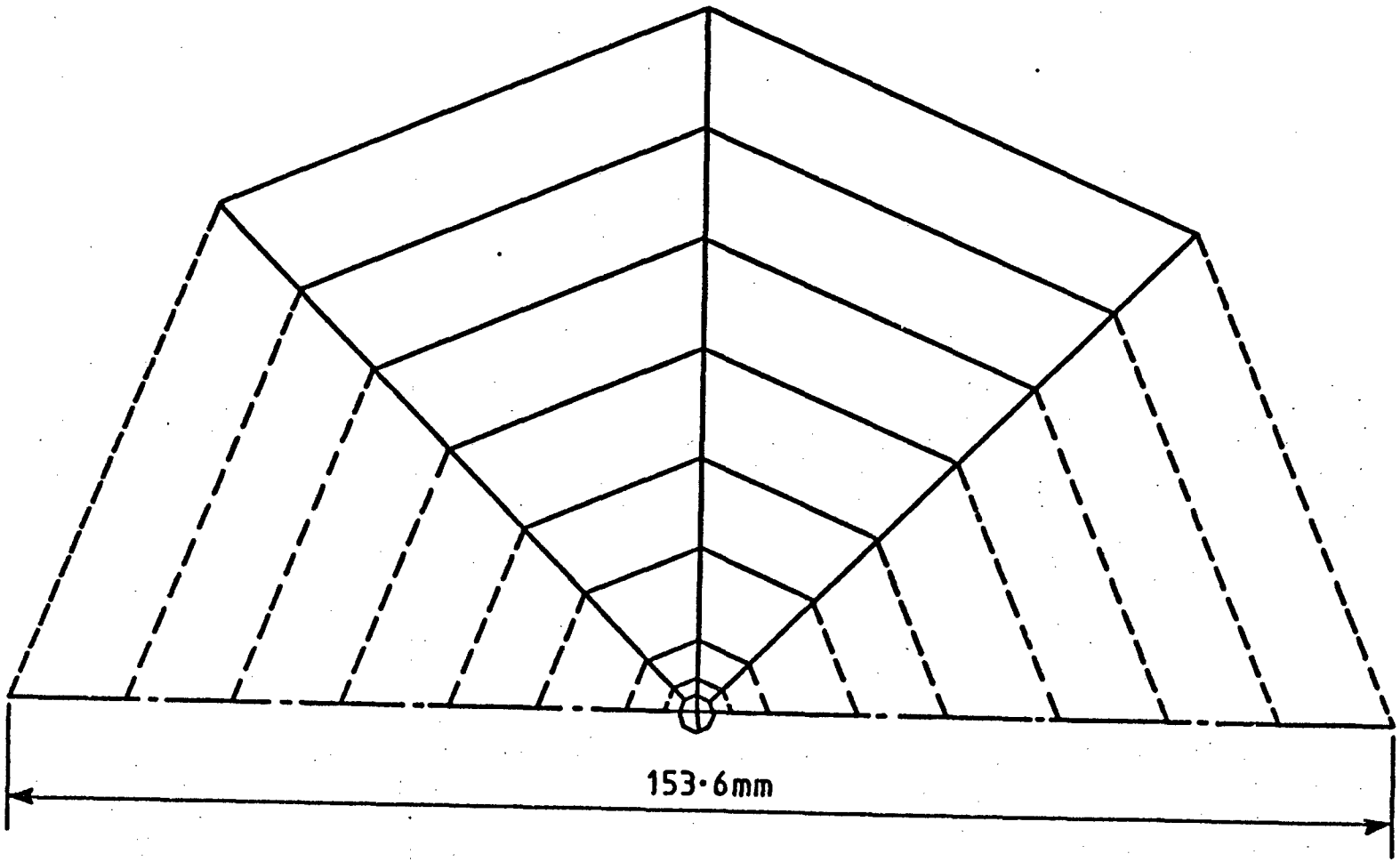

Fig 5.30. Elements of fabric (3-D model)

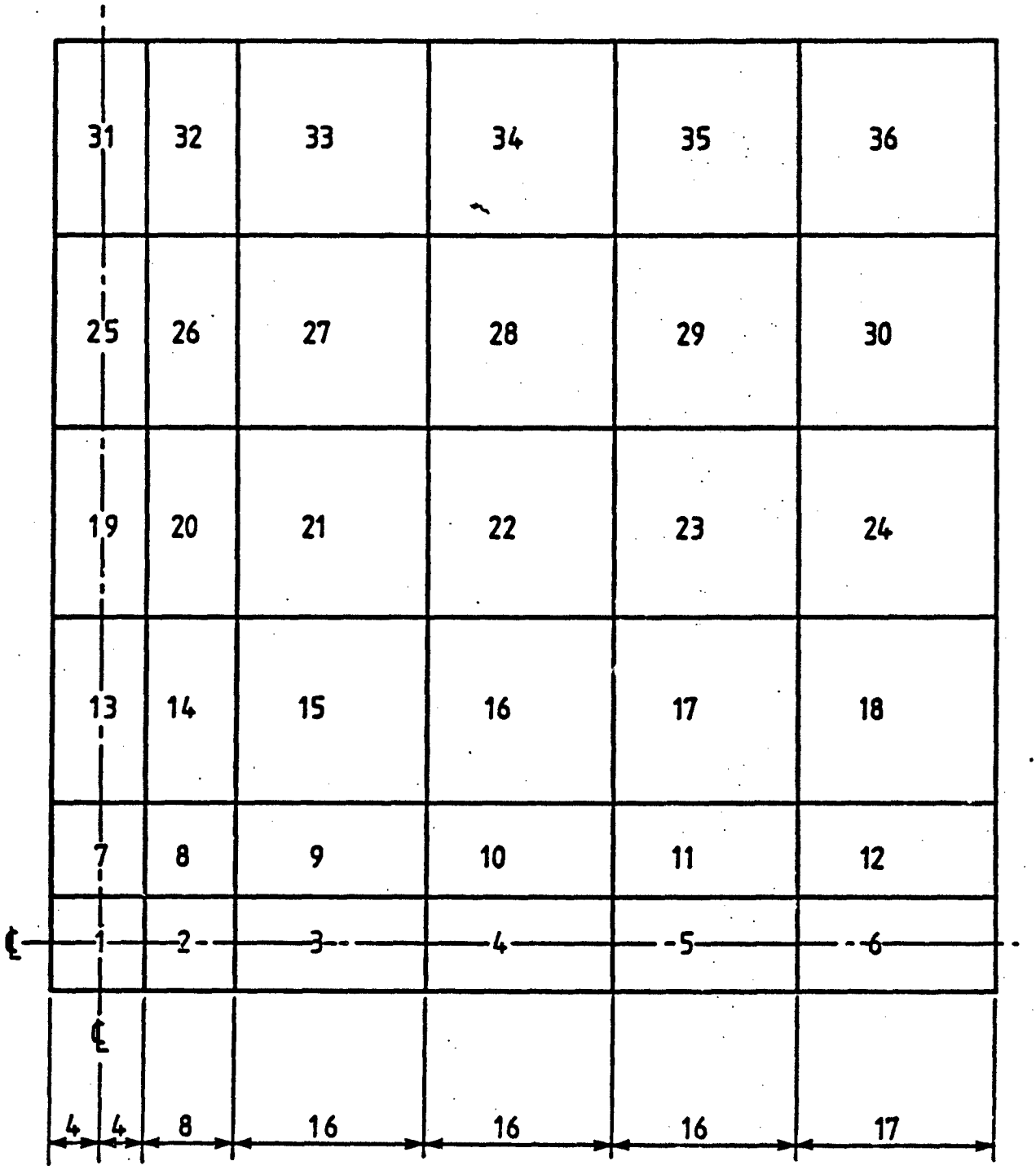

Quarter of fabric (All dimensions in mm)

36 elements 169 nodes

Fig. 5.31. Descritisation of fabric into 9-node element

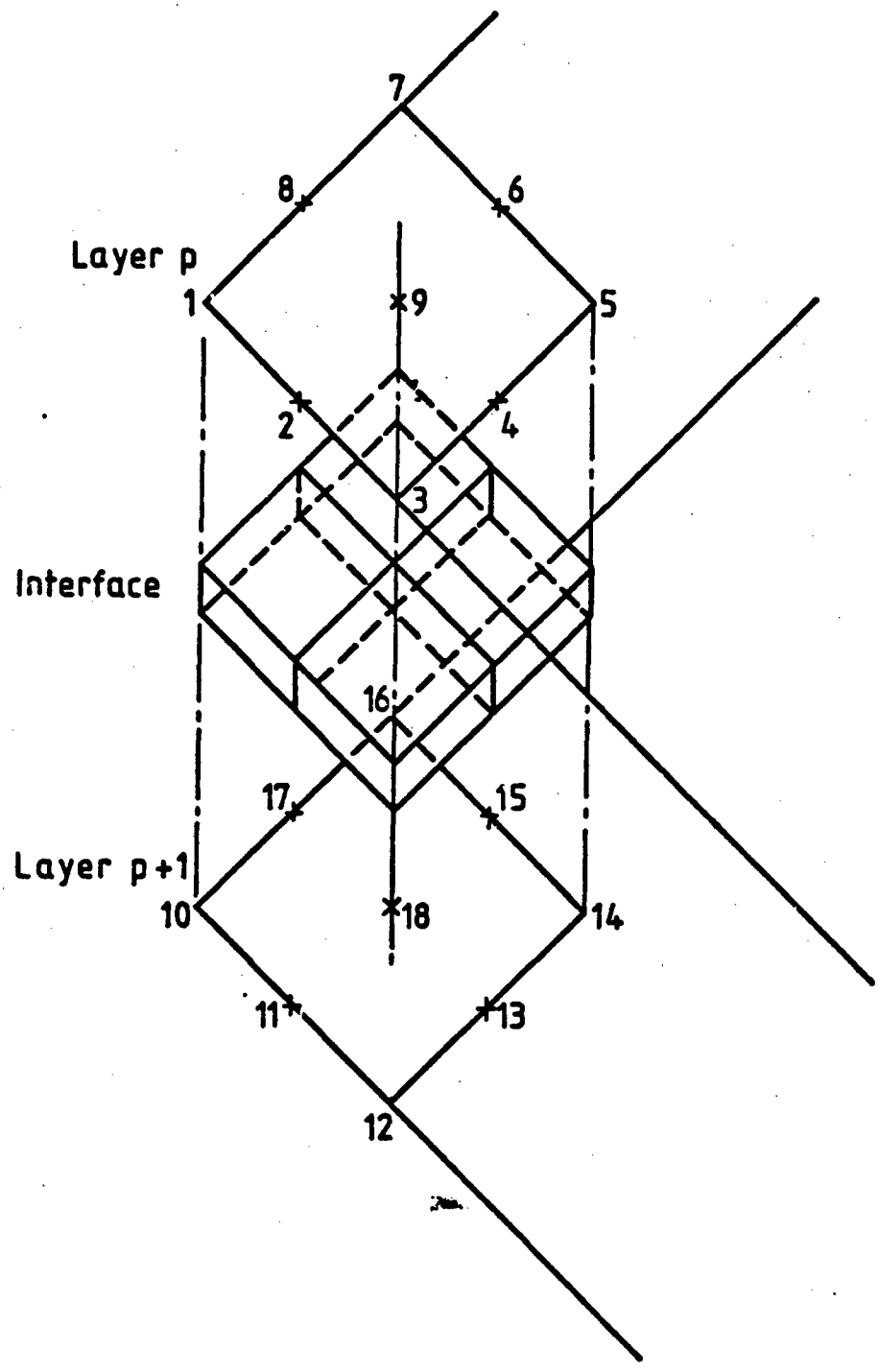

Fig. 5.32. Details of interface element (model involving 9-node membrane elements.)

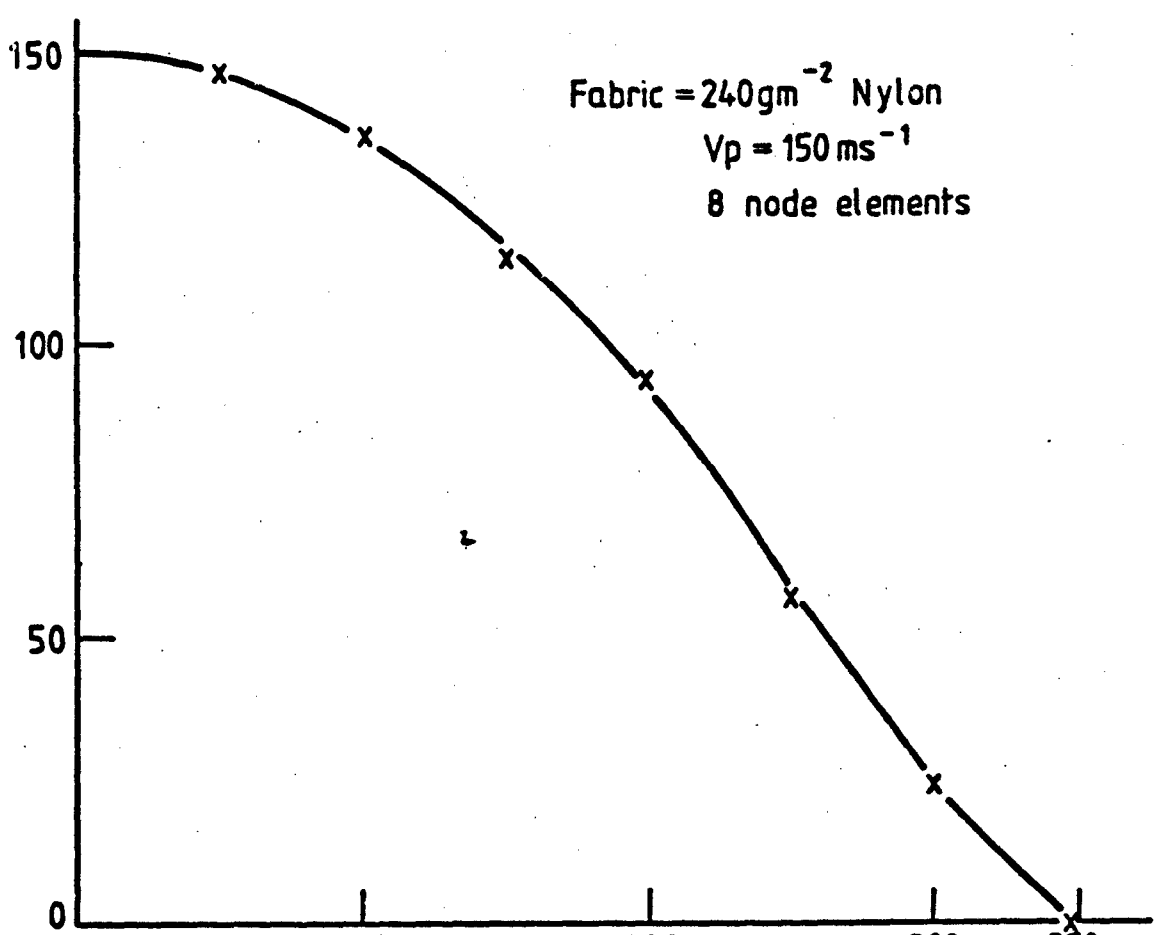

Projectile velocity against time

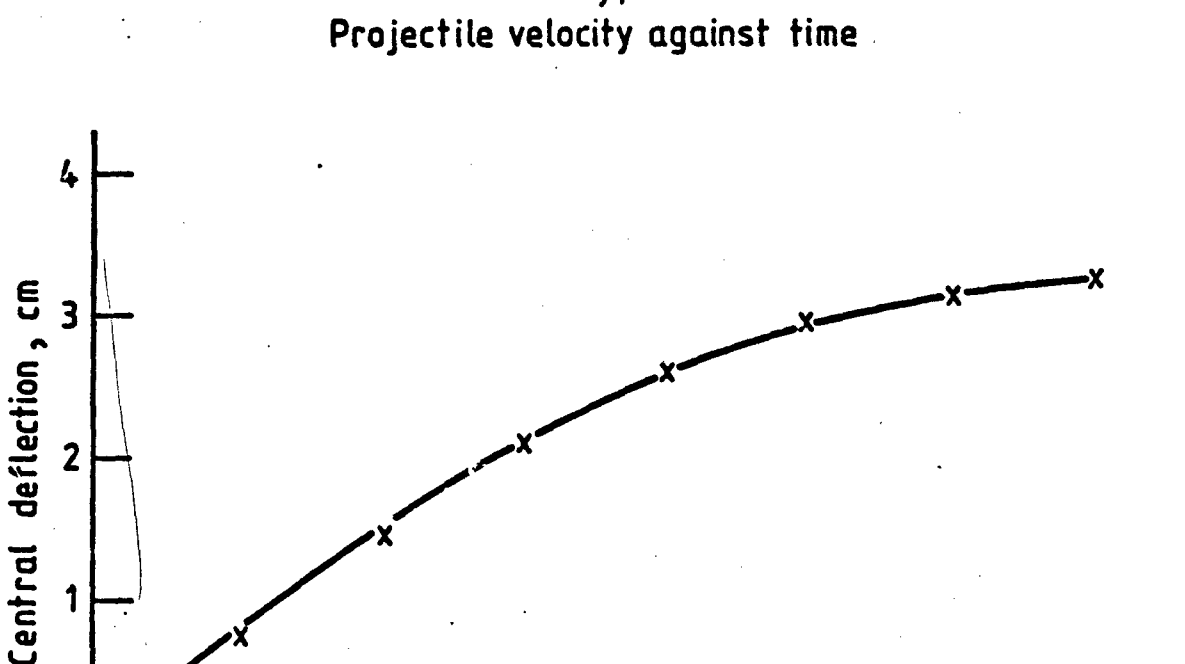

Out of plane deflection of fabric at centre

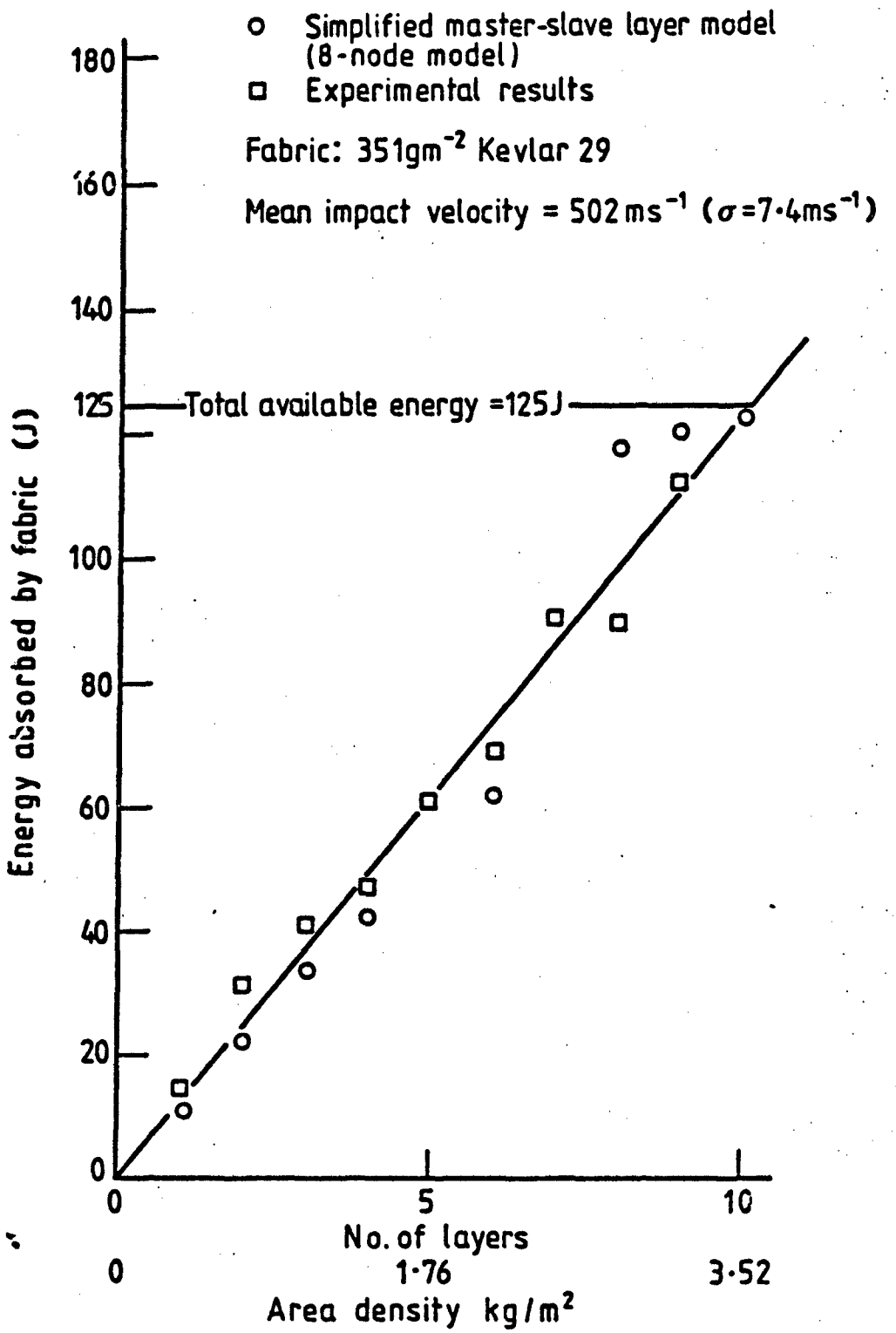
Simplified master-slave layer model (8-node model)
Experimental results
Fabric: 351gm^{-2} Kevlar 29
Mean impact velocity = 502 ms^{-1} (σ=7·4ms^{-1})
Total available energy =125J
Energy absorbed by fabric (J)
180
160
140
125
100
80
60
40
20
0
0
5
10
No. of layers
0
1·76
3·52
Area density kg/m^2

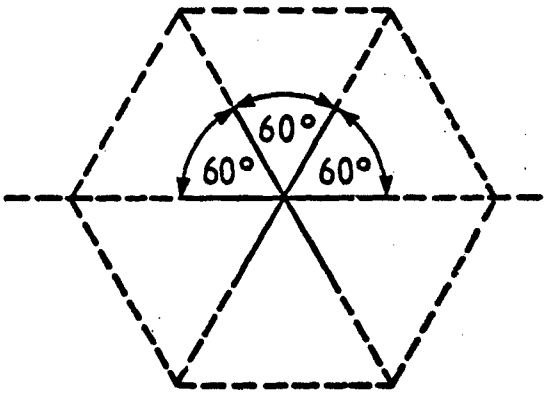

Fig.A1. 1a Typical cell in triaxially woven fabric

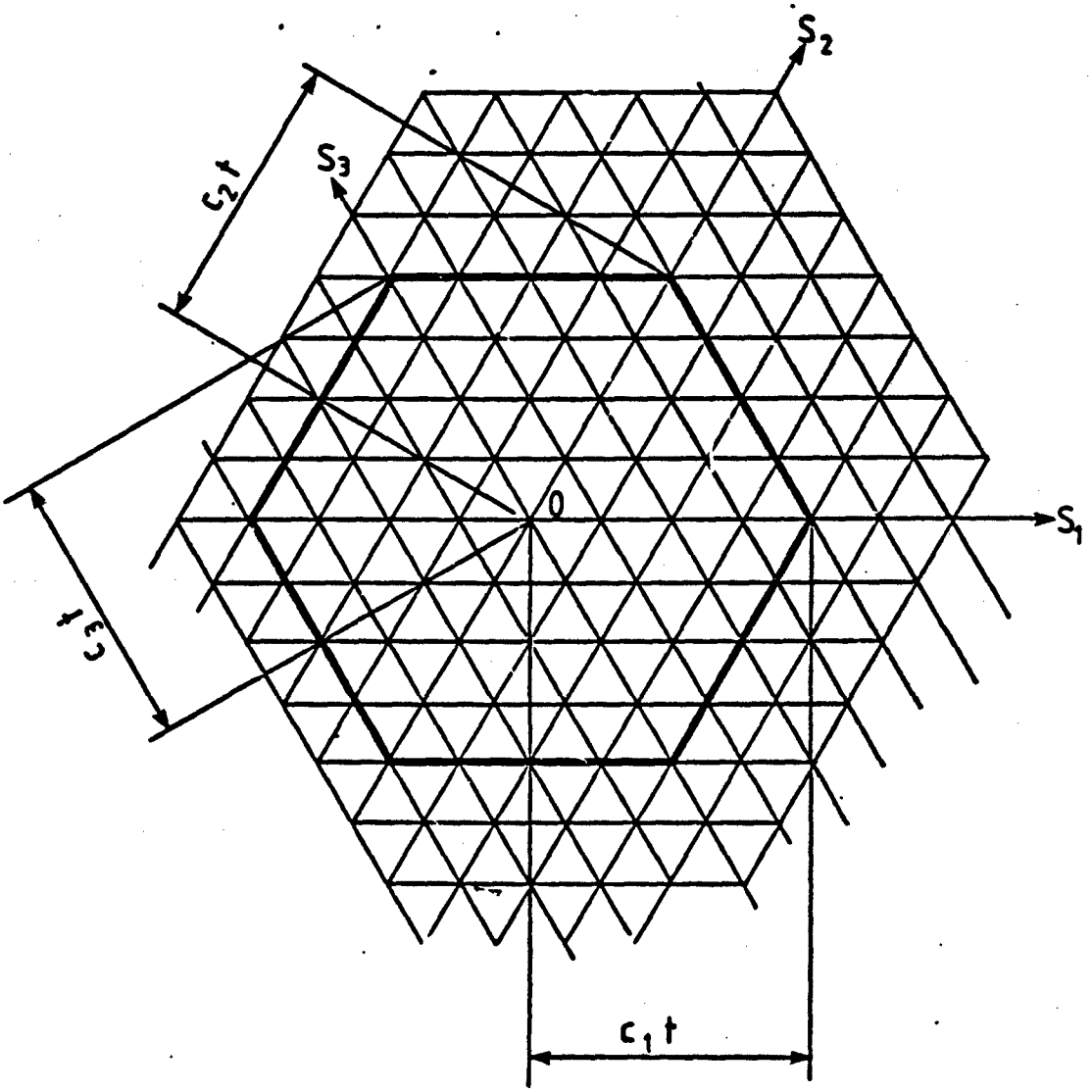

Fig.A1. 1b Hexagonal wave front in triaxially woven fabric

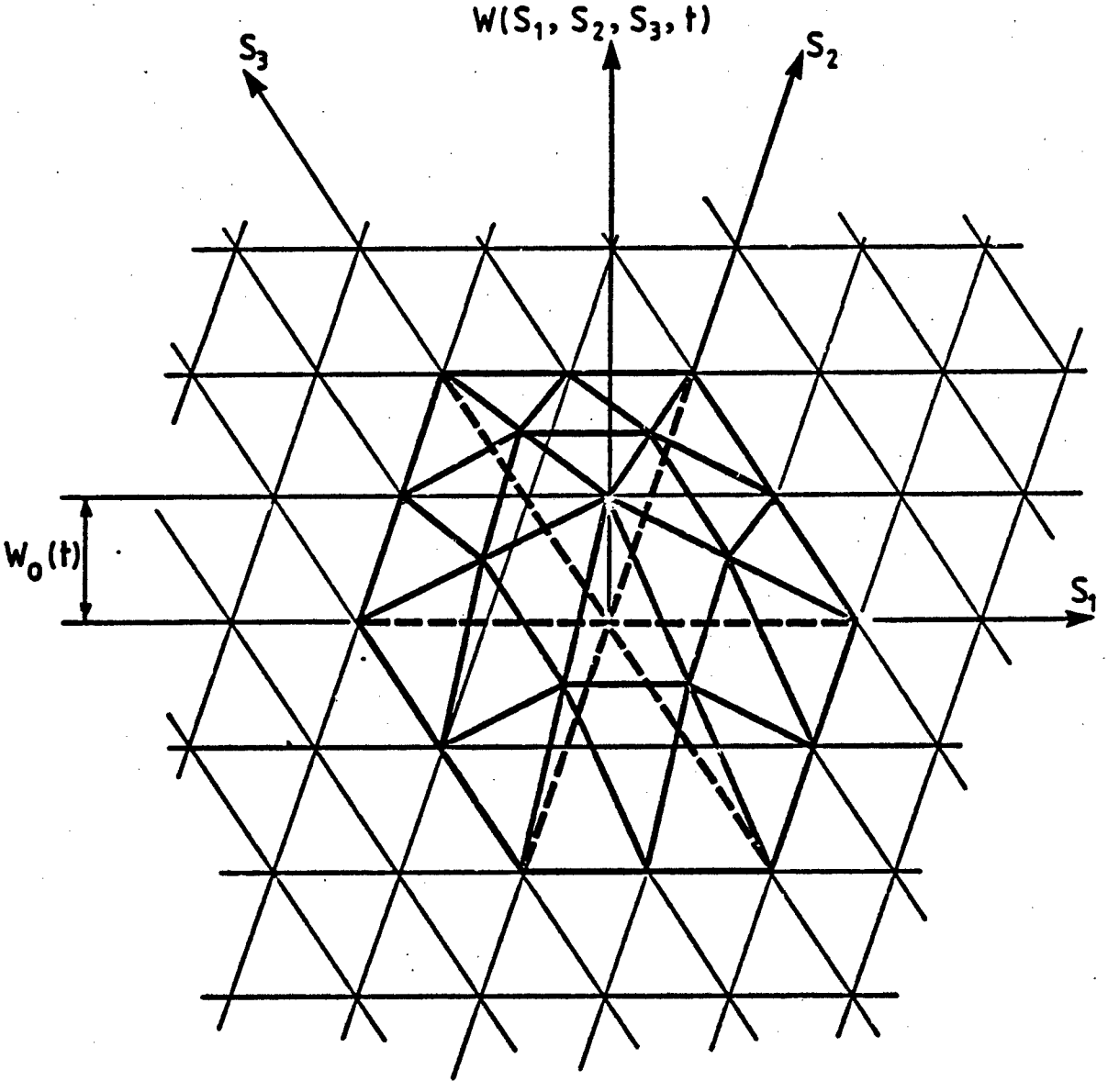

Fig.A1. 2. Pyramidial indentation of fabric

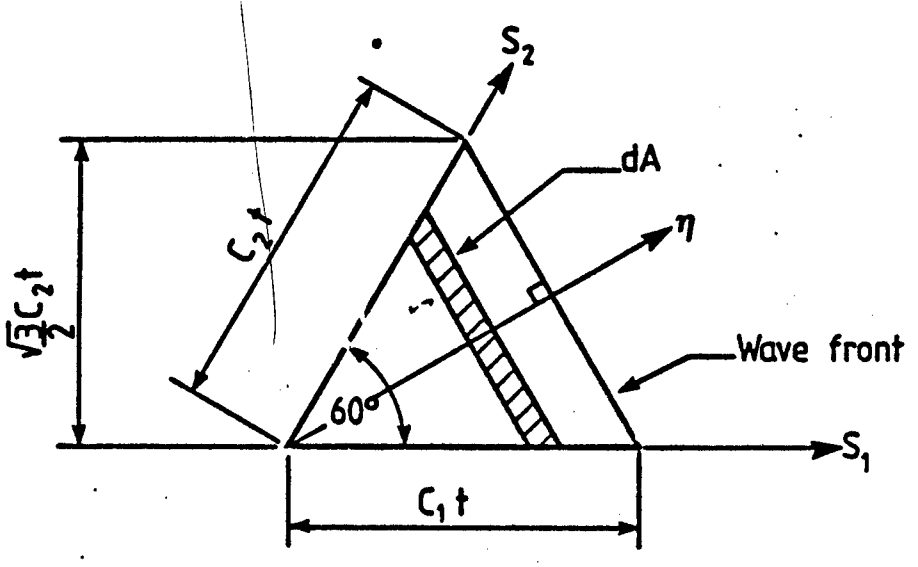

Fig.A1.3 Transversely displaced area of fabric [illegible]

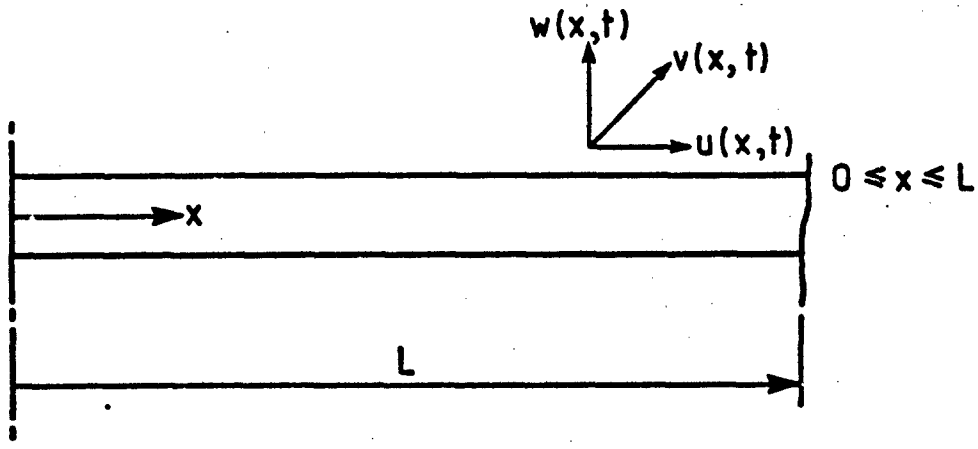

Fig. A2. 1. Typical filament

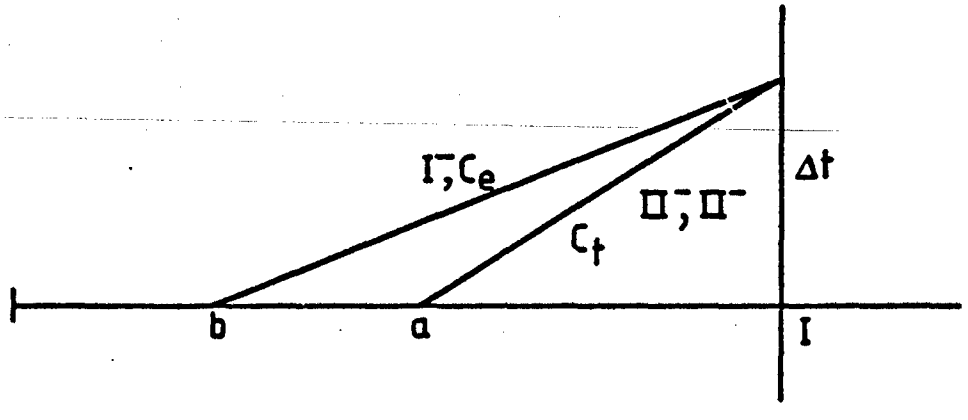

Fig. A2. 2. Extensional and transverse characteristics at I at time t+Δt